



**MONTGOMERY
& ASSOCIATES**

Water Resource Consultants

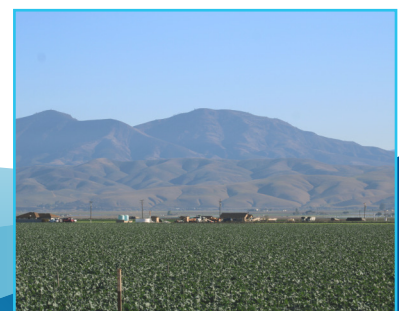
REPORT

March 2023

Salinas Valley Seawater Intrusion Model Development

Prepared for:

Salinas Valley Basin Groundwater Sustainability Agency
Salinas Valley, California



201 Hoffman Avenue, Suite 9, Monterey, CA 93940
elmontgomery.com

Contents

ACRONYMS & ABBREVIATIONS.....	vi
1 INTRODUCTION AND BACKGROUND.....	1
1.1 Purpose and Scope of Modeling.....	7
1.2 Project/Study Area	8
2 HYDROGEOLOGIC CONCEPTUAL MODEL	9
2.1 Geologic Framework.....	9
2.2 Hydrogeologic / Hydrostratigraphic Units in Study Area	14
2.2.1 Hydrostratigraphy near Study Area Center.....	15
2.2.2 Hydrostratigraphy Along Study Area Margins.....	20
2.2.3 Hydrogeologic Model.....	23
2.3 Occurrence and Movement of Groundwater.....	25
2.3.1 Groundwater Level Trends and Contours.....	25
2.3.2 Density Dependent Flow.....	31
2.4 Chloride Distribution and Seawater Concentrations.....	31
2.4.1 Mechanism and Extent of Seawater Intrusion.....	31
2.4.2 Measurement and Extent of Seawater Intrusion	32
2.5 Hydraulic Properties for Hydrogeologic Units.....	35
2.6 Surface Water Features	42
2.7 Groundwater Inflows and Outflows	48
2.7.1 Groundwater Inflows.....	48
2.7.2 Groundwater Outflows	57
2.7.3 Summary of Groundwater Flows	60
3 MODEL DEVELOPMENT	61
3.1 Modeling Code Selection.....	62
3.1.1 Important code features.....	62
3.2 Model Spatial and Temporal Discretization	62
3.2.1 Lateral discretization and grid spacing.....	62
3.2.2 Vertical discretization / layering	62
3.2.3 Temporal discretization.....	64
3.3 Initial Conditions	64
3.3.1 Initial Heads.....	64
3.3.2 Initial Concentrations	65
3.4 Pumping.....	65
3.5 Ocean Boundary.....	65
3.5.1 Variable Density Flow	69

3.6	Elkhorn Slough.....	69
3.7	Southeastern Boundary Groundwater Inflow	69
3.8	No-flow Boundaries	70
3.9	Surface Water	70
3.10	Recharge.....	71
3.11	Castroville Seawater Intrusion Program	74
3.12	Evapotranspiration.....	74
3.13	Hydrogeologic Zonation (HGUs).....	77
4	MODEL CALIBRATION	94
4.1	Calibration Datasets.....	95
4.1.1	Groundwater Levels.....	95
4.1.2	Chloride Concentrations	96
4.1.3	Streamflow Measurements	99
4.2	Calibration Results.....	99
4.2.1	Water Levels and Chloride Concentrations.....	99
4.2.2	Surface Water Flows	111
4.3	Calibrated Model Parameter Distributions	116
4.4	Model Parameter Uncertainty Runs and Matching AEM Data	121
4.4.1	Model Parameter Uncertainty Runs.....	121
4.4.2	Model Constraining Using Geophysics (AEM Data)	132
4.5	Comparison of Groundwater Flows.....	134
4.6	Calibration Summary	134
	REFERENCES	135

Tables

Table 2-1.	Hydrostratigraphic Units and Data Sources for Groundwater Level Contours.	26
Table 2-2.	Statistical Summary of Hydraulic Conductivity Measurements by Aquifer	38
Table 2-3	Measured Surface Water Flows in Study Area (WY1975-2020).....	45
Table 2-4.	Seasonal On-Farm Efficiencies by Irrigated Area	50
Table 2-5.	Estimated Total Annual Recharge in Study Area.....	51
Table 2-6.	Parameters Used to Estimate Darcy Flux at Chualar Creek.....	55
Table 2-7.	Summary of Annual Pumping by Category in Model Study Area for WYs 1975 through 2020 ...	59
Table 2-8.	Groundwater Flows	60
Table 3-1.	Summary of Model Boundary Conditions and Components	61
Table 3-2.	Model Layer Generalized Hydrogeologic Units.....	64
Table 3-3.	Repeated Water Years for Basin Boundary Surface Water Inflows	70
Table 4-1.	Water Level Calibration Statistics	102

Table 4-2. Summary of Calibrated Hydraulic Conductivity (K) and Storage Properties of the HGUs within the Model	118
Table 4-3. Calibrated Recharge Multipliers.....	120

Figures

Figure 1-1. General Location Map and Study Area.....	2
Figure 1-2. Model Study Area and CSIP Location	3
Figure 1-3. Seawater Intrusion in the 180-Foot Aquifer (from MCWRA) and Fall 2020 Water Levels	4
Figure 1-4. Seawater Intrusion in the 400-Foot Aquifer (from MCWRA) and Fall 2020 Water Levels	5
Figure 2-1. Surface Geology and Description of Geologic Units in Model Study Area.....	10
Figure 2-2. Extent and Depth to the Salinas Valley Aquitard in Model Study Area	17
Figure 2-3. Extent of Aquitard Layers in the Model Study Area	21
Figure 2-4. Example Cross Section Showing the 9 Model Layers in the Hydrogeologic Model	24
Figure 2-5. Representative Hydrographs within the 180-Foot Aquifer	28
Figure 2-6. Representative Hydrographs within the 400-Foot Aquifer	29
Figure 2-7. Representative Hydrographs within the Deep Aquifer.....	30
Figure 2-8. Relationship between Chloride and Total Dissolved Solids in Groundwater	33
Figure 2-9. Background Chloride Concentration in Groundwater	34
Figure 2-10. Hydraulic Conductivity Distribution by Aquifer or Geologic Formation.....	37
Figure 2-11. Location of Hydraulic Conductivity Measurements by Aquifer	39
Figure 2-12. Literature Estimates of Dispersivity Versus Scale of Observation	41
Figure 2-13. Surface Water Features in Study Area	44
Figure 2-14. Average Monthly Surface Water Flow on the Salinas River	46
Figure 2-15. Average Monthly Surface Water Flow at Gabilan and El Toro Creek.....	47
Figure 2-16. Urban Recharge as a Percentage of Urban Pumping	52
Figure 2-17. Recharge Component Areas	53
Figure 2-18. Recharge Areas	54
Figure 2-19. Pumping Locations and Data Sources	58
Figure 3-1. Extent of Model Grid.....	63
Figure 3-2. Model Boundary Conditions	66
Figure 3-3. Sea Level Rise at Monterey Bay	68
Figure 3-4. Historical Snapshots of Estimated Recharge	72
Figure 3-5. Estimated Monthly Spatial Distribution of Recharge in Water Year 2020	73
Figure 3-6. Historical Estimates of Potential Evapotranspiration for Selected Time Periods	75
Figure 3-7. Estimate of Potential Evaporation for Water Year 2020	76
Figure 3-8. Model Hydrogeologic Zonation in Layer 1	79
Figure 3-9. Model Hydrogeologic Zonation in Layer 2	80
Figure 3-10. Model Hydrogeologic Zonation in Layer 3	81
Figure 3-11. Model Hydrogeologic Zonation in Layer 4	81
Figure 3-12. Model Hydrogeologic Zonation in Layer 5	82

Figure 3-13. Model Hydrogeologic Zonation in Layer 6	83
Figure 3-14. Model Hydrogeologic Zonation in Layer 7	84
Figure 3-15. Model Hydrogeologic Zonation in Layer 8	85
Figure 3-16. Model Hydrogeologic Zonation in Layer 9	86
Figure 3-17. Model Hydrogeologic Zonation in Layer 10	87
Figure 3-18. Model Hydrogeologic Zonation in Layer 11	88
Figure 3-19. Model Hydrogeologic Zonation in Cross Section A-A'	89
Figure 3-20. Model Hydrogeologic Zonation in Cross Section B-B'	90
Figure 3-21. Model Hydrogeologic Zonation in Cross Section C-C'	91
Figure 3-22. Model Hydrogeologic Zonation in Cross Section D-D'	92
Figure 3-23. Model Hydrogeologic Zonation in Cross Section E-E'	93
Figure 4-1. Water Level Calibration Target Locations with their Associated Calibration Group	97
Figure 4-2. Chloride Calibration Target Locations with their Associated Calibration Group	98
Figure 4-3. Simulated and Observed 500 mg/L Chloride Concentration Contours within the 180-Foot Aquifer in 1985, 1997, 2005, 2015, and 2020	100
Figure 4-4. Simulated and Observed 500 mg/L Chloride Concentration Contours within the 400-Foot Aquifer in 1985, 1995, 2005, 2015, and 2020	101
Figure 4-5. Mean Residual Water Level Bubble Plot within the 180-Foot Aquifer and Equivalent Areas...	104
Figure 4-6. Mean Residual Water Level Bubble Plot within the 400-Foot Aquifer and Equivalent Areas...	105
Figure 4-7. Simulated and Observed Water Level Crossplot	107
Figure 4-8. Observed and Simulated Representative Hydrographs within the 180-Foot Aquifer	108
Figure 4-9. Observed and Simulated Representative Hydrographs within the 400-Foot Aquifer	109
Figure 4-10. Observed and Simulated Representative Hydrographs within the Deep Aquifers	110
Figure 4-11. Simulated and Measured Stream Flow in the Salinas River at the Gage near Chualar	112
Figure 4-12. Simulated and Measured Stream Flow in the Salinas River at the Gage near Spreckels	113
Figure 4-13. Simulated and Measured Stream Flow in Gabilan Creek	114
Figure 4-14. Simulated and Measured Stream Flow in El Toro Creek	115
Figure 4-15. Hydraulic Conductivity Pilot Points Used during Model Calibration	119
Figure 4-16. Simulated 500 mg/L Chloride Concentration Contours from 105 Null-Space Monte Carlo Models in the 180-Foot Aquifer in 1985	122
Figure 4-17. Simulated 500 mg/L Chloride Concentration Contours from 105 Null-Space Monte Carlo Models in the 180-Foot Aquifer in 1997	123
Figure 4-18. Simulated 500 mg/L Chloride Concentration Contours from 105 Null-Space Monte Carlo Models in the 180-Foot Aquifer in 2005	124
Figure 4-19. Simulated 500 mg/L Chloride Concentration Contours from 105 Null-Space Monte Carlo Models in the 180-Foot Aquifer in 2015	125
Figure 4-20. Simulated 500 mg/L Chloride Concentration Contours from 105 Null-Space Monte Carlo Models in the 180-Foot Aquifer in 2020	126
Figure 4-21. Simulated 500 mg/L Chloride Concentration Contours from 105 Null-Space Monte Carlo Models in the 400-Foot Aquifer in 1985	127

Figure 4-22. Simulated 500 mg/L Chloride Concentration Contours from 105 Null-Space Monte Carlo Models in the 400-Foot Aquifer in 1997	128
Figure 4-23. Simulated 500 mg/L Chloride Concentration Contours from 105 Null-Space Monte Carlo Models in the 400-Foot Aquifer in 2005	129
Figure 4-24. Simulated 500 mg/L Chloride Concentration Contours from 105 Null-Space Monte Carlo Models in the 400-Foot Aquifer in 2015	130
Figure 4-25. Simulated 500 mg/L Chloride Concentration Contours from 105 Null-Space Monte Carlo Models in the 400-Foot Aquifer in 2020	131
Figure 4-26. AEM Survey Flight Lines over the Seawater Intrusion Intruded Areas in 2017 and in 2019..	133

Appendices

Appendix A. Simulated and Observed Water Level Hydrographs

Appendix B. Integration of Airborne Electromagnetic Data into the Modeling of Saltwater Intrusion

ACRONYMS & ABBREVIATIONS

AEM.....	Airborne Electromagnetic
AF/yr.....	acre-feet per year
ASR.....	Aquifer Storage and Recovery
basin.....	Salinas Valley Groundwater Basin
BCM.....	Basin Characterization model
BCT.....	block centered transport
cfs.....	cubic feet per second
CHD.....	constant head boundary
CLN.....	connected linear network
CSIP.....	Castroville Seawater Intrusion Project
DDF.....	density dependent flow
DWR.....	California Department of Water Resources
ET.....	evapotranspiration
FO-SVA.....	Fort Ord-Salinas Valley Aquitard
GEMS.....	Groundwater Extraction Management System
gm/L.....	grams per liter
GSPs.....	Groundwater Sustainability Plans
HCM.....	hydrogeologic conceptual model
HGU.....	Hydrogeologic zonation or unit
MCWD GSA..	Marina Coast Water District Groundwater Sustainability Agency
MCWRA.....	Monterey County Water Resources Association
mg/L.....	milligrams per liter
Model.....	Seawater Intrusion Model
msl.....	mean sea level
NAVD88.....	North American Vertical Datum of 1988
NWT.....	Newton Raphson Solver
OFE.....	On-Farm Efficiency
PEST.....	Parameter Estimation and Uncertainty Analysis
PET.....	potential evapotranspiration
RMS error.....	root mean squared error
SGMA.....	Sustainable Groundwater Management Act
SRDF.....	Salinas River at the Salinas River Diversion Facility
SVA.....	Salinas Valley Aquitard
SVBGSA.....	Salinas Valley Basin Groundwater Sustainability Agency
SVIHM.....	Salinas Valley Integrated Hydrologic Model
SWI Model.....	Seawater Intrusion Model
TDS.....	total dissolved solids
USGS.....	U.S. Geological Survey
WY.....	Water Year

1 INTRODUCTION AND BACKGROUND

This report documents the development of a coupled flow and transport groundwater model to simulate seawater intrusion in the Salinas Valley Groundwater Basin (Basin). The Salinas Valley Groundwater Basin is an alluvial basin underlying the elongated, intermountain valley of the Salinas River. The Basin is oriented southeast to northwest, with the Salinas River draining toward the northwest into the Pacific Ocean at Monterey Bay. The study area covers the coastal portion displayed on Figure 1-1 in the northwestern portion of the Basin.

The Salinas River drains a watershed area of approximately 4,410 square miles, including the highlands of the Sierra de Salinas and Santa Lucia Range to the west and the Gabilan and Diablo Ranges to the east (Tetra Tech, 2015). The valley floor is approximately 10 miles wide in the north near the City of Salinas and narrows to about 2 miles wide in the south near San Ardo. The valley floor slopes at an average grade of approximately 5 feet per mile to the northwest, dropping from 500 feet above mean sea level (msl) (NAVD88) near Bradley to sea level at Monterey Bay.

Within the Salinas Valley, the 180-Foot and 400-Foot Aquifers have been subject to seawater intrusion for more than 70 years, as demonstrated by increased chloride in wells near the Monterey Bay coastline, west of the City of Salinas. The negative impact of seawater intrusion on local water resources and the agricultural economy has been the primary motivation for many studies dating back to 1946 (California Department of Water Resources [DWR], 1946). The Monterey County Water Resources Association (MCWRA) and others have implemented a series of engineering and management projects to halt seawater intrusion including well construction moratoriums, the Castroville Seawater Intrusion Project (CSIP) system (Figure 1-2), and the Salinas Valley Water Project. Although those actions have managed to slow the advance of intrusion and reduce its impacts, seawater intrusion remains an ongoing threat.

The extent and advance of seawater intrusion over time has been well monitored and reported by MCWRA. Monitoring seawater intrusion is currently conducted by MCWRA through a network of monitoring wells that are sampled biannually in June and August. MCWRA has published estimates of the extent of seawater intrusion over the past 70 years with recent estimates published at least every 2 years. The MCWRA maps define the extent of seawater intrusion as the inferred location of the 500 milligrams per liter (mg/L) chloride concentration (Figure 1-3 and Figure 1-4). This chloride concentration is significantly lower than is typical of seawater, but it represents a concentration that begins to impact use of the water.

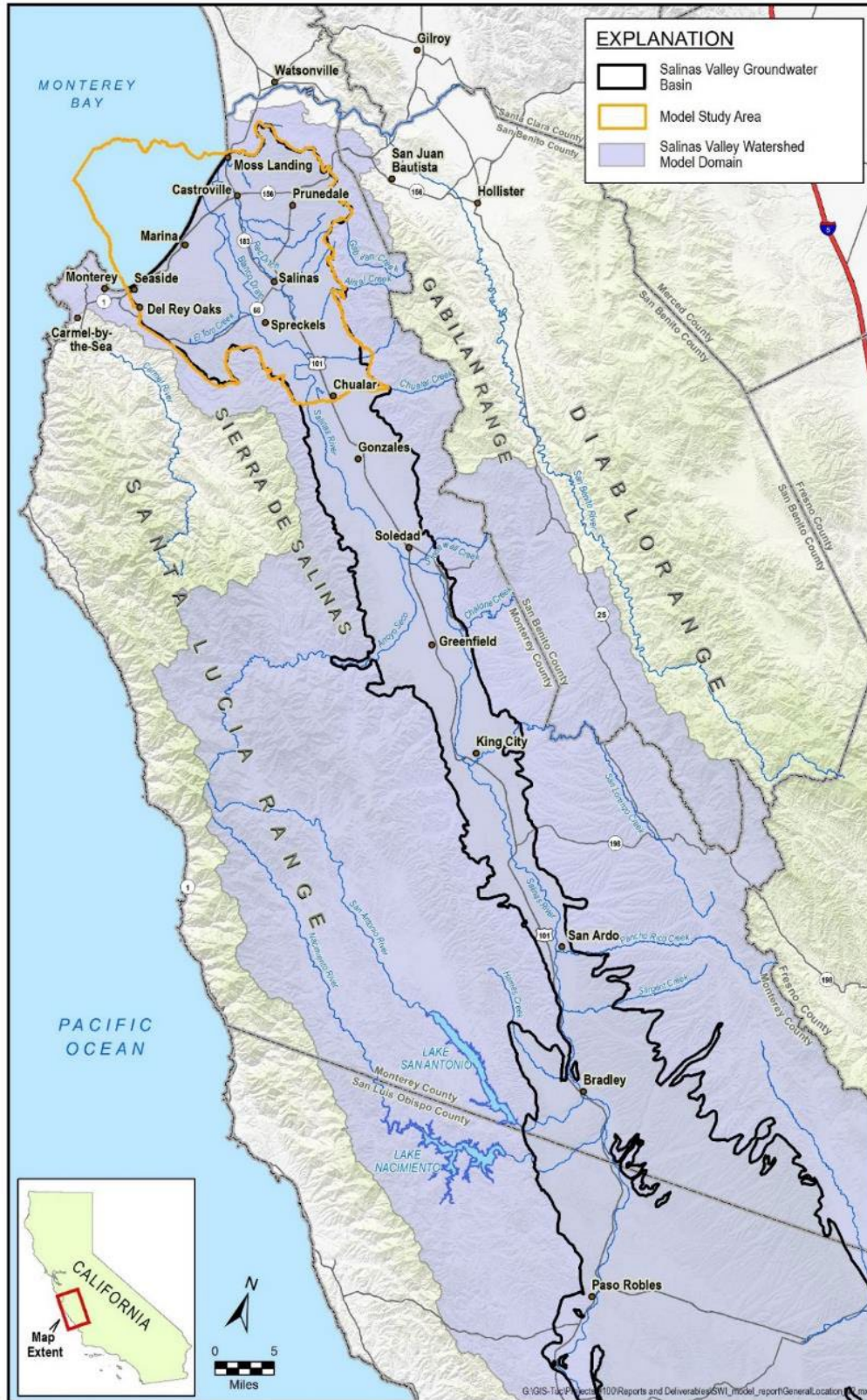


Figure 1-1. General Location Map and Study Area

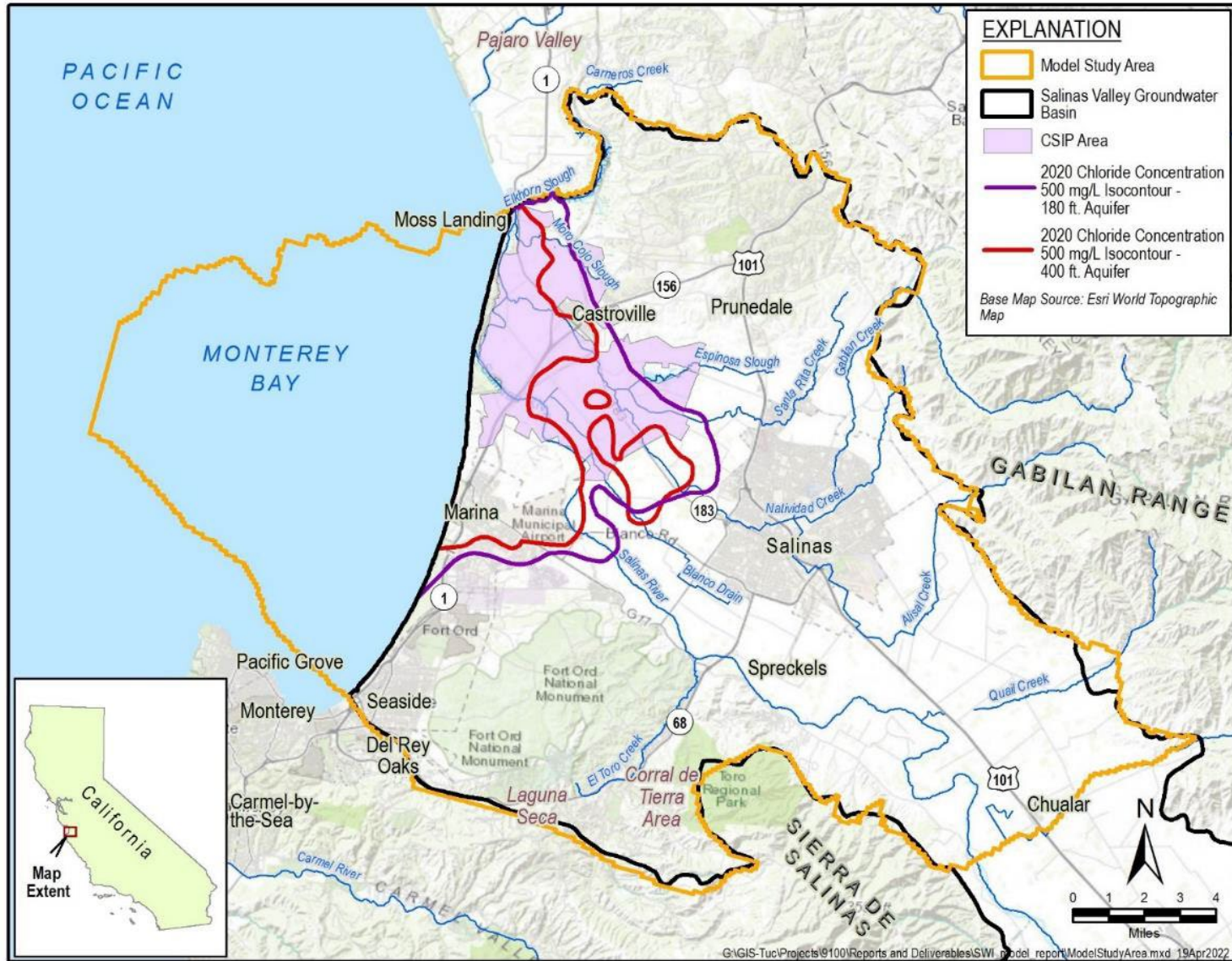


Figure 1-2. Model Study Area and CSIP Location

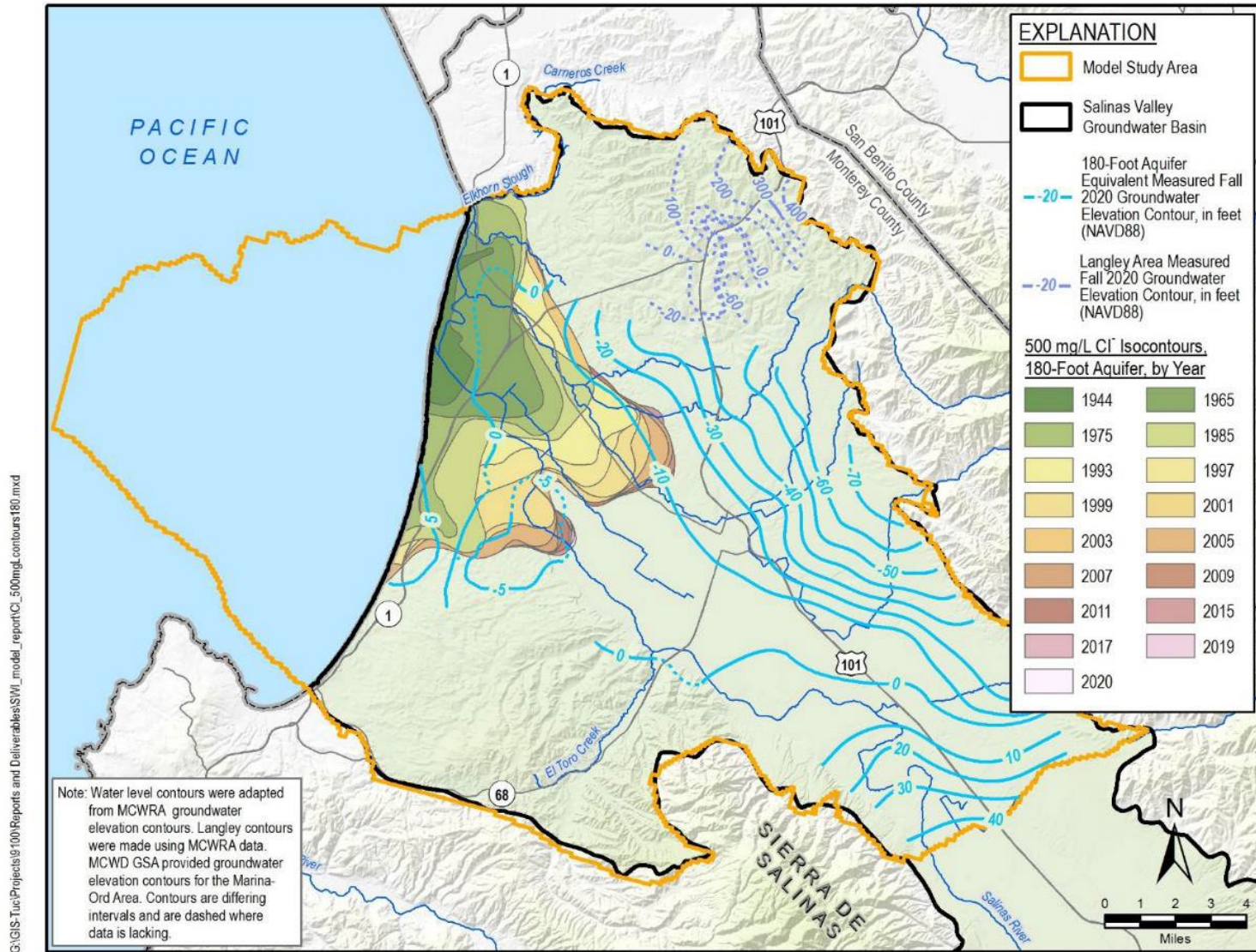


Figure 1-3. Seawater Intrusion in the 180-Foot Aquifer (from MCWRA) and Fall 2020 Water Levels

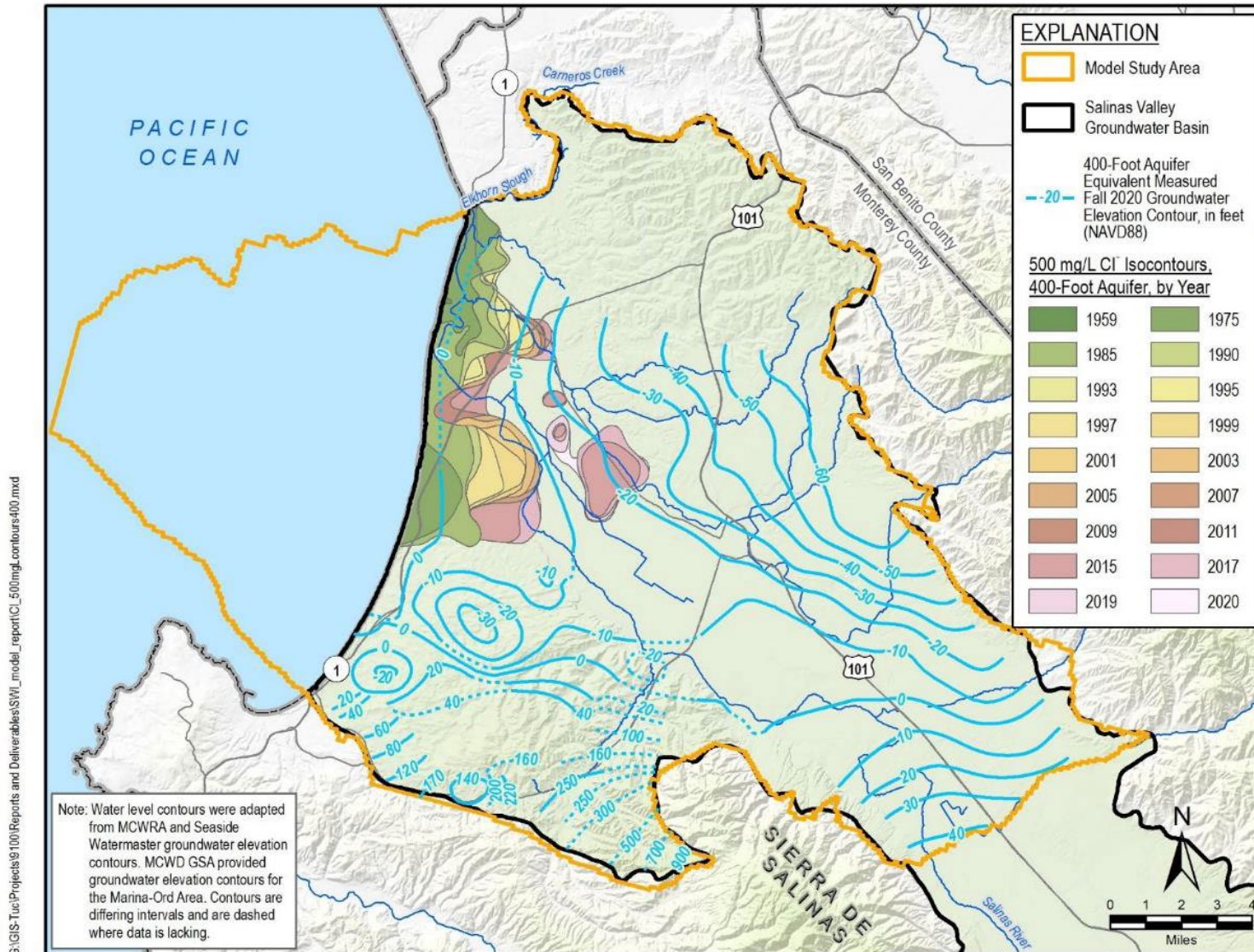


Figure 1-4. Seawater Intrusion in the 400-Foot Aquifer (from MCWRA) and Fall 2020 Water Levels

The extent of the shaded contours on Figure 1-3 and Figure 1-4 represents the extent of groundwater with chloride exceeding 500 mg/L during the 2020 monitoring period. The historical progression of the 500 mg/L extent is illustrated on these figures through the colored overlays that represent the extent observed during selected years. These figures also present the mapped Fall 2020 groundwater elevations for the 180-Foot Aquifer and the 400-Foot Aquifer, respectively. Fall groundwater levels represent roughly average groundwater elevations. Seawater intrusion occurs most rapidly when groundwater levels are at their lowest, which usually occurs in August.

Seawater intrusion in the 180-Foot Aquifer appears to generally follow hydraulic gradients (Figure 1-3.). Similarly in the 400-Foot Aquifer (Figure 1-4), seawater intrusion appears to follow hydraulic gradients toward groundwater depressions. However, the cone of depression in the Monterey Subbasin, shown with a closed -30 feet msl contour, has apparently not driven seawater intrusion as much as other gradients. Although groundwater elevations are one driver of seawater intrusion, geologic controls such as the interface between the alluvial fans (along the Gabilan Range on the northeast side of the study area) and the marine sediments of the 180/400-Foot Aquifer (and underlying sediments) also influence the rate and direction of seawater intrusion (Brown and Caldwell, 2017; Kennedy/Jenks, 2004).

The *State of the Salinas River Groundwater Basin* (Brown and Caldwell, 2017) report estimated approximately 11,000 acre-feet of seawater intrusion in the Basin every year based on previously published studies. The report focuses on the 180- and 400-Foot Aquifers and covers the entire study area. This estimate is lower than other studies which range from 11,000 (DWR, 2003) to 18,000 acre-feet per year (AF/yr) (Yates, 1988). These rates, as well as the volume of impacted aquifer, were calculated using the migration of the 500 mg/L MCWRA chloride concentration contours. While this provides a reasonable estimate of the rate and extent of seawater intrusion, the landward migration of seawater does not occur uniformly; the seawater intrusion front or 500 mg/L contour line is not migrating landward at a uniform rate. Data collection and quality are limited in some areas resulting in uncertainty in the true location of the 500 mg/L contour lines. Natural heterogeneity (both horizontally and vertically) of the aquifers as well as seawater's greater density than freshwater compounds uncertainty. These challenges complicate an accurate understanding of where seawater will further intrude and how projects and management actions will affect seawater intrusion.

To date, no widespread seawater intrusion has been observed in the Deep Aquifers. The Salinas Valley Basin Groundwater Sustainability Agency (SVBGSA), MCWRA, and partners are funding a Study of the Deep Aquifers to assess the potential risk of seawater intrusion, among other objectives.

Seawater intrusion continues to advance, although advancement has slowed in the 180-Foot Aquifer. Further intrusion threatens agricultural and drinking water supplies in the 180-Foot and 400-Foot Aquifers, and potentially the Deep Aquifers. In particular, intrusion threatens the drinking water wells for the community of Castroville and City of Salinas. In addition, in 2014 California passed the Sustainable Groundwater Management Act (SGMA) that requires groundwater basins to reach sustainability across 6 sustainability indicators, including seawater intrusion.

1.1 Purpose and Scope of Modeling

The purpose of the Salinas Valley Seawater Intrusion Model is to develop a tool that will assist in designing and assessing projects and management actions that address seawater intrusion in the Salinas Valley. The Seawater Intrusion Model (SWI Model) was initially developed for the Monterey Subbasin and was funded through the Department of Water Resources Round 3 SGMA Planning Grants. SVBGSA and MCWRA then expanded the model to the Salinas Valley's boundaries to cover the full extent of potential seawater intrusion. This model report covers model development and calibration for the entire expanded area of the model.

Existing groundwater flow models of the Salinas Valley do not have the ability to account for the differing densities of freshwater, seawater, and brackish water. The SWI Model includes the ability to account for transport due to density differences. It builds on existing groundwater models of the region, including the Monterey Subbasin Groundwater Flow Model developed by EKI Environment and Water for Marina Coast Water District Groundwater Sustainability Agency (MCWD GSA), the Salinas Valley Integrated Hydrologic Model (SVIHM)^{1,2} under development by the U.S. Geological Survey, the North Marina Groundwater Model, and the Seaside Basin Model.

Under SGMA, SVBGSA, MCWD GSA, and the Monterey County GSA must reach sustainability in the 180/400-Foot Aquifer and Monterey Subbasins according to the 6 sustainability indicators, including seawater intrusion. The Seawater Intrusion Model (Model) is a tool the agencies can use to better assess, compare, and design projects and management actions to reach their sustainability goals.

¹ These data (model and/or model results) are preliminary or provisional and are subject to revision. This model and model results are being provided to meet the need for timely best science. The model has not received final approval by the U.S. Geological Survey (USGS). No warranty, expressed or implied, is made by the USGS or the U.S. Government as to the functionality of the model and related material nor shall the fact of release constitute any such warranty. The model is provided on the condition that neither the USGS nor the U.S. Government shall be held liable for any damages resulting from the authorized or unauthorized use of the model.

² The provisional SVIHM used by M&A in this modeling was provided on February 2, 2021.

1.2 Project/Study Area

The model study area covers the full extent of potential seawater intrusion within the Salinas Valley (Figure 1-2). The northern boundary is the Elkhorn Slough, which separates the Salinas Valley from the adjacent Pajaro Valley. The Model's northeastern edge follows the edge of the Basin near the Gabilan Mountains. The southeastern extent is Chualar Creek, which was selected because it is located at a distance far enough away from seawater intrusion and severe groundwater level depressions to minimize any potential boundary effects on model results. Along the southwestern side, the study area boundary abuts the Santa Lucia Highlands.

2 HYDROGEOLOGIC CONCEPTUAL MODEL

This section provides information on the hydrogeologic conceptual model (HCM) that is the foundation for the numerical model. It summarizes the geologic framework, aquifer layering, groundwater levels and flows, recharge, discharge, aquifer hydraulic properties, and groundwater quality principally in terms of seawater intrusion. The HCM is based on best available data, technical studies, and maps that characterize the physical and hydrologic components in the model study area. Chapters 3 and 4 build on this HCM and summarize how the HCM is incorporated into model development and calibration.

2.1 Geologic Framework

The Salinas Valley Groundwater Basin is a northwest-dipping structural trough underlain by the Salinian tectonic block, a geologic basement terrane consisting of metamorphic and granitic rock of Paleozoic to Mesozoic age. The Salinian Block is bordered on both east and west by tectonic blocks of the Franciscan Complex, marked by large scale strike-slip faults: the San Andreas fault zone on the east and the Rinconada fault zone on the west, which locally includes the Reliz-King City Fault (Figure 2-1). The combination of tectonically driven land movement, structural deformation, and climatically driven sea level changes has influenced the depositional environment in the Salinas Valley. Over time, the Basin has been filled with approximately 10,000 to 15,000 feet of both marine and continental sediments. Figure 2-1 presents a geologic map of the Basin and vicinity. This geologic map was adopted from the United States Geologic Survey's (USGS) Monterey and Adjacent Area Map. (Wagner, *et al.*, 2002).

The geologic formations that comprise the aquifers in the Basin are predominantly fluvial, alluvial, and marine sedimentary sequences that are characteristic of changes in sea level over time, leading to the sequence of aquifers and aquitards present today (Tinsley, 1975; Brown and Caldwell, 2017). The transitions between marine and terrestrial depositional environments have led to complex layering of coarse and fine-grained marine and continental materials in the subsurface. This process created the variable hydrogeologic conditions encountered throughout the Basin, even within the same geologic unit.

The geology of the portion of the Basin where the model study area is located is characterized by fluvial and marine deposits encountered as the Paso Robles Formation, the Aromas Sand, and the overlying unconsolidated quaternary deposits (DWR, 2004a). The northernmost portion of the Basin is in contact with a filled-in paleochannel of the Salinas River, known as the Elkhorn Slough.

GEOLOGY EXPLANATION

QUATERNARY DEPOSITS

af	Artificial fill
Q	Alluvium
Qd	Dune sand
Qe	Eolian sand
Qs	Sand
Qcf	Canyon Fill (offshore)
Qg	Stream gravel
Qb	Basin deposits
Qfl	Flood plain deposits
Qae	Eolian facies
Qaf	Fluvial facies
Qls	Landslide deposits
Qms	Marine sediments
Qf	Alluvial fan deposits
Qo	Older alluvium
Qod	Older Dune Sand
Qrb	Relict beach deposits (offshore)
Qct	Submarine canyon terrace
Qar	Aromas Sand (undivided)
Qfa	Fan deposits of Antioch
Qfc	Fan deposits of Chualar
Qfp	Fan deposits of Placencia
Qfg	Fan deposits of Gloria
Qmt	Marine terrace deposits
QT	Plio-Pleistocene continental deposits

TERTIARY ROCKS

Puc	Unnamed Pliocene continental mudstone
Pus	Unnamed Pliocene continental sandstone
Ppu	Purisima Formation
MPE	Etchegoin Formation
Tv	Tertiary volcanic rocks
Msm	Santa Margarita Sandstone
Mmy	Monterey Formation
Msh	Organic mudstone
Mus	Unnamed Miocene sandstone
Mv	Unnamed Miocene volcanic rocks
Orb	Red beds
Ovq	Vaqueros Sandstone
Ovc	Carmeloite of Lawson
EOsj	San Juan Bautista Formation
Ebu	Unnamed Eocene sedimentary rocks
Ec	Carmelo Formation

CRETACEOUS ROCKS

Ku	Upper Cretaceous sedimentary rock
KJf	Franciscan Complex
Kgd	Granodiorite
Kgr	Granitic rocks
Kqd	Quartz diorite
Kqm	Quartz monzonite

JURASSIC ROCKS

ls	limestone
Jhg	Hornblende Gabbro of Logan quarry
PzMz	Prebatholithic metasedimentary rocks
Pzls	Prebatholithic Carbonate rocks
msc	Schist of Sierra de Salinas

GEOLOGIC SYMBOLS

---	fault, approx. located
—	fault, certain
-----	fault, concealed
.....	fault, concealed, queried
- - - -	fault, inferred
- - - ->	fault, inferred, queried
↖	thrust fault, certain
↖.....	thrust fault, concealed
↖ - - -	thrust fault, inferred
↖ - - - ?	thrust fault, inferred, queried
+	Anticline, Certain
- - + - -	Anticline, Concealed

Source: Geology from Wagner et. al 2002

The major geologic units present in the model study area are described below, starting at the surface and characterizing the geologic layers from youngest to oldest. Geologic descriptions are derived from a combination of sources (Jennings, *et al.*, 2010; Clark, *et al.*, 2000; Johnson, *et al.*, 1988; DWR, 2004a).

Quaternary Deposits

- *Alluvium, Flood Plain Deposits, Landslide Deposits, Alluvial Fans (Q/Qfl/Qls)* – Holocene Alluvium consists of unconsolidated stream and basin deposits occur at the base hillslopes in the Basin. These deposits have gradational contacts with the Floodplain Deposits that occur along tributaries to the Salinas River. The Floodplain Deposits consist predominately of unconsolidated layers of mixed sand, gravel, silt, and clay that were deposited in a fluvial environment by the Salinas River and its tributaries. Numerous landslides are present in upland portions southwest of the valley axis such as San Benancio, Harper, and Corral de Tierra Canyons, as well as in the upland areas of the Sierra de Salinas.
- *Older Dune Sand (Qod)* – This Pleistocene unit blankets most of the northwestern portions of the Basin and is the predominant surface deposit present in approximately one-third of the Monterey Subbasin. This unit is up to 250 feet thick. This sand is predominately fine- to medium-grained, with thin, gentle, to moderate crossbedding (Harding ESE, 2001).
- *Older Alluvium (Qo), Alluvial Fans (Qf)* – no surface expression mapped in model study area) – This Pleistocene unit comprises alternating, interconnected beds of fine-grained and coarse-grained deposits, predominately associated with alluvial fan depositional environments. The Older Alluvium underlies the Older Dune Sand (*Qod*) and in some reports has been referred to as Valley Fill Deposits, which is described as including an estuarine clay layer (Salinas Valley Aquitard [SVA]) and an underlying sand and gravel fluvial sequence (Harding ESE, 2001). Alluvial fans are present along the east side of the study area. These sediments are deposited in a distributary manner at the base of mountain fronts where streams emerge (Kennedy/Jenks, 2004). They consist of moderately to poorly sorted sand, silt, and gravel, and can range from unconsolidated to moderately consolidated depending on age and depth.
- *Aromas Sand (Qar)* – This Pleistocene unit is composed of cross-bedded sands containing some clayey layers (Harding ESE, 2001). This unit was deposited in predominately in an eolian, high-energy alluvial, alluvial fan, and shoreline environments, with the predominant deposition environment being eolian (Harding ESE, 2001; Greene, 1970; Dupre, 1990). The Aromas Sand likely extends into the northern portion of the center of the basin (MCWRA, 2017). The Aromas Sand is exposed

throughout the ridge and hilltops in the northern upland areas of the Basin, while the unit is buried beneath Older Dune Sand and Alluvium in the vicinity of the City of Marina. Thickness of the Aromas Sand varies within the Basin and can be up to 300 feet thick (Harding ESE, 2001; Muir, 1982). Although a clayey or hard red bed is sometimes observed at the basal contact with the underlying Paso Robles Formation, the stratigraphic relationship between the Aromas Sand and the Paso Robles Formation is difficult to discern due to lithologic similarities and the complex interface between them (Harding ESE, 2001; Dupre, 1990).

Tertiary Deposits

- *Paso Robles Formation (QT)* – This Pliocene to lower Pleistocene unit is composed of lenticular beds of sand, gravel, silt, and clay from terrestrial deposition (Thorup, 1976; Durbin, *et al*, 1978). The depositional environment is largely fluvial but also includes alluvial fan, lake, and floodplain deposition (Durbin, 1974; Harding ESE, 2001; Thorup, 1976; Greene, 1970). The individual beds of fine and coarse materials typically have thicknesses of 20 to 60 feet (Durbin, *et al*, 1978). Durham (1974) reports that the thickness of the Paso Robles Formation is variable due to erosion of the upper part of the unit. Varying thicknesses ranging from 500 feet to 2,000 feet are found within the Basin. Outcrops of the Paso Robles Formation in the Study Area occur in Corral de Tierra area.
- *Purisima Formation (Ppu)* – This formation has no surface expression within the Study Area, and is not mapped or shown on Figure 2-1. This Pliocene unit consists of interbedded siltstone, sandstone, conglomerate, clay, and shale deposited in a shallow marine environment (Greene, 1977; Harding ESE, 2001). The Purisima Formation has been encountered in boreholes closer to the coast; however, the unit is not present in the more inland portions of the Basin (Harding ESE, 2001; HydroMetrics, 2009; Geosyntec, 2007). The Purisima Formation ranges in thickness from 500 to 1,000 feet (Feeney and Rosenberg, 2003).
- *Santa Margarita Sandstone (Msm)* – The Miocene Santa Margarita Sandstone is a friable, arkosic sandstone. In the northern portions of the Basin, the Santa Margarita Sandstone interfingers with the Purisima Formation, which is overlain by the Paso Robles Formation (Durbin, 2007; HydroMetrics, 2009). Toward the boundaries with the Seaside area and the Corral de Tierra Area, the Paso Robles unconformably overlays over the Santa Margarita Sandstone. Outcrops of the Santa Margarita Sandstone are found in the Corral de Tierra Area.

- *Monterey Formation (Mmy)* – The Monterey Formation (Miocene) is a shale or mudstone deposited in a shallow marine environment (Harding ESE, 2001; Greene, 1977). The top of the Monterey Formation is generally defined as the bottom of the Basin as it is relatively impervious.
- *Older Igneous and Metamorphic Rocks (Kgd/Kqd/Kgr/Kqm/PzMz/Pzls/msc)* –The eastern and western borders of the Basin are defined by the contact between the Quaternary and Tertiary sedimentary units described above and the Cretaceous igneous and pre-Cretaceous metamorphic rocks of the Gabilan Range and Sierra de Salinas Range, respectively. These older units also make up the basement of the basin.

Several of these geologic formations crop out in the Monterey Bay, particularly along the walls of Monterey Canyon. Due to their permeability, these formations and the principal aquifers within them are also in hydraulic contact with the sea (Wagner *et al.*, 2002). If they do not directly crop out in Monterey Bay, the hydraulic connection is likely through a thin veneer of deltaic deposits (approximately 20 feet) overlying the formations (Greene 1977).

2.2 Hydrogeologic / Hydrostratigraphic Units in Study Area

Groundwater production in the Basin is primarily from sedimentary deposits that fill the Salinas Valley structural trough: the Holocene Alluvium, the Quaternary Older Alluvium, and Pliocene Paso Robles Formation. These geologic units do not define separate, individual aquifers. Although these units differ in age, they have similar distributions of sediment type and layering, and in practice they are difficult to distinguish during drilling. The lack of continuous aquitards makes it difficult to differentiate between various aquifers throughout most of the Salinas Valley. Within the study area however, the presence of laterally continuous clays distinguish the aquifers affect the following aspects of the basin hydrogeology:

- A near-surface clay layer, the SVA creates relatively shallow confined conditions in most of the central portion of the model study area, in contrast to the unconfined conditions over margins of the Basin.
- Deeper clay layers create definable aquifers along the center axis of study area, whereas other parts of the study area include only a single undifferentiated aquifer with interspersed, discontinuous clay lenses.

This HCM includes the following series of aquifers and aquitards, which have long been recognized in a multitude of studies and reports:

- Shallow Sediments, including Dune Sand Aquifer
- SVA/Fort Ord-Salinas Valley Aquitard

- 180-Foot Aquifer
- 180/400-Foot Aquitard
- 400-Foot Aquifer
- Deep Aquitard
- Deep Aquifers

This hydrostratigraphy is found in the model study area center and differs from the hydrostratigraphy near the study area boundaries as a result of varying depositional and structural influences. The undifferentiated aquifers near the study area boundary are connected to, and potentially influence, the movement of groundwater and seawater intrusion within the study area center.

2.2.1 Hydrostratigraphy near Study Area Center

Aquifers and aquitards in the layered system that define the Study Area center are described in the following sections, starting at the surface and moving downward through the system.

2.2.1.1 Shallow Sediments and Dune Sand Aquifer

The shallowest water-bearing sediments are thin, laterally discontinuous, and do not constitute a significant source of water through most of the Basin, with the exception of the Dune Sand Aquifer along the coast near the cities of Marina and Seaside. These shallow sediments are generally within 30 feet of the ground surface and are part of the Holocene Alluvium unit. Outside of Marina and Seaside, groundwater in these sediments is hydraulically connected to the Salinas River but is assumed to be relatively poorly connected to the underlying productive principal aquifers due to the presence of the underlying SVA.

The Dune Sand Aquifer is composed of fine to medium, well-sorted dune sands of Holocene age (Ahtna Engineering, 2013). This aquifer is locally defined and overlies the Fort Ord-Salinas Valley Aquitard (FO-SVA), which is an aquitard that pinches out near the coast, allowing the groundwater in the Dune Sands to potentially flow into the 180-Foot Aquifer as a result of lower groundwater elevations. The Dune Sand Aquifer is also sometimes referred to as the “A-Aquifer” beneath Fort Ord (Harding Lawson Associates [HLA], 1994; Jordan, *et al.*, 2005; Harding ESE, 2001). Groundwater in the Dune Sand Aquifer is unconfined. The aquifer is perched away from the coast, in areas where the FO-SVA exists and groundwater in the 180-Foot Aquifer has fallen below the bottom elevation of the FO-SVA. It is hydraulically connected to the underlying 180-Foot Aquifer in areas nearer to the coast. While the Dune Sands Aquifer is locally designated, there are no major production wells in this aquifer, and it is impacted by Fort Ord contamination.

2.2.1.2 Salinas Valley Aquitard/Fort Ord-Salinas Valley Aquitard

The SVA is the shallowest, relatively continuous hydrogeologic feature in the central portion of the study area. The aquitard is composed of blue or yellow sandy clay layers with minor interbedded sand lenses (DWR, 2003). The SVA correlates to the Pleistocene Older Alluvium stratigraphic unit and was deposited in a shallow sea during a period of relatively high sea level. The SVA caps the most productive aquifers and separates the aquifers from the Salinas River and other local surface water features (DWR, 1946). While this aquitard is relatively continuous in the center of the study area, it is not monolithic. The clay layer is missing in some areas and pinches out in other areas. Figure 2-2 shows the inferred extent and depth to the top of the SVA.

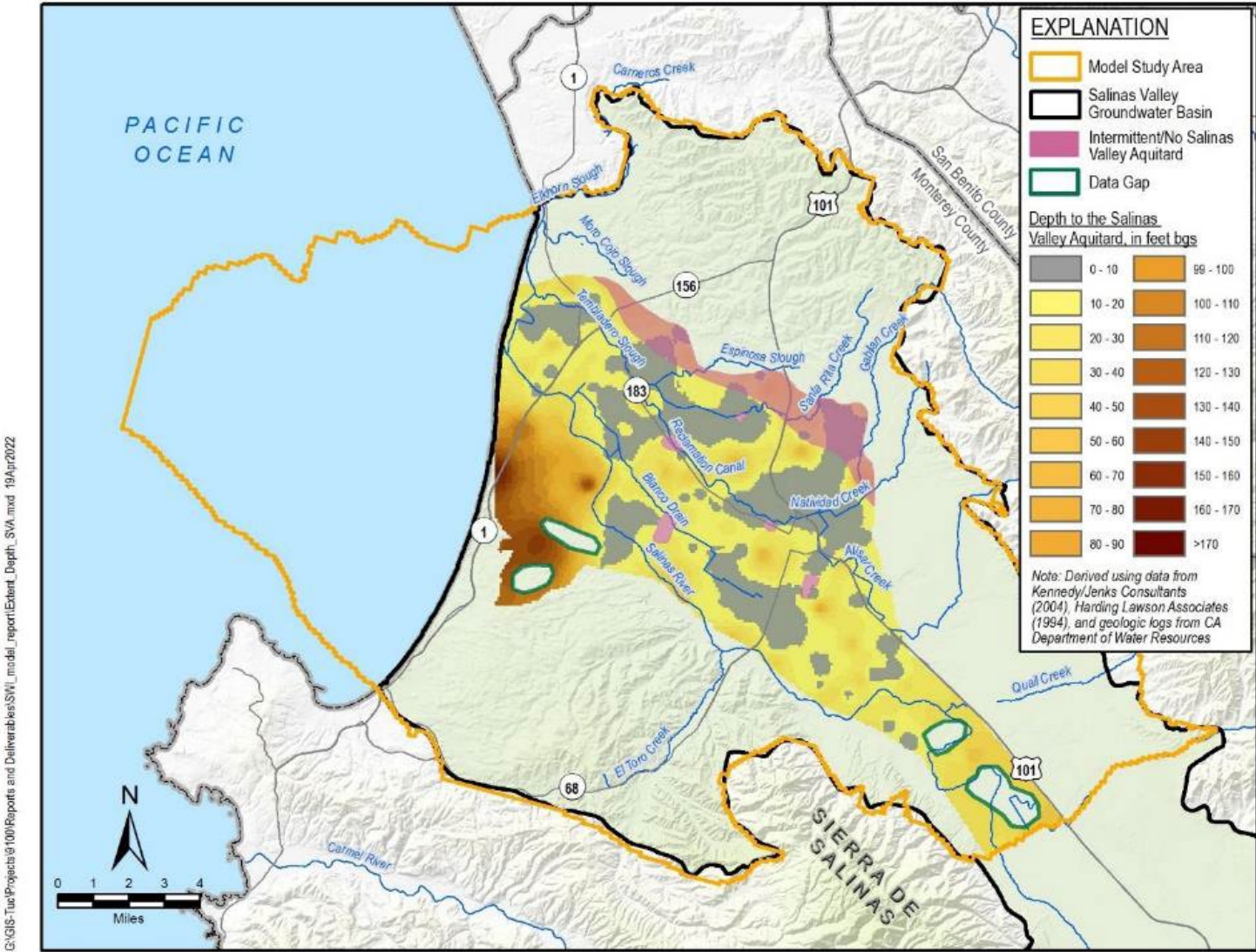


Figure 2-2. Extent and Depth to the Salinas Valley Aquitard in Model Study Area

The FO-SVA is present beneath the Dune Sands Aquifer in the west-southwest portion of the model study area. The FO-SVA is composed of laterally extensive blue or yellow sandy clay layers with minor interbedded sand lenses (Harding ESE, 2001; DWR, 2003). The FO-SVA generally correlates to the Pleistocene Older Alluvium stratigraphic unit, which is shown as Valley Fill on Figure 2-1. The FO-SVA was deposited in a shallow sea during a period of relatively high sea level. Harding ESE (2001) noted that the FO-SVA beneath the former Fort Ord might have formed under a different depositional event than the SVA unit beneath the Salinas Valley (e.g., estuarine deposits vs. flood plain deposits). However, the 2 clay units are hydraulically equivalent (Harding ESE, 2001). The FO-SVA is generally encountered at depths of less than 150 feet. This clay layer is relatively continuous in the study area, it is not monolithic across the northwest portion of the study area. The FO-SVA thins westward from the City of Marina vicinity toward the west-southwest of the study area, as well as toward the coast, where it appears to pinch out near Highway 1 (Harding ESE, 2001). The thinning and pinching out of the FO-SVA in these locations may increase the vertical hydraulic connection between the Dune Sand Aquifer and underlying 180-Foot Aquifer.

2.2.1.3 180-Foot Aquifer

The SVA overlies and confines the 180-Foot Aquifer. The 180-Foot Aquifer is the shallowest laterally extensive aquifer in the 180/400-Foot Aquifer Subbasin and within the study area. This aquifer—from 50 to 150 feet thick—consists of interconnected sand and gravel beds. The sand and gravel layers are interlayered with clay lenses. This aquifer correlates to the Older Alluvium or upper Aromas Sand formations (Harding ESE, 2001; Kennedy/Jenks, 2004). The 180-Foot Aquifer is exposed on the floor of the Monterey Bay (Todd Engineers, 1989).

In a portion of the former Fort Ord, south of the City of Marina, the 180-Foot Aquifer is separated into an upper zone of sandy deposits with some gravel and a lower zone of gravel with sand and clay lenses; the 2 zones are separated by a thin clay layer (Ahtna Engineering, 2013). Data collected within the former Fort Ord show that significant head differences exist between the upper and lower zones of the 180-Foot Aquifer.

The primary uses of the 180-Foot Aquifer are domestic, irrigation, and municipal water supply.

2.2.1.4 180/400-Foot Aquitard

The base of the 180-Foot Aquifer is an aquitard consisting of interlayered clay and sand lenses, including a marine blue clay similar to the SVA (DWR, 2003). This aquitard is known as the 180/400-Foot Aquitard. It is widespread in the center of the study area but varies in thickness and quality, and areas of hydrologic connection between the 400-Foot and 180-Foot Aquifers are known to exist (Kennedy/Jenks, 2004). In areas where the 180/400-Foot Aquitard is thin or

discontinuous, intruded seawater in the 180-Foot Aquifer can migrate downward into the 400-Foot Aquifer in response to pumping (Kennedy/Jenks, 2004).

2.2.1.5 400-Foot Aquifer

The 180/400-Foot Aquitard overlies and confines the 400-Foot Aquifer. The 400-Foot Aquifer comprises sand and gravel beds with varying degrees of interbedded clay lenses. It is usually encountered between 270 and 470 feet below ground surface. This aquifer correlates to the lower Aromas Red Sands and the upper part of the Paso Robles Formation due to its geologic composition (Yates, 2005).

Near the City of Salinas, the 400-Foot Aquifer is a single permeable bed approximately 200 feet thick; but in other areas the aquifer is split into multiple permeable zones by clay lenses (DWR, 1973). The upper portion of the 400-Foot Aquifer merges and interfingers with the 180-Foot Aquifer in some areas where the 180/400-Foot Aquitard is missing (DWR, 1973).

Recharge to this aquifer likely occurs from both the overlying 180-Foot Aquifer and outcrops of the Aromas Sand and Paso Robles Formations in and near the Corral de Tierra Area. Within the model study area groundwater flow direction in the 400-Foot Aquifer is greatly influenced by groundwater pumping.

The primary uses of the 400-Foot Aquifer are domestic, irrigation, and municipal water supply.

2.2.1.6 400-Foot/Deep Aquitard

The base of the 400-Foot Aquifer is the 400-Foot/Deep Aquitard, typically encountered within the Paso Robles Formation as an area of higher clay content rather than a competent and homogenous clay layer. This aquitard can be several hundred feet thick in some areas of the Salinas Valley Basin (Kennedy/Jenks, 2004). Boring logs in the Marina-Ord Area indicate that the 400-Foot/Deep Aquitard in this area comprises a series of aquitards separating the 400-Foot Aquifer from the Deep Aquifers. There is currently no published analysis of the spatial occurrence or geologic composition of the 400-Foot/Deep Aquitard beyond the provisional SVIHM and the North Marina Groundwater Model.

2.2.1.7 Deep Aquifers

The 400-Foot/Deep Aquitard overlies and confines the Deep Aquifers. The Deep Aquifers, historically referred to as the 800-Foot, 900-Foot, 1,100-Foot, and 1,500-Foot Aquifers, may be up to 900 feet thick and have alternating sandy-gravel layers and clay layers which do not differentiate into distinct aquifer and aquitard units (DWR, 2003). The Deep Aquifers have also historically referred to all the water-bearing sediments beneath the 400-Foot Aquifer. The Deep Aquifers comprise the middle and lower portions of the Paso Robles Formation, the Purisima

Formation, and the Santa Margarita Sandstone (Hanson, *et al.*, 2002; Yates, 2005). The Deep Aquifers are also likely laterally connected to other aquifers that are not overlain by the 400-Foot/Deep Aquitard, such as the Santa Margarita aquifer in the Seaside area (Yates, 2005). The base of the Deep Aquifers is the contact with the low permeability Monterey Formation, which is considered the bottom of the productive areas in the Basin. While the Deep Aquifers are relatively poorly studied, some well owners have indicated that there are different portions of the Deep Aquifers with different water qualities.

The recharge mechanisms for the Deep Aquifers are not well known. There is likely some recharge from overlying aquifers, in response to downward vertical gradients (Thorup, 1976; Feeney and Rosenberg, 2003). Additional recharge may come from outcrops of Santa Margarita Sandstone or Paso Robles Formation in the Corral de Tierra Area. There may also be lateral inflow from the Basin Fill Aquifer that defines the remainder of the Salinas Valley Basin as well. There are no known recharge mechanisms or pathways for the Purisima Formation other than from leakage from overlying aquifers, and there are no surficial outcrops of the Purisima Formation in the Basin (Feeney and Rosenberg, 2003). Age dating of groundwater by the USGS indicates that groundwater in the Deep Aquifers near the Monterey Coast may be 25,000 to 30,000 years old (Hanson, *et al.*, 2002). The Deep Aquifers are used primarily for irrigation and municipal water supply.

The estimated lateral extents of all aquitard layers in the model study area are shown on Figure 2-3. It is possible that some of the aquitards extend past the model study area boundary. The confining nature of each aquitard differs between aquitards, with the SVA being one of the more confining and most easily recognizable. The deeper confining units are less discernable as distinct features, with the 400-Foot/Deep Aquitard being more a zone of higher clay content than a contiguous clay lens. The extent of Seaside Clay and the clay within Elkhorn Slough are uncertain as well.

2.2.2 Hydrostratigraphy Along Study Area Margins

The hydrostratigraphy near the margins of the Study Area represent structural and depositional transitions from the Basin margins to the main center of the Basin. This means the hydrostratigraphic descriptions above do not fully represent these key areas. Study Area margins refer to the areas outside the color-shaded areas shown on Figure 2-3. The hydrostratigraphy in these areas are generally described below, and in greater detail in draft Groundwater Sustainability Plans (GSPs) for each subbasin within the study area. The geologic formations that comprise portions of known aquifers in the center of the Study Area, also comprise portions of the water-bearing zones in the margins of the Study Area as well. There is likely hydraulic connectivity between the margins and the central portion of the Study area, contributing to recharge for the principal aquifers of the Study area. The margins' hydrostratigraphy is described below.

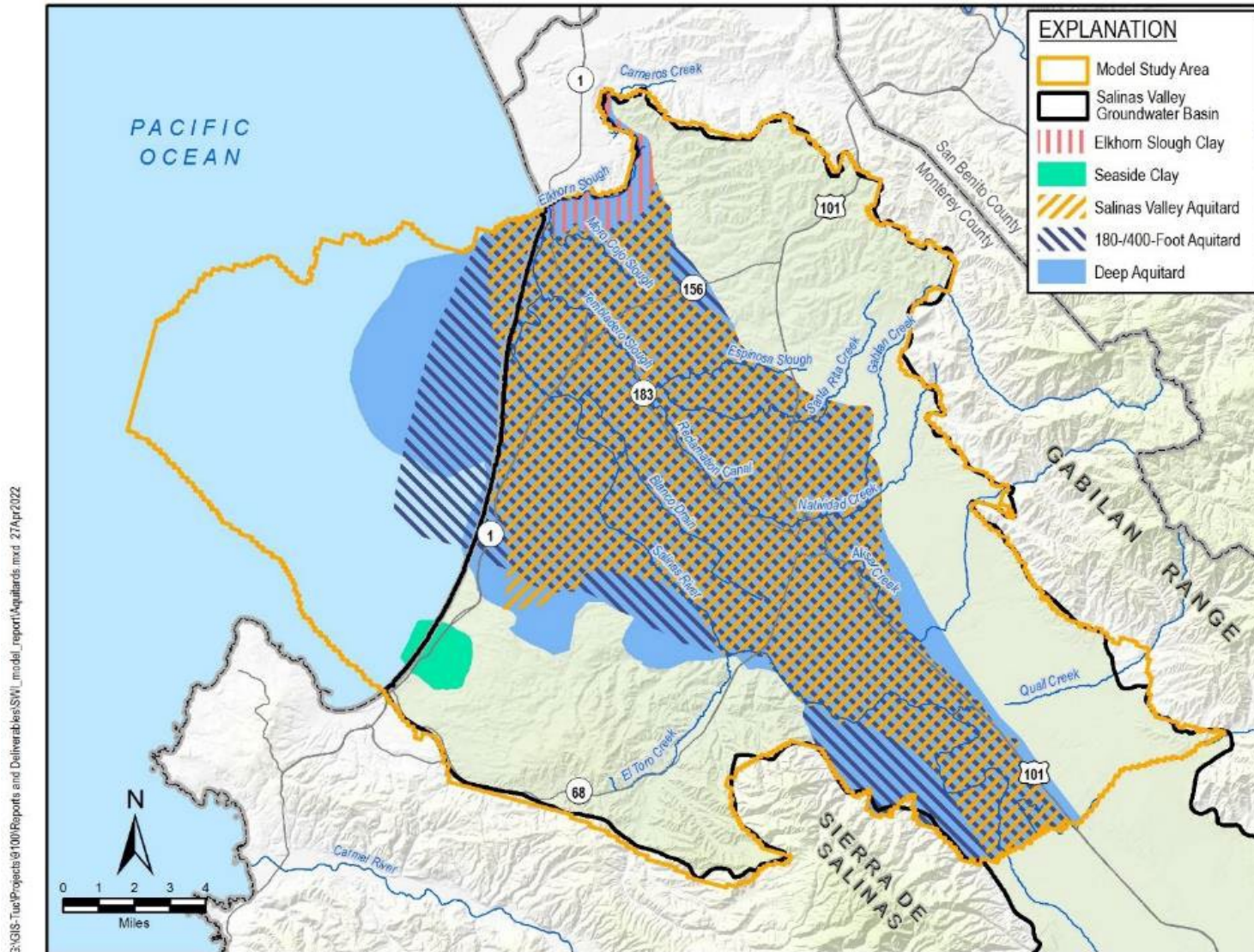


Figure 2-3. Extent of Aquitard Layers in the Model Study Area

Southwestern Margins

In the southwest region of the study area, near the City of Seaside and near the Corral de Tierra area, the hydrostratigraphy consists of the Dune Sands, the Paso Robles Formation, and the Santa Margarita Sandstone. The Paso Robles Formation and Santa Margarita Sandstone are typically designated shallow and deep, respectively, in the Seaside well names. Portions of the Paso Robles Formation may be laterally continuous with the 400-Foot Aquifer and the Deep Aquifers as it forms portions of both the 400-Foot Aquifer and Deep Aquifers elsewhere in the study area.

In the Corral de Tierra Area, many wells are screened across both the Paso Robles Formation and the Santa Margarita Formation formations, and groundwater management plans have grouped these 2 formations into the El Toro Primary Aquifer System for this area. This area is included in the Study Area due to the recorded hydraulic connectivity with the Laguna Seca area to the northwest, and presumed hydraulic connectivity with the 180/400-Foot Aquifers to the northeast where Toro Creek meets the Salinas River. Hydraulic connectivity from the Corral de Tierra area through former Fort Ord towards Marina is less well known, and may be impacted by structural changes mapped through this area.

Eastern Margins

Two generalized water-bearing zones have been recognized within the alluvial fan aquifer system in the eastern portion of the study area: the Eastside Shallow Zone and the Eastside Deep Zone. Many wells are screened across both zones and are sometimes named Eastside Both. While the designations of Deep and Shallow have been useful for geologic investigations into the morphology of the area, they are not identified as distinct aquifers by most investigators because there is no continuous aquitard separating them.

The single aquifer in the eastern portion of the study area appears to be somewhat hydraulically connected to the 180- and 400-Foot Aquifers in the center of the basin, despite noted facies changes discussed in the 2004 *Final Report, Hydrostratigraphic Analysis of the Northern Salinas Valley*, (Kennedy/Jenks, 2004). This connectivity is partially evidenced by the eastwardly decreasing groundwater elevations near Salinas (Brown and Caldwell, 2017). However, this area has an abundance of clay in the subsurface, which may limit hydraulic connectivity between the 2 depositional environments that generally define the subbasins.

Northern Margins

In the northern portion of the study area, groundwater can be found throughout most of the Aromas Red Sands and the fractured granite underneath. Water is generally drawn from the single, unconfined aquifer comprising unconfined sands and gravels that characterize the Aromas Red Sands, with a few wells also drawing from the fractured granite. There is no significant and

laterally extensive aquitard separating the Aromas Red Sands from fractured granite, indicating potential hydraulic connection. The fractured granite is not a source of abundant water supply, as fracture systems are largely unreliable zone of production. Additionally, this area shallows quickly towards the Gabilan Range, which is a granitic mountain that forms an impervious boundary with the Basin. While there may be some water in the fractured granite, and this may be connected to the Aromas Sands above, it should not be viewed as a reliable or plentiful source of groundwater.

The Aromas Red Sands also forms portions of the 400-Foot Aquifer in the center of the study area (DWR, 2004a), and therefore this northeastern single aquifer in the Study Area appears to be hydraulically connected to the 180- and 400-Foot Aquifers in the study area center.

2.2.3 Hydrogeologic Model

A continuous 3D, volumetric representation of the hydrostratigraphic framework for the study area was prepared using the geologic modeling software Leapfrog® Geo, developed by Seequent. The Leapfrog geologic model is based on aquifer layering from 2 previously developed, overlapping groundwater models. One model is the SVIHM, developed by the USGS. It is a coarsely detailed regional model that covers the entire Salinas Valley Groundwater Basin. The second model is the Monterey Subbasin Groundwater Flow Model, developed by EKI Environment & Water. It is a finely detailed model of the Monterey Subbasin and some area to the north. A third model, the Seaside Watermaster Model, developed by Hydrometrics WRI, was also considered but was not used because its layers are defined by geologic formations, which do not align with the hydrogeologic units (HGUs) used by the other 2 models.

Like the provisional SVIHM on which it is based, the Leapfrog geologic model has 9 layers representing 9 HGUs. Figure 2-4 shows the HGUs in cross section. In order from youngest (Layer 1) to oldest (Layer 9), the HGUs are: Shallow Sediments, SVA, 180-Foot Aquifer, Middle Aquitard, 400-Foot Aquifer, Deep Aquitard, Paso Robles Formation, Purisima Formation, and Monterey Formation. Layer 9 may also include units that are older than the Monterey Formation.

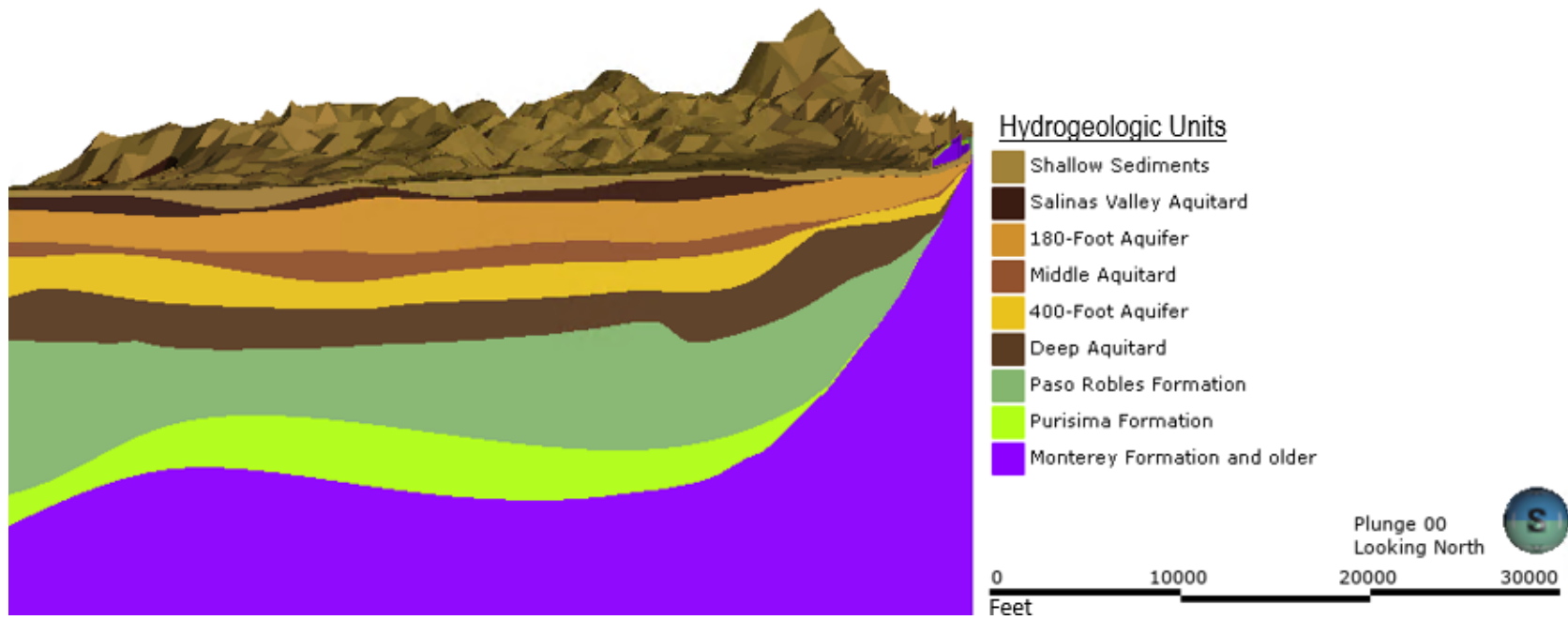


Figure 2-4. Example Cross Section Showing the 9 Model Layers in the Hydrogeologic Model.

Where the 2 input models overlap, the aquifer layering represented in the Monterey Subbasin Model is generally preferred over the provisional SVIHM in the Monterey Subbasin, since it was developed for the GSP with more data and calibration points than the provisional SVIHM. However, the Monterey model does not subdivide the Deep Aquifer into the Paso Robles and Purisima Formations like the provisional SVIHM does. Therefore, where the 2 models overlap, the Monterey Model was used for layers 2 through 6 and the provisional SVIHM was used for layers 7 through 9. The top of Layer 1 comes from a 30-meter digital elevation model of the Earth's surface.

The contacts between Leapfrog layers were adjusted up or down based on 48 georeferenced cross sections from 10 publications. Where there were discrepancies between intersecting or closely spaced cross sections, more weight was given to cross sections that showed boreholes with detailed lithology close to the area of interest.

2.3 Occurrence and Movement of Groundwater

Prior to any anthropomorphic stresses on the groundwater system, natural groundwater flow is believed to have generally followed topography. Flow would have been from the upland areas towards the center of the basin and the Salinas River. From the center of the basin, flow would be to the northwest along the axis of the valley and discharge into Monterey Bay. This is assumed to be the case with all confined and unconfined aquifers within the basin, based on the assumption that the confined aquifers are recharged along the basin boundaries and discharge into Monterey Bay.

As anthropomorphic stresses were introduced in the Salinas Valley Basin, this natural flow field changed. Agricultural practices and municipal pumping introduced changes to surficial recharge and to the hydraulic gradients across the basin. Pumping within the model study area has had a profound impact on water levels creating water level depressions in both the 180-Foot Aquifer and the 400-Foot Aquifer, resulting in water levels more than 100 feet below msl (Figure 1-3 and Figure 1-4). The water level depressions modify the hydraulic gradients within the subsurface inducing groundwater flow toward the low points. These cones of depression below sea level induce landward migration of seawater, causing the seawater intrusion observed along the coast.

2.3.1 Groundwater Level Trends and Contours

MCWRA annually produces groundwater elevation contour maps for the Basin using data collected from their annual August trough and fall measurement programs. In general, the August water level contours represent the annual low groundwater levels, and the Fall measurements represent average groundwater levels in the Salinas Valley. In August, increased agricultural pumping lowers groundwater levels. Seawater intrusion likely advances at the fastest rate during this time. Groundwater contours for Fall 2020 for the 180-Foot and 400-Foot Aquifers are shown on Figure 1-3 and Figure 1-4, respectively.

The 180-Foot and 400-Foot Aquifers do not extend across the full model study area. However, aquifers along the valley margins are hydraulically connected to these aquifers. Groundwater elevation contours from multiple data sources were combined and adapted to provide coverage over the full basin. These contours are used to help guide model calibration. Table 2-1 lists the hydrostratigraphic units and the data sources for each set of contours.

Table 2-1. Hydrostratigraphic Units and Data Sources for Groundwater Level Contours.

Region	180-Foot and Connected Aquifers	400-Foot and Connected Aquifers
Valley Center	180-Foot Aquifer – developed by MCWRA	400-Foot Aquifer – developed by MCWRA
Northeastern Margin	Unconsolidated deposits – developed by M&A	No data available for hydraulically connected aquifers
Marina Ord Area	Upper 180-Foot Aquifer – Developed by MCWD GSA	Lower 180-Foot and 400-Foot Aquifer - Developed by MCWD GSA
Corral de Tierra Area	No Hydraulically connected aquifer	El Toro Primary Aquifer System – Developed by M&A
Southwestern Margin	No contours available for hydraulically connected aquifers	Paso Robles Formation - Seaside Watermaster

Groundwater generally flows from the south and from adjacent basins toward the north-northwest, with localized depressions around pumping centers, such as northwest of the City of Salinas. The contours indicate that groundwater flow directions are similar in the 180-Foot and 400-Foot Aquifers. However, based on these contours, groundwater elevations in the 400-Foot Aquifer are generally lower than groundwater elevations in the 180-Foot Aquifer, indicating a downward vertical hydraulic gradient between these aquifers.

Groundwater elevations in the center of the study area, except for the south and southwest areas, are mostly below sea level, as indicated by the negative values on the contour lines. The lowest groundwater elevations in the study area occur north of the City of Salinas. The horizontal hydraulic gradients differ throughout the subbasin and are difficult to quantify based on variable groundwater elevations. Groundwater elevations in the study area increase to the west toward Monterey Bay. They also increase to the south toward the upper portions of the Basin, and southwest toward the City of Marina and Monterey. Groundwater level data and contours are described in detail for each Subbasin in draft GSPs and Annual Reports submitted to the DWR.

The primary aquifer in the Langley area, located near the northeastern study area margin, is characterized by unconfined sands and gravels. Water levels in this area are distinctly different from other parts of the study area but are most closely aligned with elevations found in the 180-Foot Aquifer. While some evidence suggests that the Langley area is hydraulically

connected to the 180-Foot Aquifer, data is limited and variable, and the extent of connection is uncertain. In general, groundwater in the Langley area flows from the northeast to the southwest. The hydraulic gradient differs across the Langley area due to variable groundwater elevations and thus is difficult to approximate.

In the Marina Ord and Corral de Tierra areas, the Paso Robles formation is the primary shallow aquifer. This unit is hydraulically connected to the 400-Foot Aquifer. In the Marina Ord area, groundwater generally flows from the southeast to the ocean. Pumping cones of depression exist near the cities of Seaside and Marina. Complex geologic structures along the southern study area margin may create a groundwater flow divide. Further investigation of the hydraulic properties of the Laguna Seca anticline or the Ord Terrace fault is warranted to confirm the location and extent of the hydraulic barrier to flow. In the Corral de Tierra area, groundwater generally flows from the southeast towards the valley center.

As discussed above, pumping within the model study area has resulted in declining water levels. Figure 2-5 and Figure 2-6 show representative hydrographs within the 180-Foot Aquifer and the 400-Foot Aquifer. The hydrographs illustrate the historical water level changes due to pumping. In both the 180-Foot, 400-Foot, and equivalent aquifers, water levels are generally declining. However, many wells are exhibiting minimal declines. This illustrates the complex and locally variable hydrogeologic system that exists within the model study area. Additional detail on water level conditions is provided in the GSPs for each subbasin.

MCWRA does not produce groundwater elevation maps of the Deep Aquifers. Insufficient data currently exist to map flow directions and groundwater elevations in the Deep Aquifers across the entire study area. Initial analysis indicates that groundwater flow directions may be similar to overlying units; however, more data are required to confirm this observation. Representative hydrographs for the Deep Aquifers are shown on Figure 2-7. The hydrograph data generally show higher groundwater levels to the south and along the study area margins with lower groundwater elevations near the coast. This indicates that groundwater is potentially flowing towards the ocean in the deep aquifer. In general, Deep Aquifer wells tend to show less seasonal variation than wells in the 180-Foot and 400-Foot and equivalent aquifers. Water level trends are either relatively flat or declining in the deep aquifer between 1990 and 2020. The Robley Deep Well (South), located near the southern study area margin, shows the greatest decline of approximately 70 feet over the 30-year period. Both upward and downward vertical hydraulic gradients appear to occur between the Deep Aquifers and the overlying 400-Foot Aquifer.

The groundwater elevations and related trends described above are used to calibrate the seawater intrusion model. Further detail on the calibration dataset is provided in Chapter 1.

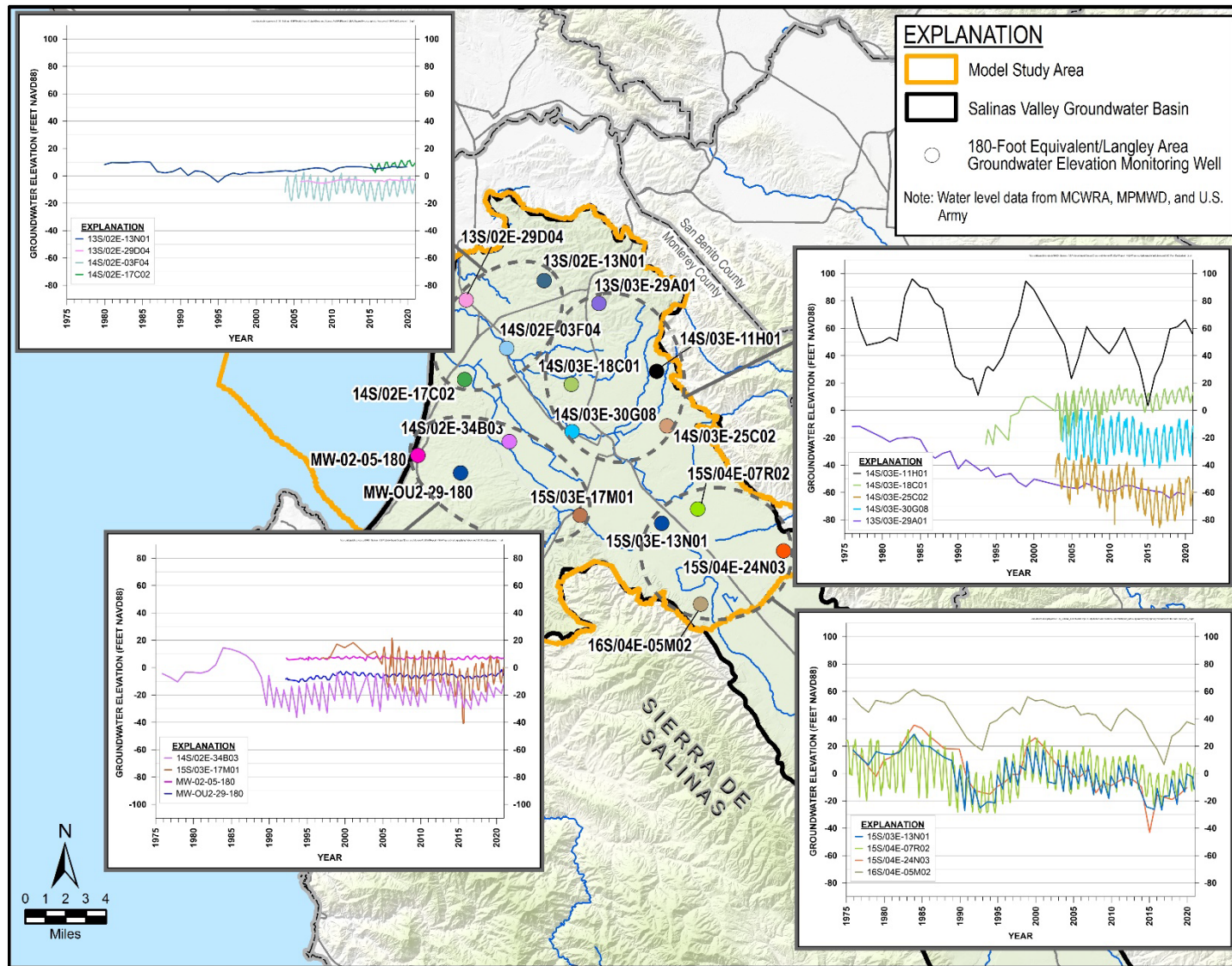


Figure 2-5. Representative Hydrographs within the 180-Foot Aquifer

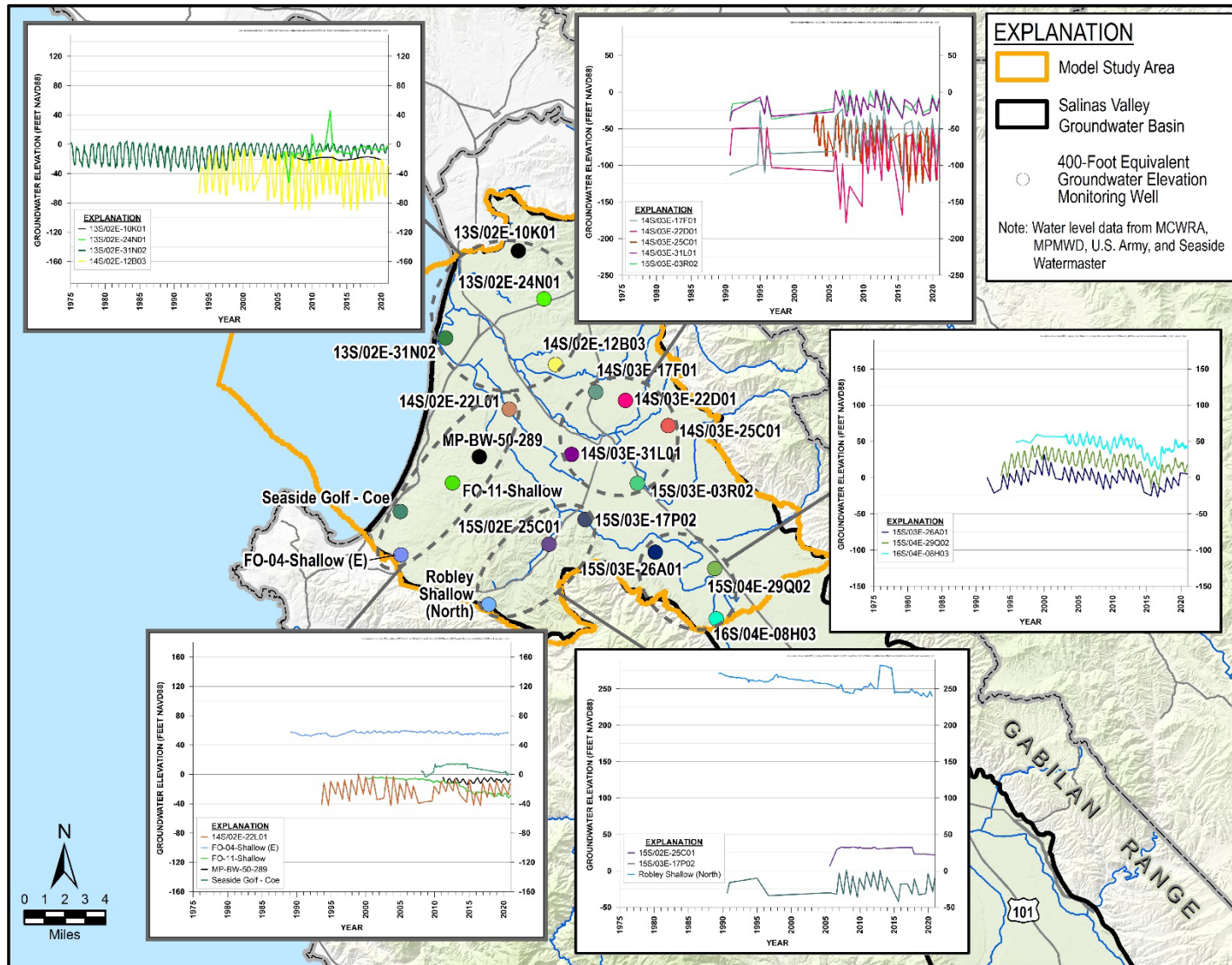


Figure 2-6. Representative Hydrographs within the 400-Foot Aquifer

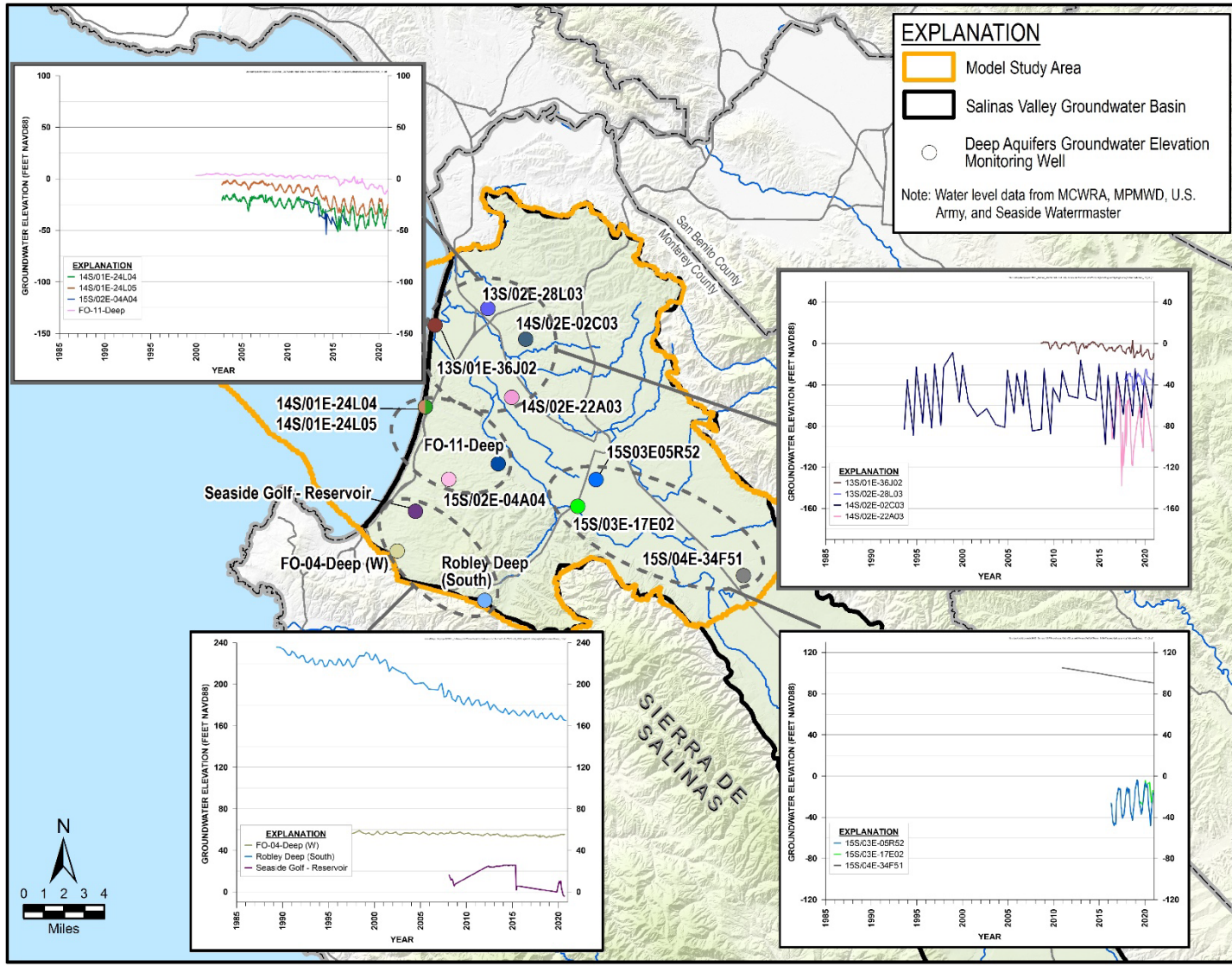


Figure 2-7. Representative Hydrographs within the Deep Aquifer.

2.3.2 Density Dependent Flow

In its simplest form, groundwater flow (Q) can be expressed as the product of the hydraulic conductivity (K) and the hydraulic gradient (i):

$$Q = Ki \quad (1)$$

The hydraulic gradient is a measure of the spatial variability of fluid pressure and is calculated as the difference in hydraulic head between 2 points divided by the distance between the 2 points. Hydraulic head (h) is the measured groundwater elevation, and is calculated from several factors through the following relationship:

$$h = \frac{P_N}{\rho_f g} + Z_N \quad (2)$$

where P_N is the fluid pressure at the measurement point (N); ρ_f is the fluid density; g is the gravitational constant; and Z_N is the elevation at the measurement point (N). Equation (2) shows that given 2 fluids with differing densities, the fluid with the larger density (ρ_f) would need higher pressure (P_N) to result in an identical head (h). Seawater is denser than freshwater, with a larger fluid density, ρ_f . Therefore, seawater exerts a higher pressure than fresh water for the same measured groundwater elevation. Without accounting for the differing fluid densities, 2 fluids with the same head would produce a zero hydraulic gradient. However, by accounting for differing densities, there is a hydraulic gradient from the denser fluid (e.g., saline or seawater fluid) to the less dense fluid (e.g., freshwater).

In the case of coastal aquifers, as found in the model study area, there is a density difference between the freshwater within the inland groundwater system and the saline water within the ocean and seaward groundwater system. This density difference is sufficient to influence groundwater flow and can induce seawater intrusion.

2.4 Chloride Distribution and Seawater Concentrations

2.4.1 Mechanism and Extent of Seawater Intrusion

Detailed characterizations of seawater intrusion in Salinas Valley can be found in multiple previous studies (Greene, 1970; DWR, 1973; Todd Engineers, 1989; Kennedy/Jenks, 2004). Three primary mechanisms driving seawater intrusion in the Valley include:

- Pumping induced cones of depressions result in landward groundwater gradients within the 180-Foot and 400-Foot Aquifers

- Inter-aquifer seawater intrusion due to the discontinuous nature of the aquitards and poorly constructed or abandoned wells
- Density differences between seawater and fresh water, as described above

Evidence for the inter-aquifer seawater intrusion due to both natural aquitard gaps and improperly constructed and abandoned wells includes the large islands of saline water appearing ahead of the seawater intrusion leading edge. This downward migration is driven by the downward head gradient between the 2 aquifers.

The mechanisms that have facilitated seawater intrusion in the 180-Foot and 400-Foot Aquifers may also pose a risk of seawater intrusion into the Deep Aquifers. The formations that comprise the Deep Aquifers are in contact with seawater in Monterey Bay. Groundwater elevations have been declining with increased extraction over time, and the aquitard that separates the 400-Foot Aquifer from the Deep Aquifers is poorly studied and understood. Additionally, some wells completed in the deeper portions of the 400-Foot Aquifer may also be in connection with the shallower portions of the Deep Aquifers.

2.4.2 Measurement and Extent of Seawater Intrusion

The seawater intrusion monitoring program by MCWRA and mapped intrusion extents are described in Section 1 and shown on Figure 1-3 and Figure 1-4. Chloride concentrations are often used as an analogue for presence of seawater in groundwater, and MCWRA uses the 500 mg/L chloride isocontour as the extent of seawater intrusion. To increase the number of measurements available for the calibration dataset, measurements of total dissolved solids (TDS) were converted to estimates of chloride concentration when TDS measurements were available and chloride were not. Figure 2-8 shows the relationship between chloride and TDS measurements in the model study area. A conversion factor of 0.571 was determined to convert between TDS and chloride concentration data.

Background groundwater concentration data was compiled from available sources and is shown on Figure 2-9. Median background chloride concentration was calculated as 55 mg/L in the model study area.

The Granite Canyon Monitoring Station, operated by the Moss Landing Marine Laboratory, measures ocean salinity in Monterey Bay. TDS was measured at 33,694 mg/L compared to global mean seawater TDS of 35,176 mg/L (Geoscience, 2014; JGOFS 1997). Applying the ratio of the Granite Canyon Monitoring Station Ocean TDS and the global mean seawater TDS ($33,694 / 35,176$) to the global mean seawater chloride concentration (19,352 mg/L) yields a seawater chloride concentration in Monterey Bay of 18,537 mg/L.

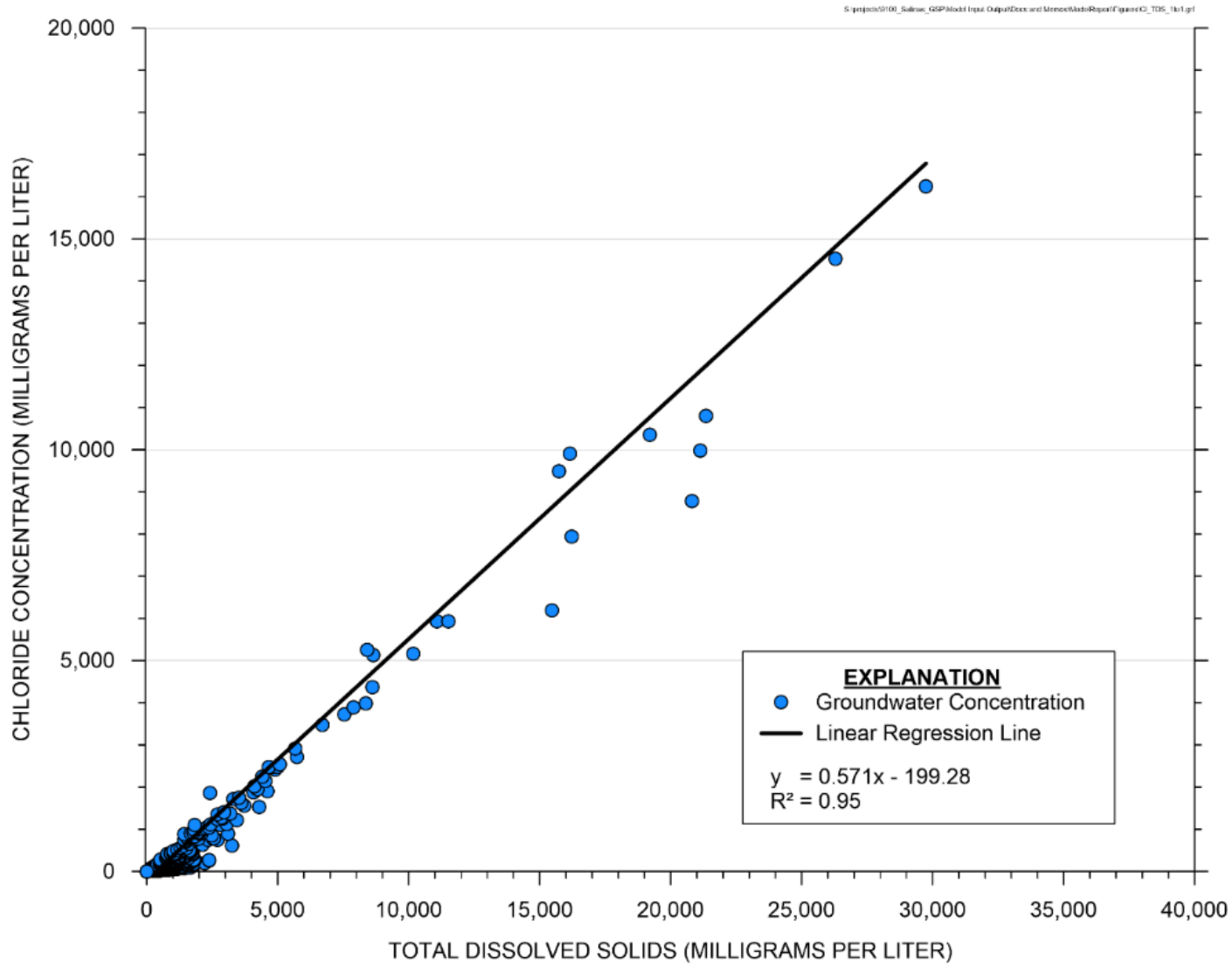


Figure 2-8. Relationship between Chloride and Total Dissolved Solids in Groundwater

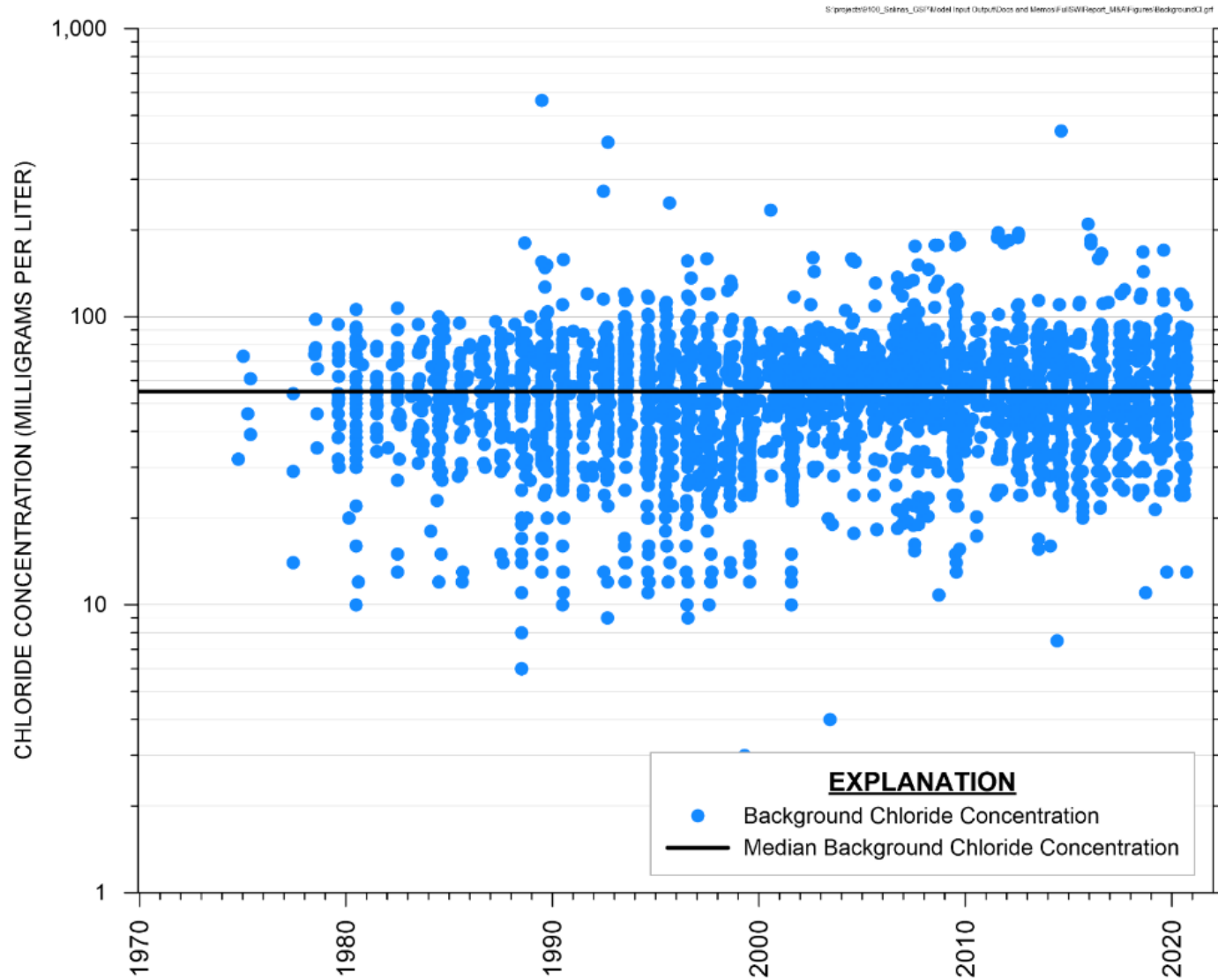


Figure 2-9. Background Chloride Concentration in Groundwater

2.5 Hydraulic Properties for Hydrogeologic Units

Aquifer properties define how groundwater is stored and how groundwater moves in the subsurface. The movement and storage of groundwater through an aquifer is dependent on the structural and geological characteristics that are then described through hydraulic parameters. The 2 general types of aquifer properties relevant to groundwater modeling are aquifer transmission properties (hydraulic conductivity) and aquifer storage properties (specific yield and specific storage). Aquifer transmission properties control the relationship between hydraulic gradients and the rate of groundwater flow. Aquifer storage properties control the relationship between the volume of groundwater stored in the aquifer and the groundwater elevations measured in the aquifer. The values and distribution of aquifer properties in the Basin have not been well characterized and documented. There is a relatively sparse amount of measured aquifer properties throughout the Basin.

Most measured hydrogeologic properties are found at well or borehole locations at the site of Former Fort Ord where cleanup activities for tetrachloroethylene and trichloroethylene have occurred. There are fewer locations northward, eastward, and southward from the Fort Ord area, and subsequently aquifer properties have been estimated through the process of numerical model calibration. Aquifer property calibration has been completed for numerous published modeling studies completed in the Basin, including studies by Durbin (1974), Yates (1988), WRIME (2003), and the provisional SVIHM developed by the USGS.

Hydraulic conductivity data were obtained from DWR, the CSIP wells, and from previous studies. Figure 2-10 shows a box and whisker plot of hydraulic conductivity measurements by aquifer. The boxes represent the first and third quartiles and the whiskers show the 2.5 and 97.5 percentiles. Individual data points are plotted to show the distribution and range of all data for each aquifer.

Hydraulic conductivity measurements vary within the same aquifer both vertically and areally. Measurements within the same aquifer can range by multiple orders of magnitude. Summary statistics of hydraulic conductivity measurements are listed in Table 2-2.

Aquifers with a lower number of hydraulic conductivity measurements show a tighter range, suggesting that the data likely do not cover the full range of actual hydraulic conductivity for that aquifer. Additionally, the data are likely skewed higher than the true average for the aquifer. The majority of the available data comes from specific capacity tests on wells that are used for municipal or agricultural pumping. These wells are purposely installed in more productive areas of the aquifer with higher hydraulic conductivities. Figure 2-11 shows the locations of hydraulic conductivity measurements by aquifer.

Estimated storage properties are lacking from the aquifer testing results which are limited to hydraulic conductivity and / or transmissivity (Figure 2-10 and Table 2-2). However, for the aquifer units, estimates of specific yield and specific storage utilized within numerical models of the area (provisional SVIHM, Monterey Subbasin Groundwater Flow Model, Seaside Watermaster Model, and the North Monterey County Groundwater Model) generally range between 0.05 to 0.30 and 0.001 to 1.0×10^{-7} feet⁻¹, respectively.

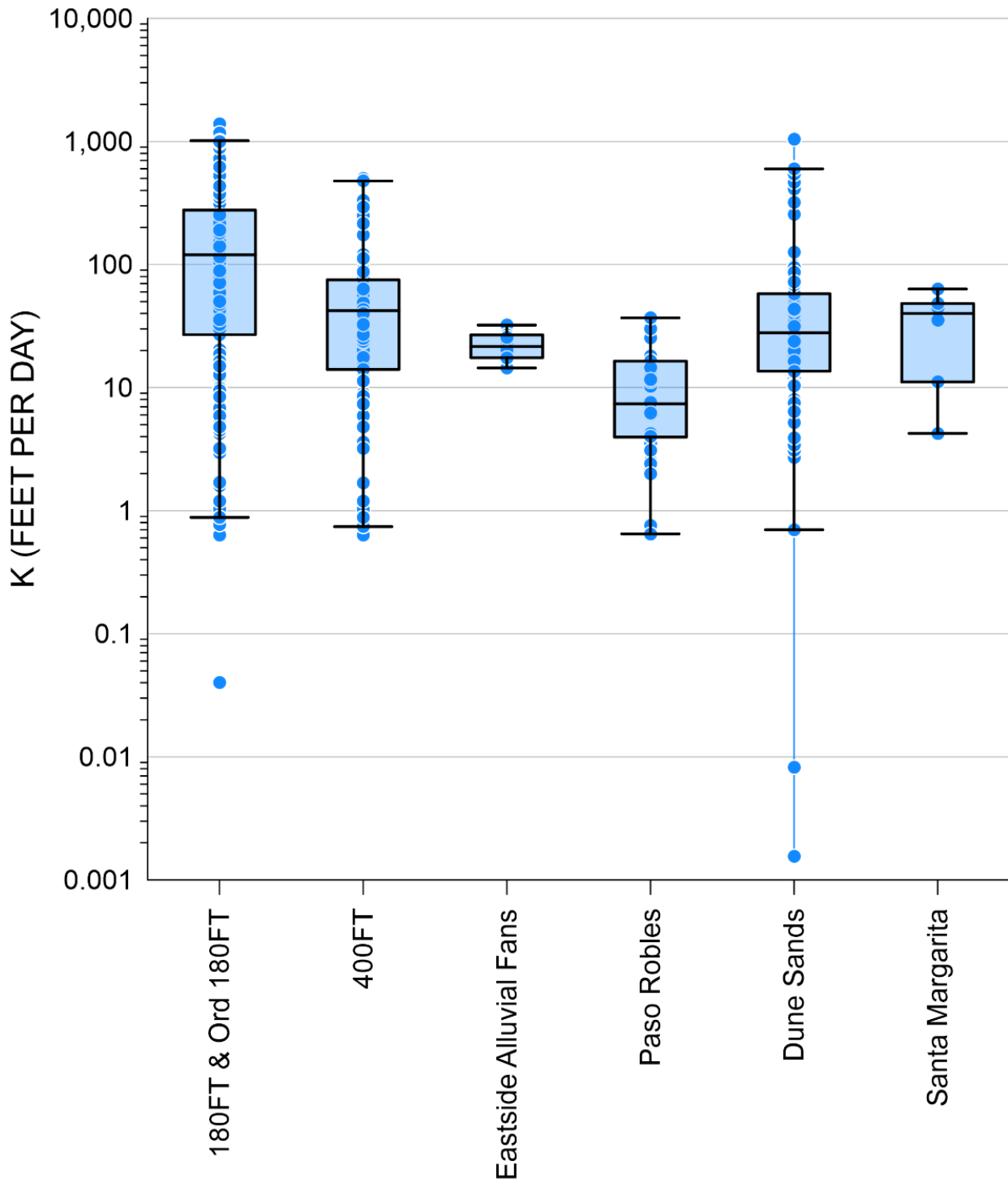
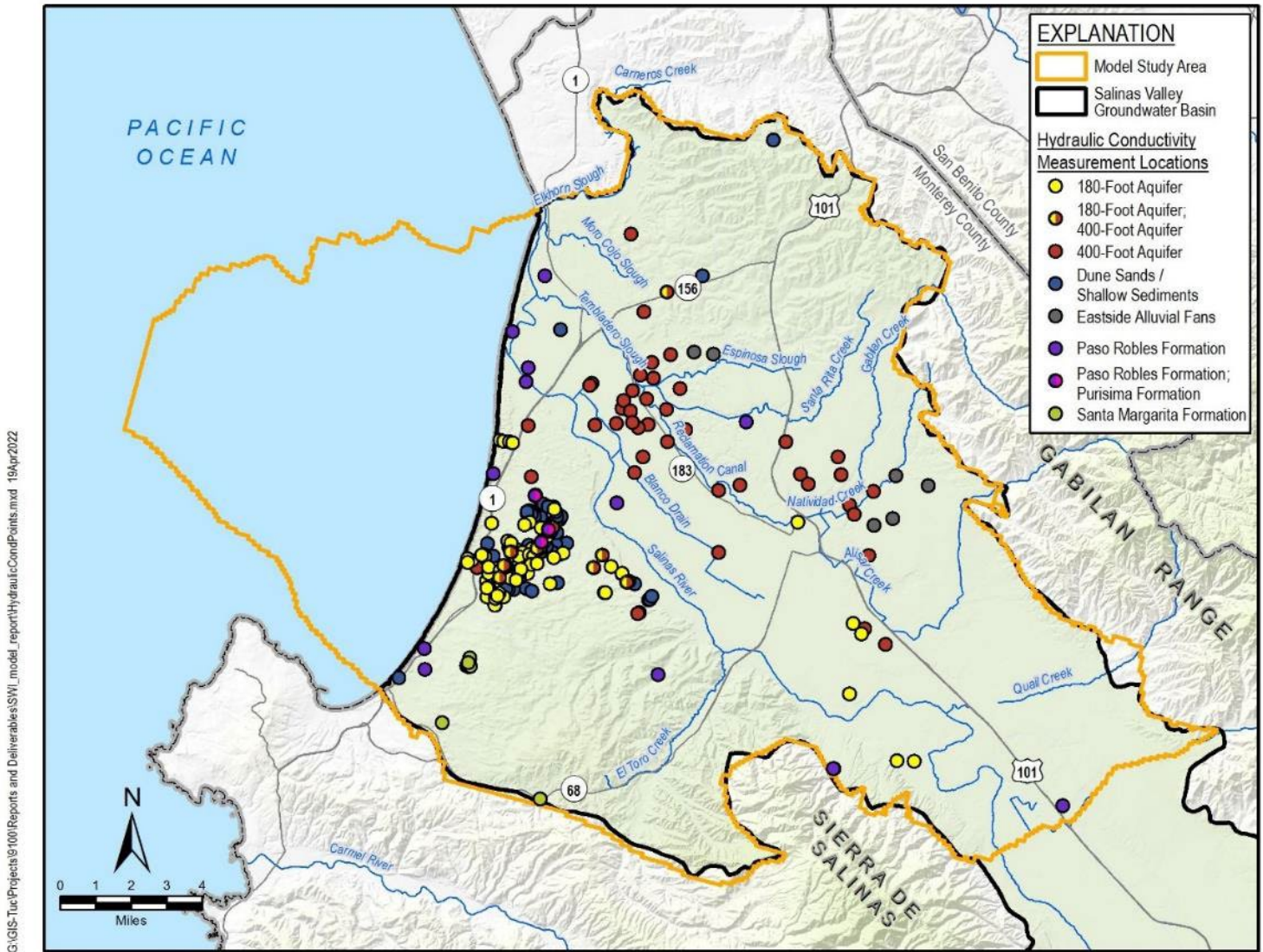


Figure 2-10. Hydraulic Conductivity Distribution by Aquifer or Geologic Formation

Table 2-2. Statistical Summary of Hydraulic Conductivity Measurements by Aquifer

Aquifer/Formation	180-Foot & Ord 180-Foot	400-Foot	Eastside Alluvial Fans	Paso Robles	Dune Sands	Santa Margarita
Maximum (ft/day)	1396.0	500.4	32.2	36.9	1047.0	63.4
Minimum (ft/day)	0.040	0.635	14.438	0.648	0.002	4.247
Arithmetic Mean (Average) (ft/day)	207.1	69.9	22.6	10.9	73.1	34.5
Geometric Mean (ft/day)	72.7	29.4	22.0	7.3	25.0	24.7
Median (ft/day)	119.8	42.2	21.6	7.4	27.9	40.0
Standard deviation (ft/day)	261.0	98.2	5.6	9.4	151.1	20.8
Number of measurements	139	74	7	34	107	6

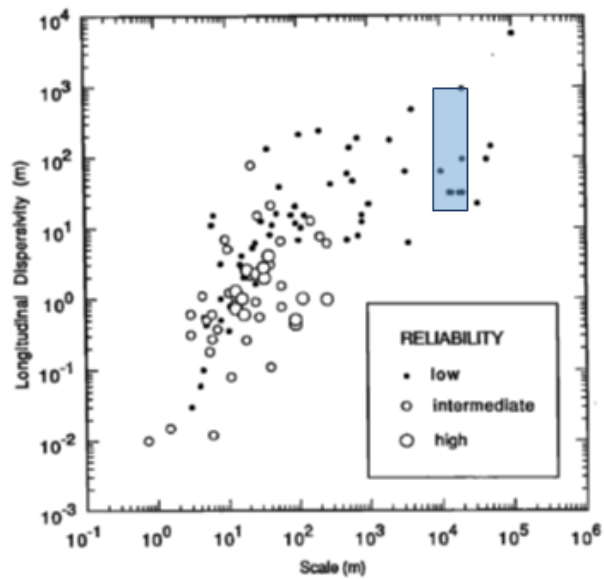


G:\GIS-Tuc\Projects\1001\Reports and Deliverables\SWI_model_report\HydraulicCondPoints.mxd 19Apr2022

Figure 2-11. Location of Hydraulic Conductivity Measurements by Aquifer

Chloride is transported by being carried along with the moving groundwater (advection), and spreads longitudinally, transversely, and vertically due to groundwater velocity variation and flow path tortuosity (dispersion). Dispersion in porous media is controlled by the dispersivity parameter. However, there is significant uncertainty in estimates of dispersivity. Figure 2-12 shows estimates of longitudinal dispersivity from a variety of study sites outside the study area prepared by Gelhar *et al.* (1992) and Xu and Eckstein (1995). Both studies show that dispersion is not a single value, but rather it increases with the extent of intrusion. In the study area, the extent of seawater intrusion is approximately 2 to 6 miles, or 3,000 to 10,000 meters. Using the correlations provided on Figure 2-12, dispersivity ranges from approximately 20 to 1,000 meters, or 65 to 3,280 feet. Both Gelhar, *et al.* (1992) and Xu and Eckstein (1995) classify estimates over this scale as having low reliability. Both the wide range in dispersivity estimates over this scale and the low reliability classification indicates significant uncertainty in dispersivity estimates. While there is a large range reported, the actual range in dispersivity within the study area is likely substantially narrower.

Gelhar et al. (1992)



Xu and Eckstein (1995)

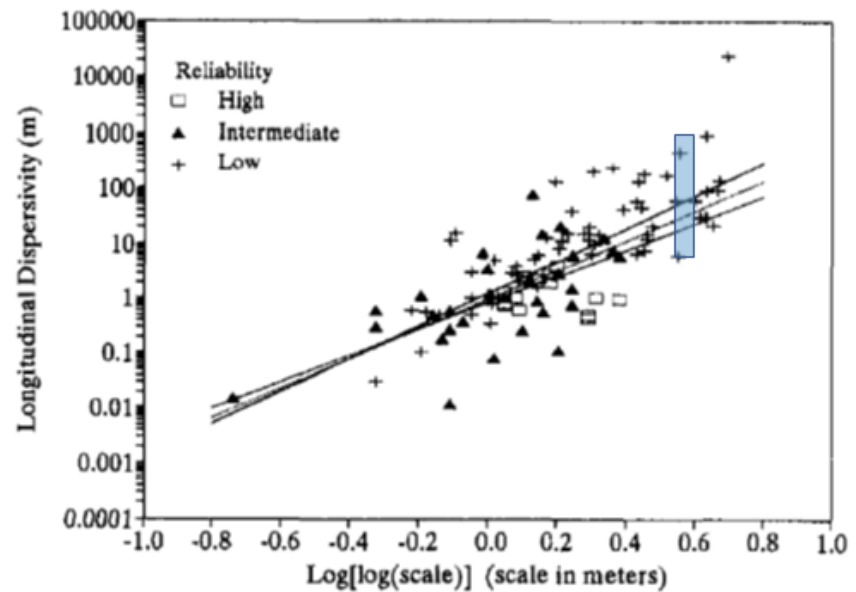


Figure 2-12. Literature Estimates of Dispersivity Versus Scale of Observation

2.6 Surface Water Features

Besides the Pacific Ocean, the primary surface water feature in the model study area is the Salinas River. This river runs the entire length of the Basin and is fed by local tributaries that drain the Sierra de Salinas and Gabilan Range (Figure 1-1). Additionally, 2 reservoirs outside of the study area control flow into the Salinas River. The Nacimiento and San Antonio reservoirs near Bradley, control the amount of water in the channel for several purposes, including:

- Flood control
- Water conservation
- Maintaining flows for recreation and ecological requirements
- Dam safety

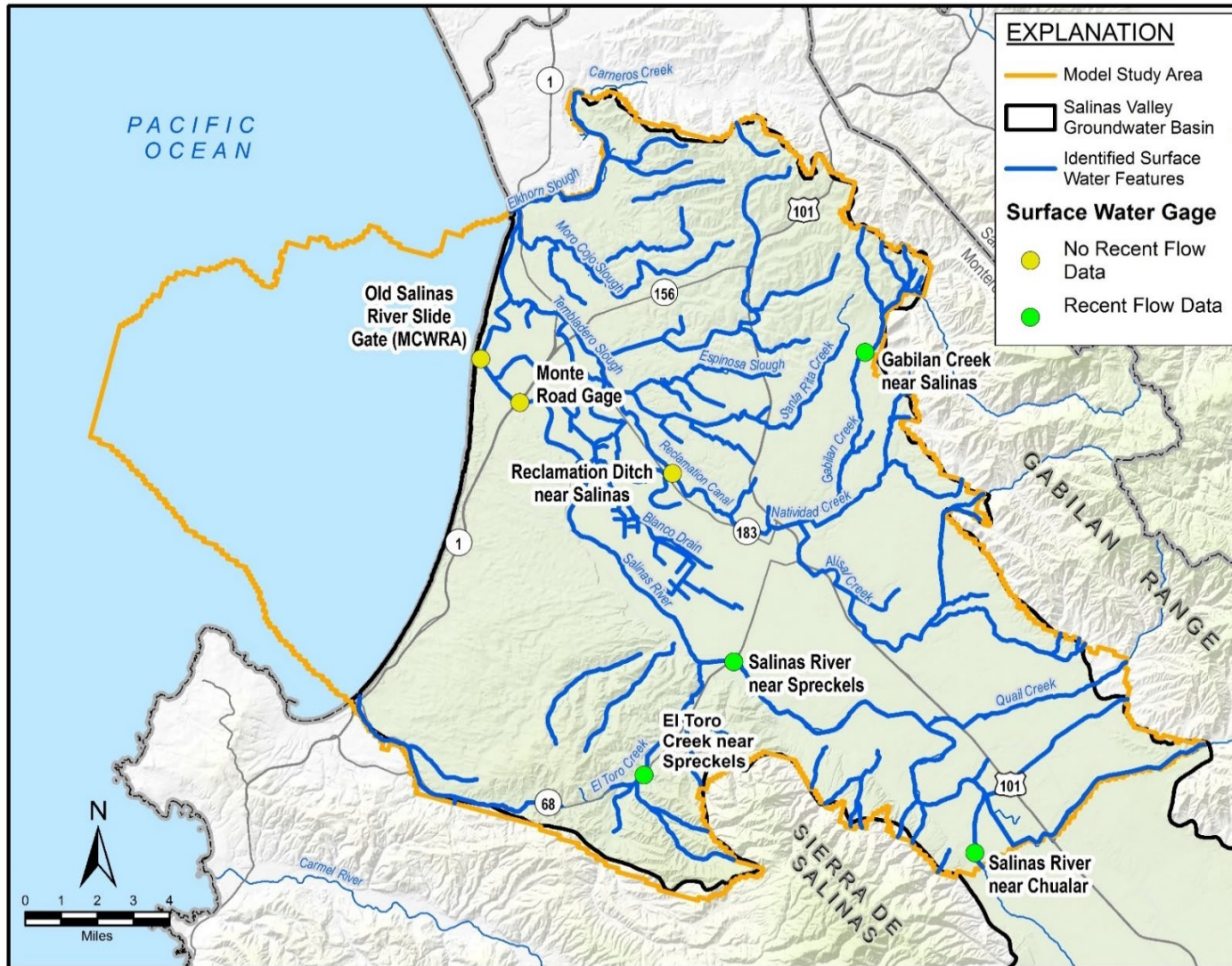
Calculated from data provided by MCWRA, the average monthly release rate between 1975 and 2018 for the San Antonio and Nacimiento reservoirs were approximately 88 and 264 cubic feet per second (cfs), respectively.

There are 4 stream gages which have recent surface water flow measurements in the study area. The Salinas River has 2 gages, one near Chualar (USGS 11152300) and one near Spreckels (USGS 11152500). Two additional stream gages are located along Gabilan Creek (USGS 11152600) and El Toro Creek (USGS 11152540). Surface water features and stream gages in the study area are shown on Figure 2-13.

Monthly surface water data at both active gages along the Salinas River are shown on Figure 2-14. Monthly data are available at the Chualar gage beginning in October 1976 and at the Spreckels gage beginning in October 1941. During periods of high surface water flow (1978, 1980, 1983, and 1998), flow at Spreckels frequently exceeds flow at Chualar. This is likely due to the addition of runoff flows from the tributaries between the gages, such as Chualar Creek and Quail Creek. However, on an average monthly basis, flow at Chualar is slightly greater, but not discernable at the scale of the graph on Figure 2-14. Table 2-3 provides statistics of monthly measured surface water flows at USGS gaging stations between water year (WY) 1975 through 2020. Multiple months for each gage have zero flow. The maximum monthly flow in each gage occurred in February 1998. Between the reservoirs and the Chualar gage, the Salinas River gains and loses water from/to groundwater. Runoff within the watershed and flows from tributaries also contribute to the flow downstream of the reservoirs. Monthly flows at the surface water gages along Gabilan Creek and El Toro Creek, which are 2 of the larger tributaries to the Salinas River in the study area, are shown on Figure 2-15.

Overall, most surface water features in the model study area lose water through streambed infiltration; however, they are largely disconnected from the principal aquifers of the Basin due to the presence of the SVA.

Water is diverted from the Salinas River at the Salinas River Diversion Facility (SRDF). Additional information on how this water is used is described in Sections 2.7.1.1 and 1.



G:\GIS-Tuc\Projects\100\Reports and Deliverables\SW_model_report\SWfeatures20230228.mxd 28Feb2023

Figure 2-13. Surface Water Features in Study Area

Table 2-3 Measured Surface Water Flows in Study Area (WY1975-2020)

Surface Water Gage	Maximum Monthly Flow February 1998 (cfs)	Average Monthly Flow (cfs)
Salinas River near Chualar (USGS 11152300)	14,350	385
Salinas River near Spreckels (USGS 11152500)	16,260	356
El Toro Creek near Spreckels (USGS 11152540)	90	2
Gabilan Creek near Salinas (USGS 11152600)	239	4

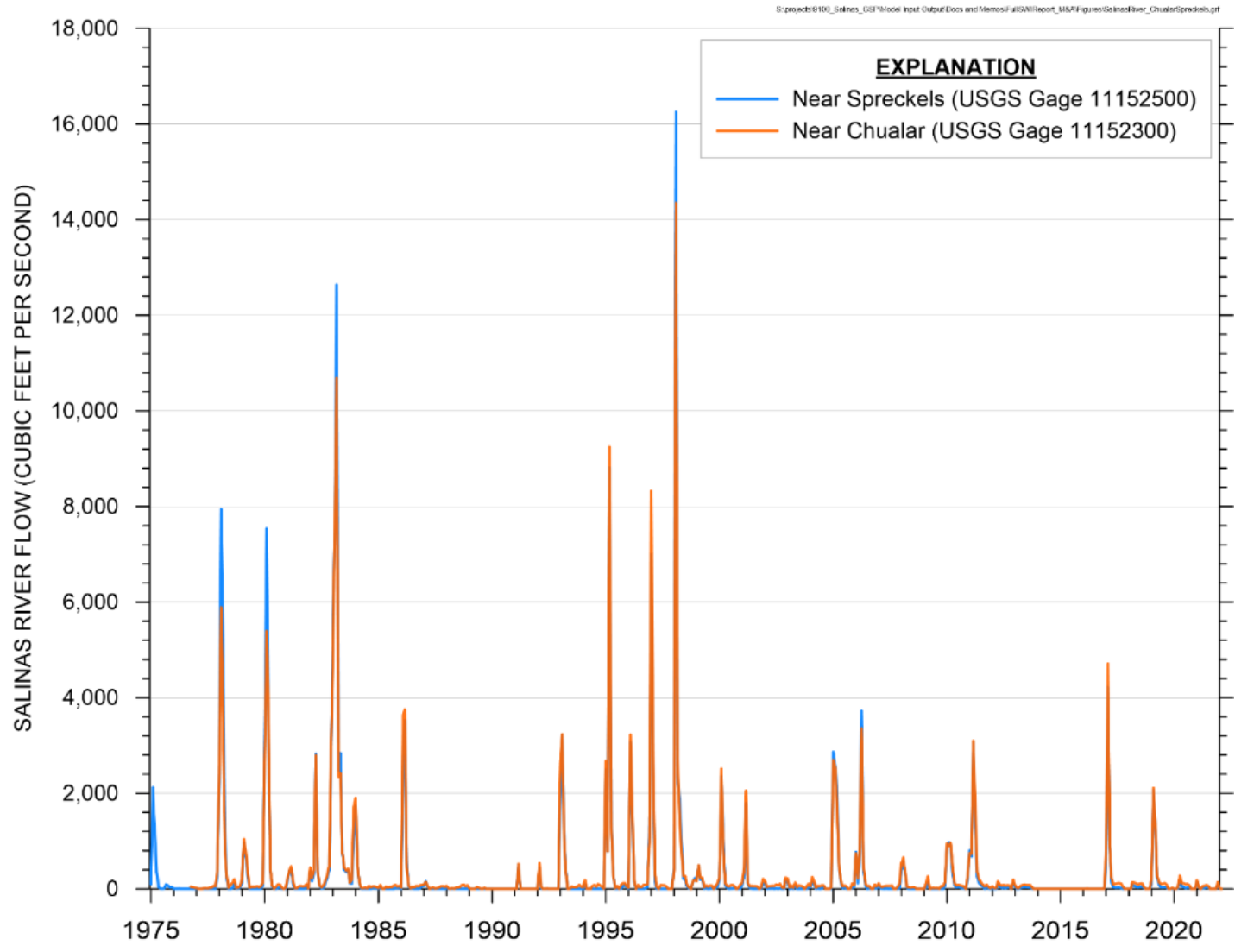


Figure 2-14. Average Monthly Surface Water Flow on the Salinas River

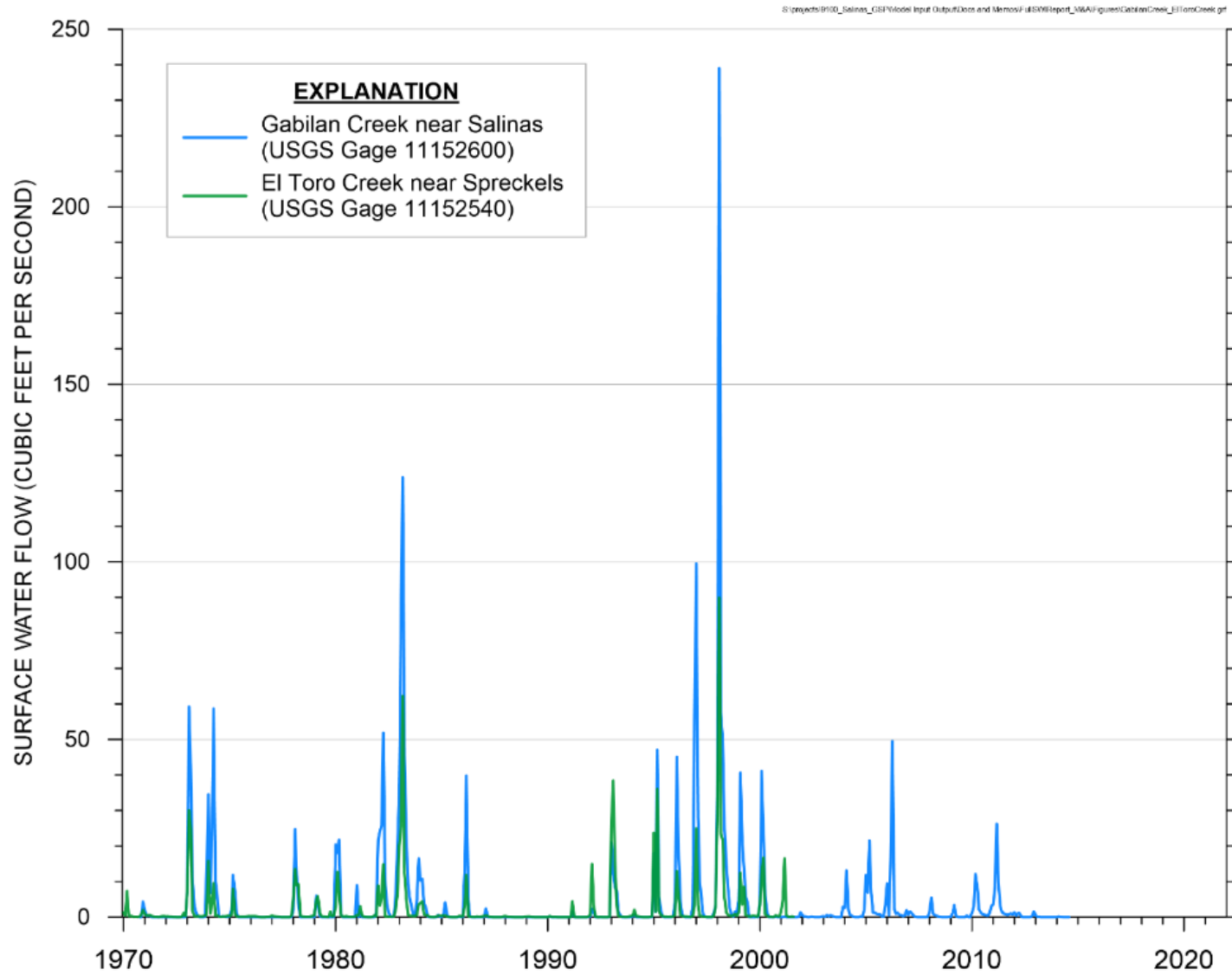


Figure 2-15. Average Monthly Surface Water Flow at Gabilan and El Toro Creek.

2.7 Groundwater Inflows and Outflows

The following section details estimates of water budget components within the study area. When reported data were not available, water budget components were estimated using previously developed tools, including other modeling studies.

2.7.1 Groundwater Inflows

Groundwater inflows to the model study area include (1) recharge including agricultural deep percolation, urban deep percolation, and deep percolation of precipitation, (2) underflow from adjacent basins, (3) underflow from the ocean, (4) injection from aquifer storage and recovery (ASR) operations, and (5) seepage from the surface water network. The latter inflow component is reported herein as the net groundwater-surface water exchange, as described in Section 2.7.1.6.

2.7.1.1 Recharge

Recharge is water that infiltrates to the groundwater via deep percolation. There are several components of recharge in the model study area, including natural recharge, rural domestic recharge, urban recharge, and irrigation return flow. Natural recharge is derived from precipitation or precipitation runoff and is assumed to apply over the entire model study area outside of urban areas. Rural domestic recharge from septic tanks is assumed to contribute a significant component to the water budget only in the Langley and Corral de Tierra areas. Urban recharge is the water that infiltrates to groundwater within urban areas. Irrigation return flow occurs beneath agricultural fields and comprises infiltration of applied irrigation water not consumed by crop evapotranspiration.

Total recharge at any given location comprises the sum of the various recharge components. Each recharge component was estimated separately and then summed to estimate recharge across the model study area as follows:

- **Deep percolation of precipitation:** To account for natural recharge from precipitation outside of urban areas, recharge rates were extracted from the USGS Basin Characterization Model (BCM) (Flint 2014). The BCM is a grid-based, water balance model that covers the entire state of California with 270-meter spatial resolution and monthly timesteps. The BCM uses maps of soils and geology and historical climate data to develop water budget components including recharge, runoff, and 16 other parameters. BCM rates were spatially averaged for the model study area. Natural recharge represents approximately 18,000 AF/yr of recharge in the model study area.
- **Leakage from urban infrastructure:** A 7% loss rate was assumed for water deliveries to cities in the model study area to account for leaks and conveyance losses from water

delivery systems and sewer systems (Santa Cruz Mid County GSA, 2022). These conveyance losses percolate to the groundwater. Figure 2-16 shows a breakdown of the percentage of urban pumping that becomes recharge to groundwater. Of total urban pumping, 7% is assumed to be lost from leakage in the initial delivery. Of the remaining 93% of urban pumping, 70% is assumed to be used for indoor use and 30% is used outdoors. An estimate of 90% of indoor use ends up in the sewer system where the same 7% loss rate was assumed to percolate as recharge as the water travels to a wastewater treatment facility. Additionally, 10% of outdoor use is assumed to return to the groundwater system as recharge. Applying these losses, a 7% loss rate in delivery and sewer systems corresponds with approximately a 14% recharge rate of urban pumping. This results in an estimated average of 3,200 AF/yr of urban recharge.

- **Rural Domestic Recharge:** Most of the Basin outside urban areas is assumed to be serviced by septic systems. However, in rural areas, return flow from septic tanks is a trivial component of recharge compared to irrigation return flow. In the northeast uplands of the Langley Area and the Corral de Tierra area, domestic water use and subsequent return flow from septic tanks constitutes a much larger proportion of the water budget than in the rest of the model study area due to limited agricultural pumping in these areas. As a result, we assumed return flow from septic tanks is a non-trivial component of the water budgets in the Langley and Corral de Tierra areas. Rural domestic recharge in these 2 areas was calculated as 70% from indoor use (deep percolation from septic tanks) and 30% from outdoor use (deep percolation of irrigated landscape). Of the outdoor use, 10% is considered to recharge to groundwater. Of the indoor use, 90% of the water is assumed to make it to the septic system and return to groundwater. Figure 2-17 shows the estimated locations of rural domestic recharge. Domestic recharge locations are based on domestic well location information from DWR's Online System for Well Completion Reports. The estimated average annual total rural domestic recharge in the model study area is approximately 600 AF/yr, which represents approximately 70% of domestic pumping. There is considerable uncertainty in any of the assumptions used to estimate domestic recharge. This conceptualization was developed with the understanding that the estimates would be adjusted during model calibration. Adjusted recharge values are discussed in Section 3.10.
- **Irrigation Return Flow:** Values for monthly On-Farm Efficiency (OFE), or the percentage of applied irrigation water that is consumed by crop evapotranspiration, were extracted from the provisional SVIHM and averaged into 2 seasons: summer and winter. The summer season is April through October, and the winter season is November through March. Figure 2-18 shows the provisional SVIHM irrigated areas where different OFE values were applied. Table 2-4 lists the summer season and winter season OFE for each

irrigated area. All recharge areas shown on Figure 2-18 are irrigated, at least partly, using groundwater. Agricultural recharge is calculated as:

$$\text{Volume of applied water} \times (1 - OFE)$$

OFE values across the model study area indicate that approximately 30% of applied water becomes irrigation return flow.

A portion of irrigation return flow is derived from non-groundwater sources. To reduce the amount of groundwater pumped, and thus reduce seawater intrusion, coastal farmland surrounding Castroville receives a combination of recycled water, groundwater, and surface water through the CSIP. Surface water diversions provide water to agriculture, and additional surface water is diverted through a pneumatic diversion dam known as the SRDF. This dam is located on the Salinas River near Marina. The SRDF diverts water from the river to the CSIP distribution system to offset groundwater pumping. MCWRA maintains records of CSIP deliveries that range from approximately 9,300 to 20,700 AF/yr between 1999 and 2020. The CSIP area has an estimated OFE of 75% (Figure 2-18). Using this OFE, CSIP deliveries contribute between 2,300 and 5,200 AF/yr of recharge with an average recharge rate of approximately 3,500 AF/yr.

On average, OFEs applied to Groundwater Extraction Management System (GEMS) agricultural pumping and reported CSIP deliveries indicate approximately 45,200 AF/yr of irrigation return flow each year across the model study area.

Table 2-4. Seasonal On-Farm Efficiencies by Irrigated Area

Irrigated Area	Summer On-Farm Efficiency	Winter On-Farm Efficiency
CSIP Area	75%	75%
Highlands South	89%	0%
Granite Ridge	89%	0%
Corral De Tierra	85%	75%
Blanco Drain Area	75%	75%
East Side	85%	76%
Pressure Northeast	75%	70%
Pressure Southwest	72%	70%
Southwest Region	85%	0%

Note: Values are from the provisional SVIHM.

Table 2-5 summarizes recharge by category for each WY from 1975 through 2020. On average, irrigation return flow is the largest component of recharge. However, in particularly wet years, such as 1998, deep percolation of precipitation can be the dominant component of recharge in the model study area. BCM estimates of deep percolation of precipitation can vary over multiple

orders of magnitude year to year. Rural domestic and urban recharge make up a comparatively small percentage of recharge.

Table 2-5. Estimated Total Annual Recharge in Study Area

Annual Recharge (AF/yr)	Irrigation Return Flow	Deep Percolation of Precipitation	Rural Domestic	Leakage from Urban Infrastructure	Total
Minimum (<i>Year</i>)	24,400 (<i>1998</i>)	3 (<i>2012</i>)	500 (<i>1975</i>)	1,100 (<i>2016</i>)	34,900 (<i>2012</i>)
Maximum (<i>Year</i>)	73,400 (<i>1992</i>)	166,500 (<i>1998</i>)	700 (<i>2020</i>)	6,600 (<i>1994</i>)	193,200 (<i>1998</i>)
Average	45,200	18,000	600	3,200	67,300

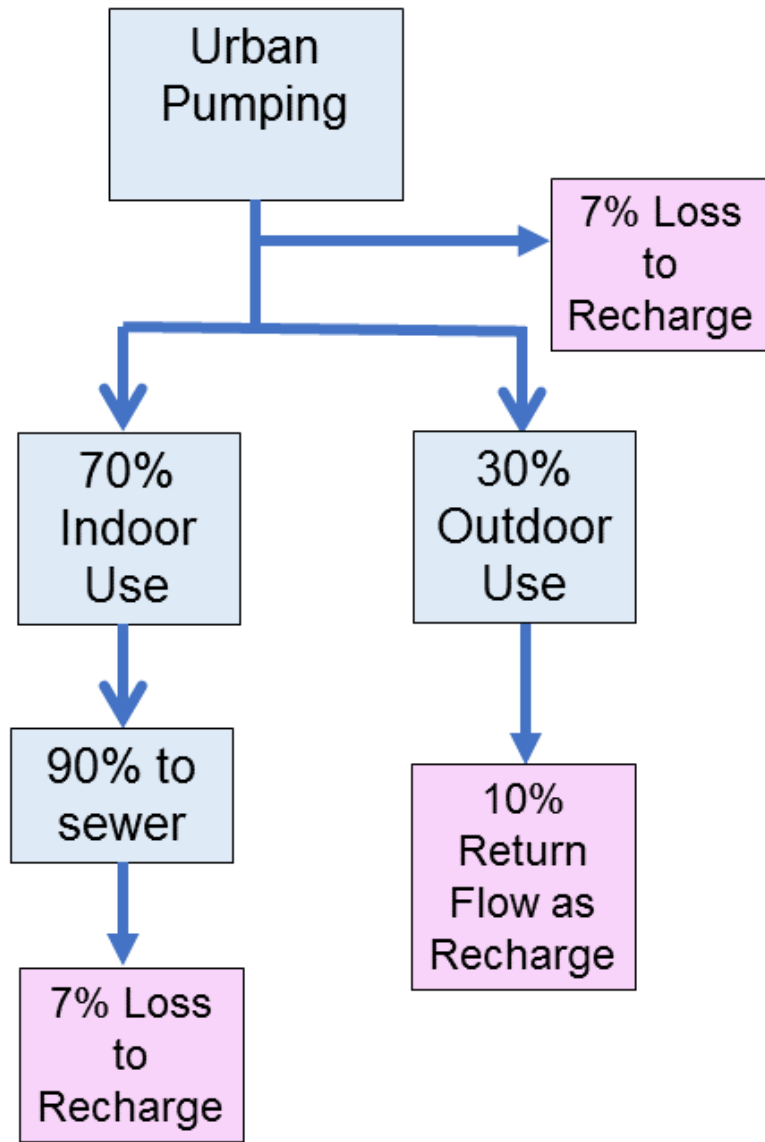
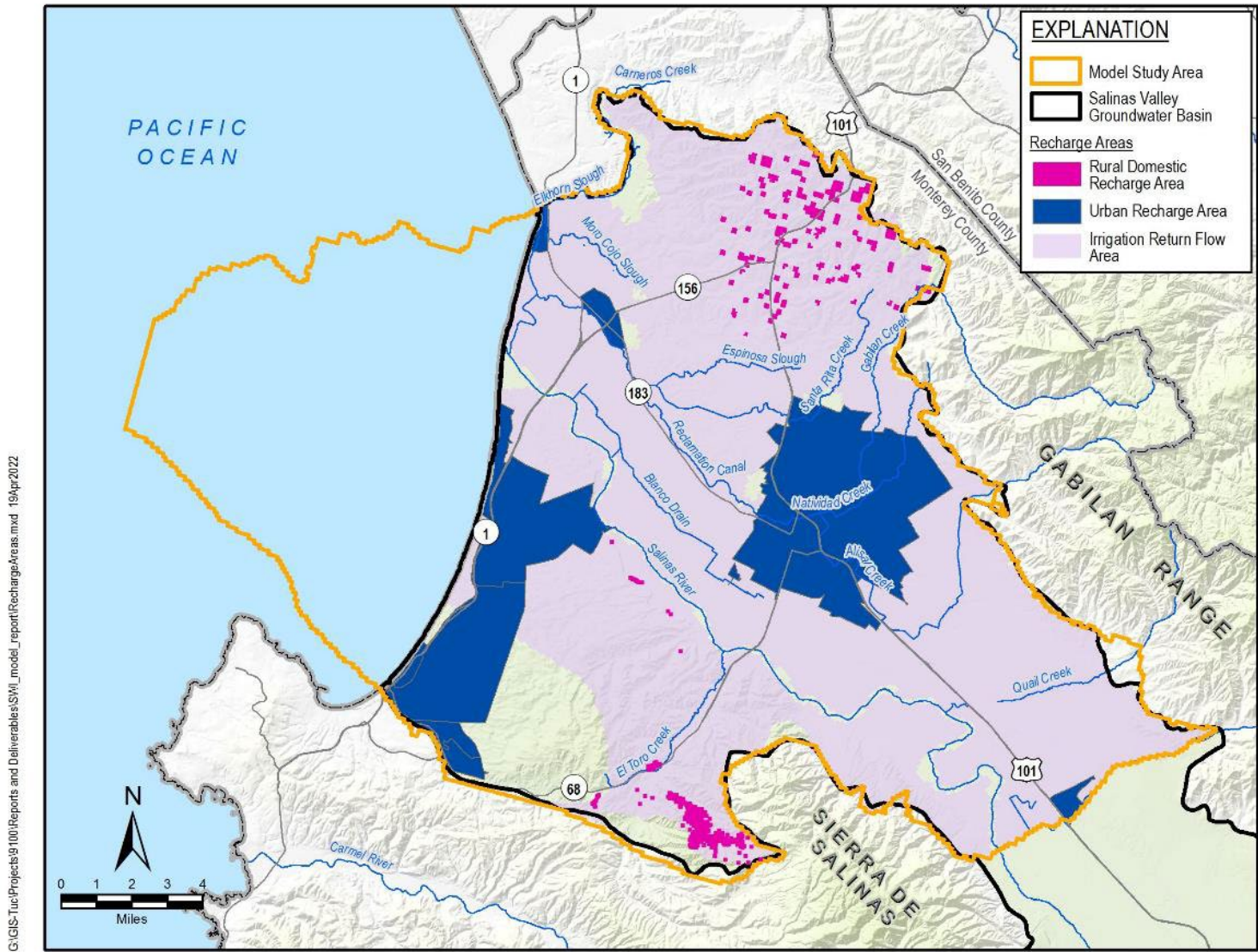
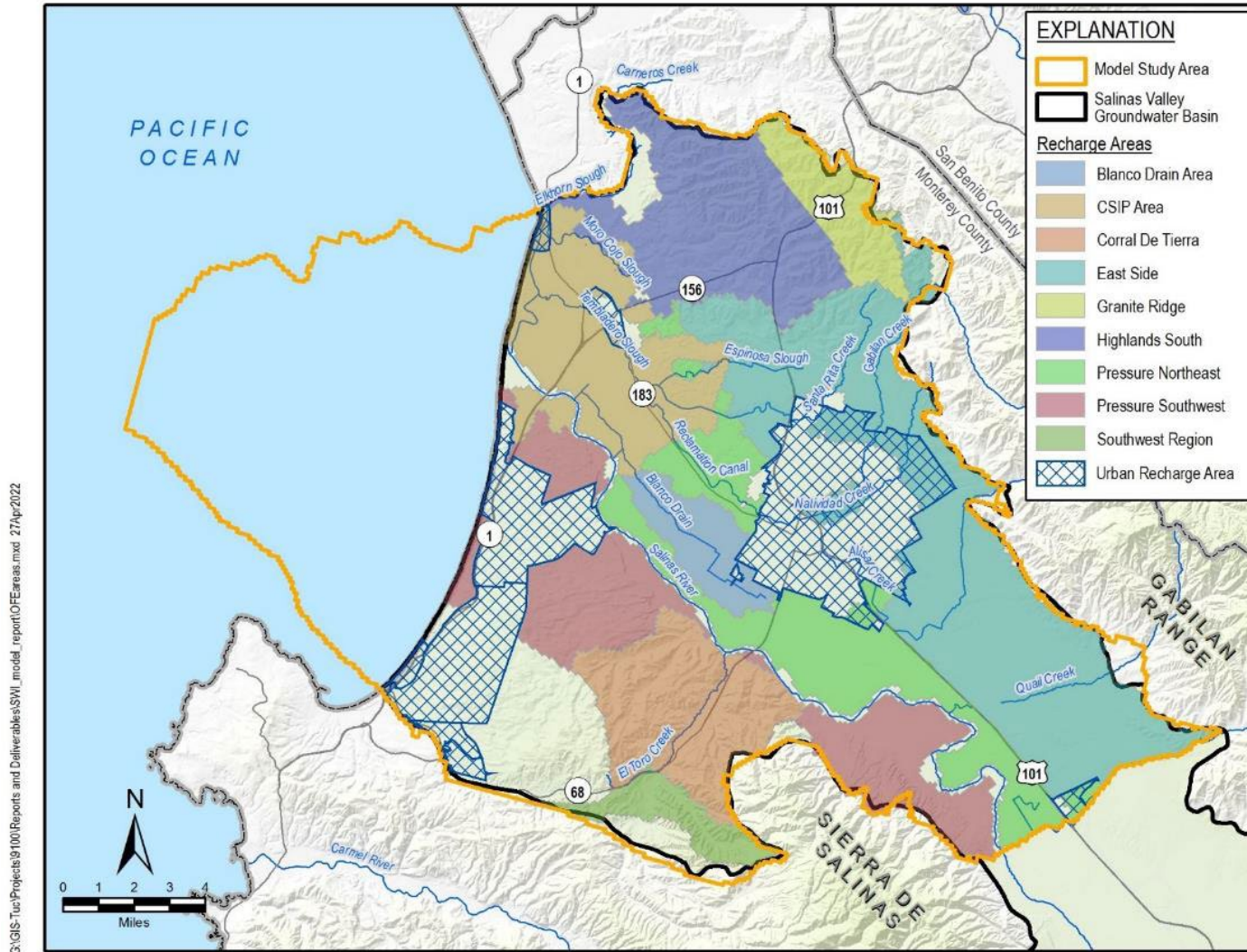


Figure 2-16. Urban Recharge as a Percentage of Urban Pumping



G:\GIS-Tuc\Projects\100\Reports and Deliverables\SWI_model_report\rechargeAreas.mxd 19-Apr-2022

Figure 2-17. Recharge Component Areas



G:\GIS-Tuc\Projects\9100\Reports and Deliverables\SWI_model_report\OFEAreas.mxd 27Apr2022

Figure 2-18. Recharge Areas

2.7.1.2 Underflow from Adjacent Basins

The Salinas Valley is bounded by low permeability basement rock. The Model assumes that no significant underflow occurs from these basement rocks. However, the entire Basin is not included in the model study area. At the upgradient boundary of the model study area near Chualar Creek, groundwater in both the 180-Foot and 400-Foot Aquifers enters the model study area from upgradient parts of the Basin, as indicated by measured groundwater levels.

A Darcy-flux calculation was used to approximate groundwater flows into the model study area at the upgradient boundary near Chualar Creek. Groundwater flow (flux) is equal to hydraulic conductivity multiplied by the cross-sectional area of flow multiplied by the hydraulic gradient. The parameters used in the calculations are summarized in Table 2-6. A cross-sectional width of 3.6 miles (about 19,000 feet) was used for the calculations. Hydraulic gradients are based on Fall 2020 groundwater contours (Figure 1-3 and Figure 1-4). At present, there is insufficient groundwater elevation data to prepare contours for the deeper portions of the Paso Robles Formation and for the Santa Margarita Formation. As a result, the gradient calculated for the 400-Foot Aquifer is used for the deeper formations. Hydraulic conductivity values represent the geometric mean of reported aquifer test results for each aquifer. Cross sectional areas are generalized from the geologic model described in section 3.2.2.

Table 2-6. Parameters Used to Estimate Darcy Flux at Chualar Creek

Parameter	Shallow/180 Foot	Deep/400-Foot	Paso Robles	Santa Margarita
Hydraulic gradient	0.0026	0.0020	0.0020	0.0020
Hydraulic Conductivity (ft/d)	72.7	29.4	7.3	24.7
Estimated Thickness (ft)	117	220	936	930
Assumed Shape	Rectangular	Rectangular	Triangular	Triangular
Darcy Flux (ft ³ /d)	926,531	551,392	290,345	980,030
Darcy Flux (AF/yr)	7,764	4,620	2,433	8,212

Summing the fluxes for each aquifer gives a total inflow of approximately 23,000 AF/yr at the study area boundary near Chualar Creek. This approximated flow rate is substantially larger than subsurface flows simulated by the provisional SVIHM. This discrepancy is likely a result of the uncertainty in the parameters used in the Darcy-flux calculation which could cause an overestimate of flows. Results from the provisional SVIHM indicate that historic average subsurface outflow from the Forebay Subbasin, located about 8 miles upgradient from this model boundary, is about 3,900 AF/yr. This range of flow estimates is used as a conceptual guide for developing the numerical groundwater model.

2.7.1.3 Elkhorn Slough

The Elkhorn Slough area is underlain by a low-permeability, sediment-filled paleochannel. This estuary and marshy area is located along the northeast boundary of the model study area. While surface water flows freely through the channel, the underlying sediments are rich in clay and have limited permeability. Water in the slough is saline at the outlet near the ocean. Monitoring data indicates water at the northern end of the slough is brackish (California Fish and Game, 2022). Based on the provisional SVIHM, net groundwater flow in the aquifers underlying the slough is anticipated to be northward towards Pajaro Valley. The provisional SVIHM estimates an average annual net flow of approximately 200 AF/yr into Elkhorn Slough.

2.7.1.4 Inflow from Ocean

As shown on Figure 1-3 and Figure 1-4, seawater intrusion has been observed in the 180-Foot and 400-Foot Aquifers. Groundwater pumping in vicinity of the City of Salinas has resulted in a cone of depression in the aquifers, resulting in a reversal of the hydraulic gradient in that area with respect to the ocean. The reversed hydraulic gradient results in groundwater movement from the coast towards the inland pumping center. Estimated sea water intrusion inflows range from 11,000 to 18,000 AF/yr, as described in Section 1.1.

2.7.1.5 Injection from Aquifer Storage and Recovery (ASR)

ASR occurs within the city limits of Seaside. Up to 2,300 AF/yr is injected into the Paso Robles and Santa Margarita Formations. However, average injection is approximately 600 AF/yr for WYs 1998-2020.

2.7.1.6 Net Groundwater-Surface Water Exchange

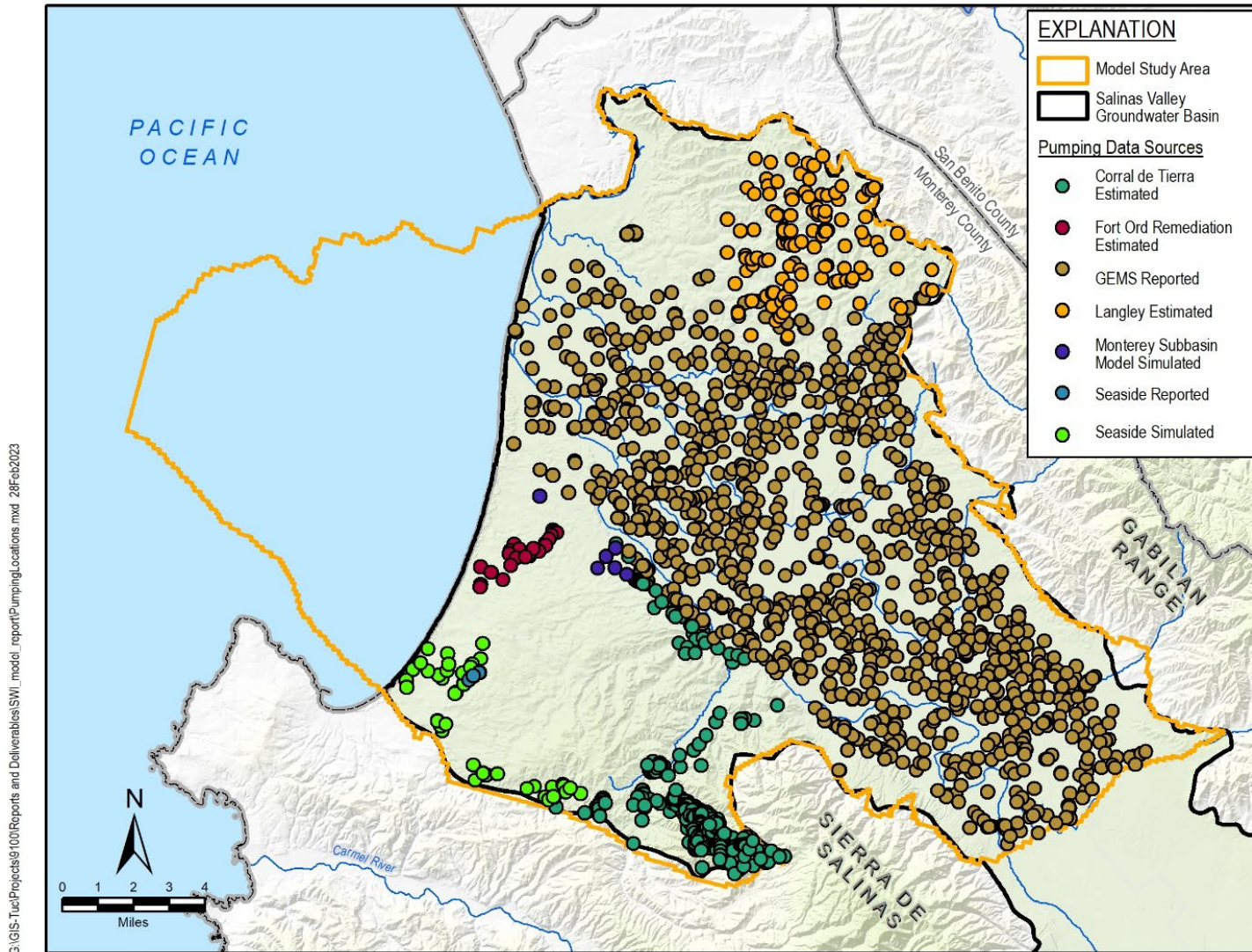
The exchange between surface water and groundwater varies dramatically over space and time, and is consequently difficult to measure on a basin or even subbasin scale. In some parts of the Basin, groundwater discharges to streams, while in other parts of the Basin streams lose water to the aquifer due to streambed seepage. Overall, the surface water network in the study area is primarily losing water to groundwater and act as an inflow to the groundwater system. The provisional SVIHM predicts a net inflow of approximately 16,000 AF/yr to the groundwater system from surface water network within the study area. This rate is supported by measured flow rates at stream gages along the Salinas River; average streamflow at the Chualar gage is approximately 16,000 AF/yr greater than average flow downstream at the Spreckels gage. This decrease in streamflow indicates that this reach of the Salinas River is losing water to groundwater via streambed seepage.

2.7.2 Groundwater Outflows

Groundwater outflows from the model study area include (1) groundwater pumping, (2) evapotranspiration by riparian vegetation, and (3) groundwater flow to the ocean.

2.7.2.1 Groundwater Pumping

Groundwater extraction rates were compiled from available sources that were considered reliable. These sources include reported pumping from GEMS and MCWD GSA, simulated pumping from the provisional SVIHM, simulated pumping from the Seaside Model, and estimated pumping in the Langley and Corral de Tierra regions. M&A compiled pumping data used to develop water budgets for the subbasin GSPs. These pumping datasets were combined to provide an estimate of pumping within the model study area. Pumping data sources used for estimating pumping rates within the model study area are summarized in the following section. Pumping well locations are shown on Figure 2-19. Provisional SVIHM pumping locations were only used prior to 1995 and are not shown on the Figure below. The provisional SVIHM pumping locations are similar, but not identical to GEMs reported pumping locations.



G:\GIS-Tuc\Projects\9100\Reports and Deliverables\SWI_model_report\PumpingLocations.mxd 28Feb2023

Figure 2-19. Pumping Locations and Data Sources

- **SVIHM (Pre 1995):** Prior to 1995, monthly municipal and agricultural pumping rates were extracted from the provisional SVIHM. Simulated pumping in the provisional SVIHM increases between 1975 and 1994.
- **GEMS:** For 1995 through 2020, municipal and agricultural pumping was aggregated from the GEMS database and distributed on a monthly basis.
- **Corral de Tierra Estimate:** In the Corral de Tierra area, pumping was estimated by the Wallace Group (2021) and adapted through 2020. Within water service areas, well locations were based on existing water service connections with rates supplied by the water service operators. Outside of water service areas, wells were located based on parcel data and a rate of 0.75 AF/yr was assumed for each residence.
- **Seaside Area:** For 1975 through 2017, simulated pumping rates for the Seaside Subbasin were extracted from the historical Seaside model. Reported monthly within the model study area. Table 2-7 lists summary statistics of each pumping category for Water Years (WYs) 1975 through 2020 within the model study area.

Table 2-7. Summary of Annual Pumping by Category in Model Study Area for WYs 1975 through 2020

Pumping Statistic	Domestic	Urban	Agricultural	Remediation (1975-1986)
Minimum	757	31,238	113,993	3,385
Maximum	1,044	49,140	200,593	5,763
Average	875	39,133	149,432	4,806

2.7.2.2 Riparian Groundwater Evapotranspiration

Groundwater evapotranspiration (ET) is assumed to only occur within riparian areas. Riparian areas are defined in the study area as the 400-foot buffer along the tributaries to and along the Salinas River and the Riparian Corridor identified in the provisional SVIHM. Potential Evapotranspiration (PET) represents the maximum ET that could occur for a given location. However, actual ET will be dependent on depth to groundwater. PET rates were taken from the BCM. PET rates for any given month range from 0.04 in/day to 0.24 in/day. On an annual basis, PET for the model study area ranges from approximately 110,700 to 146,600 AF/yr with actual groundwater ET being much less.

2.7.2.3 Groundwater Flow to Ocean

Based upon review of the provisional SVIHM, groundwater outflow to the ocean is approximately 2,000 AF/yr from aquifers in the model study area.

2.7.3 Summary of Groundwater Flows

Table 2-8 details the average annual conceptual water budget. As described in the previous sections, water budget components were estimated from measured and simulated sources. Each water budget component represents a summary value and likely has a large margin of error. The level of uncertainty is high enough such that estimates of change in storage calculated only from data in the following table are potentially unreliable. For example, actual ET will be much lower than PET. Change in storage calculated by the seawater intrusion model is considered more reliable; the information presented in the table and the associated descriptions is used as a guide for calibration of the numerical groundwater model described in Chapter 3.

Table 2-8. Groundwater Flows

Inflows		Minimum	Maximum
Recharge	Urban	1,100	6,600
	Irrigation Return Flow	24,400	73,400
	Domestic Return Flow	200	400
	Deep percolation of precipitation	3	166,500
	CSIP	2,300	5,200
Subsurface Inflow	Valley Upgradient Inflow near Chualar	3,900	23,000
	Seawater Intrusion	11,000	18,000
Injection	ASR - Seaside	12	2,312
Outflows			
Pumping	Irrigation	113,739	134,769
	Urban	24,868	31,596
	Monterey/Seaside	7,044	10,267
	Domestic	537	628
Potential Groundwater Evapotranspiration	Riparian	110,700	146,500
Subsurface Outflow	Valley Outflow to Ocean		19,000
Net Stream Exchange		8,956	92,231

3 MODEL DEVELOPMENT

Section 2 of this report provides the background data and HCM for developing the seawater intrusion numerical model. This section provides the link between the HCM and the numerical model by describing how the HCM was translated into the numerical model. This section summarizes the primary components of the Model and their linkage with the HCM data and information (Table 3-1). Additionally spatial and temporal discretization is presented.

Table 3-1. Summary of Model Boundary Conditions and Components

Model Component Type	Model Component / Boundary Condition	Model Package	Source
Inflows	Recharge	RCH	Estimated using rates derived from BCM and percentages of agricultural, urban, and domestic pumping. These rates were adjusted during calibration
	Valley Upgradient Inflow near Chualar	CHD	Estimated heads are applied to the model. The SWI Model calculates flow across this boundary
	Injection	WEL	Reported
	CSIP	RCH	Reported application rates
Outflows	Pumping	WEL/CLN	Reported data used when available. Estimated rates from previous models and other studies used when reported data not available
	Groundwater Evapotranspiration	EVT	Estimated PET from the BCM is input to the model. The SWI Model calculates actual evapotranspiration based on simulated groundwater levels
Net Flow	Net Flow to/from Ocean	GHB	Reported Sea Level - SWI Model calculates flow
	Net Stream Exchange	CLN	Groundwater surface water interaction is calculated by SWI Model. Surface water inflows at model boundaries were estimated using the Salinas Valley Watershed model
Model Structure	Model Layering	DIS	Developed from published cross sections and previously published models
	Zonation	LPF & others	Zonation was developed from geologic and hydrogeologic reports, published models, published cross sections, and professional knowledge
	Hydraulic Properties	LPF & others	Literature values, aquifer tests, hydrogeologic reports. These values are adjusted during calibration.

CLN - connected linear network

GHB- general head boundary package

3.1 Modeling Code Selection

The USG-Transport program was selected as the numerical code for the groundwater flow and transport model. USG-Transport is an expanded version of MODFLOW USG and, like MODFLOW-USG, uses an integrated finite difference framework to simulate heterogeneous, 3D advective-dispersive chemical species flow and transport with equilibrium and non-equilibrium retardation (Panday 2021, Panday *et al.*, 2013).

3.1.1 Important code features

USG-Transport uses the Newton (NWT) solver. NWT includes upstream weighting which aids in model convergence when model cells dry and rewet due to changes in simulated groundwater levels (Niswonger 2011). USG-Transport also includes the block centered transport (BCT) package which allows MODFLOW to solve for transport in unstructured grid settings in conjunction with the connected linear network (CLN) package. Coupled with the BCT package is the density dependent flow (DDF) package which allows for variable density flow to be simulated. Variable density flow simulation is necessitated by the density differences between seawater and freshwater.

3.2 Model Spatial and Temporal Discretization

3.2.1 Lateral discretization and grid spacing

Figure 3-1 shows the extent of the model grid, lateral discretization, and the active model extent. The active model extent was generated based on the model study area defined in Section 2. The grid contains 419 rows and 250 columns with a grid size of 500 feet. There are 11 layers with 104,750 nodes per layer for a total of 1,152,250 cells.

3.2.2 Vertical discretization / layering

Model layer surfaces were extracted from the Leapfrog hydrogeological model described in Section 2.2.3. These model layer surfaces were imported into the groundwater modeling interface software Groundwater Vistas, developed by Environmental Simulations Inc. Table 3-2 lists the generalized HGUs associated with each layer of the model.

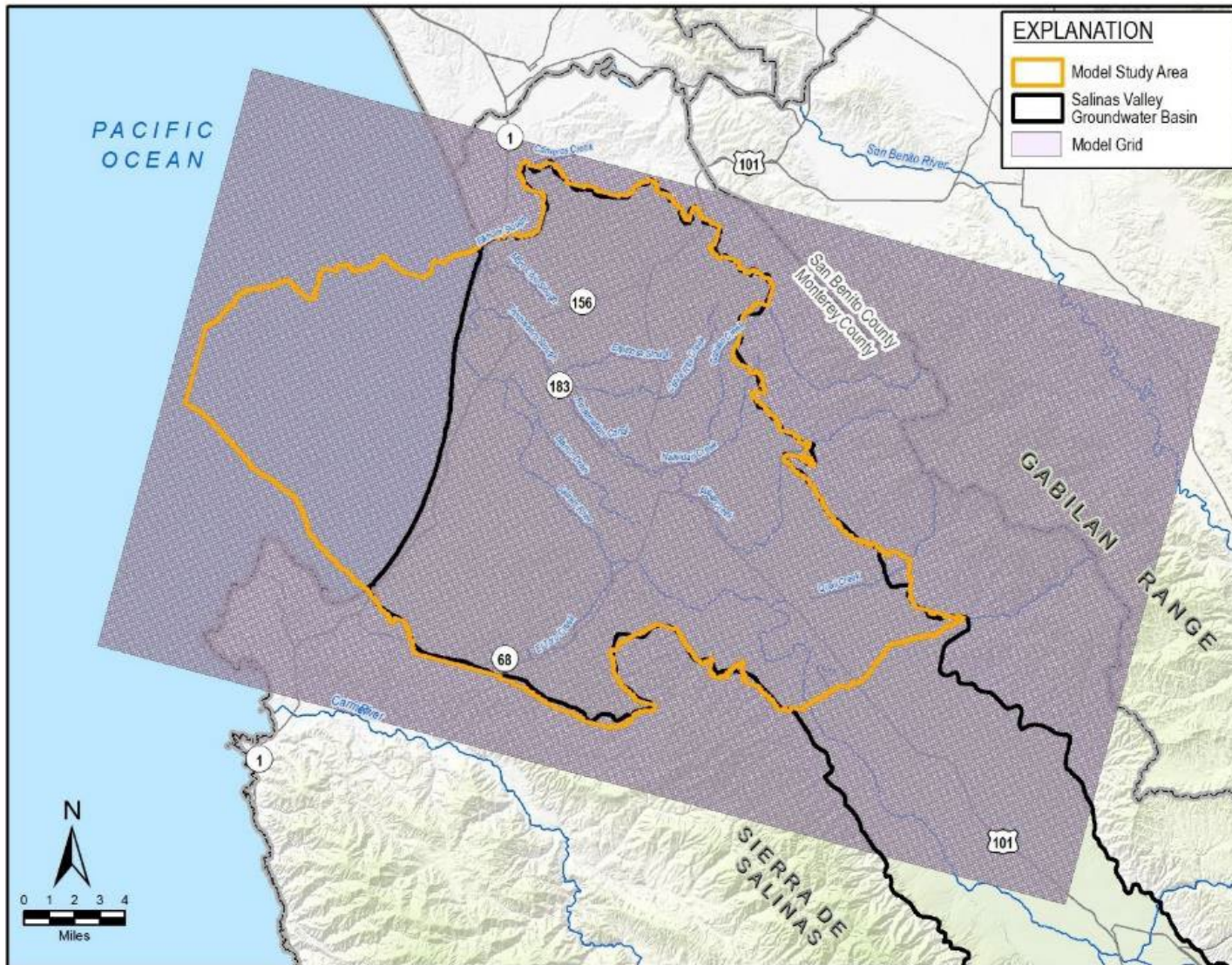


Figure 3-1. Extent of Model Grid

Table 3-2. Model Layer Generalized Hydrogeologic Units

Model Layer	Generalized Hydrogeologic Unit
1	Shallow Sediments
2	Salinas Valley Aquitard
3	180-Foot Aquifer
4	
5	
6	180/400 Foot Aquitard
7	400-Foot Aquifer
8	Deep Aquitard
9	Paso Robles Formation
10	Purisima Formation
11	Monterey Formation (Bedrock)

3.2.3 Temporal discretization

The primary time period for which seawater intrusion is simulated within the model is from the beginning of WY 1985 through WY 2020. Due to limited calibration data and to reduce model run times, variable length stress periods were used. Due to the transient nature of the seawater intrusion, an initial stress period of 500 years was used to develop a (pseudo-) pre-anthropomorphic influenced seawater wedge. The second stress period of approximately 60 years was then applied to represent anthropomorphic stresses through October 31, 1984, and serves as a seawater intrusion ramp-up period for the model.

The simulated period from November 1, 1984, through October 30, 1997, is represented by semi-annual stress periods 3 through 28. The stress periods split each WY into a 7-month summer (April-October) and a 5-month winter (November-March). From November 1, 1997, through September 30, 2020 (stress periods 29-303), monthly stress periods were used.

3.3 Initial Conditions

3.3.1 Initial Heads

The initial water levels assigned to every cell in the model at the beginning of the first 500-year stress period were determined by extracting the provisional SVIHM simulated heads from the end of September 1974 and preparing head contours for each model layer. As the model was developed and calibrated, simulated water levels from the end of this first stress period from 1 simulation were used as initial heads in subsequent simulations. A benefit of iteratively updating the initials heads resulted in improved model run times.

3.3.2 Initial Concentrations

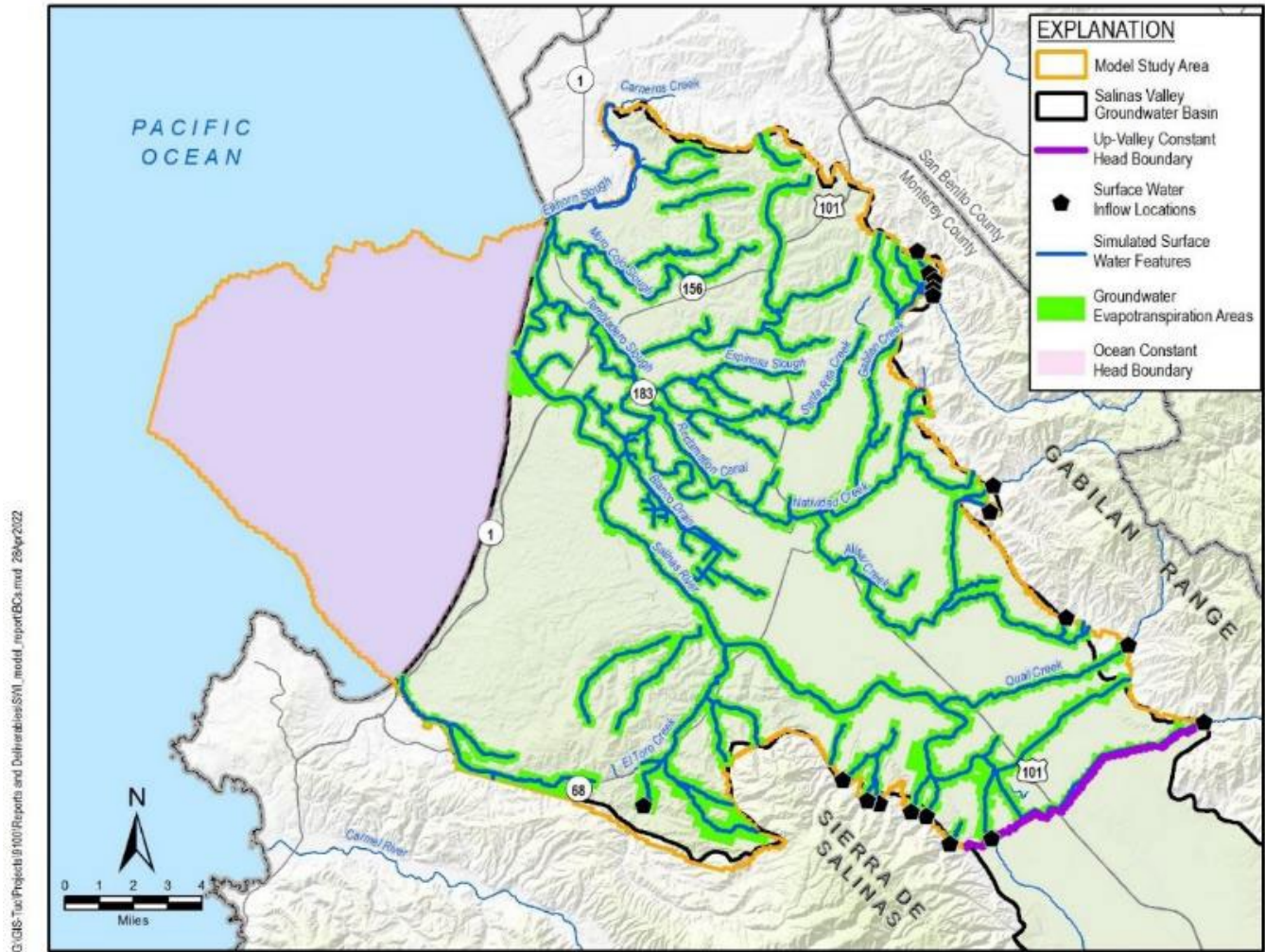
Initial chloride concentrations were developed similarly to the initial heads. At first, a background chloride concentration (55 mg/L) was applied to all model layers with the exception of Monterey Bay and the model cells beneath it, which had initial concentrations equal to seawater (18,537 mg/L). As the first 500-year stress period progressed a seawater wedge formed beneath the coast. To improve model run times, simulated chloride concentrations from the end of the 500-year stress period of previous model runs were used as initial concentrations for subsequent model runs. With each model run, the 500-year stress period allowed the seawater wedge to reach a quasi-steady state location. Review of Gottschalk (2020) indicates that freshwater / seawater transition zone was approximately 1.5 to 2 miles wide along the coastline. The simulated transition zone at the end of the first stress period also exhibited a similar width.

3.4 Pumping

Groundwater pumping is implemented using the MODFLOW WEL package. Details on the rates and locations applied to the model are described in section 2.7.2.1. Monthly pumping rates from reported and estimated sources were averaged over the length of each stress period. Some data sources only provided annual estimates of pumping and were distributed over the monthly stress periods.

3.5 Ocean Boundary

The ocean is modeled as a time-varying constant head boundary (CHD package). Figure 3-2 shows the area covered by constant head cells in the ocean as well as other boundary conditions in the model.



G:\GIS\Tuc\Projects\9100\Reports and Deliverables\911_model_report\BCs.mxd 28Apr2022

Figure 3-2. Model Boundary Conditions

From WY 1975 through WY 2020, sea level at Monterey varied by +/- 0.6 foot. Figure 3-3 shows a time series of variations in Sea Level for Monterey from the National Oceanic and Atmospheric Administration Tides and Currents webpage. This time series was applied to the ocean constant head cells. Of note is that this data and figure assume a msl of zero whereas the vertical datum (NAVD88) used in the model and in estimating groundwater levels places mean sea level at 2.97 feet. A conversion of the data was incorporated for model input.

Ocean TDS was measured at 33,694 mg/L at the Granite Canyon Monitoring Station (Geoscience, 2014) which is approximately 95.8% of the global seawater concentration of 35,176 mg/L (JGOFS 1997). Multiplying this percentage to the global seawater chloride concentration of 19,352 mg/L results in a local chloride concentration of 18,537 mg/L for Monterey Bay. This concentration was applied for all constant head cells representing the bay.

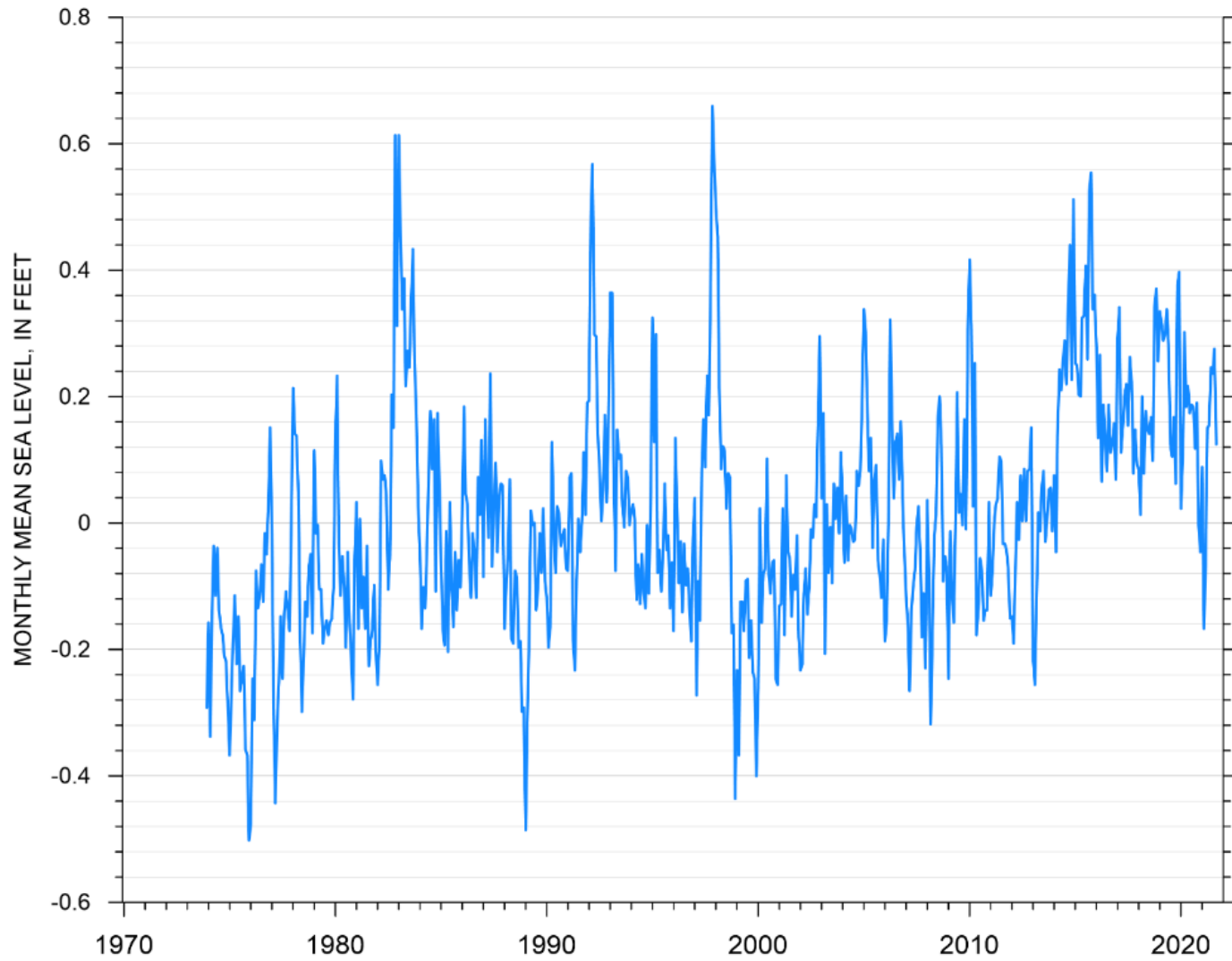


Figure 3-3. Sea Level Rise at Monterey Bay

3.5.1 Variable Density Flow

Variable density flow is implemented through the DDF package. This package only requires 3 additional input values: density of freshwater (1,000 gm/L), the reference density of the solution (1,024 gm/L – the density of seawater), and the reference concentration (18,537 mg/L – the chloride concentration of seawater). Thus, depending upon the simulated concentration, between background (55/mg/L) and seawater (18,537 mg/L), a density of the fluid can be determined.

3.6 Elkhorn Slough

The Elkhorn Slough is represented in the model using the CLN package. CLNs represent one-dimensional water conveyance features that are significantly longer than they are wide and allow for the simulation of flow in features, such as wells or streams, at scales significantly smaller than the groundwater model grid (Panday 2013). The sediments underlying the Elkhorn Slough are clay rich and thus impede flow perpendicular or across the slough and thus limit the flow between the Salinas Valley to the south and Pajaro Valley to the north. This flow is represented through the MODFLOW GHB. The actual slough is represented through a CLN into top layer (layer 1). The heads or water levels at the seaward outflow end of the CLN are specified as equal to the ocean water levels and vary as ocean levels vary (Figure 3-3). The ocean side of the Slough is set constant to seawater concentration (18,537 mg/L chloride) while concentrations are allowed to vary through the remainder of the slough.

3.7 Southeastern Boundary Groundwater Inflow

The southeastern extent of the active model was selected to be the valley transect at Chualar Creek (Figure 3-2). This extent was selected to minimize boundary effects on the seawater intruded area and the cone of depression caused by pumping in and around the city of Salinas. The southeastern boundary groundwater inflow is simulated using a CHD time-variant specified head. The CHD boundary spans the valley transect in active model cells in layers 2 through 11. Simulated heads from the provisional SVIHM were extracted and aerially averaged over the seawater intrusion model grid for WY 1975 through 2017. The last year of head values was repeated for WY 2018 through 2020. Heads in layer 1 are controlled by the surface water flow in Chualar Creek and the Salinas River. The provisional SVIHM results show groundwater flow out across a portion of this boundary toward a simulated cone of depression east-southeast of Chualar. The cone of depression simulated in the model is not consistent with groundwater level contours prepared from measured groundwater levels. The apparent discrepancy between simulated and observed flow conditions along this portion of the model boundary is located far away from the area of interest for this model (coastal area) and does not impact simulated seawater intrusion.

3.8 No-flow Boundaries

All other model cells along the model’s boundaries (apart from the up-valley boundary cells along and beneath Chualar Creek – Section 3.6; and the boundary cells along and beneath the Elkhorn Slough Section 3.7) are defined as no flow boundaries and generally represent hydrologic boundaries (see Figure 3-2). The southwestern boundary of the model coincides with a surface water divide as well as a groundwater flow divide. The remaining active extent of the model roughly corresponds to the extent of basin fill sediments, similar to the provisional SVIHM. No flow boundaries represent the juxtaposition of basin fill sediments on the surrounding lower permeability basement rock.

3.9 Surface Water

The Salinas River is the primary surface water feature in the model study area. Flow is monitored by the USGS near Chualar at the southern extent of the model area (gage number 11152300). Figure 2-14 shows monthly surface water flows at this gage, which were assumed to be equal to flow at the study area boundary. No other measured surface water data is available for the tributaries to the Salinas River near the model boundary. Since measured data were not available for the tributaries, surface water inflows were estimated using results from a watershed hydrologic model developed and calibrated by the USGS for input to the provisional SVIHM. Surface water channels and diversions are simulated using the CLN package and are shown on Figure 3-2. The simulated tributaries are based on the provisional SVIHM surface water network. Stream parameters, including width and surface water inflows, were extracted from the provisional SVIHM and applied to the same streams at the model active extent boundary. Monthly inflows from the provisional SVIHM were averaged and applied to the SWI Model for WY 1975 through WY 2018. The provisional SVIHM inflows were calculated using the BCM in conjunction with the USGS watershed model. For consistency, inflows for WY 2018 through WY 2020 were generated by repeating inflows from WYs with similar WY classifications. Table 3-3 lists the classifications and WYs used for the inflow estimates for these years.

Table 3-3. Repeated Water Years for Basin Boundary Surface Water Inflows



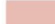





Water Year	Water Year Classification	Water Year to Repeat Inflow Values
2018	Very Dry	2015
2019	Very Wet	2011
2020	Dry	2016

Chloride concentration data was downloaded from the USGS National Water Information System for all surface water bodies in the active extent of the model. The only gage with data available was USGS #11152500, located near Spreckels, California, on the Salinas River. A log-average chloride concentration of 74 mg/L was used for all surface water inflows.

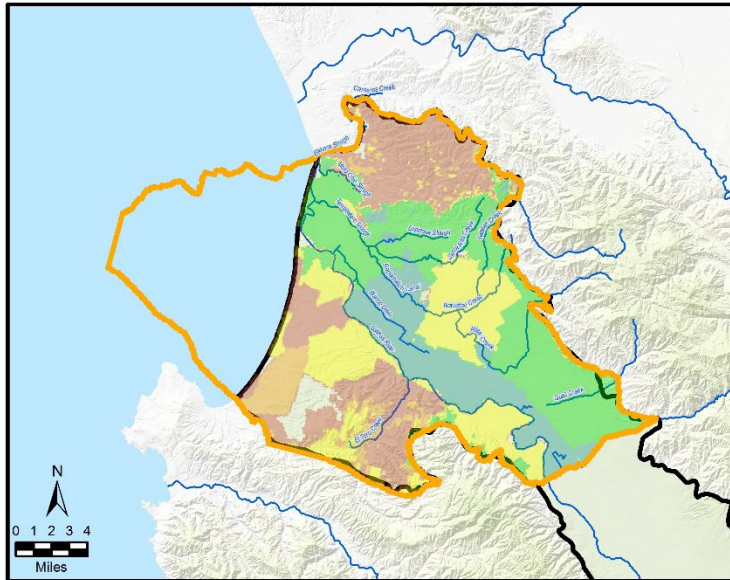
3.10 Recharge

Recharge is implemented in the model using the RCH package. Time-varying recharge rates for each model cell were determined by combining agricultural, domestic, urban, and natural recharge rates as described in Section 2.7.1.1. Recharge was applied in the model directly to the simulated water table. Recharge rates and their spatial distribution are also described in Section 2.7.1.1, and examples of the model applied recharge distribution are shown on Figure 3-4 and Figure 3-5.

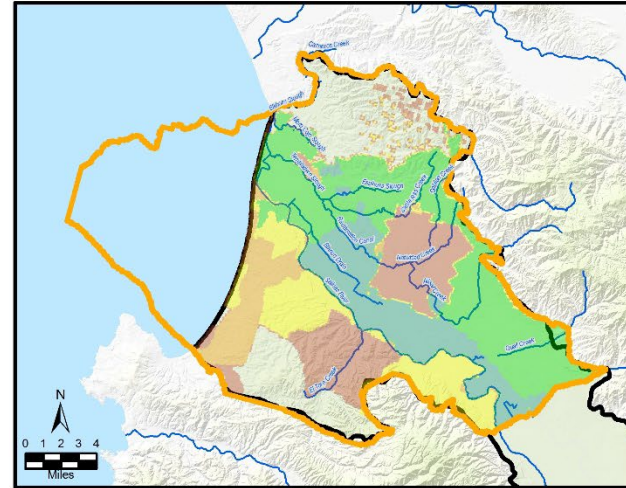
EXPLANATION

-  Model Study Area
-  Salinas Valley Groundwater Basin
- Groundwater Recharge (inches/year)**
-  0.001 - 1
-  1 - 2
-  2 - 4
-  4 - 8
-  8 - 16
-  16 - 34

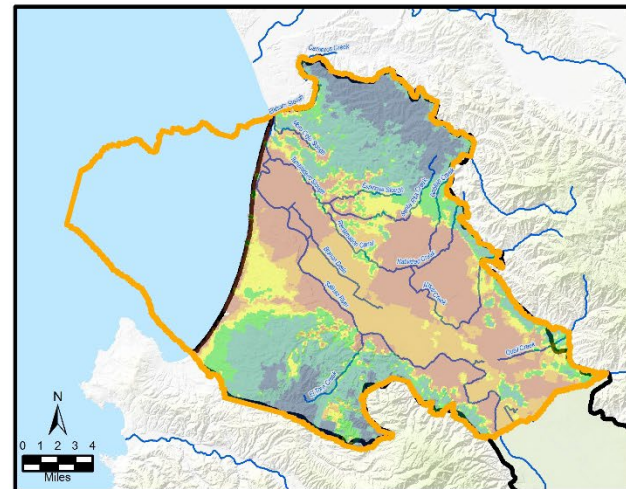
G:\GIS\Tuc\Projects\100\Reports and Deliverables\SWI_model_report\Recharge_First&SemiannualStressPeriods_2023\302.mxd 2March2023



Stress Period 2:
October 1, 1924 - October 31, 1984



Stress Period 24:
April 1, 1995 - October 31, 1995



Stress Period 25:
November 1, 1995 - March 31, 1996

Figure 3-4. Historical Snapshots of Estimated Recharge

EXPLANATION

Groundwater Recharge
(inches/year)

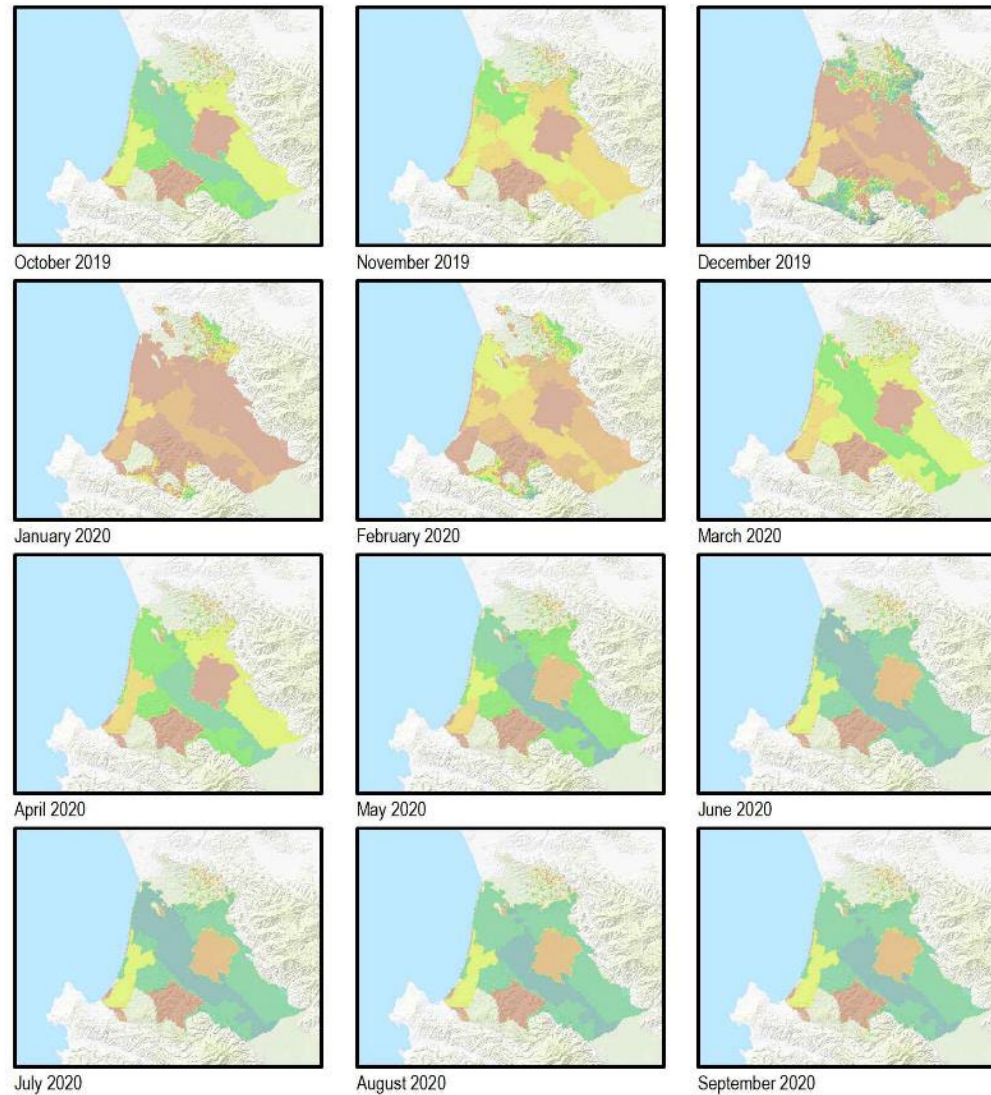
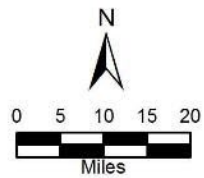


Figure 3-5. Estimated Monthly Spatial Distribution of Recharge in Water Year 2020



3.11 Castroville Seawater Intrusion Program



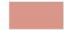

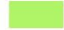
Salinas River and recycled water CSIP diversions are implemented in the model as an outflow from the CLN surface water network. Prescribed rates based on reported values are extracted from the surface water network. Water from CSIP is used to reduce groundwater pumping and is applied as irrigation to crops. A percentage of this applied water enters the groundwater system as described in Section 2.7.1.1.

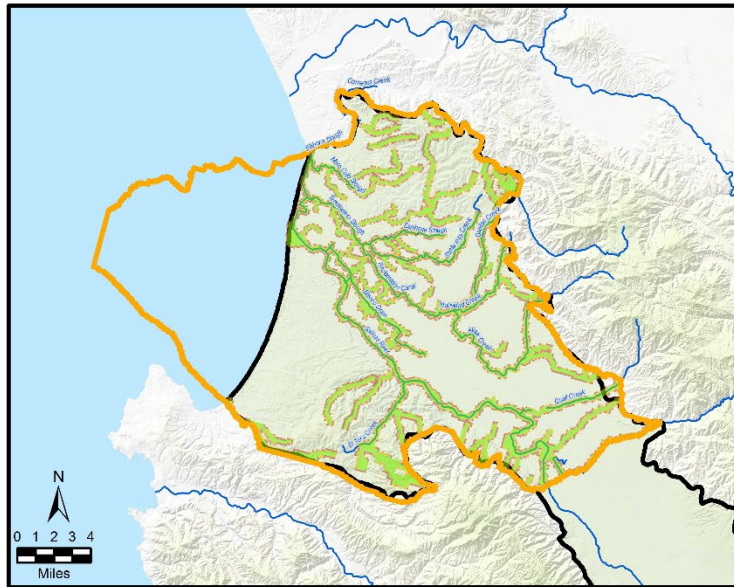
3.12 Evapotranspiration

Evapotranspiration was applied using the EVT package. ET was applied by assigning a time-varying PET rate to each model cell in the areas surrounding surface water channels, as described in Section 2.7.2.2. Figure 3-6 and Figure 3-7 show historical snapshots of the estimated spatial distribution of PET. An extinction depth of 3 feet was used for the ET areas described above. In these areas, if the depth to groundwater is less than the extinction depth in a given timestep, groundwater ET occurs at a rate dependent on water level elevation, and is calculated based on the linear interpolation between 0 in/yr at the extinction depth to the full PET rate at land surface. Maximum PET rates are described in Section 2.7.2.2.

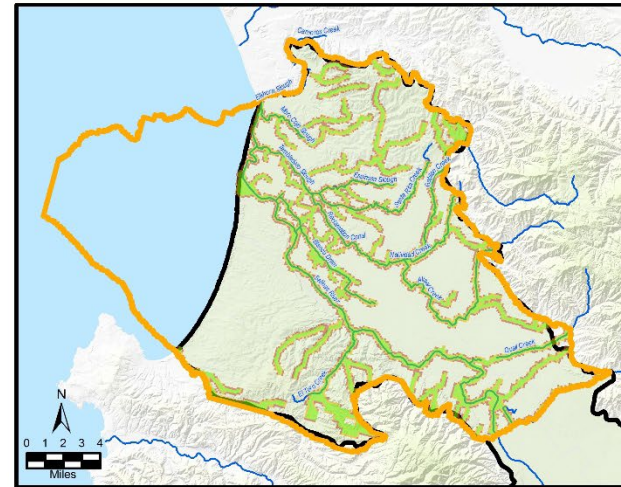
G:\GIS_Tuc\Projects\100\Reports and Deliverables\SWI_model_report\PotentialET_First&SemiannualStressPeriods_20230302.mxd 2/Mar/2023

EXPLANATION

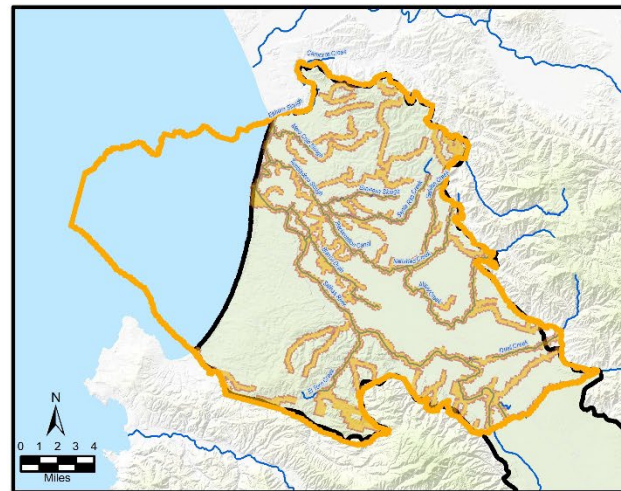
-  Model Study Area
-  Salinas Valley Groundwater Basin
- Potential Evapotranspiration (inches/day)**
-  0.001 - 0.05
-  0.05 - 0.1
-  0.1 - 0.15



Stress Period 2:
October 1, 1924 - October 31, 1984



Stress Period 24:
April 1, 1995 - October 31, 1995



Stress Period 25:
November 1, 1995 - March 31, 1996

Figure 3-6. Historical Estimates of Potential Evapotranspiration for Selected Time Periods

G:\GIS-Tue-Projects\100\Reports and Deliverables\SWI_model_report\PotentialET_Last12StressPeriods.mxd 29Apr2022

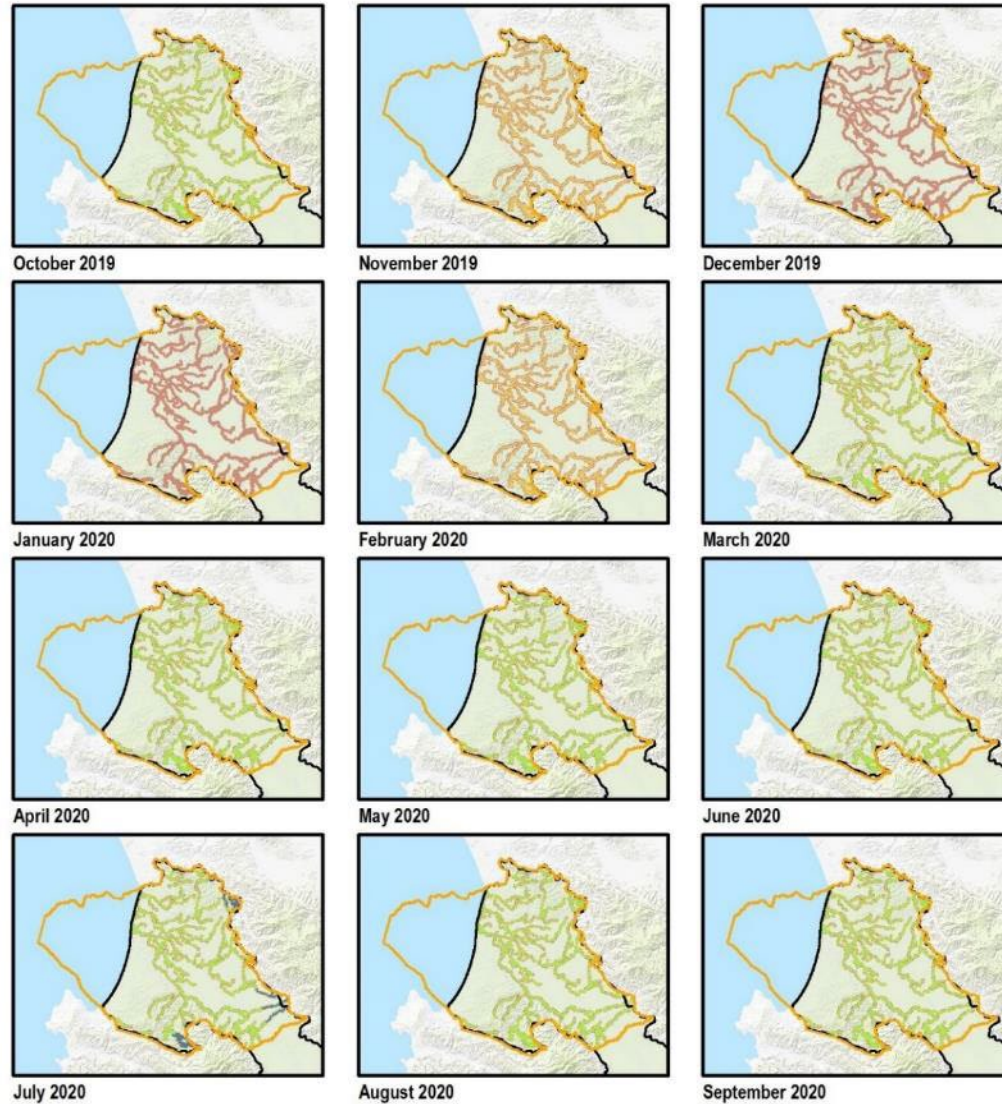
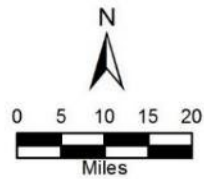
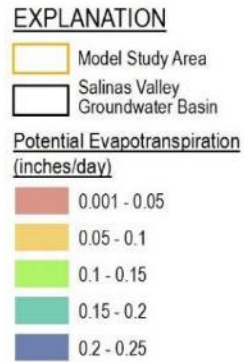


Figure 3-7. Estimate of Potential Evaporation for Water Year 2020



3.13 Hydrogeologic Zonation (HGUs)

HGUs were developed by applying the conceptual understanding presented in Section 2 to the groundwater model layering. Estimates of hydraulic parameters were assigned to the model based upon aquifer testing and estimates from existing models such as the provisional SVIHM, Monterey Subbasin Groundwater Flow Model, Seaside Watermaster Model, and the North Monterey County Groundwater Model. The applied model zonation for each model layer is shown on Figure 3-8 through Figure 3-18 with 5 cross sections through the model depicted on Figure 3-19 through Figure 3-23.

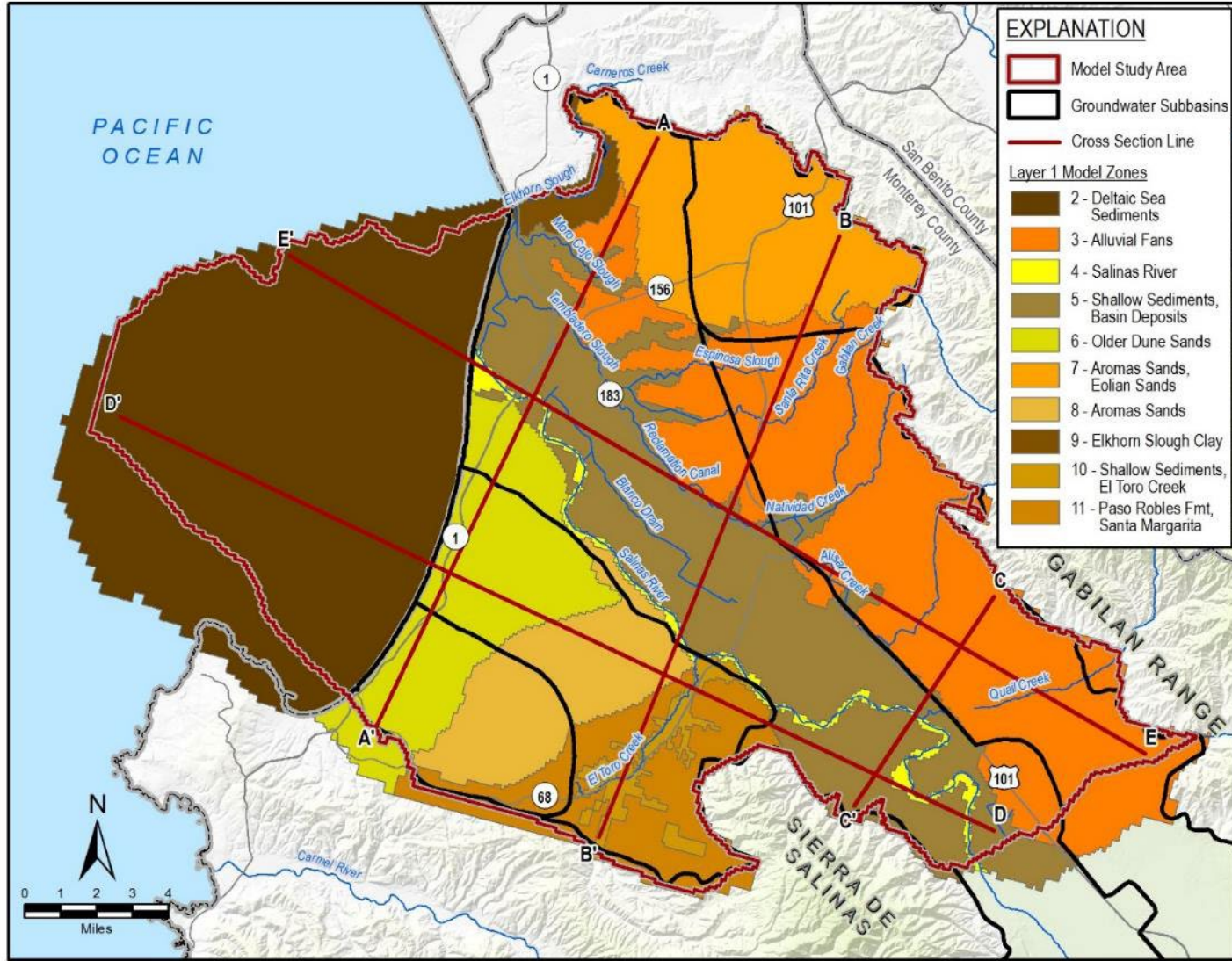


Figure 3-8. Model Hydrogeologic Zonation in Layer 1

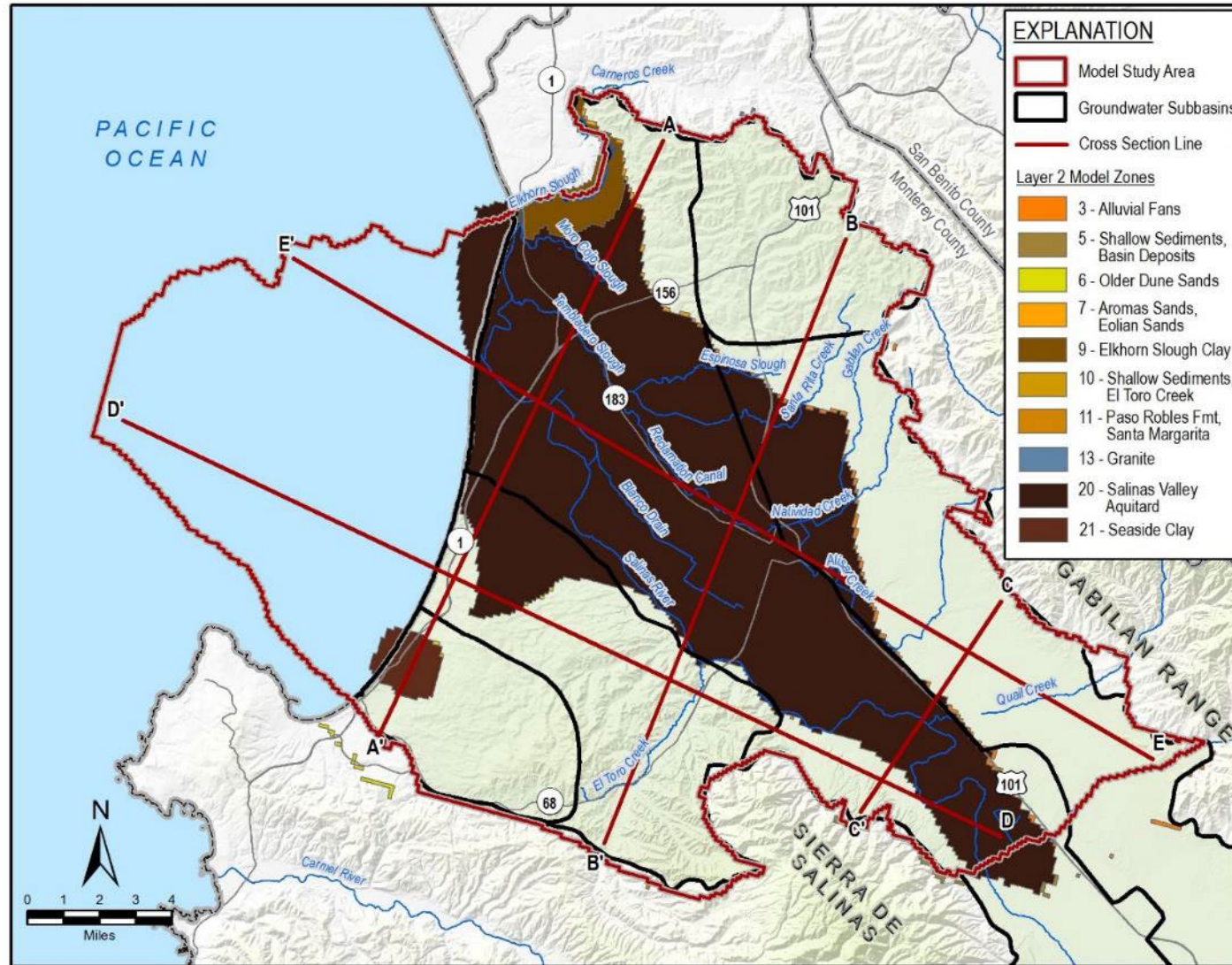


Figure 3-9. Model Hydrogeologic Zonation in Layer 2

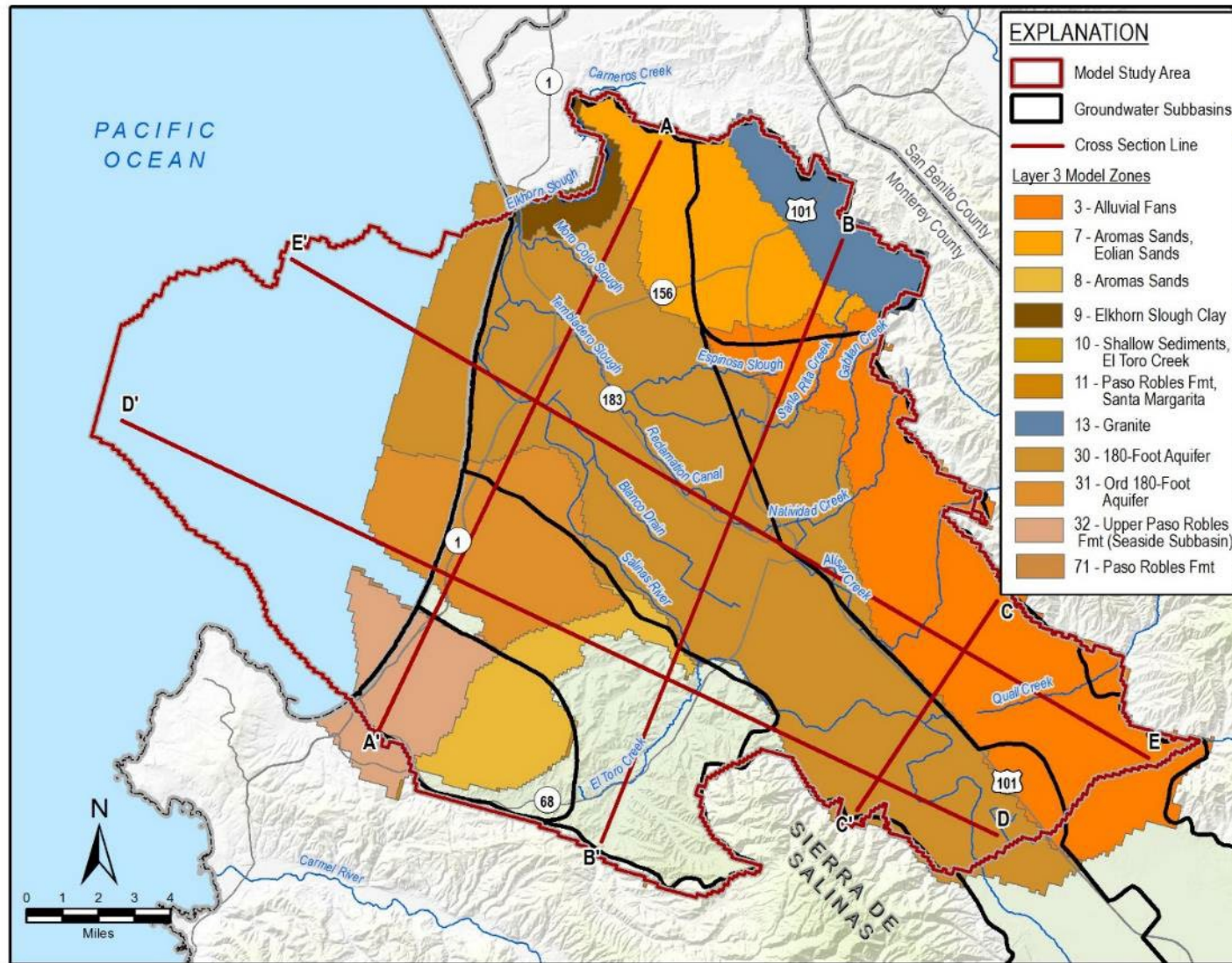


Figure 3-10. Model Hydrogeologic Zonation in Layer 3

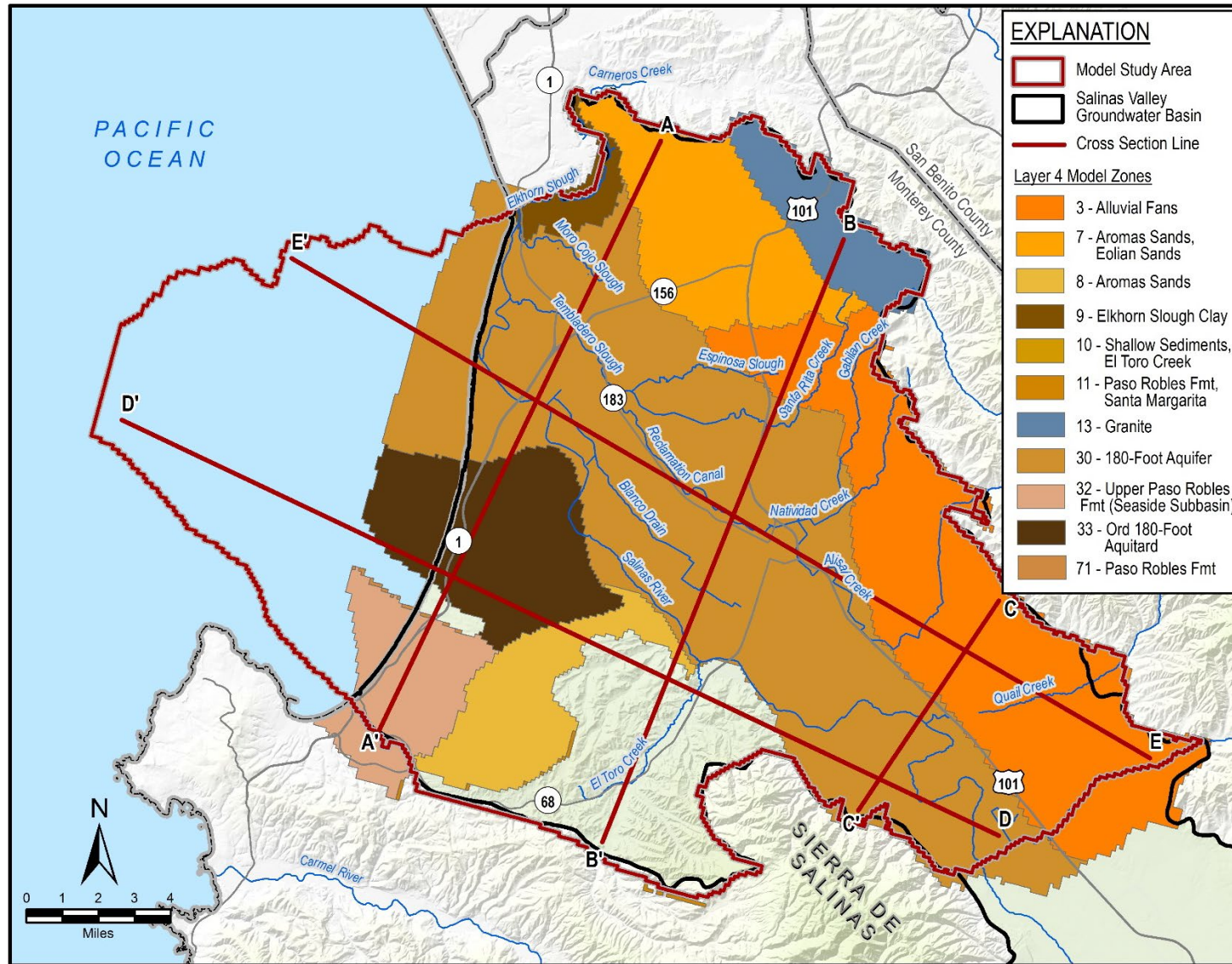


Figure 3-11. Model Hydrogeologic Zonation in Layer 4

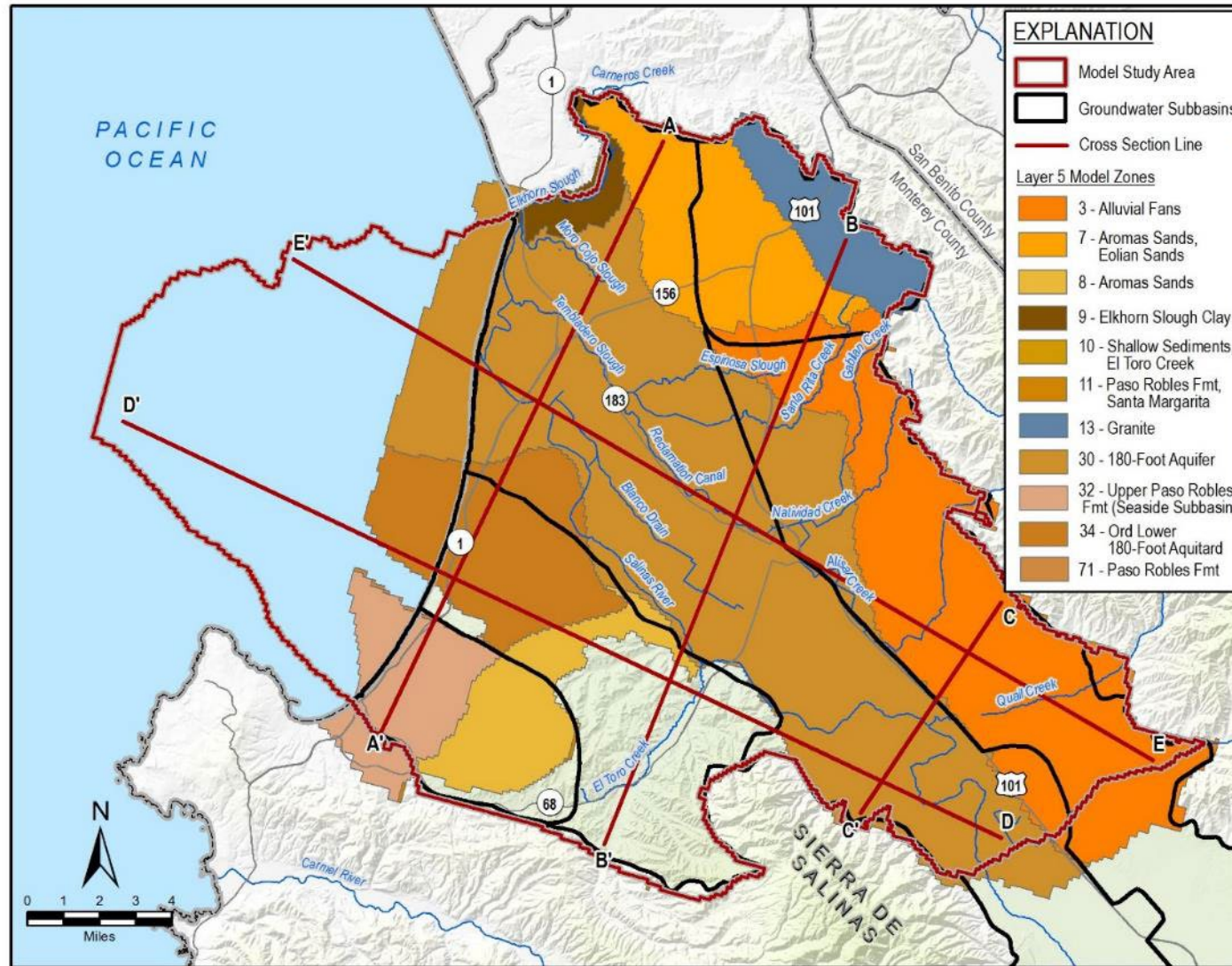


Figure 3-12. Model Hydrogeologic Zonation in Layer 5

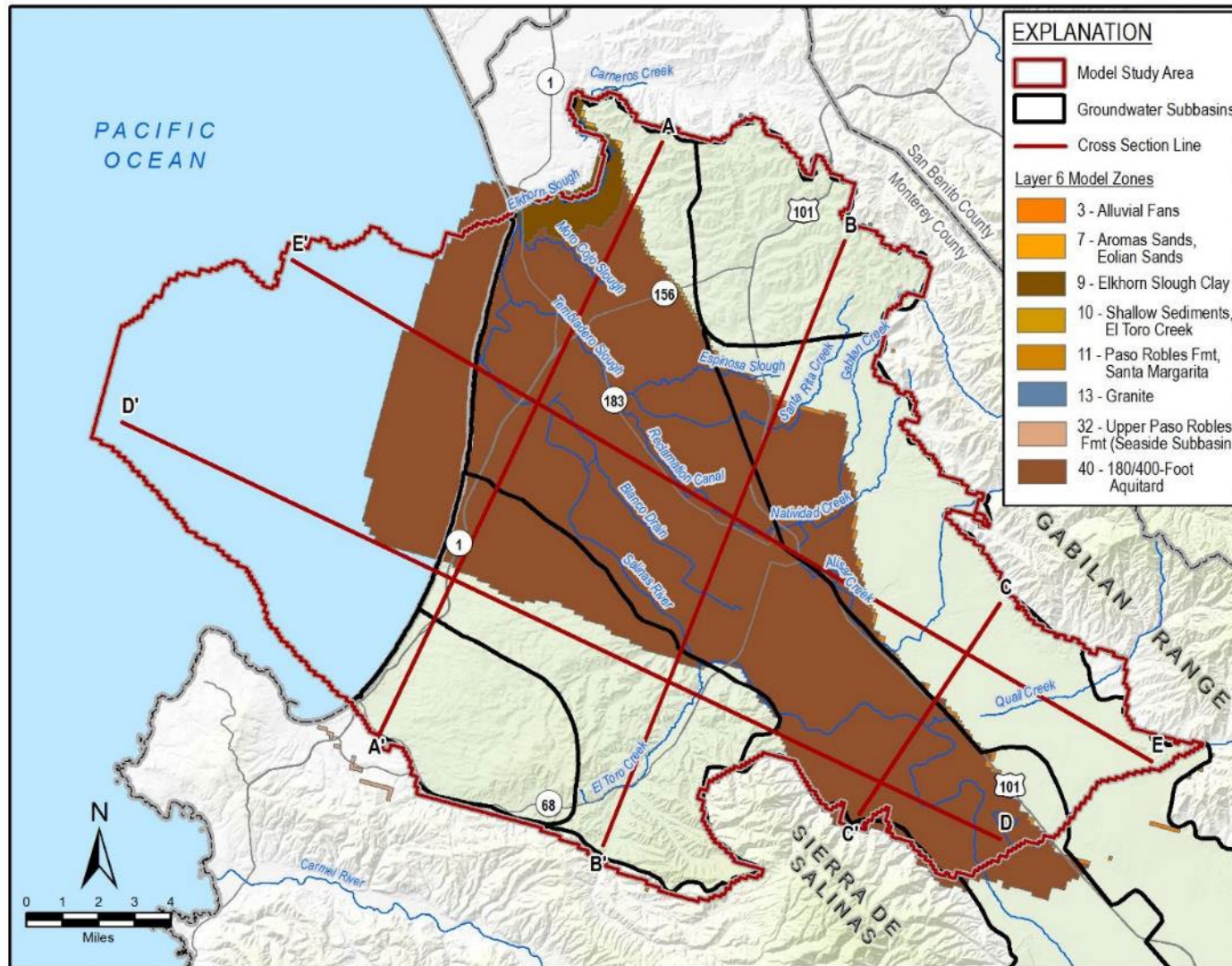


Figure 3-13. Model Hydrogeologic Zonation in Layer 6

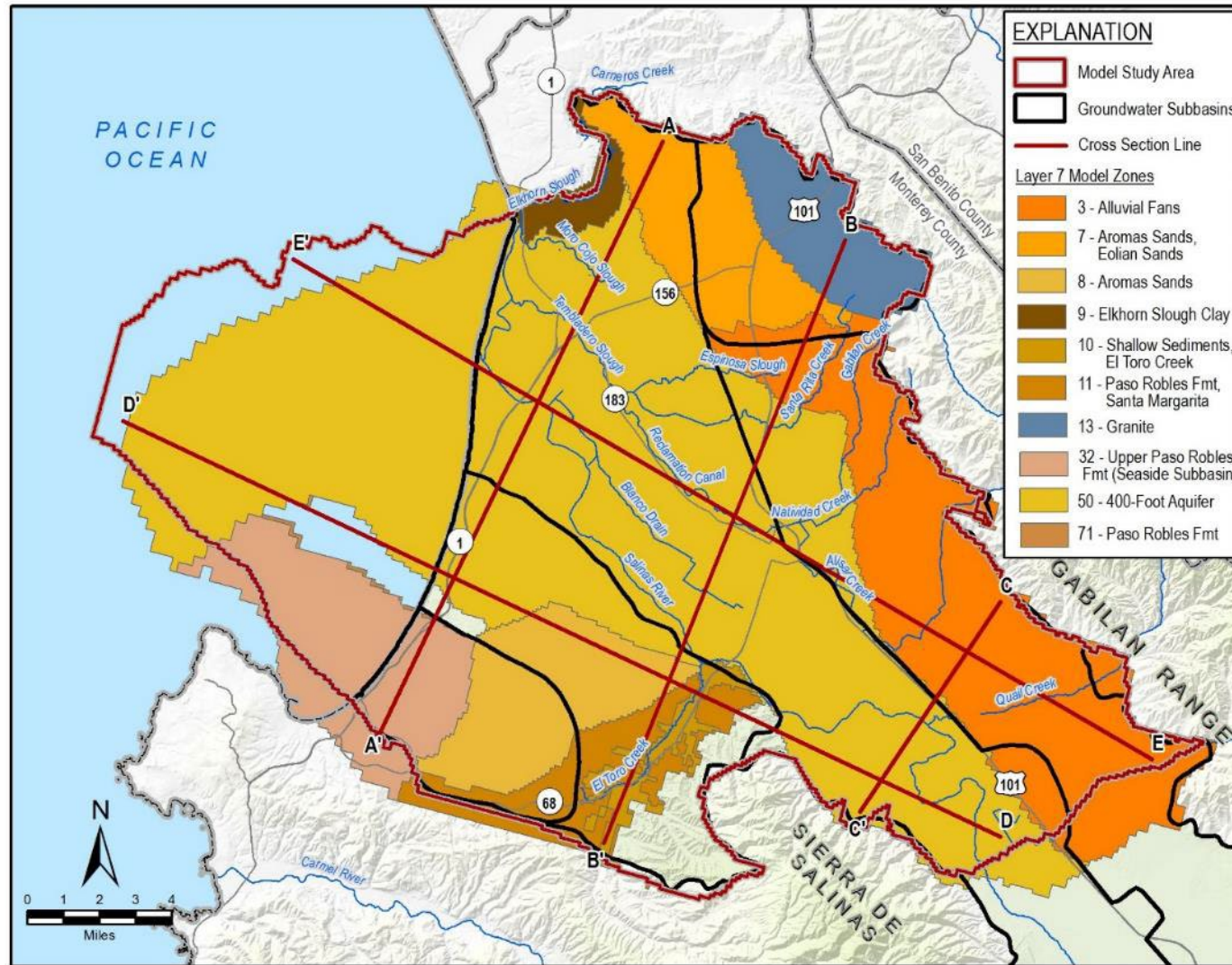


Figure 3-14. Model Hydrogeologic Zonation in Layer 7

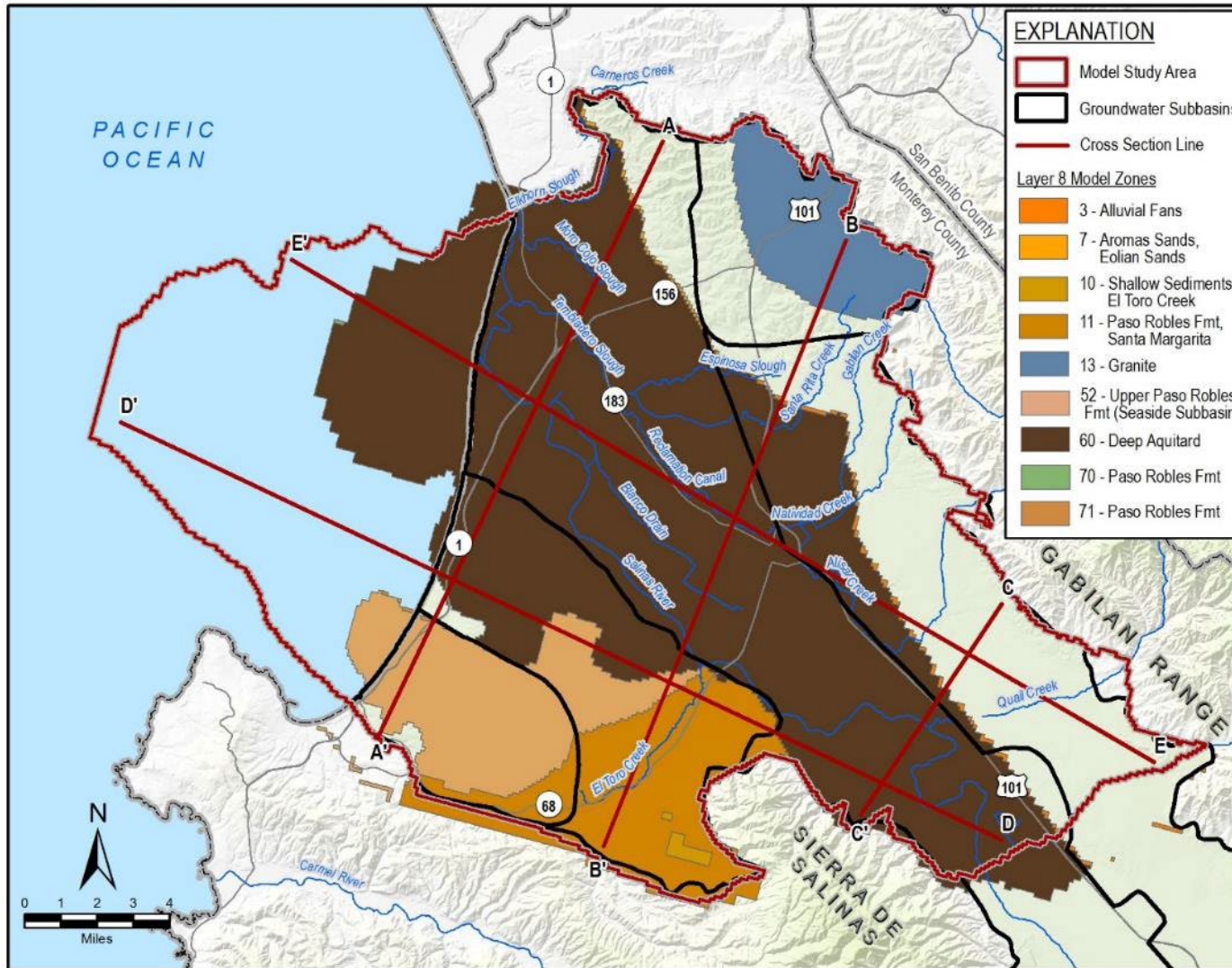


Figure 3-15. Model Hydrogeologic Zonation in Layer 8

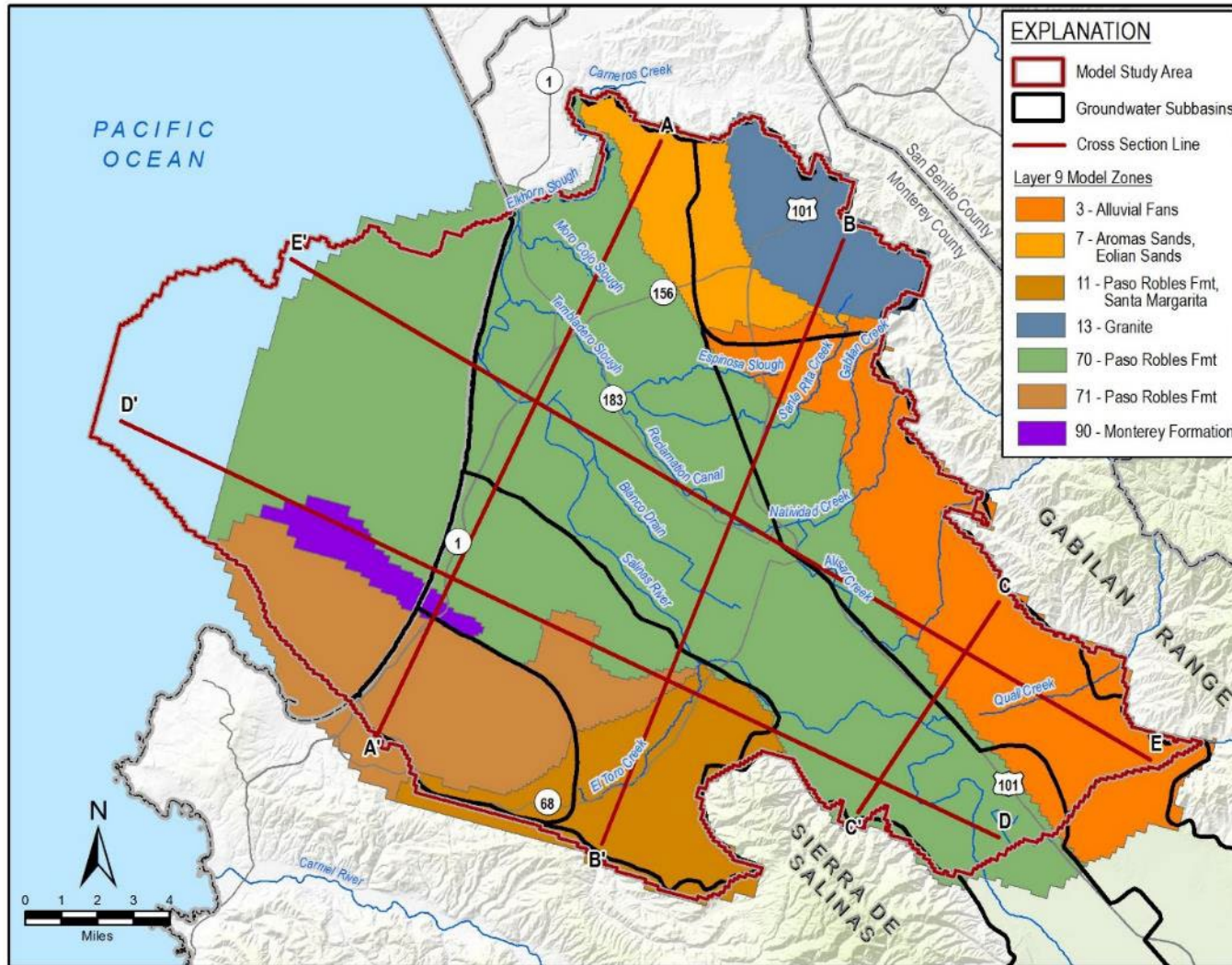


Figure 3-16. Model Hydrogeologic Zonation in Layer 9

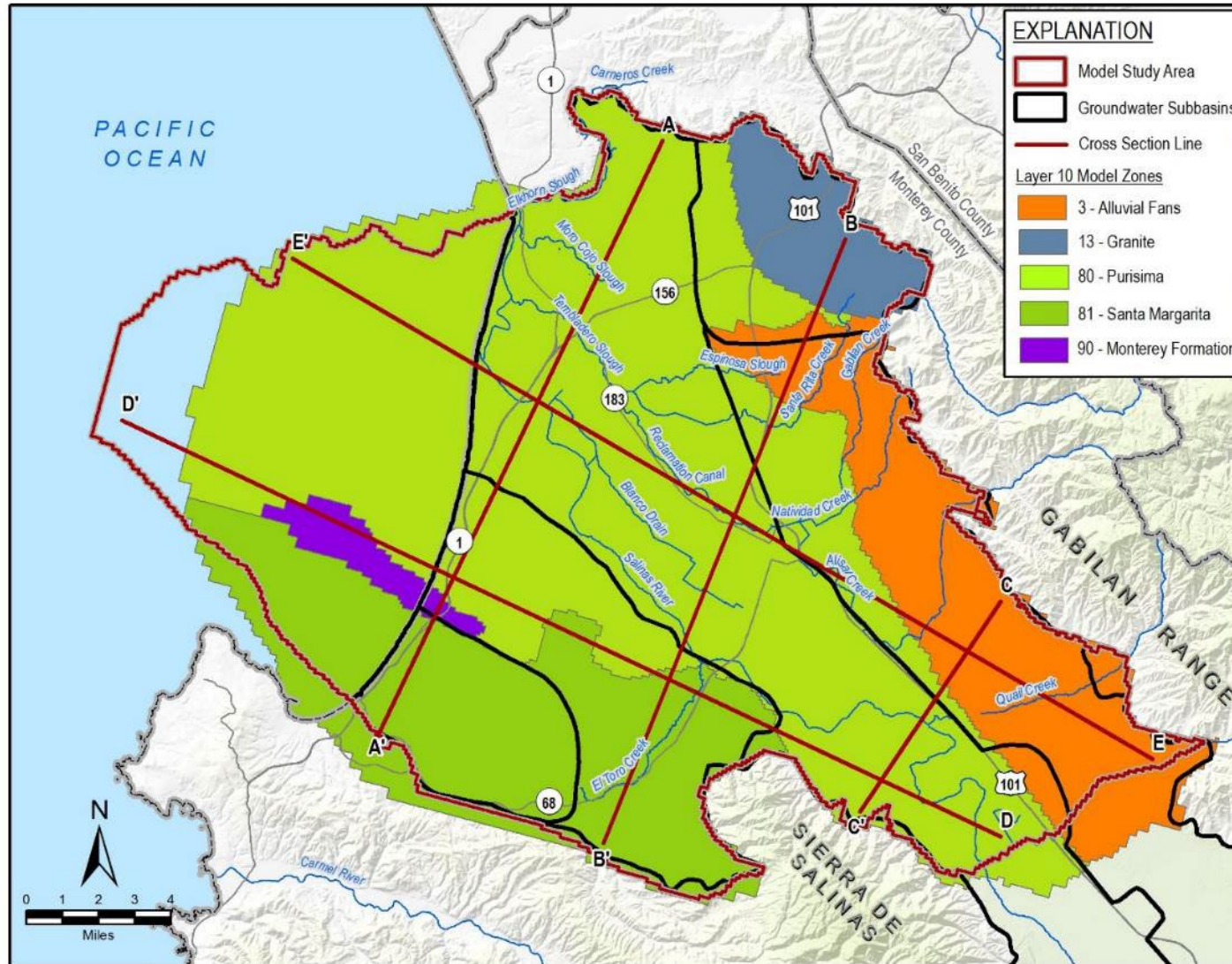


Figure 3-17. Model Hydrogeologic Zonation in Layer 10

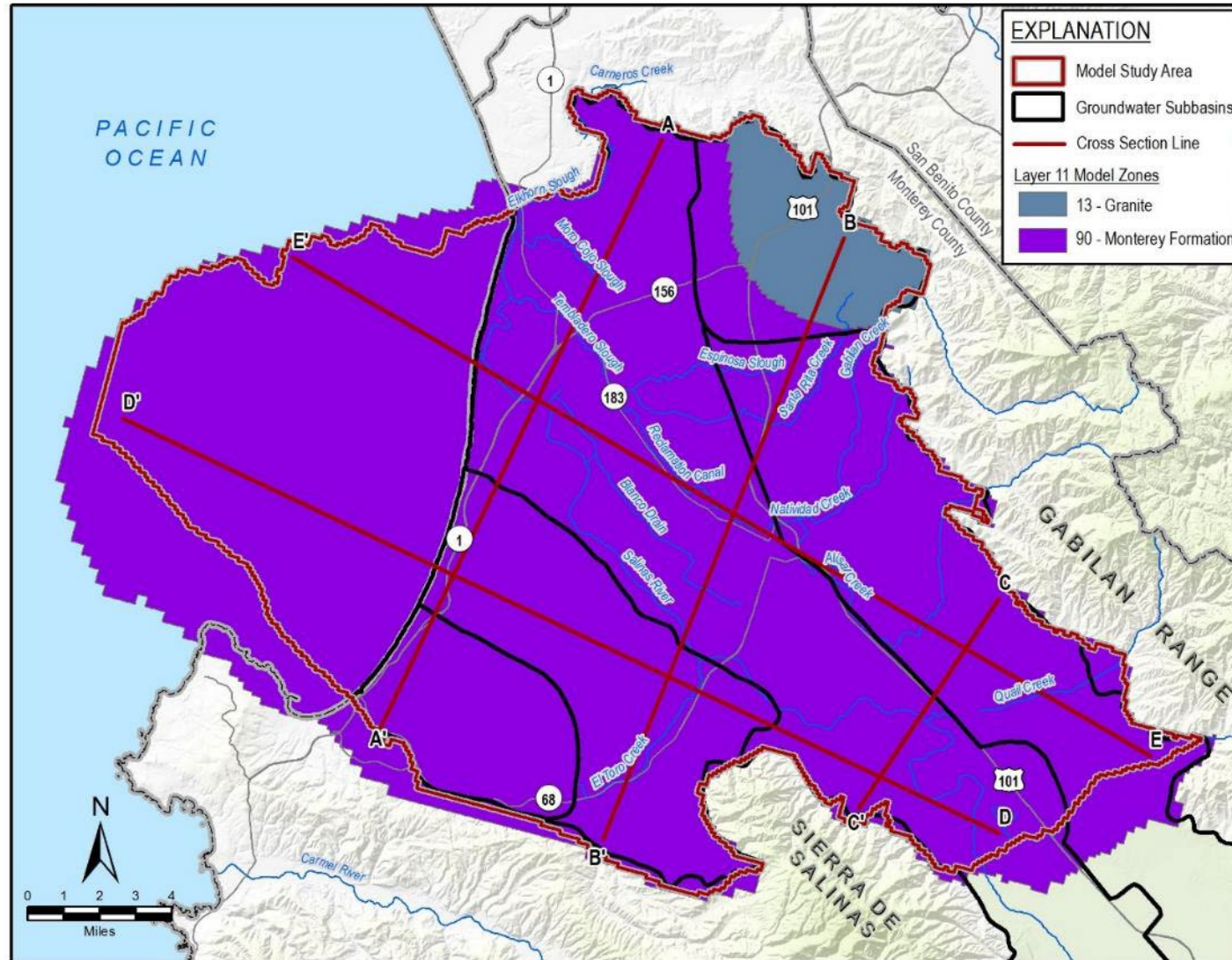


Figure 3-18. Model Hydrogeologic Zonation in Layer 11

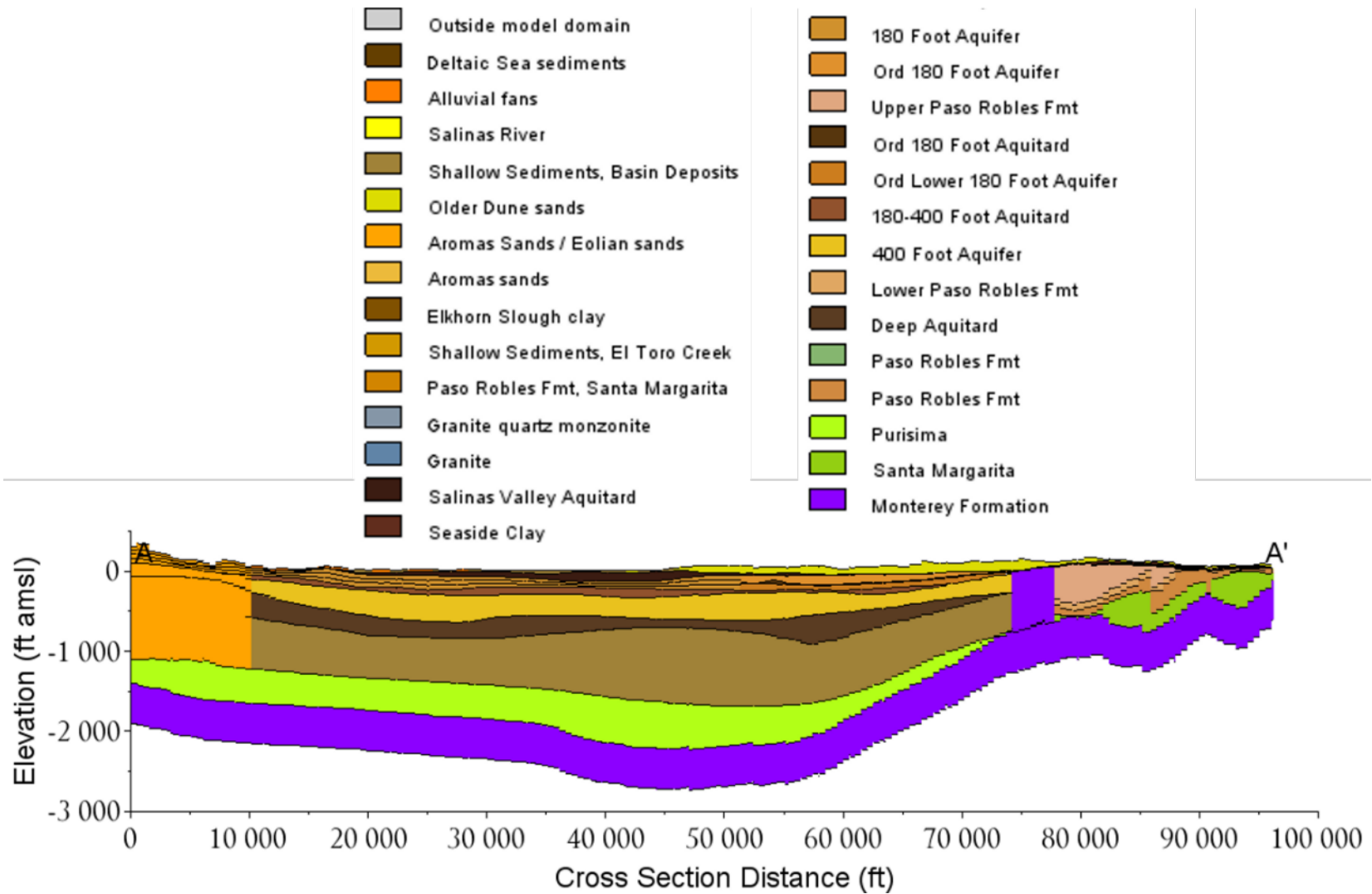


Figure 3-19. Model Hydrogeologic Zonation in Cross Section A-A'

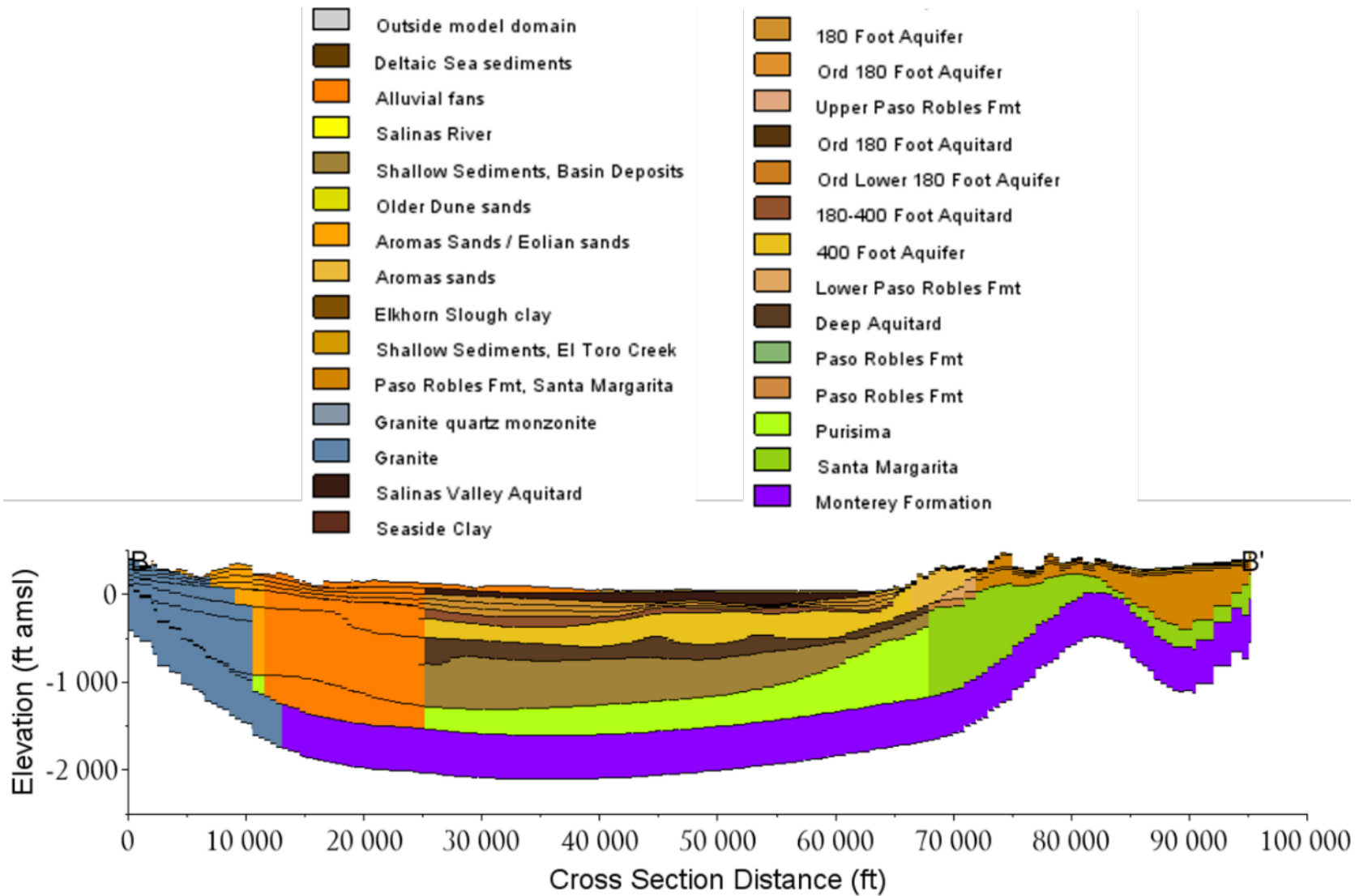


Figure 3-20. Model Hydrogeologic Zonation in Cross Section B-B'

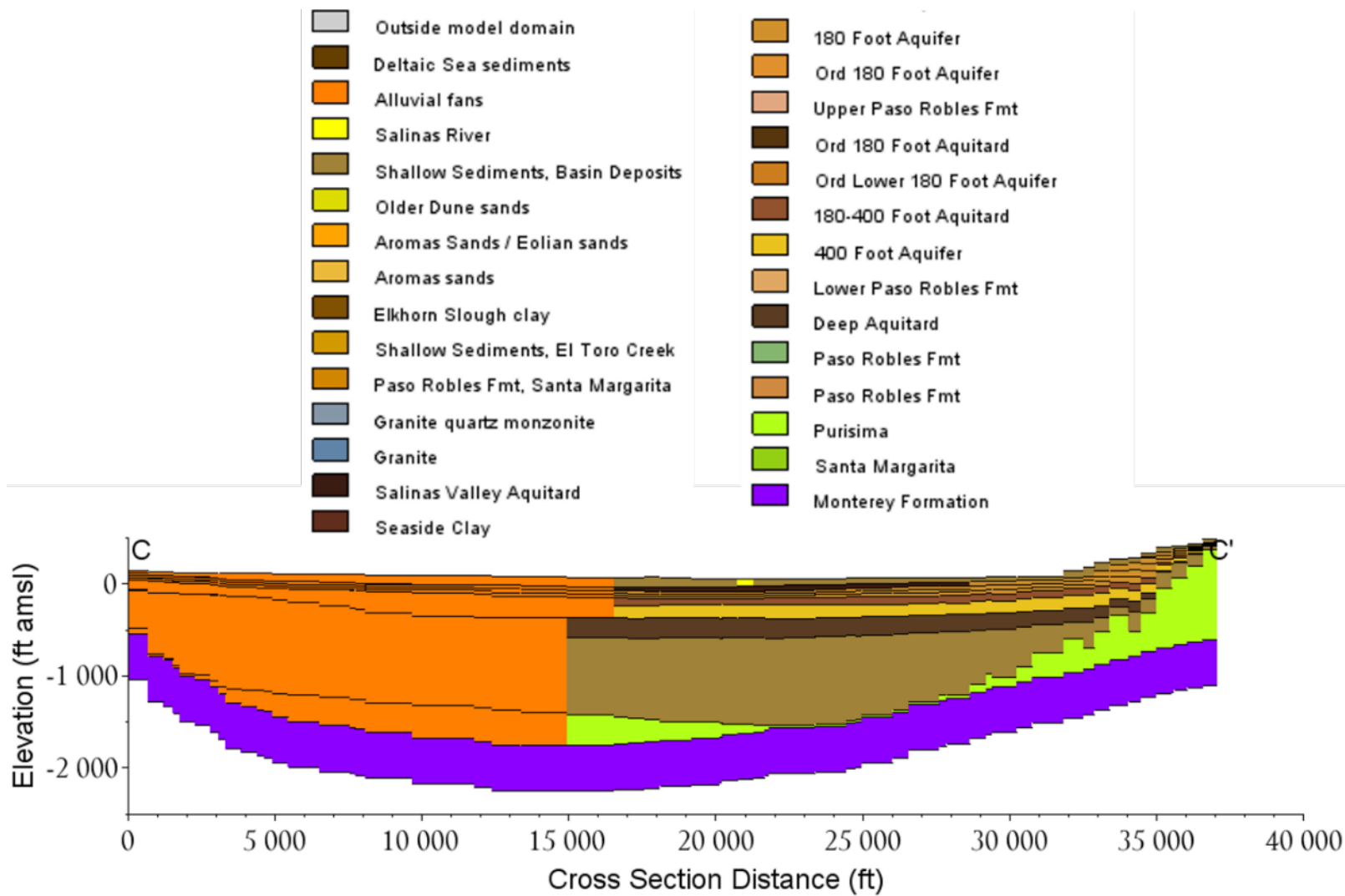


Figure 3-21. Model Hydrogeologic Zonation in Cross Section C-C'

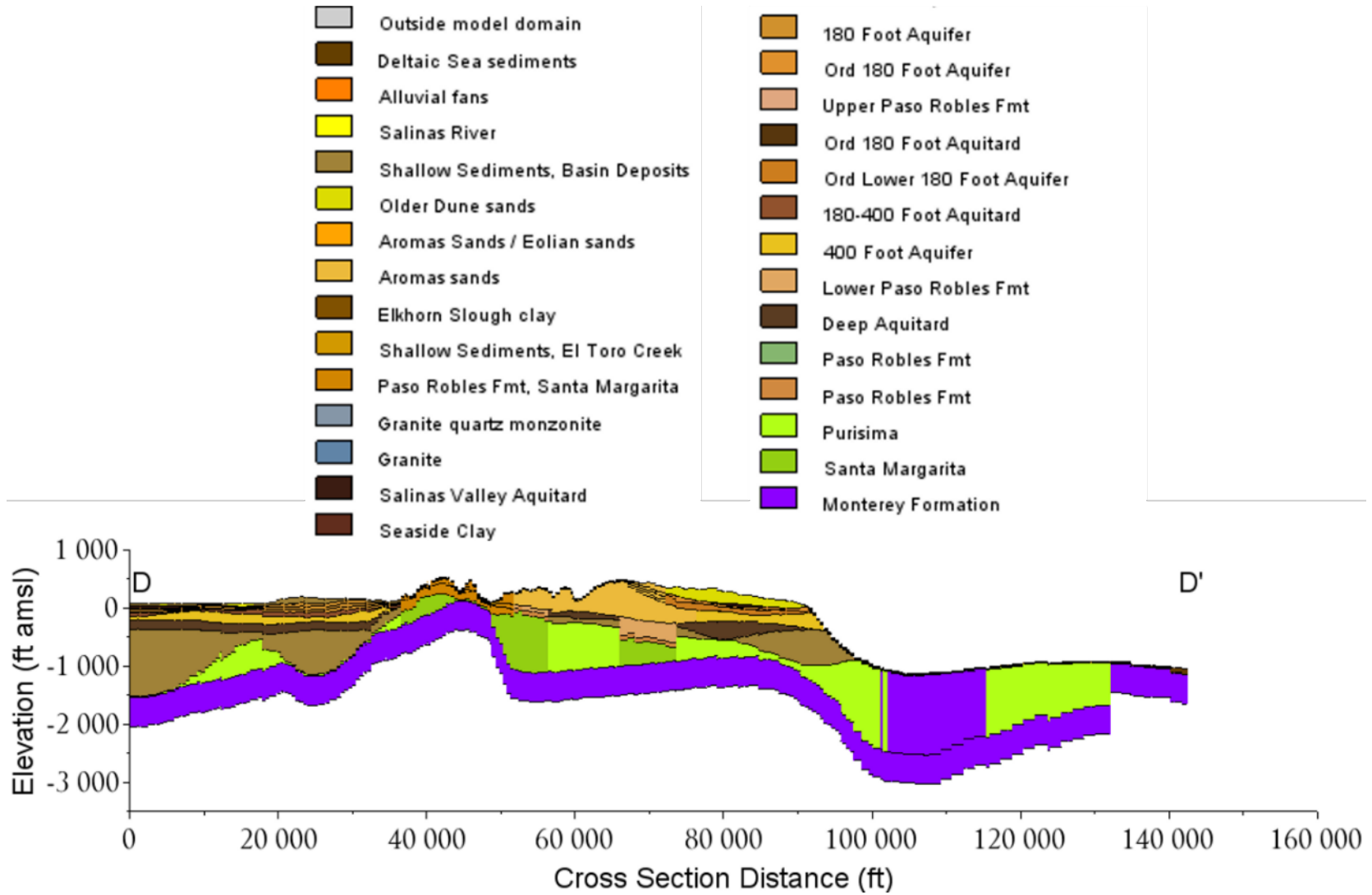


Figure 3-22. Model Hydrogeologic Zonation in Cross Section D-D'

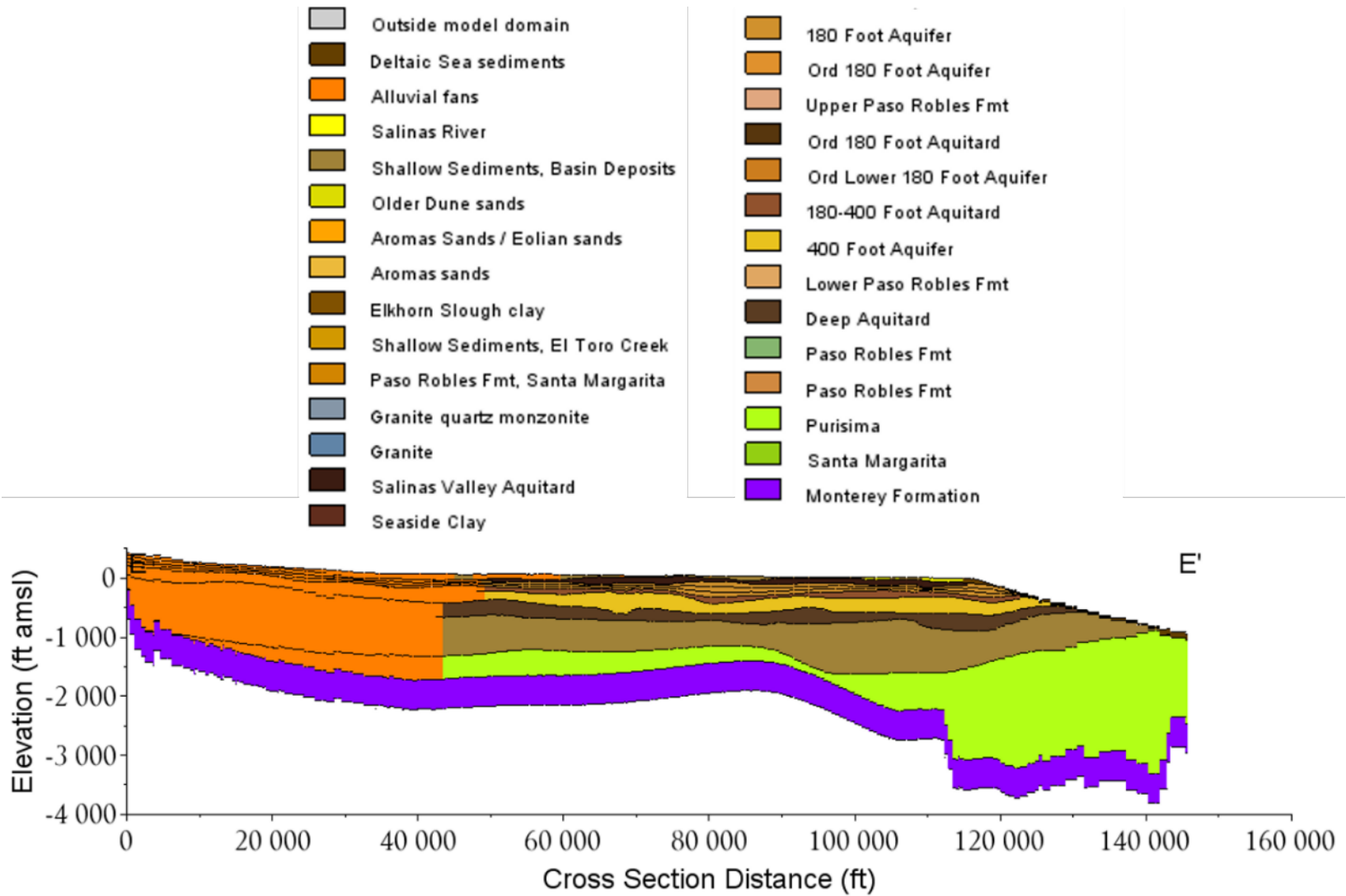


Figure 3-23. Model Hydrogeologic Zonation in Cross Section E-E'

4 MODEL CALIBRATION

Numerical model calibration is the process by which models are used to simulate hydrogeologic conditions measured in the past and adjust model parameters such that simulated historical conditions are approximated. Often this process is called history matching because the numerical model is used to match historical conditions. The hydrogeological historical conditions generally include historical groundwater levels and changes in levels, surface water flows, groundwater flows (e.g., groundwater budgets), and concentration (e.g., chloride concentration as a proxy for seawater intrusion).

Calibration is generally performed to condition the numerical model for simulation of future hydrogeologic stresses; if the model reasonably represents historical conditions, it is assumed that it would then be able to reasonably represent future stresses.

This section describes the SWI Model calibration results. The calibration of the SWI Model consisted of the following:

- Manual and automated calibration to hydrogeologic conditions at the end of WY 1984. This included calibration to groundwater levels and seawater intrusion between 1974 and 1985.
- Calibration of the historical period between 1985 and 2020. Calibration was focused on matching the extent of the historical seawater intrusion as depicted from the 500 mg/L chloride contour lines from MCWRA in the 180-Foot and 400-Foot Aquifers.
- Using the PEST software utilities, a set of models were developed that each reasonably matched both groundwater level data and chloride data. The set consisted of 105 versions of the SWI Model with hydraulic properties varying from model to model.
- Each of the 105 SWI Model versions were used to create electrical resistivity models. The resistivity models (and by analogue the SWI Model versions) were used to simulate AEM geophysical data collected in the area in 2017 and 2019. A comparison was made between the modeled AEM data and the measured AEM and each of the 105 SWI Model versions was ranked based on how well the AEM data were matched. See Section 4.4.
- One of the 105 SWI Model versions was selected as the calibrated model based upon its ranking of matching the AEM data, relative groundwater level calibration, and matching of historical 500 mg/L chloride concentration contours in the 180-Foot and 400-Foot Aquifers. It is this selected model whose calibration results are presented in this Section. See Section 4.4.



The following sections describe the various datasets used in the model calibration, the calibration results, and the development of the 105 SWI Model versions to assess uncertainty in model parameters. This includes the ranking of the model versions through matching the versions to AEM data. Finally, this section includes a discussion on simulated groundwater inflows and outflows.

4.1 Calibration Datasets

The SWI Model was calibrated to different types of data:

1. Groundwater levels
2. Chloride concentrations
3. Streamflow measurements
4. Airborne electromagnetic (AEM) measurements (geophysical data) (see Section 4.4)

Additionally, the calibrated model water budget was compared to independent estimates of water budget components to assess reasonableness.

4.1.1 Groundwater Levels

An initial water level dataset was developed from 174,804 measured water levels at 1,037 wells. This dataset was reduced in the following manner:

- A single water level was selected at each well location, for each model stress period. The median water level was selected when multiple water levels were present within a given stress period (e.g., water levels at different times within a stress period from the same location). The exception was for the stress period containing the 1975 to 1985 time period in which 2 water levels were selected: the earliest water level post-1975 and the latest water level pre-1985 which resulted in a water level target near 1975 and a second near 1985. This process reduced the number of water levels from 174,804 to 62,331.
- Water level wells located within the same model node were combined into 1 water level target location reducing the number of locations from 1,037 wells to 794 water level target locations. The wells were combined by combining the water level datasets from the wells. The water levels were then reduced again (as described above) so that only a single water level was utilized in each stress period.
- Additional de-clustering of target locations were accomplished by comparing target hydrographs of locations within a 750 feet radius horizontally and 300 feet vertically. For similar hydrographs, the targets were combined into a single location with water levels

combined as described above. This resulted in reducing the number of water level target locations from 794 to 671.

- Outliers on hydrographs were assigned a target weight of zero, removing it from the calibration. This reduced the number of water level targets from 62,331 to 45,515.
- Water level calibration locations were arranged into 5 groups: shallow sediments (or surficial sediments), 180-Foot Aquifer (or equivalent), 400-Foot (or equivalent), Deep Aquifers, and aquitards and bedrock (Monterey Formation).

Locations of water level target are shown on Figure 4-1. The target locations within the figure are arranged according to the HGU for which they represent.

4.1.2 Chloride Concentrations

The chloride concentration calibration dataset comprises 2 different types of data: chloride (or associated TDS) concentration measurements from water samples, and MCWRA-published 500 mg/L chloride concentration contours. A primary objective of the modeling was to simulate the second type of data or to simulate the 500 mg/L chloride concentration contour.

The chloride concentration dataset consisting of 812 locations and 14,915 measurements (Section 2.4) was reduced in a similar manner to the water level dataset, including:

- Reducing the number of locations from 812 to 633 by combining locations within the same model node
- Reducing the number of targets from 14,915 to 9,259 by using the median measurement within each stress period
- In areas outside of the seawater intrusion zone – where concentrations would be at background, measured chloride concentrations that varied from the background concentration of 55 mg/L were set to the background concentration (55 mg/L).

MCWRA regularly estimates the extent of the 500 mg/L contour line related to seawater intrusion (see Section 1 and Figure 1-3 and Figure 1-4) in both the 180-Foot Aquifer and 400-Foot Aquifer. To match these contours in the calibration, chloride concentration targets were created at various locations along the MCWRA contours for each data available. This added 144 chloride concentration targets.

The chloride calibration locations were grouped into the same 5 groups as the water levels targets. The target locations (colored according to the HGU to which they correspond) are shown on Figure 4-2.

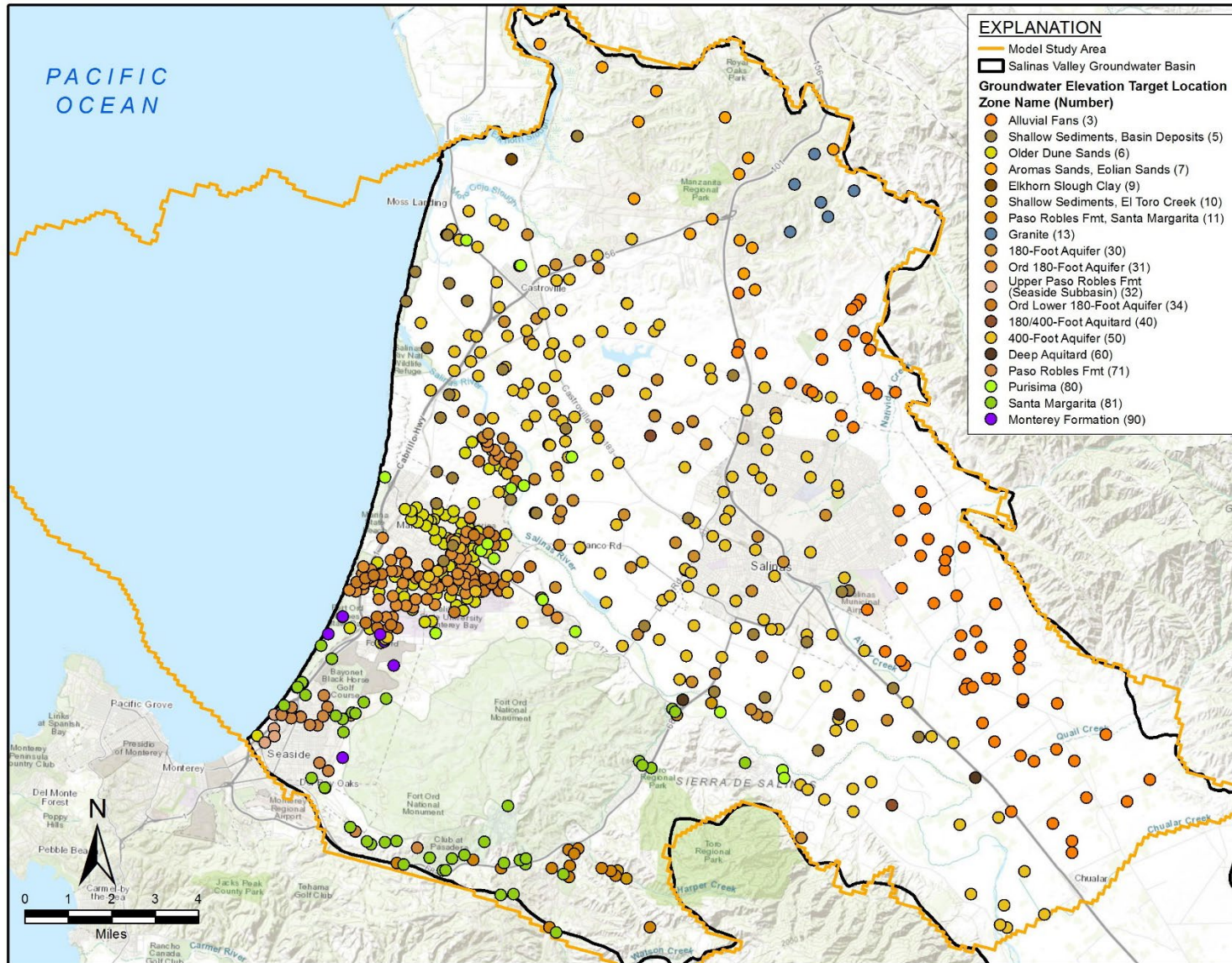


Figure 4-1. Water Level Calibration Target Locations with their Associated Calibration Group

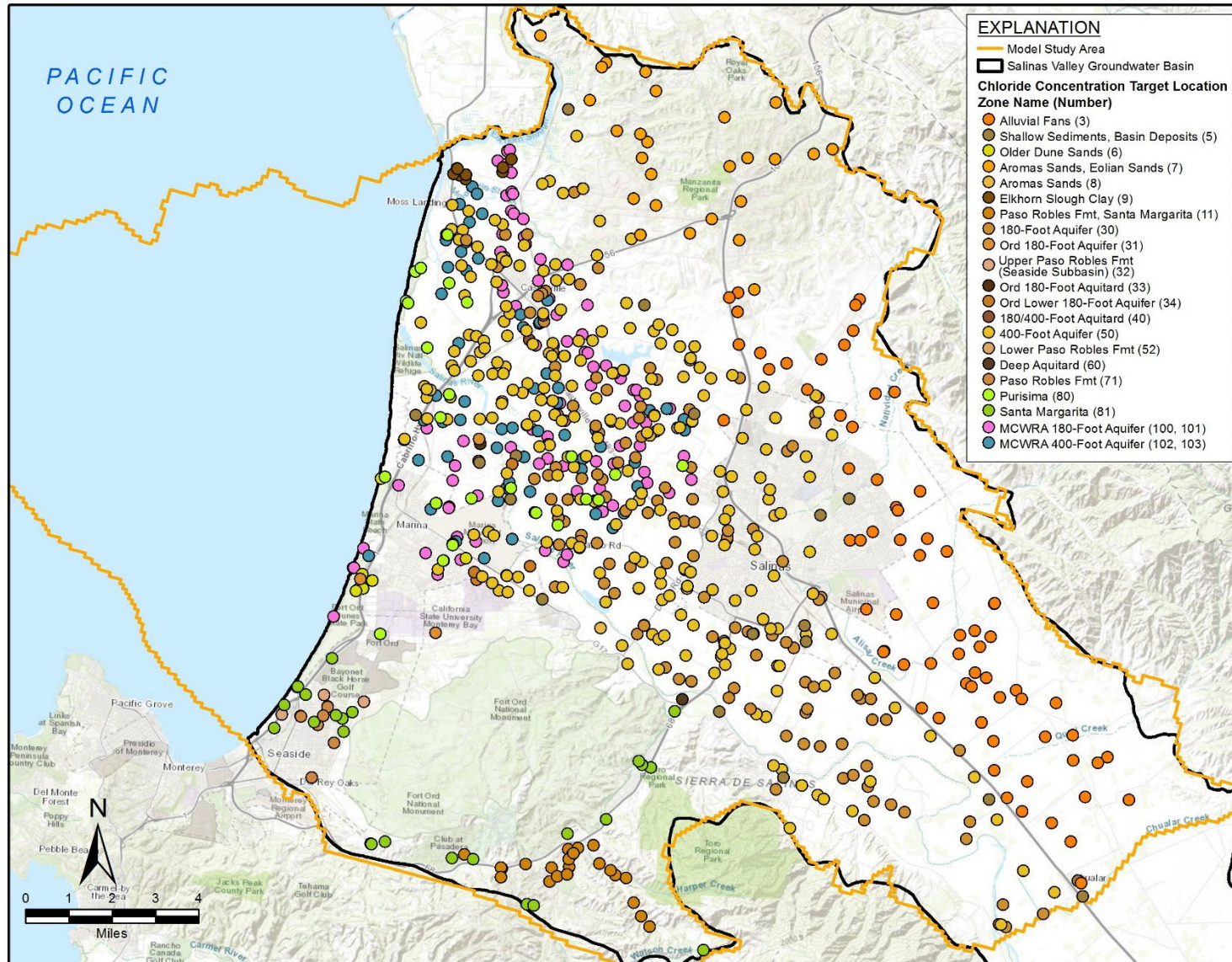


Figure 4-2. Chloride Calibration Target Locations with their Associated Calibration Group

4.1.3 Streamflow Measurements

Streamflow measurements from 4 stream gages within the model area are available (Figure 2-13 and Table 2-3). Two of these gages are on the Salinas River near Chualar and near Spreckels (Figure 2-14). Another gage is located on El Toro Creek and the fourth gage is located on Gabilan Creek (Figure 2-15). Data from the 2 Salinas River gages span the entire model time period (1975 through 2020). Data from the El Toro Creek gage is available from 1975 to 2001. Gabilan Creek gage data is available from 1975 to 2014.

4.2 Calibration Results

A combination of manual and automated methods were used to calibrate the SWI Model. Manual methods were used to make adjustments to the hydraulic conductivity with a focus on improving the match between the simulated extent of seawater intrusion in the 180-Foot and 400-Foot Aquifers and the published extent of the 500 mg/L chloride contour. Methods utilizing Parameter Estimation and Uncertainty Analysis (PEST) software (Watermark Numerical Computing 2020) automated the adjustment of hydraulic conductivity, specific yield and effective porosity, specific storage, dispersivity, and recharge to improve the fit between measured and simulated water levels and extent of seawater intrusion.

4.2.1 Water Levels and Chloride Concentrations

As described in Section 2.3, prior to anthropomorphic stresses to the groundwater system, groundwater movement within the basin is believed to have followed topography with groundwater flowing from the basin extents toward the axis and center of the basin and then along the axis toward ultimate discharge in Monterey Bay. As anthropomorphic stresses (e.g., groundwater pumping) were introduced in the basin, groundwater flow directions changed (and in some cases reversed) inducing seawater intrusion. By the middle of the twentieth century MCWRA had already begun monitoring and mapping the seawater intrusion. The model simulates a decline in water levels over time and a progression of seawater intrusion in both the 180-Foot and 400-Foot Aquifers. The simulated 500 mg/L Cl contour lines on Figure 4-3 and Figure 4-4 moves progressively inland through time following a progression similar to what was of the contours as reported by MCWRA.

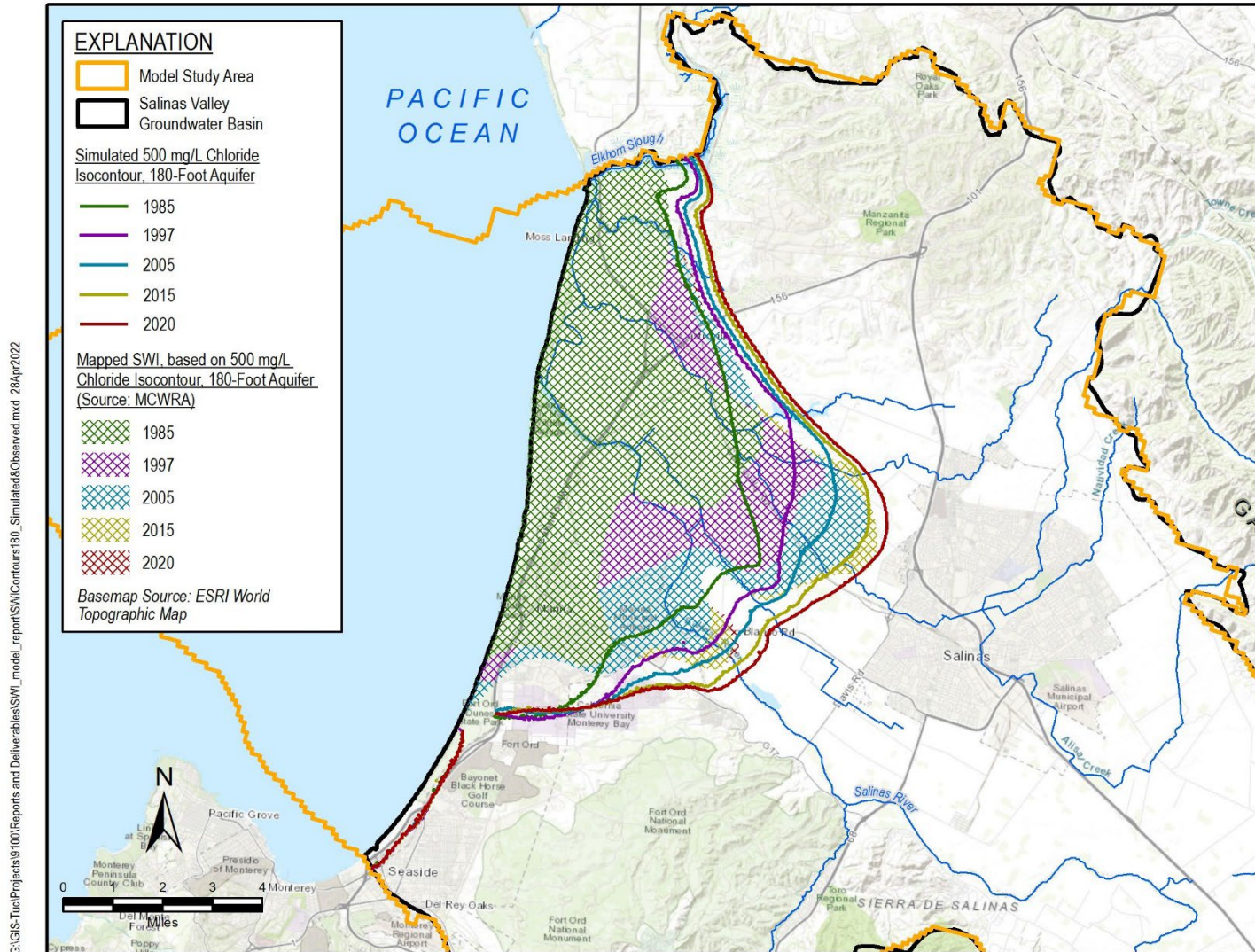


Figure 4-3. Simulated and Observed 500 mg/L Chloride Concentration Contours within the 180-Foot Aquifer in 1985, 1997, 2005, 2015, and 2020

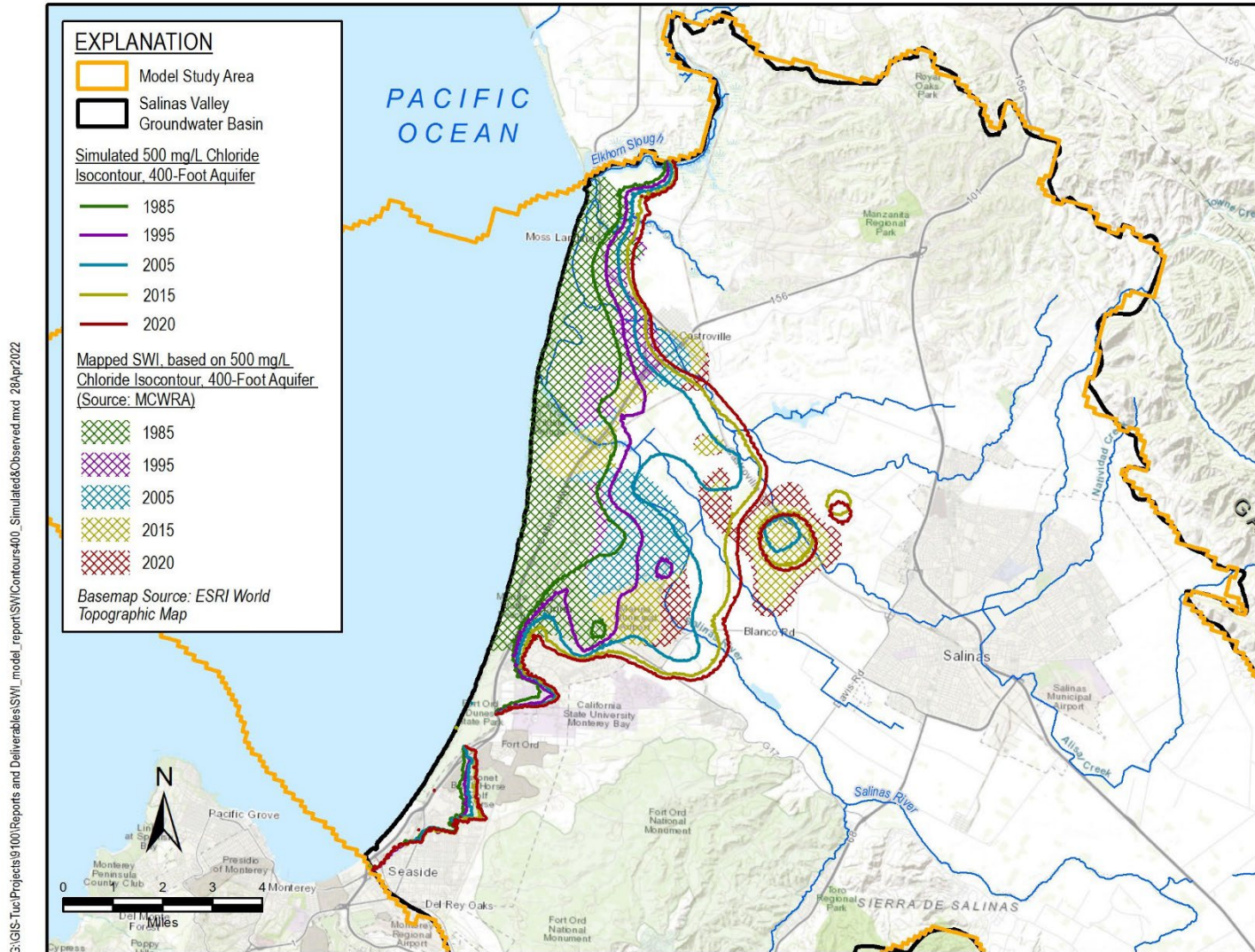


Figure 4-4. Simulated and Observed 500 mg/L Chloride Concentration Contours within the 400-Foot Aquifer in 1985, 1995, 2005, 2015, and 2020



The area focused on during the calibration process was surrounding the seawater intruded area along the coast. This calibration emphasis included groundwater levels and chloride concentrations. However, the primary calibration driver was the simulated extent of the 500 mg/L chloride contour line within the 180-Foot and 400-Foot Aquifers (Figure 4-3 and Figure 4-4). Beyond this area, simulate and observe water level differences are observed (as discussed below). However, throughout the area adjacent to the coast, there is a noticeable improvement in calibration both with respect to water levels and to chloride concentration.

4.2.1.1 Water Level Calibration

Table 4-1 shows the model groundwater level calibration statistics across the model and for equivalent aquifer model layers. The mean residual (observed minus simulated) is the mean of the residuals for a given location. If a water level mean residual for a given location were positive, then on average the simulated model would underpredict the water level for that location. The water level mean residual for the model is 33 feet, meaning that the model generally simulates groundwater levels that are 33 feet below measured. The model’s water level root mean squared error (RMS error) is 62 feet, indicating that simulated water levels are 62 feet off in either direction from measured. Calculated by the range in the measured values, the scaled RMS error and scaled residual mean are 7.46% and 3.95%, indicating that the model can be considered calibrated because these statistics are below 10%.

Calibration statistics for the surficial sediments (model layer 1 or the topmost layer of the model), the 180-Foot Aquifer model layers (model layers 3, 4, and 5), the 400-Foot Aquifer model layer (model layer 7), and the Deep Aquifers model layers (model layers 9 and 10) are listed in Table 4-1. The mean residual water level calibration statistic for all aquifers are positive showing that the model underestimates water levels. The mean residual water level statistics for each aquifer is lower than the whole model with the exception of the 400-Foot Aquifer which is 19 feet higher indicating the simulated water levels are underpredicted by a larger margin.

Table 4-1. Water Level Calibration Statistics

	Surficial Sediments	180-Foot Aquifer	400-Foot Aquifer	Deep Aquifers	All Data
Mean Residual (ft)	27.44	28.69	52.09	23.01	32.91
RMS Error (ft)	65.42	45.10	73.52	51.79	62.09
Number of Observations	14,709	12,781	9,751	7,251	45,599
Range in Observations (ft)	833	464	252	498	833
Scaled RMS Error	7.86%	9.72%	29.14%	10.41%	7.46%
Scaled Residual Mean	3.30%	6.18%	20.64%	4.62%	3.95%

Figure 4-5 and Figure 4-6 show the mean residual for each water level target in the model layers of the 180-Foot and 400-Foot Aquifers respectively. Green bubbles indicate the mean residual for that location is positive and simulated water levels underestimate measured. Orange bubbles indicate the mean residual for that location is negative and simulated water levels overestimate measured. If for a given location some of the simulated water levels are overpredicted (negative residual) and others were underpredicted (positive residual), the mean residual would be closer to zero because both positive and negative residuals were being averaged. As seen in the figures, the bubbles are mostly green showing the model underestimates water levels. Furthermore, in both figures, smaller bubbles (e.g., residual mean is smaller and indicative of a better calibration to measured values) are concentrated near the coast and progressively increase in size further inland. Meaning that simulated water levels along the coast (in areas most impacted by seawater intrusion) are better calibrated. This was expected as calibration in the seawater intrusion area was emphasized. In both figures, the larger bubbles are associated with the simulated water level depression to the south and southwest of the City of Salinas. The bubble plot for the 400-Foot Aquifer model layer (Figure 4-6) has noticeably larger bubbles than the plot for the 180-Foot Aquifer model layers (Figure 4-5) as is expected because the mean residual for the 400-Foot Aquifer model layer (~52 feet) is larger than that from the 180-Foot Aquifer model layers (~29 feet). Of note on Figure 4-6 is the cluster of orange bubbles along the southeastern portions of the model indicating the model overpredicts water levels whereas just to the south the bubbles are green and the model underpredicts water levels. Furthermore, the larger bubbles are concentrated in areas along the periphery of the model (to the northeast and to the south in the Coral de Tierra area) and it is likely that these areas – where the bubbles are larger – are responsible for the higher calibration statistics for the 400-Foot Aquifer (or equivalent) model layers.

The underprediction of water levels within the model is evidenced in the simulated and observed water level cross plot (Figure 4-7) by the majority of the points plotting below the 1-to-1 line. On this plot, the water levels that are representative of the better calibration are those that lie along or near the 1-to-1 line and are generally those between -100 ft bsl and 50 ft asl (along both axis – Observed and Simulated). These are the points that generally lie along the coast and those with smaller bubbles in the bubble plots (Figure 4-5 and Figure 4-6). The yellow circles (water level targets from the 400-Foot Aquifer model layer) that extend furthest below the 1-to-1 line would be those associated with the water level depression to the south and southwest of the City of Salinas.

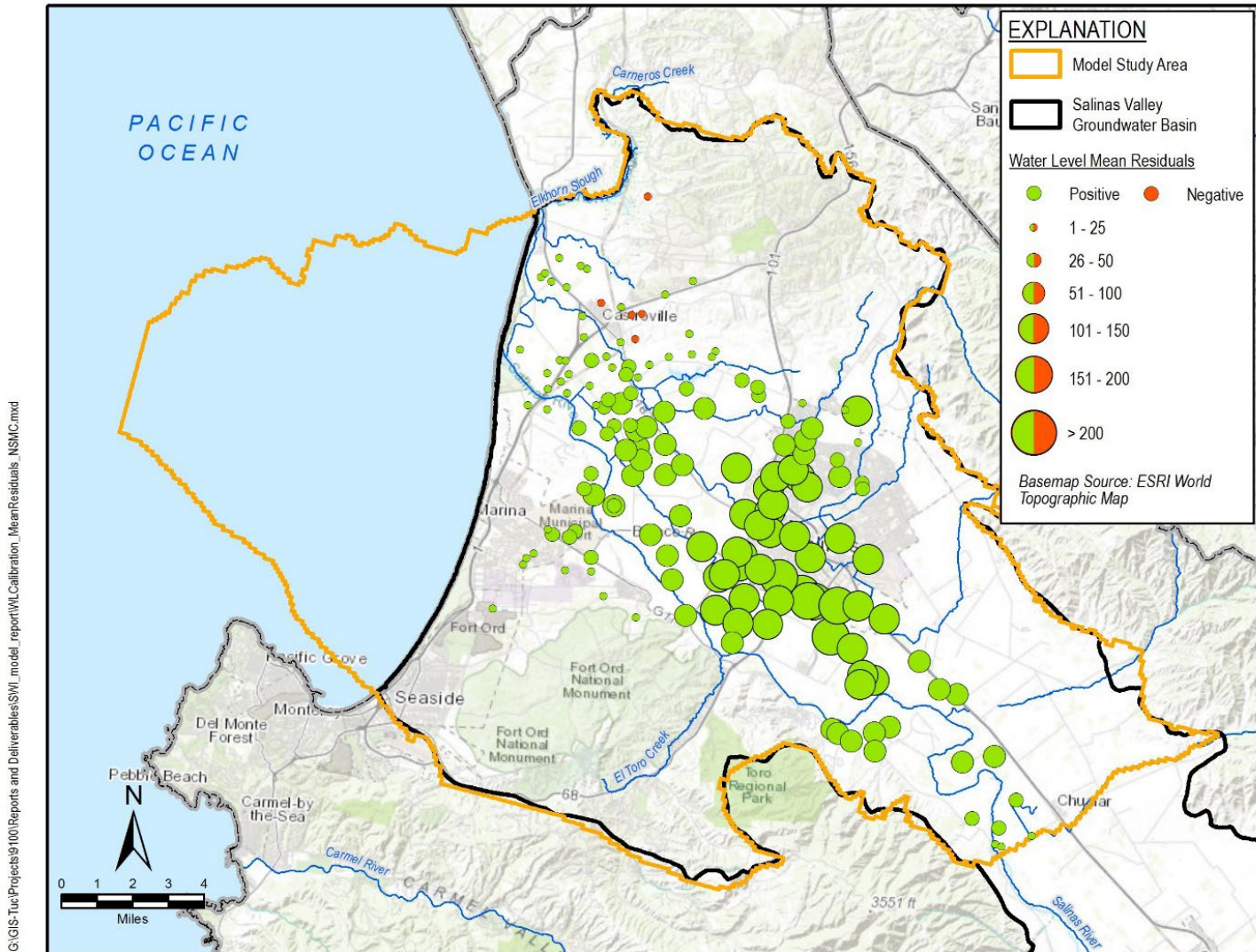
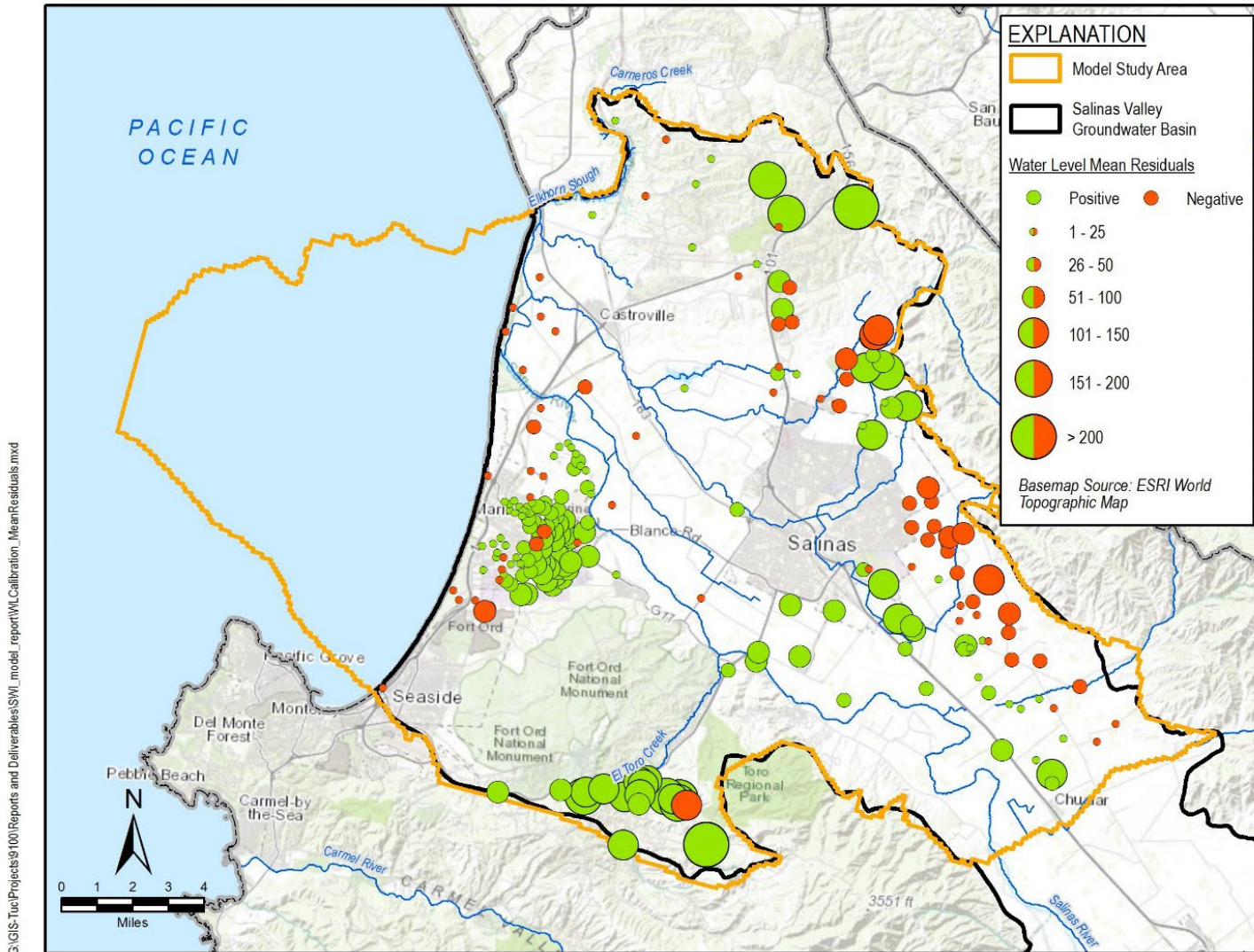


Figure 4-5. Mean Residual Water Level Bubble Plot within the 180-Foot Aquifer and Equivalent Areas



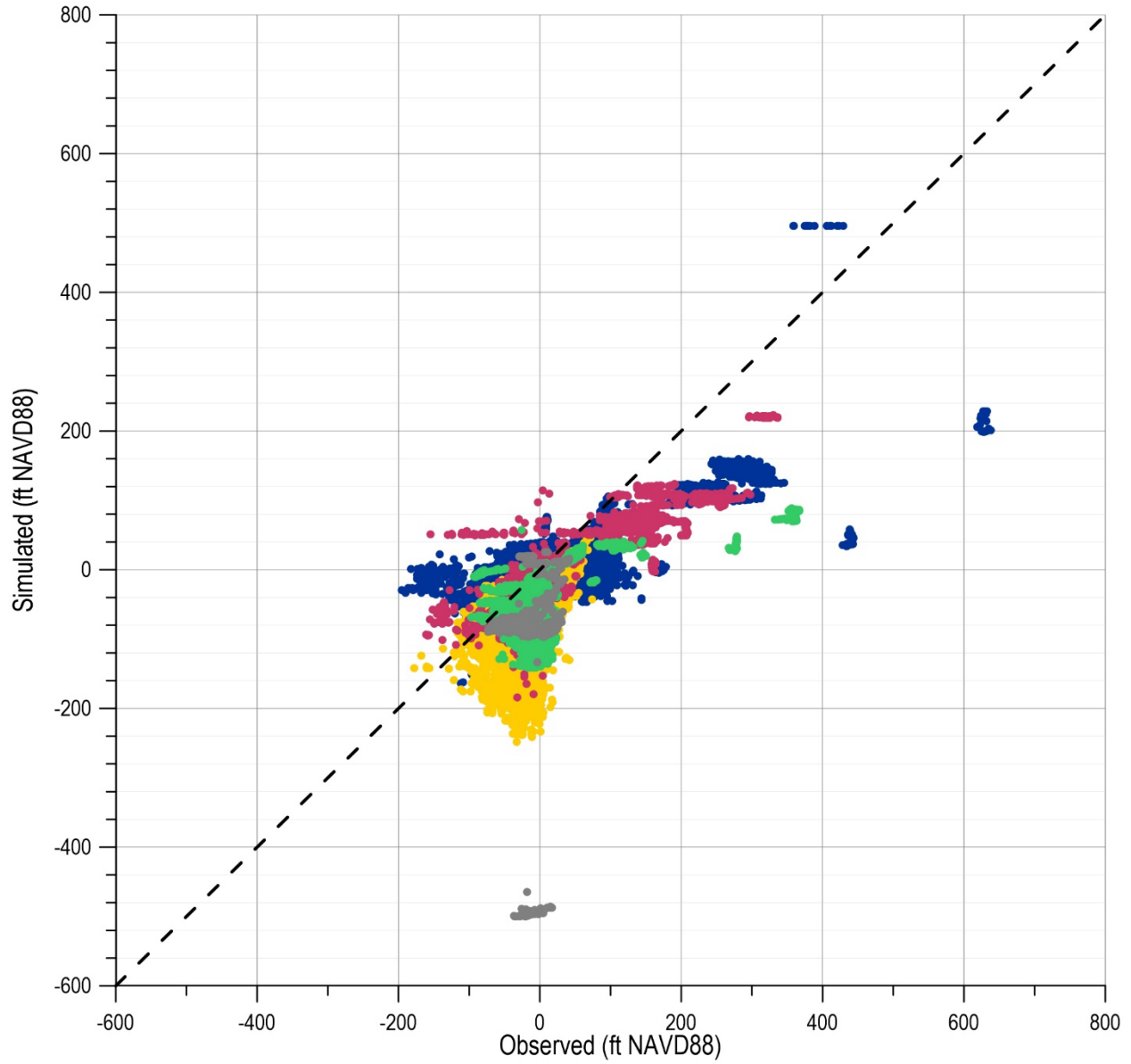
G:\GIS\Tuc\Projects\91001\Reports and Deliverables\SWI_model_report\WIL\Calibration_MeanResiduals.mxd

Figure 4-6. Mean Residual Water Level Bubble Plot within the 400-Foot Aquifer and Equivalent Areas

The red circles (water level targets from the Deep Aquifers model layers) that fall below the 1-to-1 line with observed water levels greater than 100 feet are from target locations in Seaside, Corral de Tierra, or the Ord National Monument where the topography can be generally elevated and the HGUs are those of the Deep Aquifers (e.g., Purisima, Santa Margarita, etc., and why they are grouped with the Deep Aquifers) but are currently not defined as part of the Deep Aquifers. Also, these locations are generally in topographically higher locations where the model does not simulate higher water levels well and where there is a greater underprediction of water levels. These areas generally aren't experiencing seawater intrusion and a focused calibration of these areas was not undertaken. Similarly, the blue circles (Surficial Sediments layer) below the 1-to-1 line with observed water levels greater than 100 feet are in Langley with higher topography where the model does not simulate higher water levels well.

As discussed in Section 2.3.1, water levels have been declining within the basin with varying rates over the past 30-plus years. Representative water level hydrographs in the 180-Foot Aquifer (Figure 2-5), 400-Foot Aquifer (Figure 2-6), and in the Deep Aquifers (Figure 2-7) are repeated here along with simulated hydrographs from the SWI Model (Figure 4-8, Figure 4-9, and Figure 4-10). All simulated and observed hydrographs are included in the Google Earth KMZ file distributed with the report (Appendix A). As discussed previously, the simulated hydrographs plot below the observed values (e.g., the simulated lines plot below the observed points in each of the charts). In most instances the simulated hydrograph trends match the observed (e.g., the observed water level trends are generally declining and the simulated water levels decline at roughly the same rates). The model is able to match seasonal trends in the hydrographs well in some cases and not in others which was expected as these seasonal trends (seasonal rise and fall of water levels) are likely related to seasonal variability in pumping with the model pumping having substantial uncertainty in regard to seasonal changes.

Simulated vs. Observed Water Levels



EXPLANATION	
● Surficial Sediments	● Deep Aquifer
● 180-Foot Aquifer	● Aquitards & Monterey Fmt
● 400-Foot Aquifer	- - 1:1 line

\\tuc-data\public\projects\9100_Salinas_GSP\Model Input Output\Docs and Memos\FullSWRReport_M&A\Tables\SV_SWL_uni_01k_NSMC_2.3b_WL_Calibration_1to1plot.gpj 3/10/2023

Figure 4-7. Simulated and Observed Water Level Crossplot

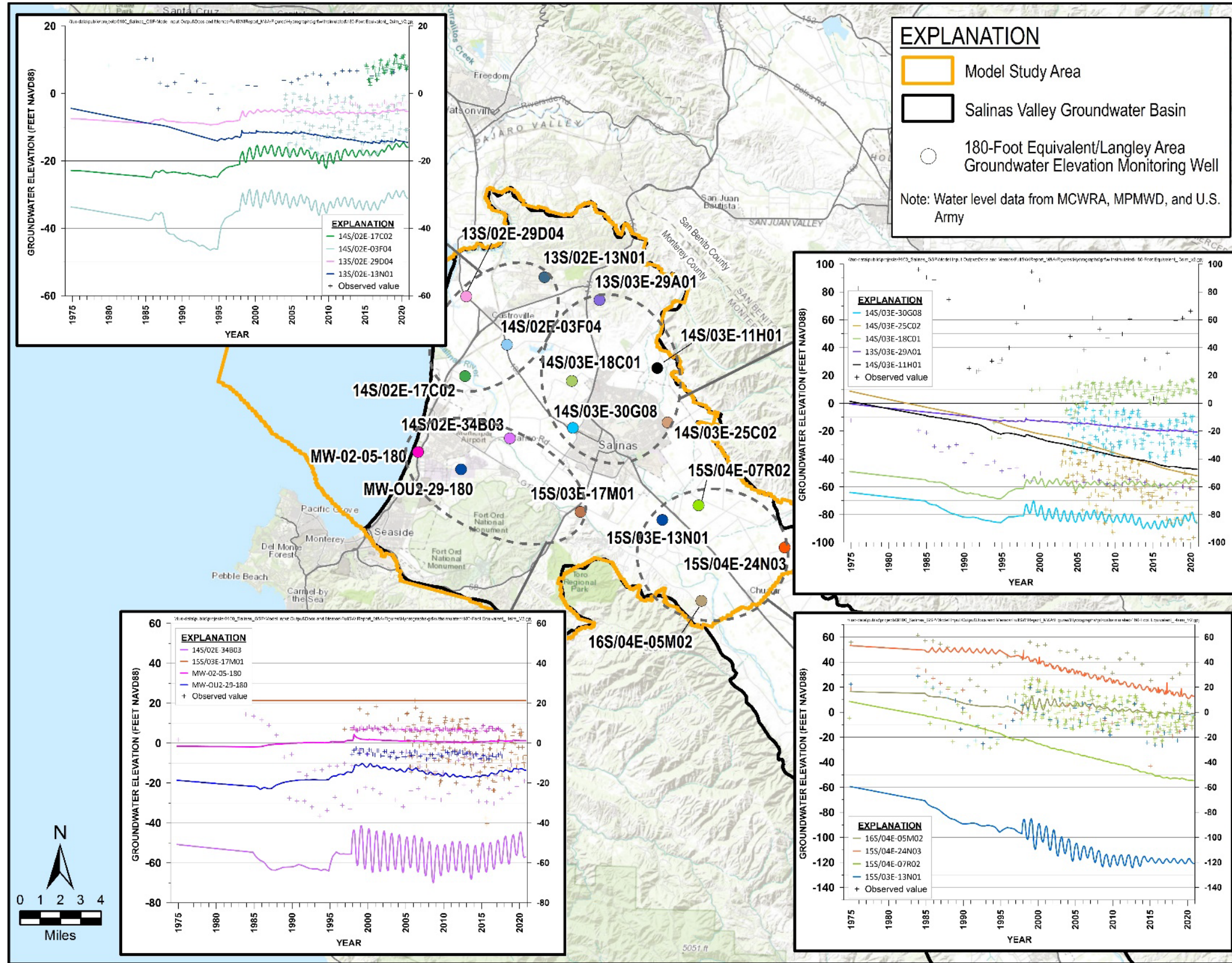


Figure 4-8. Observed and Simulated Representative Hydrographs within the 180-Foot Aquifer

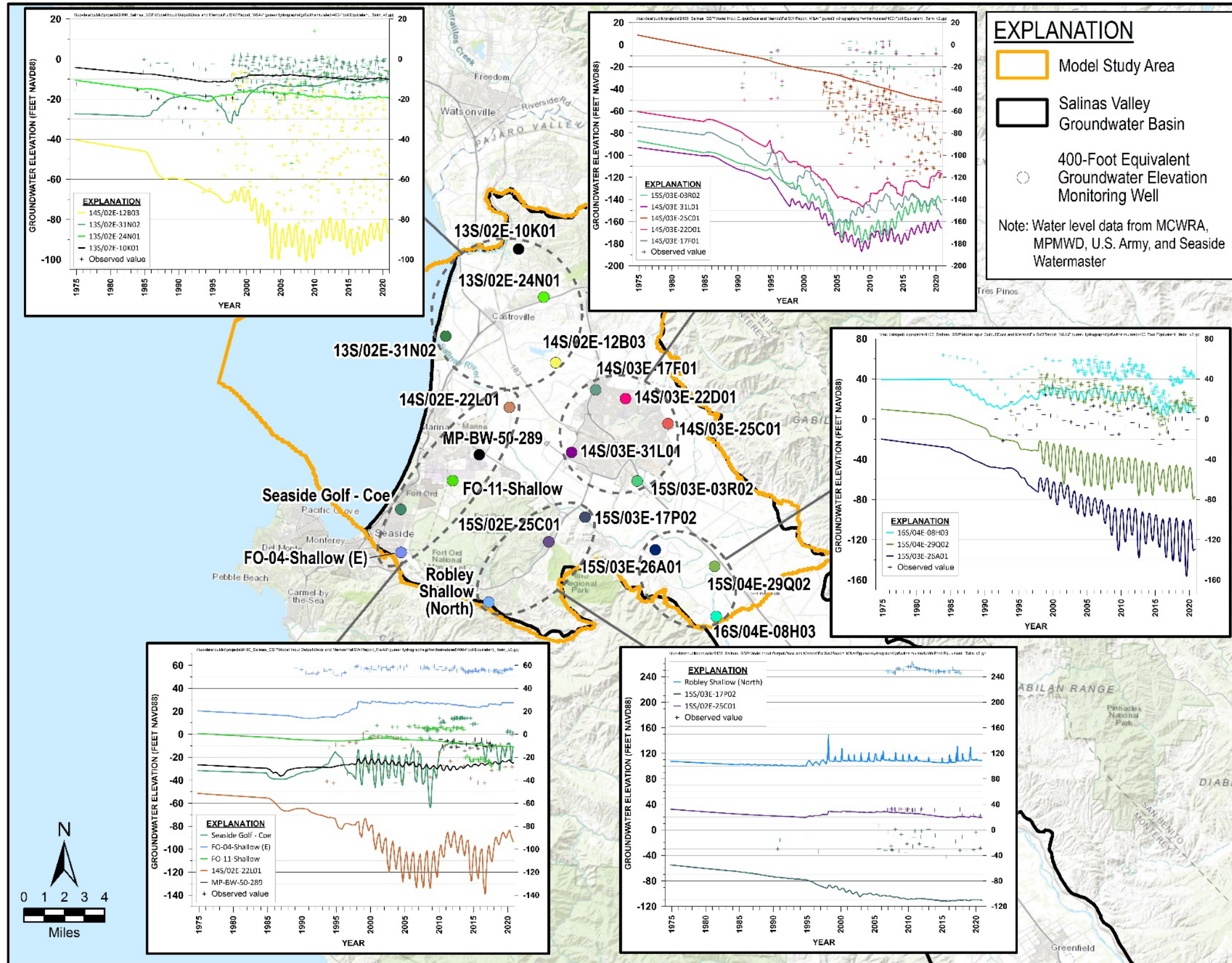


Figure 4-9. Observed and Simulated Representative Hydrographs within the 400-Foot Aquifer

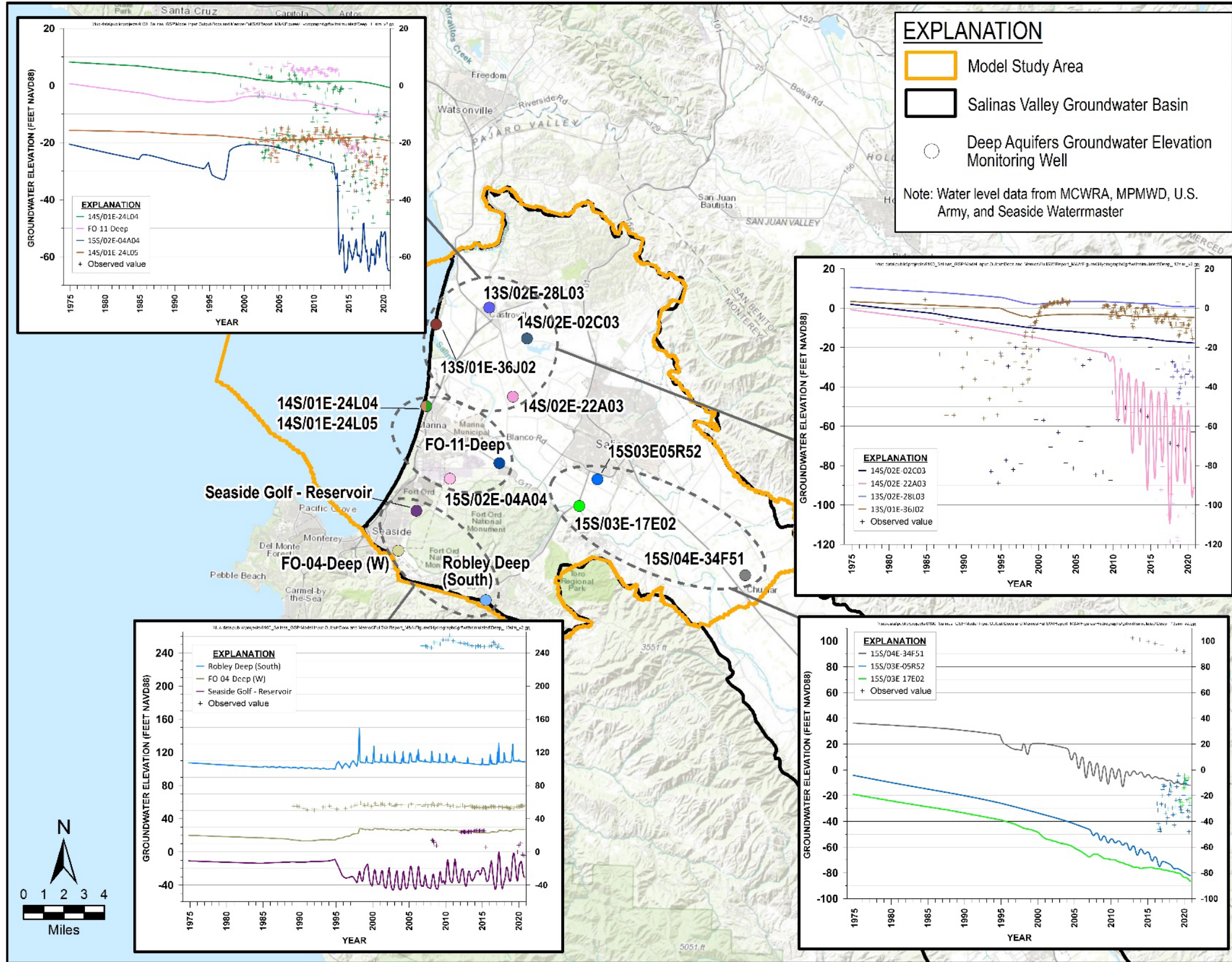


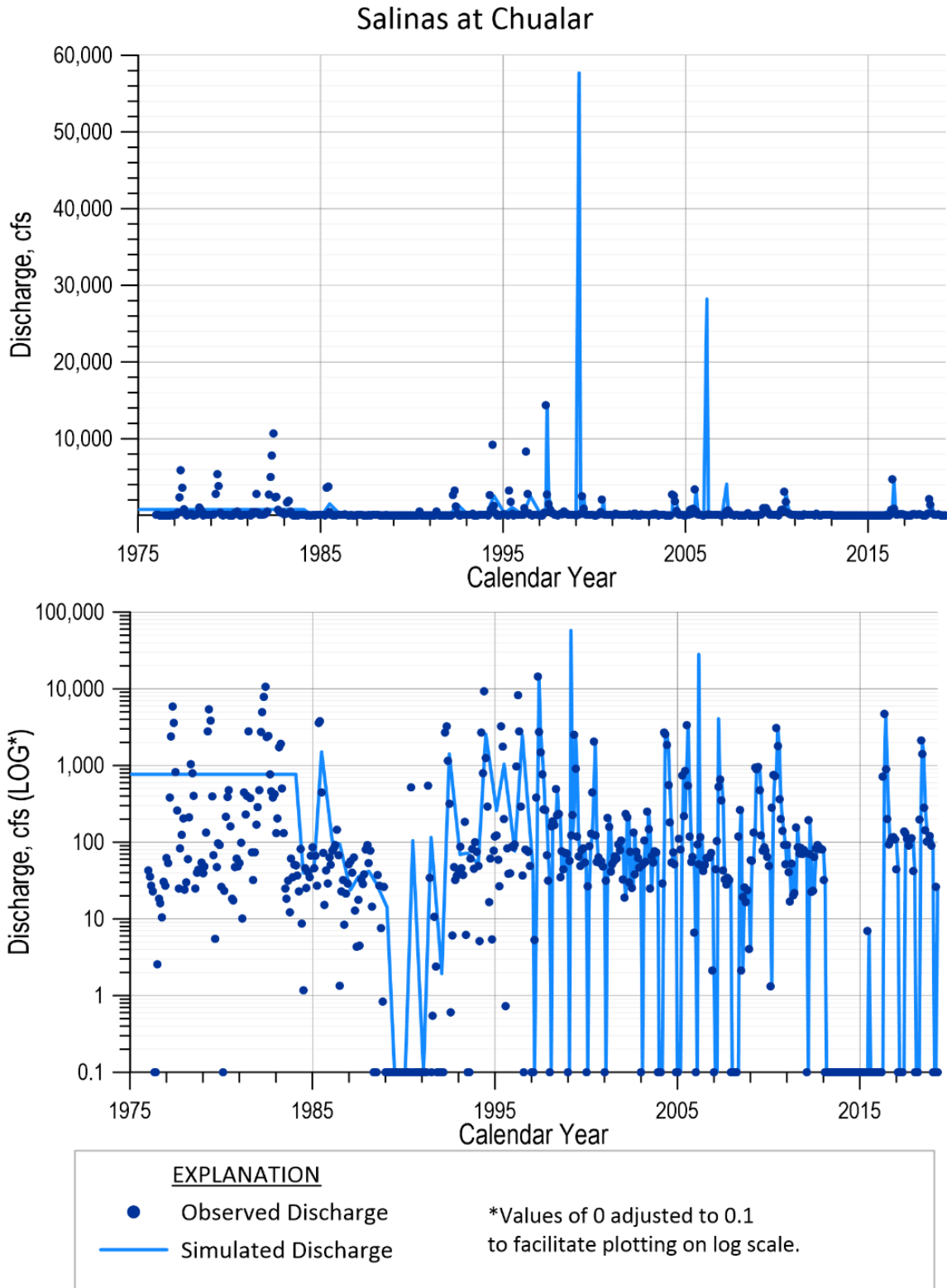
Figure 4-10. Observed and Simulated Representative Hydrographs within the Deep Aquifers

4.2.1.2 Chloride Concentrations Calibration

The landward migration of the 500 mg/L chloride concentration contour has historically been a measure of the extent of seawater intrusion in Salinas Valley (see Section 1) in both the 180-Foot and 400-Foot Aquifers. The primary focus of model calibration was to match this migration in both aquifers (see Figure 4-3 and Figure 4-4). In 1985 for the 180-Foot Aquifer, both the measured and simulated 500 mg/L chloride contours extend landward approximately 4.5 miles from the coast. However, that the measured maximum extent is approximately 2.5 miles to the north of the simulated maximum extent. This difference is likely due to model uncertainties in the hydrogeologic variability along the coast within the 180-Foot Aquifer and in model uncertainty of pumping rates and distribution prior to 1985. This uncertainty also largely contributes to the difference between observed and simulated water level depression (see Figure 4-5). The simulated 500 mg/L concentration contour was expected to increasingly resemble the measured contours as pumping information became more accurate in recent years. This is indeed the case as the maximum extent of the simulated and observed contours largely coincide beginning in 1997. The shapes of the simulated contour lines are also more representative of measured conditions than pre-1997. There are noticeable differences between the 2 – the simulated seawater intrusion to the south in Marina is more extensive than the observed contour line. There is also an area to the north of Blanco Road where no seawater intrusion is observed, but seawater intrusion is simulated there. This difference is likely due to hydrogeologic variations that are not fully captured in the model.

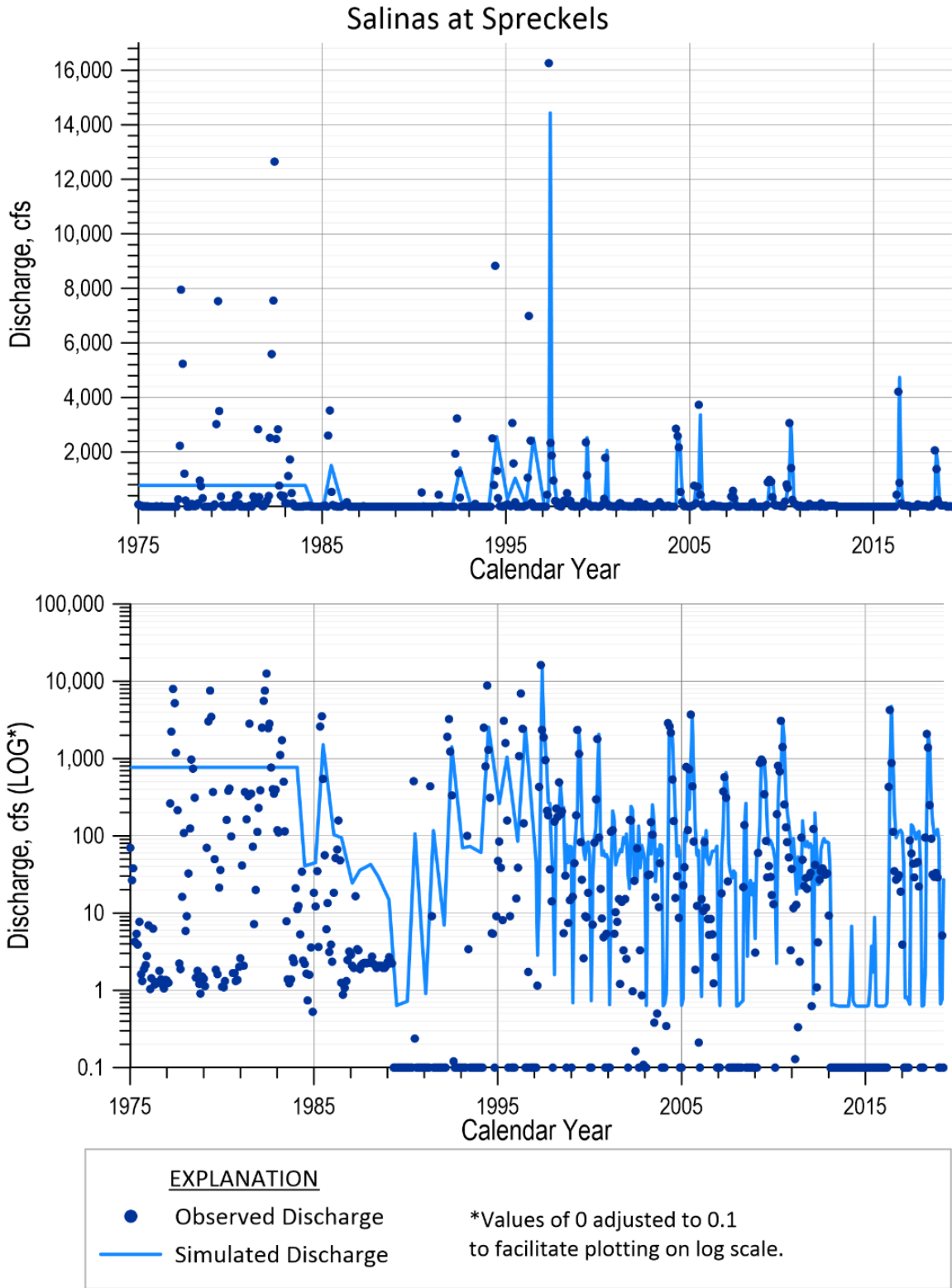
4.2.2 Surface Water Flows

The simulated and measured stream flows at the 4 gages in the model are shown on Figure 4-11 through Figure 4-14. In the Salinas River at Chualar (Figure 4-11) and the Spreckels gages (Figure 4-12), the simulated and measured river flows line up well. Similarly simulated and measured flow in Gabilan Creek (Figure 4-13) also match well. For each plot the simulated line passes through the observed points – both the highs and lows. Early in the simulation, from 1975 to 1985 when flows are held constant, the simulated stream flows are all constant yet pass through the middle of the observed data. In El Toro Creek the simulated flow appears to be less than measured but is still reasonable (Figure 4-14).



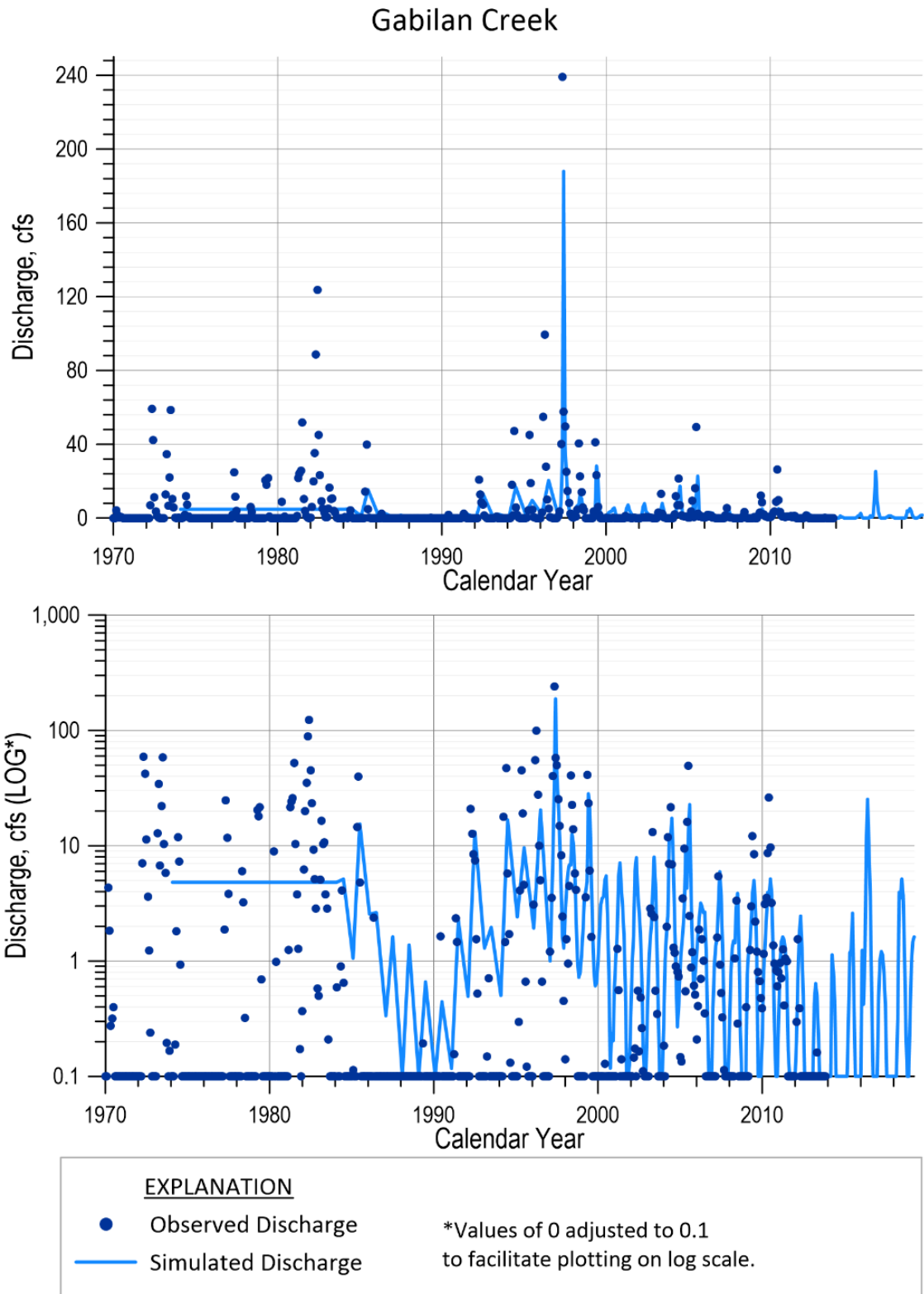
\\tuc-data\public\projects\9100_Salinas_GSP\Model Input Output\Docs and Memos\Full\SWIRReport_M&A\Figures\Hydrographs\Streamflow hydrograph\Stream_hydrograph_Salinas_Chualar.gpj 3/10/2023

Figure 4-11. Simulated and Measured Stream Flow in the Salinas River at the Gage near Chualar



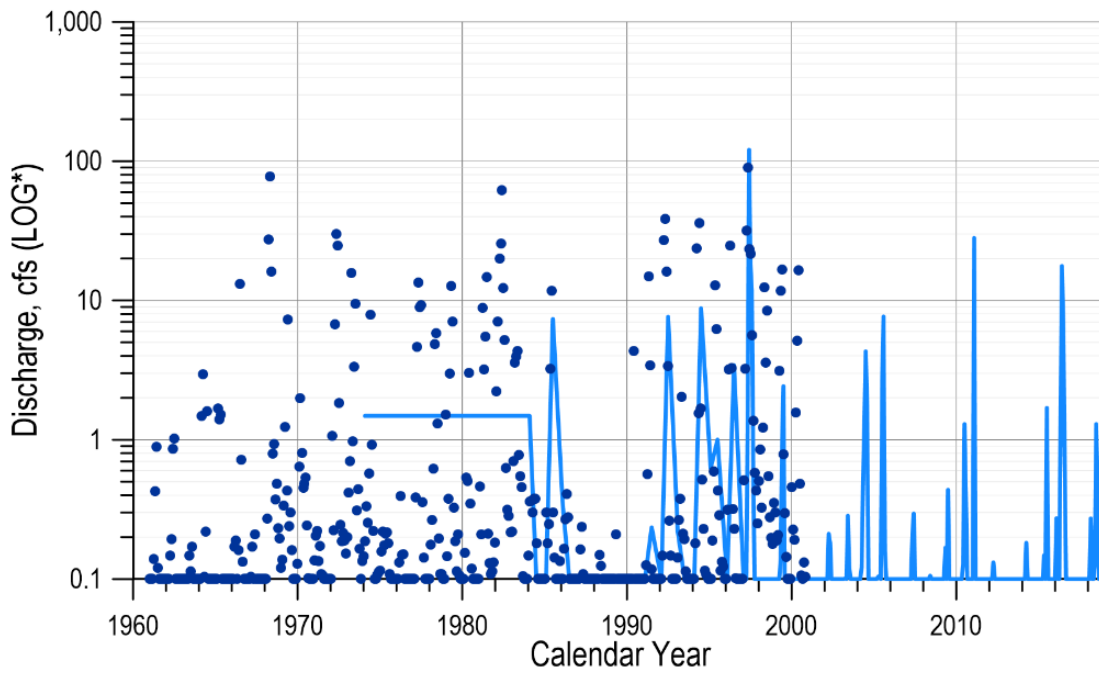
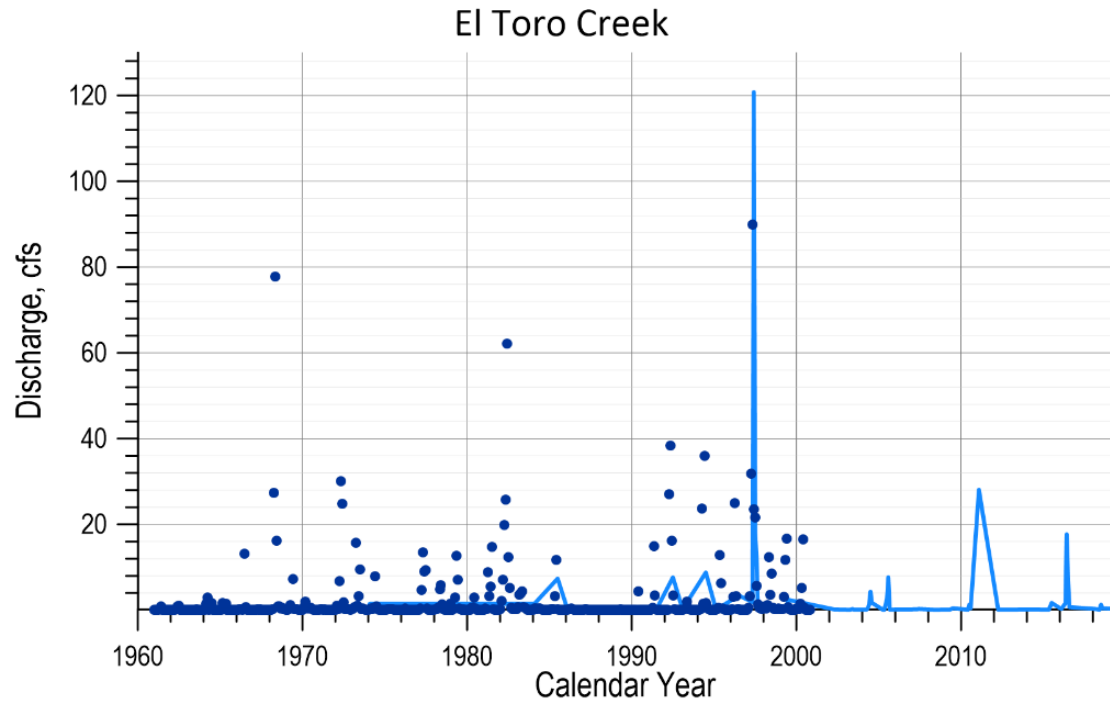
\\tuc-data\public\projects\9100_Salinas_GSP\Model Input Output\Docs and Memos\FullSWR\Report_M&A\Figures\Hydrographs\Streamflow hydrograph\Stream_hydrograph_Salinas_Spreckels.gpj 3/10/2023

Figure 4-12. Simulated and Measured Stream Flow in the Salinas River at the Gage near Spreckels



\\tuc-data\public\projects\9100_Salinas_GSP\Model Input Output\Docs and Memos\FullSWR\Report_M&A\Figures\Hydrographs\Streamflow hydrograph\Stream_hydrograph_Gabilan_Creek.gpj 3/10/2023

Figure 4-13. Simulated and Measured Stream Flow in Gabilan Creek



EXPLANATION	
●	Observed Discharge
—	Simulated Discharge
*Values of 0 adjusted to 0.1 to facilitate plotting on log scale.	

\\tuc-data\public\projects\9100_Salinas_GSPModel Input Output\Docs and Memos\FullSWIRReport_M&A\Figures\Hydrographs\Streamflow hydrograph\Stream_hydrograph_El_Toro_Creek.gpj 3/10/2023

Figure 4-14. Simulated and Measured Stream Flow in El Toro Creek

4.3 Calibrated Model Parameter Distributions

The model parameters that were adjusted during the calibration of the model include the following:

- **Hydraulic conductivity K (ft/day)** – both horizontal K (K_h) and vertical K anisotropy (K_{va} ; vertical K divided by horizontal K: K_h / K_v). Measured hydraulic conductivity for a given HGU generally varies spatially across several orders of magnitude (see Figure 2-10). Hydraulic conductivity (both K_h and K_{va}) vary between HGUs (see Figure 3-8 through Figure 3-23). In addition to varying by zone, K_h is varied within the zone using the pilot point methodology (Doherty *et. al.*, 2010). Each pilot point in a zone is assigned a K_h and K_{va} value and kriging of the pilot points within the zone is used to assign a spatially interpolated K value to each cell in the zone. Zones with only 1 pilot point have a uniform K distribution (homogeneous) within the zone (i.e., all model cells within the zone are assigned the same K value). Horizontal K varied spatially within the aquifers of the model but remained homogeneous within the aquitards (e.g., the SVA, etc.). Conversely the vertical hydraulic conductivity anisotropy is assumed to be homogeneous within each aquifer but varied spatially within the aquitards which allowed for spatial variation in the leakiness of the aquitards.

A summary of the K properties by zone (HGU) is included in Table 4-2. The parameter values presented in Table 4-2 represent the calibrated values used in the final calibration model and attainment of the values is discussed further in Section 4.4. Comparison of the hydraulic conductivity ranges of the pilot points from Table 4-2 to the measured ranges from Figure 2-10 show they are in agreement. The 180-Foot Aquifer pilot points (HGU zones 30, 31, and 32) range from 11 to 191 ft/day and fall with the measured ranges. Likewise, the 400-Foot Aquifer (HGU zone 50) pilot point K ranges from 2 to 32 and is within the lower two-thirds of the measure range. The measured range of the Eastside Alluvial fans is narrow due to limited data, thus the pilot points for this HGU (zones 3 and 53) have a broader range. The pilot point K range for the Paso Robles Formation (HGU zones 11, 32, 52, 70, and 71) lies between 1 and 23 ft/day which is within the measured range. The Dune Sands and the Aromas Sands (HGU zones 6, 7, and 8) pilot point K values range from 12 to 50 ft/day which is within the middle of the measured range. As with the Eastside Alluvial fans, the Sant Margarita measure range is somewhat narrow with the simulated value of the HGU (HGU zone 81) falling just below the measured range at 3 ft/day. Figure 4-15 shows the locations of the pilot points and how they are distributed throughout the model area. The hydraulic conductivities of the pilot points were varied throughout the calibration process with particular focus on the pilot points of the 180-Foot and 400-Foot Aquifers to better match the measured 500 mg/L chloride contours.



- **Storage parameters.** Both specific yield (S_y) and specific storage (S_s) (ft^{-1}) were varied during the calibration process and were zonal properties meaning they were homogeneous within each HGU, but were varied between HGUs. For transport, effective porosity was assumed to be equal to S_y . Storage parameters for each HGU are listed in Table 4-2. The parameter values presented in Table 4-2 represent the calibrated values used in the final calibration model and attainment of the values is discussed further in Section 4.4.
- **Dispersivity (ft).** Based upon review of literature values (see Section 2.5 and Figure 2-12) an initial longitudinal dispersivity of 30 feet was applied across the entire model domain with transverse dispersivity equal to 10% of longitudinal (3 feet) and vertical dispersivity 10% of transverse (0.3 feet) (Gelhar *et al.*, 1992). During calibration, the dispersivity varied with a final value at 60 feet, 6 feet, and 0.6 feet for the longitudinal, transverse, and vertical dispersivity respectively.
- **Recharge.** As discussed in Section 2.7.1.1 and Section 3.10 recharge varied both temporally and spatial in the model. Static recharge multipliers were applied to recharge zones (Figure 2-18); the final multiplier values are listed in Table 4-3.

Table 4-2. Summary of Calibrated Hydraulic Conductivity (K) and Storage Properties of the HGUs within the Model

HGU Zone Number	HGU Description	K _h and K _{va} Number of Pilot Points	K _h Pilot Point (ft/day)		K _{va} (K _v / K _h)		Specific Yield (Sy) Effective Porosity	Specific Storage (S _s) (ft ⁻¹)
			Minimum	Maximum	Minimum	Maximum		
2	Deltaic Sea Sediments	1	398	398	0.095	0.095	0.0821	0.0043
3	Alluvial Fans (Shallow)	12	2.05	10.5	0.034	0.037	0.195	0.00074
4	Salinas River	1	176	176	0.12	0.12	0.232	0.0015
5	Shallow Sediments, Basin Deposits	6	11.0	32.8	0.045	0.10	0.185	0.0010
6	Older Dune Sands	13	12.3	72.9	0.11	0.44	0.263	0.0010
7	Aromas Sands Eolian sands	4	49.5	49.5	0.11	0.11	0.220	0.00062
8	Aromas Sands	3	50.2	50.2	0.090	0.090	0.165	0.000062
9	Elkhorn Slough clay	1	1.34	1.34	0.0010	0.0010	0.102	0.000090
10	Shallow Sediments, El Toro Creek	1	79.3	79.3	0.13	0.13	0.168	0.0014
11	Paso Robles Formation, Santa Margarita	5	1.85	1.85	0.10	0.10	0.168	0.00014
13	Granite	1	0.688	0.688	0.94	0.94	0.208	0.0000051
20	Salinas Valley Aquitard	8	0.0125	0.0125	0.063	0.14	0.120	0.000010
21	Seaside Clay	1	0.00843	0.00843	0.14	0.14	0.120	0.000010
30	180-Foot Aquifer	19	11.4	184	0.038	0.77	0.117	0.000036
31	Ord 180-Foot Aquifer	11	30.0	191	0.042	0.048	0.160	0.000036
32	Upper Paso Robles Formation	3	3.75	3.75	0.097	0.097	0.168	0.00014
33	Ord 180-Foot Aquitard	4	0.00557	0.00557	0.30	0.30	0.128	0.0000036
34	Ord Lower 180-Foot Aquifer	9	87.5	169	0.028	0.028	0.160	0.000036
40	180-400 Foot Aquitard	8	0.00812	0.00812	0.031	0.14	0.120	0.000010
50	400-Foot Aquifer	21	2.25	32.0	0.086	0.22	0.153	0.00010
52	Lower Paso Robles Formation	2	5.01	5.01	0.0040	0.0040	0.168	0.00014
53	Alluvial Fans (Deep)	6	4.00	15.0	0.0038	0.011	0.195	0.00074
60	Deep Aquitard	6	0.00807	0.00807	0.085	0.15	0.120	0.000010
70	Paso Robles Formation	11	1.10	19.0	0.053	0.11	0.168	0.00014
71	Paso Robles Formation	3	23.5	23.5	0.079	0.079	0.168	0.00014
80	Purisima	5	1.49	1.49	0.33	0.33	0.150	0.000075
81	Santa Margarita	5	3.00	3.00	0.12	0.12	0.150	0.000075
90	Monterey Formation	1	0.00684	0.00684	0.093	0.093	0.150	0.00010

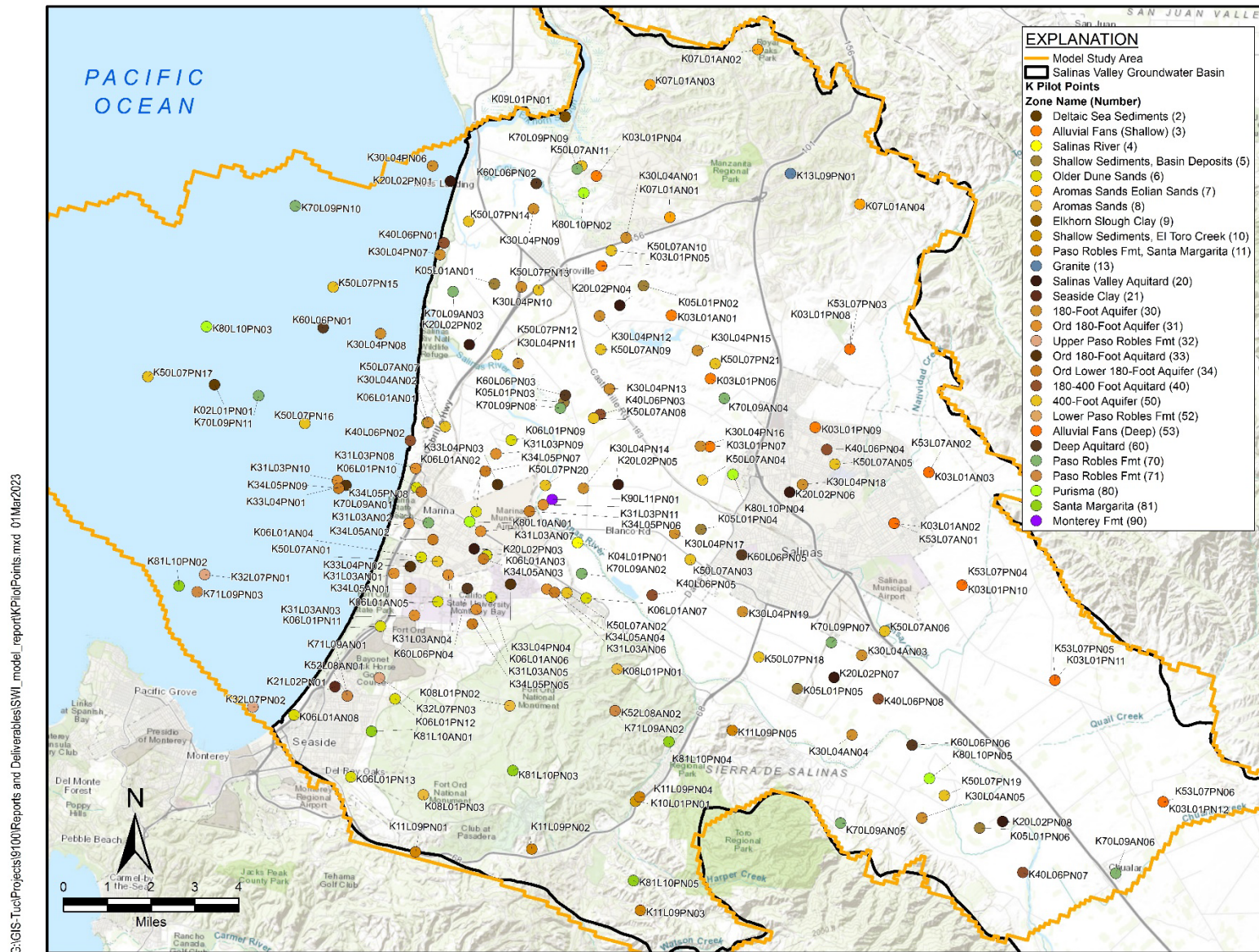


Figure 4-15. Hydraulic Conductivity Pilot Points Used during Model Calibration

Table 4-3. Calibrated Recharge Multipliers

Recharge Zone	Recharge Area	Comment	Recharge Multiplier
1	Urban – City of Salinas		1.27
2	Urban – City of Marina		0.948
3	Urban – City of Seaside		1.07
4	Urban – Castroville and Chualar		0.926
5	Granite Ridge		0.926
6	Highlands South		0.926
7	CSIP Area		1.02
8	Pressure Northeast	West of Salinas	0.861
9	Pressure Southwest	West of Salinas	1.00
10	East of Seaside		1.00
11	Southwest Region		0.962
12	Corral De Tierra		0.962
13	Blanco Drain Area		0.994
14	Eastside	Northwest of Salinas	0.890
15	Eastside	East of Salinas	1.00
16	Pressure Northeast	East of Salinas	1.01
17	Pressure Southwest	East of Salinas	1.01
18	Salinas River		1.00

4.4 Model Parameter Uncertainty Runs and Matching AEM Data

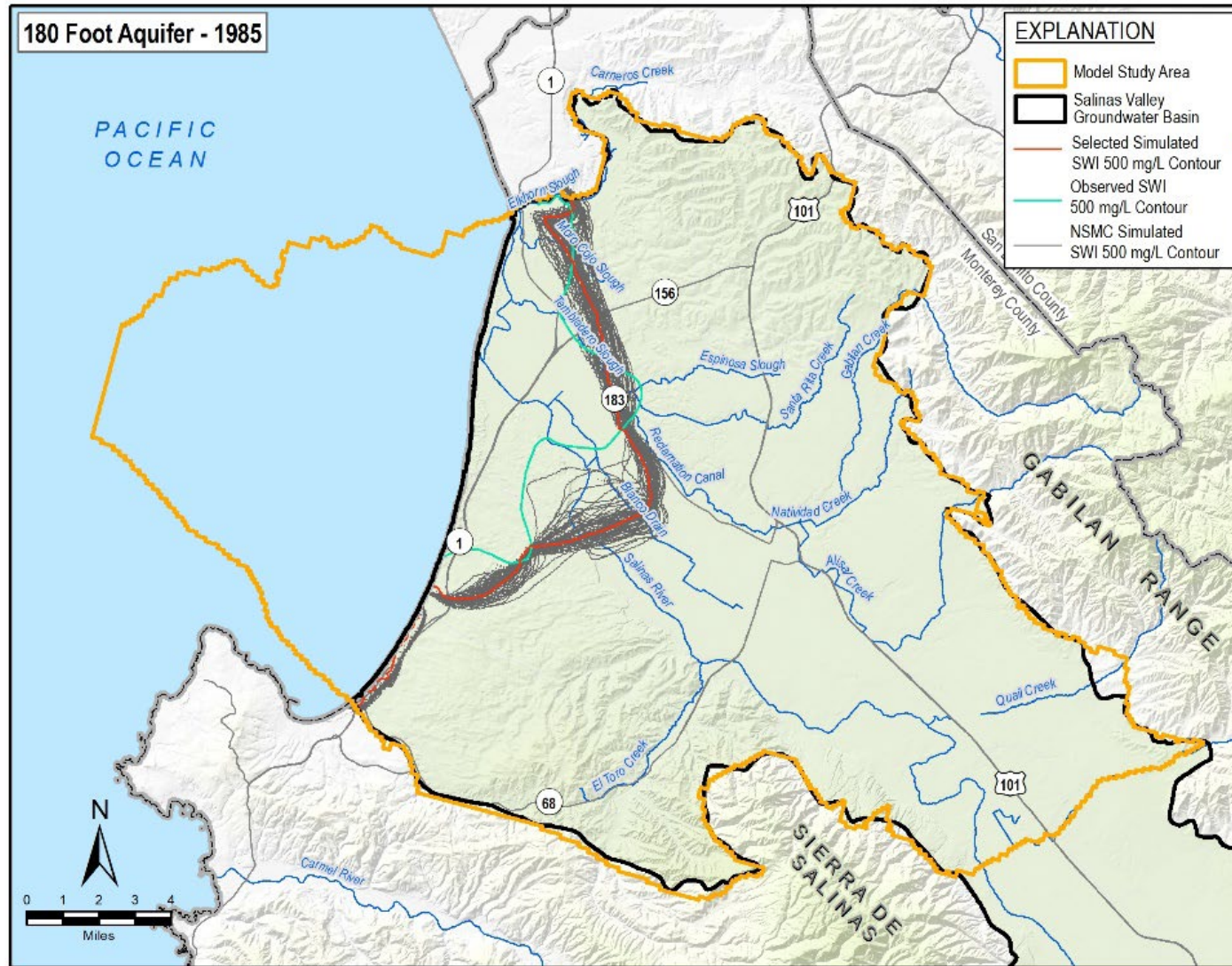
4.4.1 Model Parameter Uncertainty Runs

The PEST software suite was used to create 105 versions of the SWI Model with varying aquifer parameters with each model still remaining within calibration. The models were created using the Null-Space Monte Carlo methodology employed in the PEST software (Watermark Numerical Computing 2021; Doherty 2015). Parameters that varied between each of these models include the following:

- Horizontal hydraulic conductivity of the HGUs – both zonally and between pilot points
- Vertical hydraulic conductivity anisotropy – both zonally and between pilot points
- Specific yield (and effective porosity)
- Specific storage
- Recharge multipliers
- Dispersivity

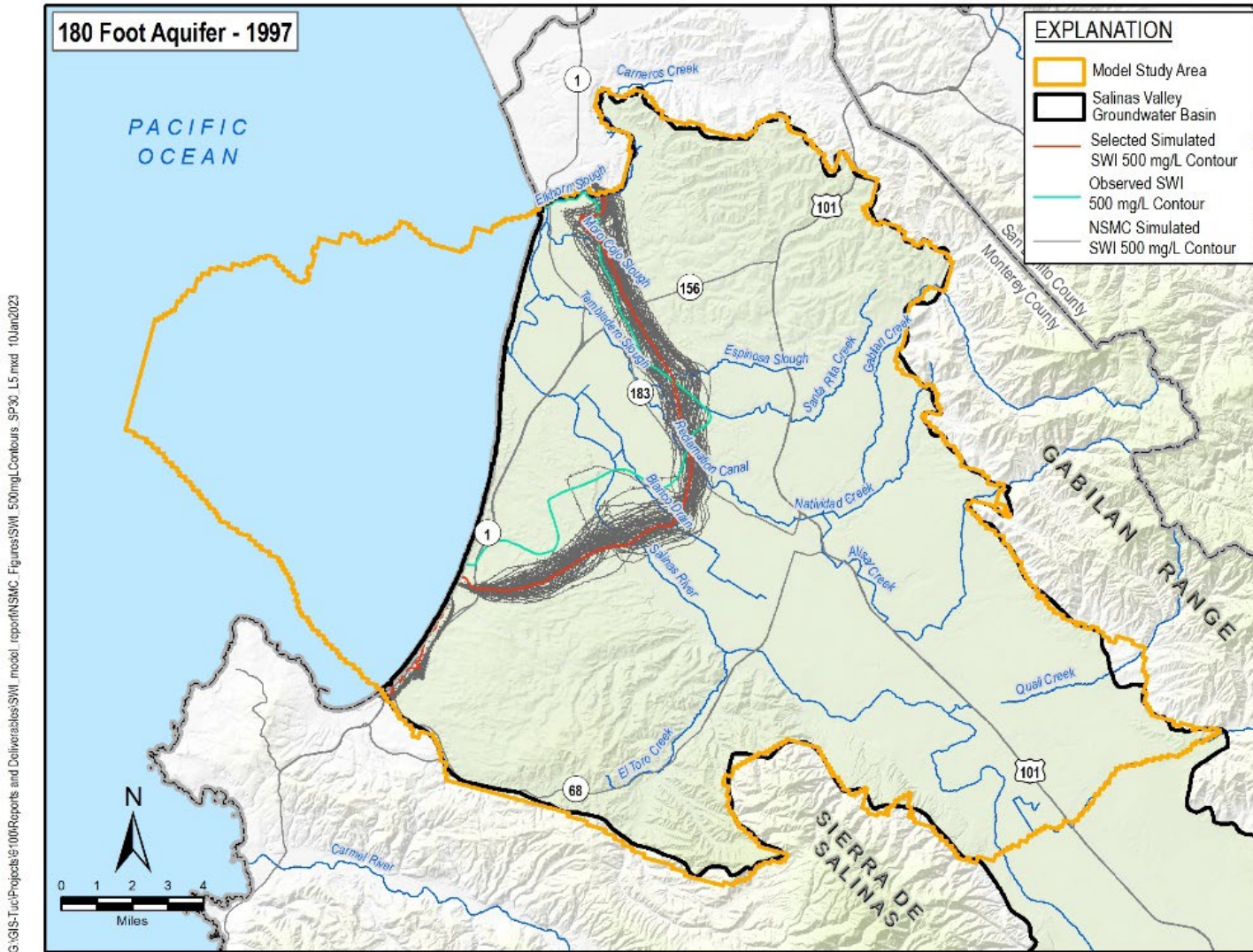
Parameter distributions were reviewed to ensure that parameters were not set at unrealistic values. As seen on Figure 4-16 through Figure 4-25 the simulated 500 mg/L contour lines from each model (gray lines in the figures) all lie reasonably close to the observed contour line. The variation in the simulated 500 mg/L chloride contour from all of the models does not vary greatly and persists through time. This is particularly evident in the 180-Foot Aquifer figures (Figure 4-16 through Figure 4-20).

This set of model runs is a sampling of the model parameter uncertainty. Each model was calibrated to water level and chloride concentration data. These model parameter uncertainty models were then used as input into an electrical resistivity model to compare to measured AEM data. This comparison to AEM data would be used to reduce the uncertainty by eliminating models that did not match the AEM data sufficiently (see Section 4.4.2).



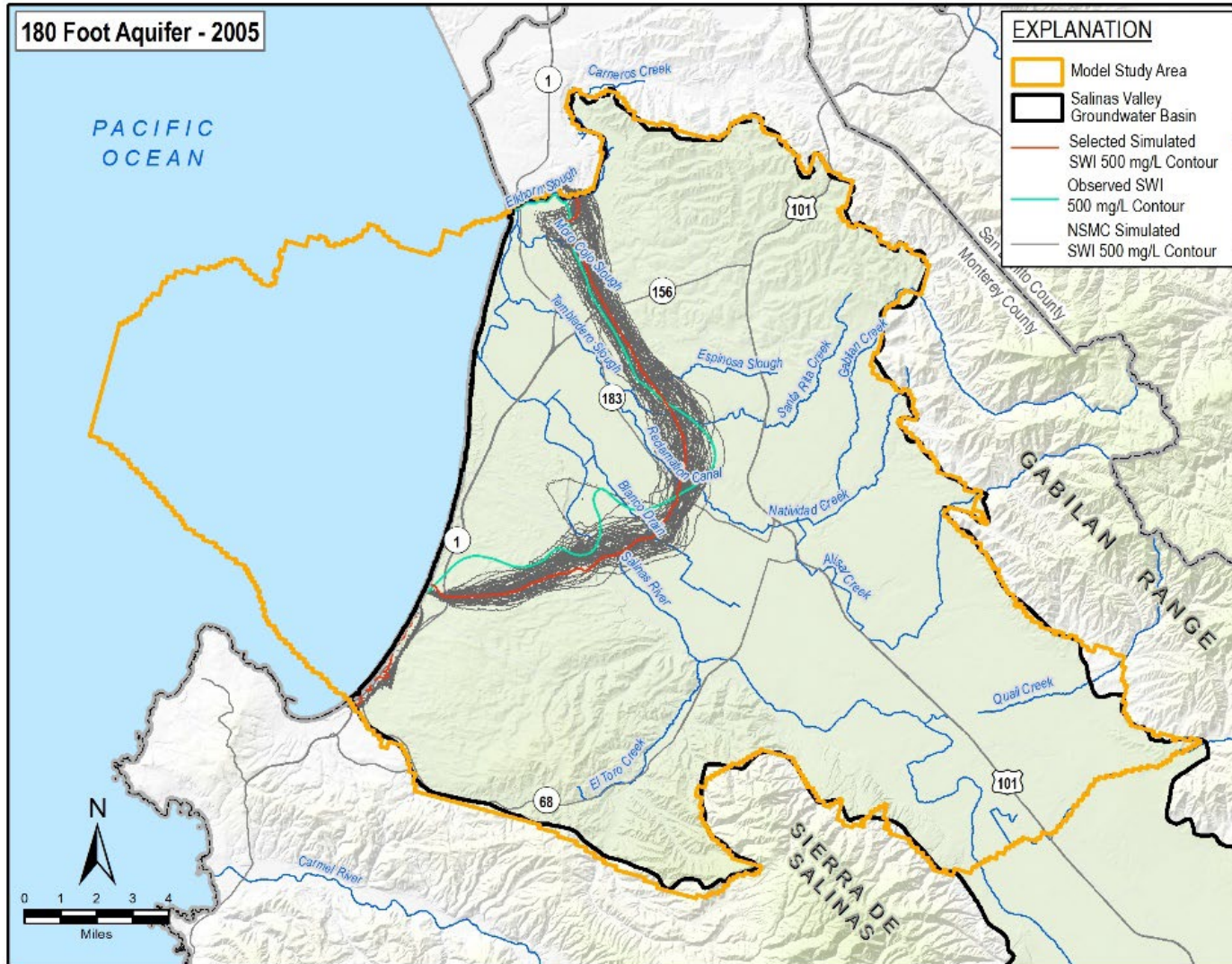
G:\GIS\Tuc\Projects\100\Reports and Deliverables\SWI_model_report\NSMC_Figures\SWI_500mgLContours_SP4_L5.mxd 10Jan2023

Figure 4-16. Simulated 500 mg/L Chloride Concentration Contours from 105 Null-Space Monte Carlo Models in the 180-Foot Aquifer in 1985



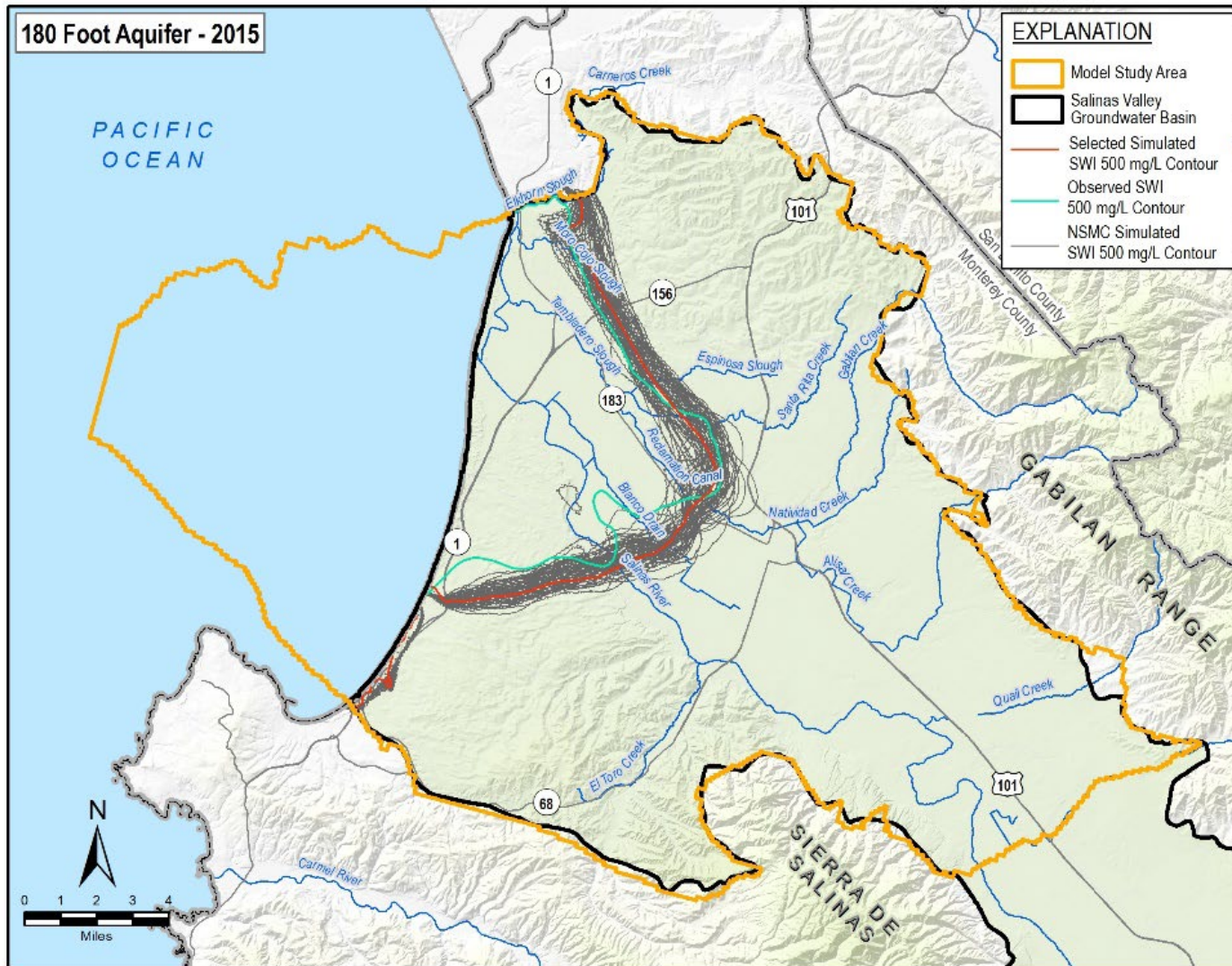
G:\GIS-1\Projects\1004\Reports and Deliverables\SWI_model_report\NNSMC_Figures\SWI_500mgLContours_SPS30_L5.mxd 10/Jan/2023

Figure 4-17. Simulated 500 mg/L Chloride Concentration Contours from 105 Null-Space Monte Carlo Models in the 180-Foot Aquifer in 1997



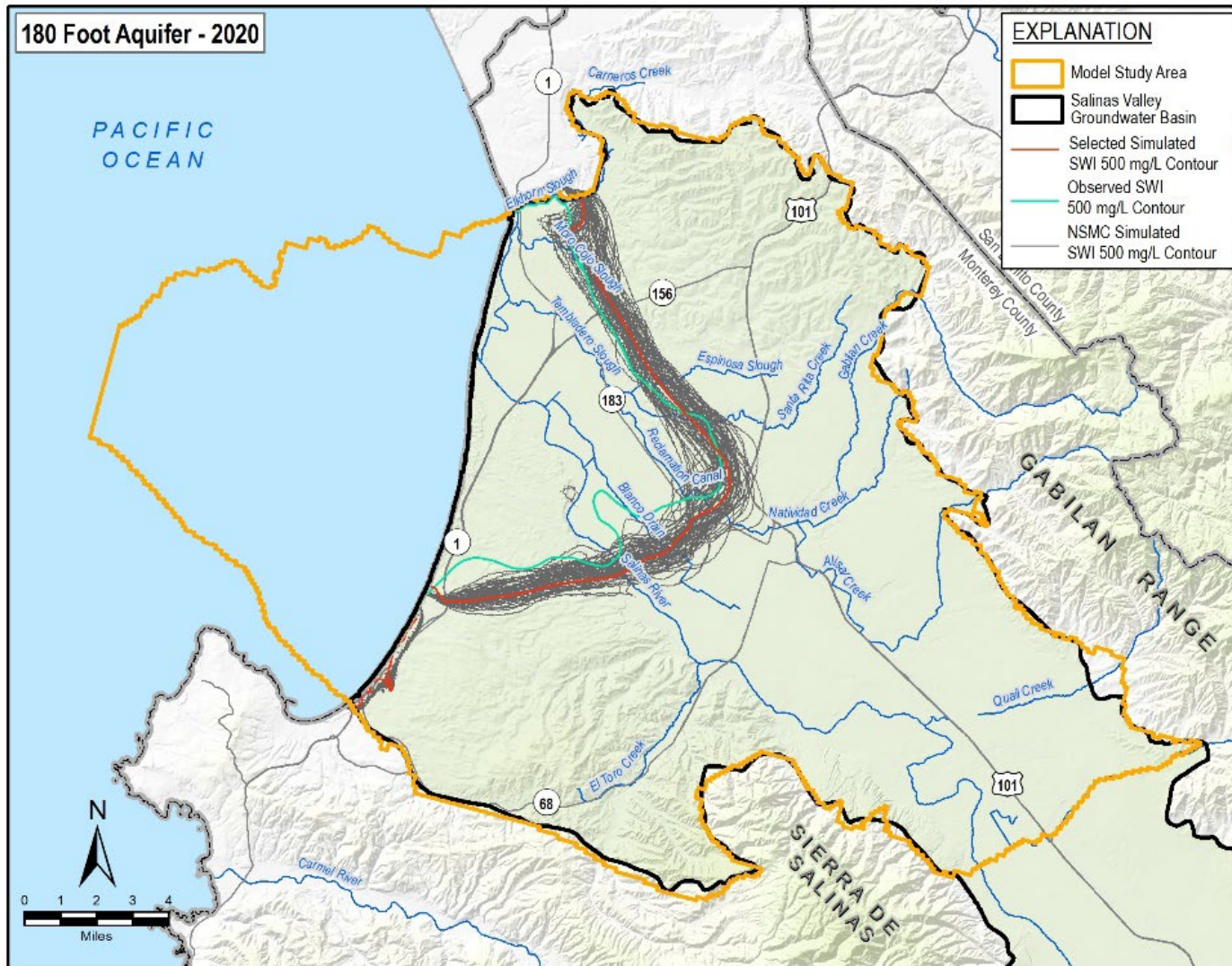
G:\GIS-1\Projects\100\Reports and Deliverables\SWI_model_report\NNSMC_Figures\SWI_500mgLContours.SP126_L5.mxd 11Jan2023

Figure 4-18. Simulated 500 mg/L Chloride Concentration Contours from 105 Null-Space Monte Carlo Models in the 180-Foot Aquifer in 2005



G:\GIS-1\Projects\100\Reports and Deliverables\SWI_model_report\NNSMC_Figures\SWI_500mgLContours.SP246_L5.mxd 11Jan2023

Figure 4-19. Simulated 500 mg/L Chloride Concentration Contours from 105 Null-Space Monte Carlo Models in the 180-Foot Aquifer in 2015



G:\GIS-1\Projects\100\Reports and Deliverables\SWI_model_report\NNSMC_Figures\SWI_500mgLContours_SPC33_L5_sym.mxd 11-Jan-2023

Figure 4-20. Simulated 500 mg/L Chloride Concentration Contours from 105 Null-Space Monte Carlo Models in the 180-Foot Aquifer in 2020

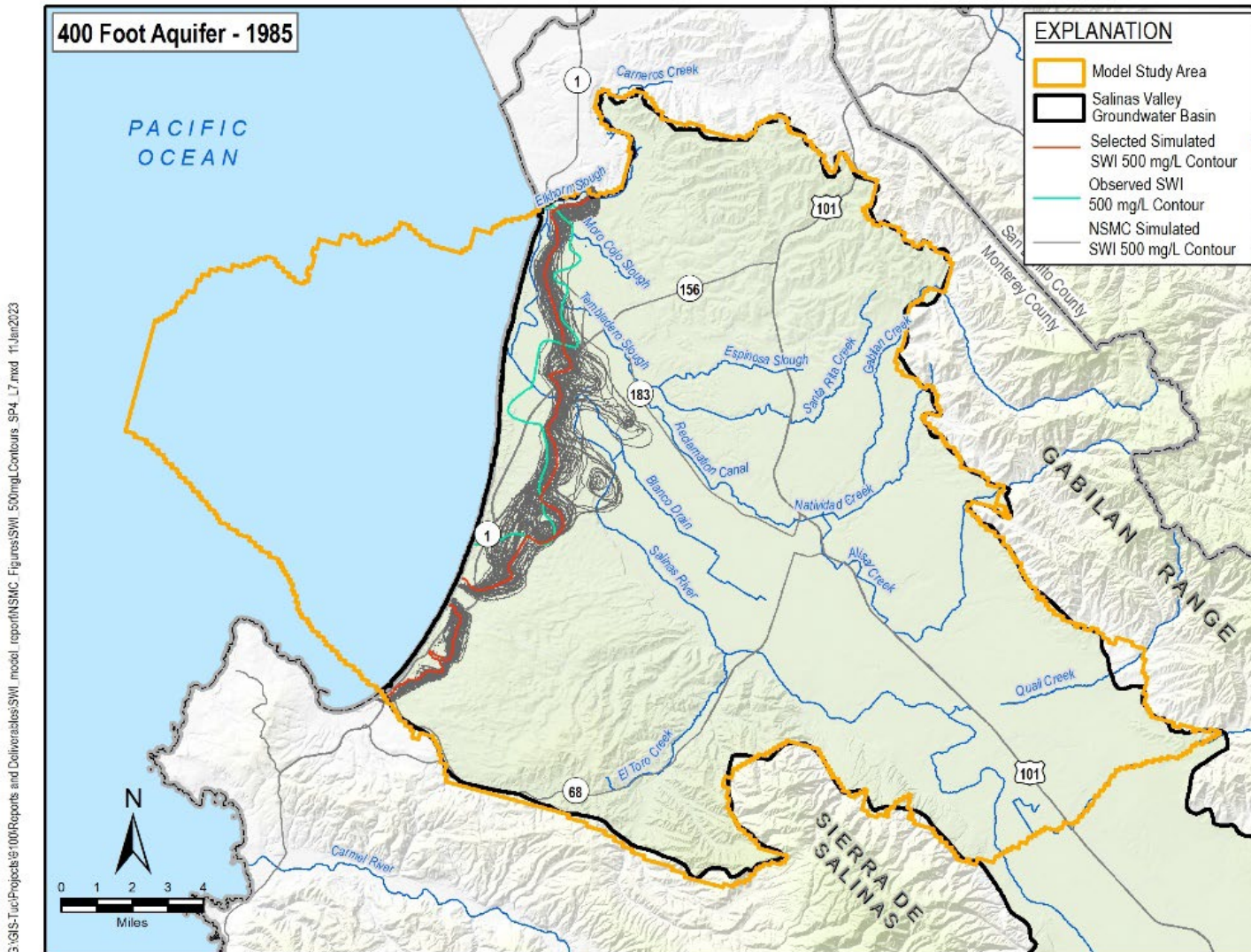
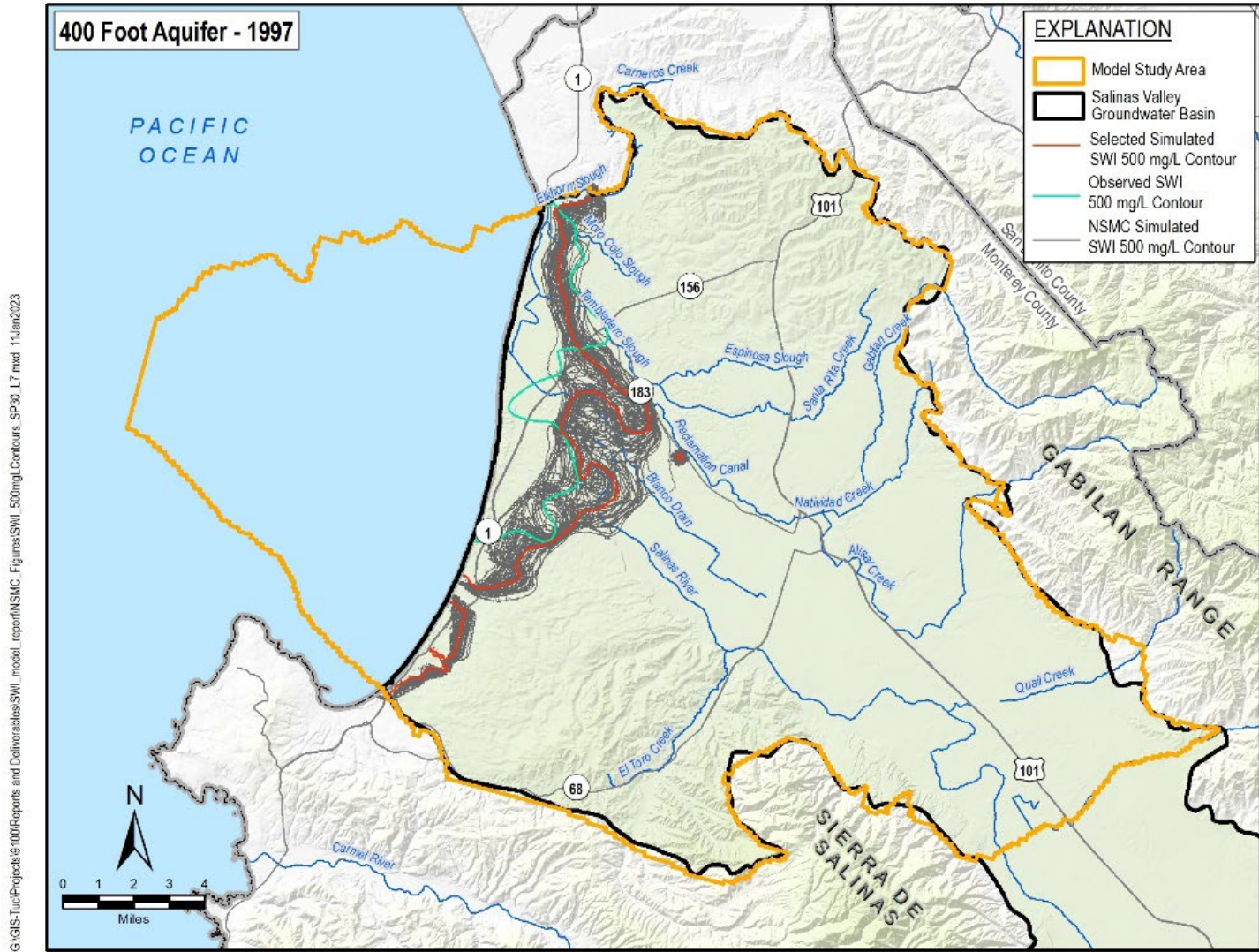
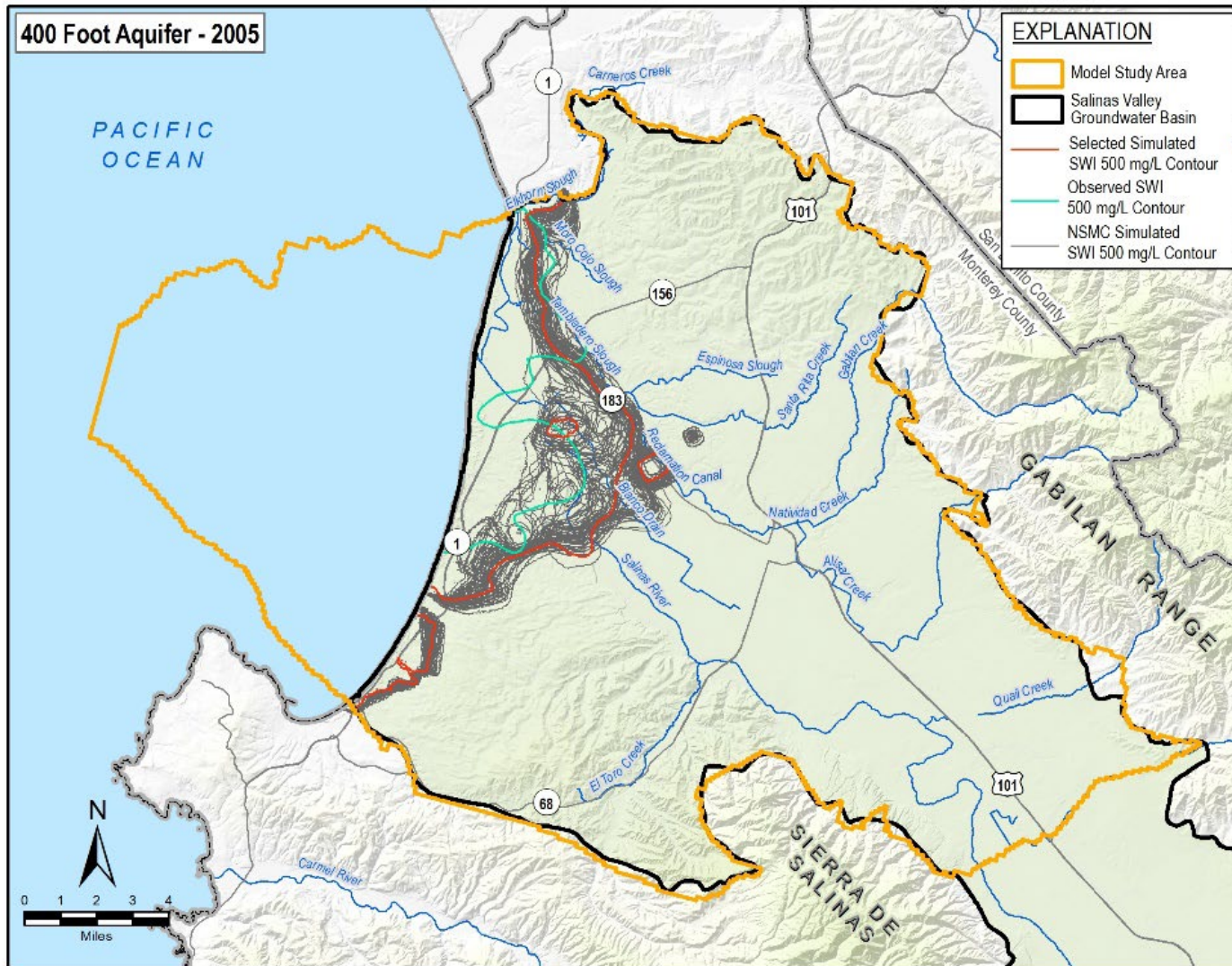


Figure 4-21. Simulated 500 mg/L Chloride Concentration Contours from 105 Null-Space Monte Carlo Models in the 400-Foot Aquifer in 1985



G:\GIS-1\Projects\100\Reports and Deliverables\SWI_model_report\NNSMC_Figures\SWI_500mgLContours_SF30_L7.mxd 11-Jan-2023

Figure 4-22. Simulated 500 mg/L Chloride Concentration Contours from 105 Null-Space Monte Carlo Models in the 400-Foot Aquifer in 1997



G:\GIS-1\Projects\100\Reports and Deliverables\SWI_model_report\NSMC_Figures\SWI_500mgLContours_SP126_L7.mxd 11Jan2023

Figure 4-23. Simulated 500 mg/L Chloride Concentration Contours from 105 Null-Space Monte Carlo Models in the 400-Foot Aquifer in 2005

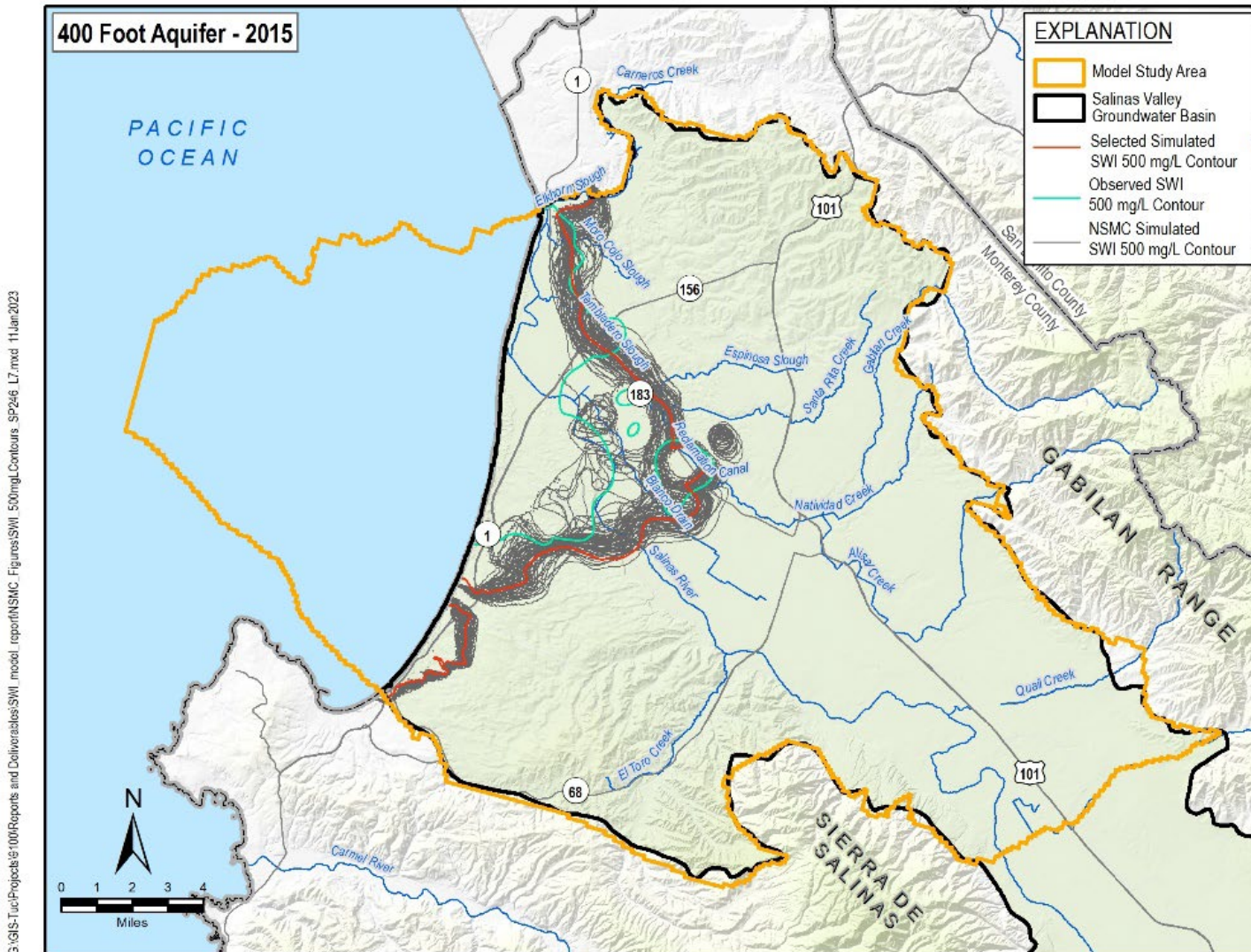


Figure 4-24. Simulated 500 mg/L Chloride Concentration Contours from 105 Null-Space Monte Carlo Models in the 400-Foot Aquifer in 2015

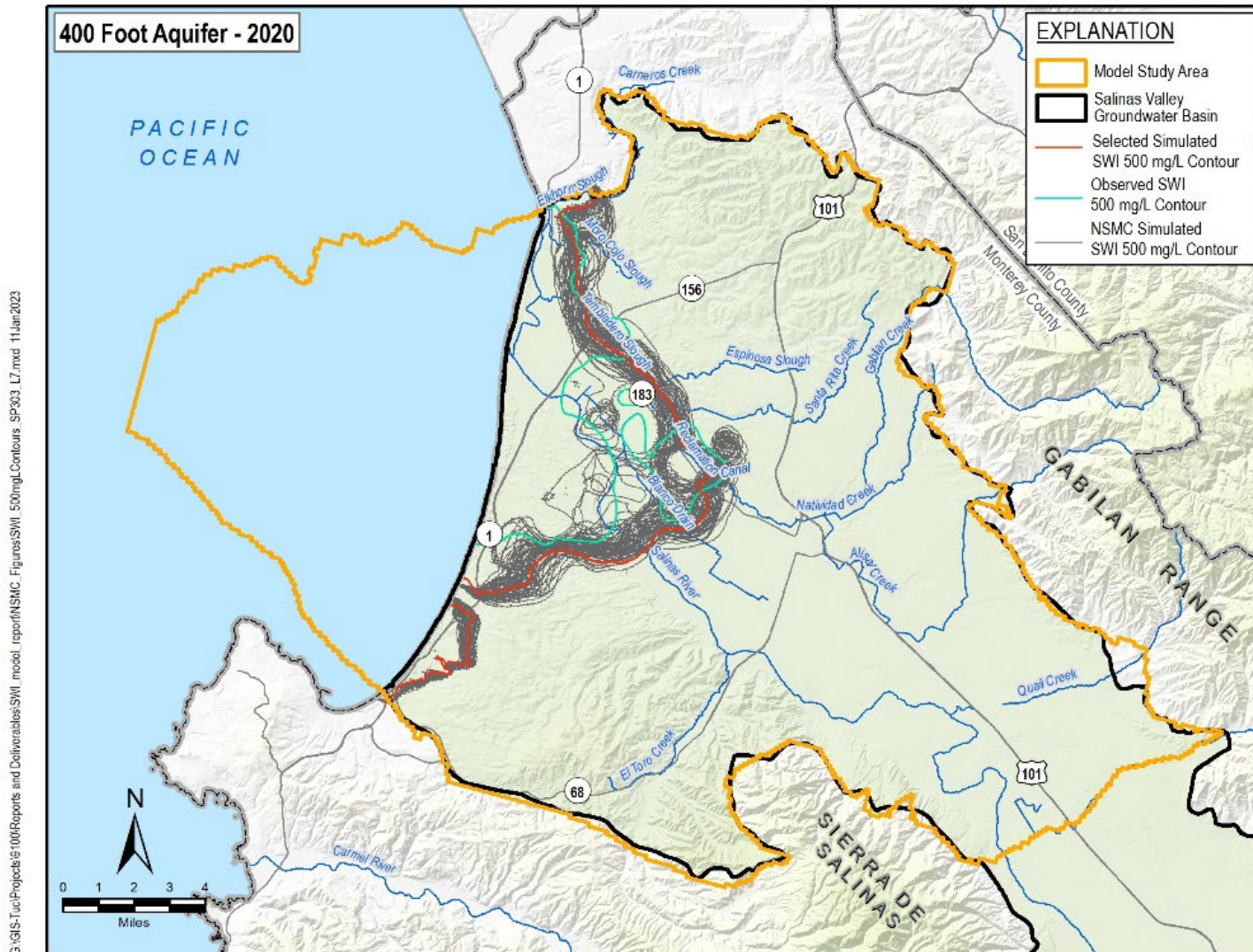


Figure 4-25. Simulated 500 mg/L Chloride Concentration Contours from 105 Null-Space Monte Carlo Models in the 400-Foot Aquifer in 2020

4.4.2 Model Constraining Using Geophysics (AEM Data)

AEM geophysical surveys were conducted in 2017 and 2019 over the seawater intrusion intruded areas in the model study area (Figure 4-26). The results of these surveys were used to estimate hydrogeologic zonation, seawater intrusion areas, and subsurface electrical resistivity. A rock physics relationship was developed by Kang *et al.* (2023) that relates subsurface hydraulic conductivity, porosity, and fluid chloride concentration to electrical resistivity measured and estimated from the AEM surveys. Using the 105 parameter uncertainty models and the rock physics relationship, the 105 models were ranked according to how well they recreated the AEM results. In essence the AEM data represent another calibration dataset. With utilization of the AEM ranked models and comparing the water level and chloride concentration calibration between the models, a final SWI Model was selected that best matches all datasets. The selected model is the calibrated model presented previously herein. The geophysical analysis and modeling is described in Appendix B – the Kang *et al.*, (2023) report.

The process by which the parameter uncertainty models were assessed using the AEM data is as follows:

- For each of the 105 models, the hydrogeologic properties (hydraulic conductivity, porosity, chloride distribution, and saturation) were transformed into an electrical resistivity model. Due to the nature of the rock physics relationship used to do this transformation, multiple resistivity models could be created for each of the 105 models with a total of 500 resistivity models created. This resulted in multiple resistivity models related to a single SWI hydrogeologic model.
- Each of the 500 resistivity models was used to simulate the AEM data.
- AEM residuals were calculated from the simulated AEM data and from the measured AEM data. The RMS residual value for the AEM data was calculated. The resistivity models (and by direct relationship, the SWI hydrogeologic models) were ranked by this RMS residual value. A lower RMS residual indicated a better match to AEM data.

The 105 versions of the SWI Model were ranked by the AEM RMS residual with the best 25 models selected for further comparison. The water level calibration statistics and match to the measured 500 mg/L contour lines were compared between these 25 models with one model selected as the calibrated SWI Model. It is this calibrated model and its results that has been described and presented above.

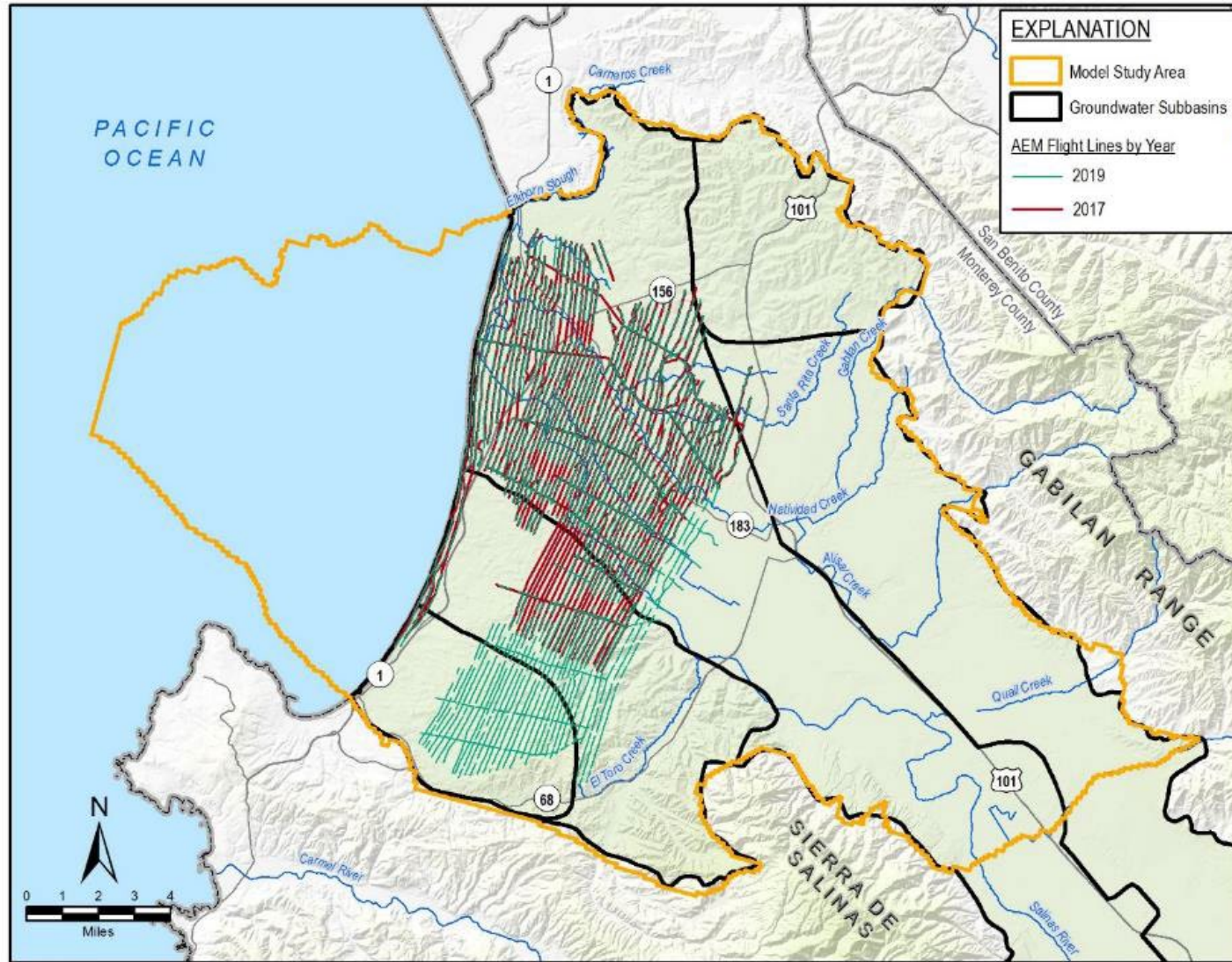


Figure 4-26. AEM Survey Flight Lines over the Seawater Intrusion Intruded Areas in 2017 and in 2019

4.5 Comparison of Groundwater Flows

Following the selection of the final calibrated model, as described in Section 4.4, simulated groundwater flows were compared to groundwater flows estimated for the conceptual model.

- Historical annual recharge (groundwater inflow) was estimated to vary between 35,000 and 190,000 AF/yr. This recharge is from direct precipitation, irrigation return flow, domestic return flow, and CSIP. The SWI Model simulated recharge within this range and an average of 65,000 AF/yr.
- Estimated groundwater inflow into the model from upgradient (into the model at the boundary beneath Chualar Creek –Figure 3-2) varies from approximately 3,900 to 20,000 AF/yr. The model on average simulates a net inflow of 2,500 AF/yr which is close to the estimated range.
- The rate of seawater intrusion is the rate of seawater entering the groundwater system underneath Monterey Bay. There is considerable uncertainty in estimates of this value, but it has been estimated to range between 11,000 and 18,000 AF/yr (see Section 1), as there is no method to measure this flow directly. Additionally, review of the provisional SVIHM models predict seawater intrusion rates as low as 5,000 AF/yr and as high as 25,000 AF/yr. The SWI Model predicts an average rate of 22,000 AF/yr.
- Potential ET estimates within the model area are as high as 147,000 AF/yr. Actual groundwater ET would be much lower than the potential rate because groundwater is not proximal to the ground surface, where the potential (maximum) ET rate generally occurs. Simulated groundwater ET within the model is 4,400 AF/yr and is in line with the assumption that it would be much less than potential ET.

4.6 Calibration Summary

The SWI Model was initially calibrated to groundwater levels and chloride concentrations. The calibration was focused along the coast in the seawater intruded areas. Emphasis in the calibration process was on the matching of measured 500 mg/L chloride contours for the 180-Foot and 400-Foot Aquifer. Once a reasonable match to the groundwater levels and chloride concentrations was achieved, a set of 105 versions of the SWI Model were created using PEST's null-space Monte Carlo methodology to sample the model parameter uncertainty. From these model parameter uncertainty runs resistivity models were created and used to generate simulated AEM data. The simulated AEM data were then compared to measured AEM data. The 25 model parameter uncertainty runs with the best fit to measured AEM data were compared to select a single, best calibrated model which became the calibrated SWI Model.

The objective of this modeling effort was to develop a SWI Model that simulated the seawater intrusion in the Salinas Valley. The SWI Model presented herein reasonably reproduces measured seawater intrusion (see Figure 4-3 and Figure 4-4).

REFERENCES

- Ahtna Engineering, 2013. Final Annual Report of Quarterly Monitoring October 2011 through September 2012 Groundwater Monitoring Program Sites 2 and 12, OU2, OUCTP and OU1 Off-Site Former Fort Ord, California, June 2013.
- Anderson, M.P., and W.W. Woessner. 1992. Applied Groundwater Modeling Simulation of Flow and Transport. Academic Press.
- Brown and Caldwell. 2017. State of the Salinas River Groundwater Basin - Hydrology Report. Monterey County Water Resources Agency Water Reports.
- California Fish and Game, 2022. <https://coast.noaa.gov/nerrs/reserves/elkhorn-slough.html>. Accessed December of 2022.
- Clark, Joseph C., Earl E. Brabb, and Lewis I. Rosenberg. 2000. Geologic Map and Map Database of the Spreckels 7.5-Minute Quadrangle, Monterey County, California. <https://pubs.usgs.gov/mf/2001/2349/>.
- Department of Water Resources (DWR). 1946. Salinas Basin Investigation Summary Report. Bulletin 52-B.
- _____. 1973. Seawater Intrusion Lower Salinas Valley. Bulletin 118 Interim Update 1973.
- _____. 2003. California's Ground Water. Bulletin 118 Update 2003. https://water.ca.gov/-/media/DWR-Website/Web-Pages/Programs/Groundwater-Management/Bulletin-118/Files/Statewide-Reports/Bulletin_118_Update_2003.pdf.
- _____. 2004a. Salinas Valley Groundwater Basin, 180/400-Foot Aquifer Subbasin. Bulletin 118 Interim Update 2004; https://water.ca.gov/LegacyFiles/pubs/groundwater/bulletin_118/basindescriptions/3-4.01.pdf.
- _____. 2004b. Salinas Valley Groundwater Basin, Eastside Aquifer Subbasin. Bulletin 118 Interim Update 2004. https://water.ca.gov/-/media/DWR-Website/Web-Pages/Programs/Groundwater-Management/Bulletin-118/Files/2003-Basin-Descriptions/3_004_02_EastsideAquiferSubbasin.pdf.
- Doherty, J. 2015. Calibration and uncertainty analysis for complex environmental models. Watermark Numerical Computing, Brisbane, Australia.
- Doherty, J.E., M.N. Fienen, and R.J. Hunt. 2010, Approaches to highly parameterized inversion: Pilot-point theory, guidelines, and research directions: U.S. Geological Survey Scientific Investigations Report 2010-5168, 36 p.
- Dupre, 1990. Maps showing geology and liquefaction susceptibility of quaternary deposits in the Monterey, Seaside, Spreckels, and Carmel Valley Quadrangles, Monterey County, California, June 4, 1990.

- Durbin, Timothy J. 1974. Digital simulation of the effects of urbanization on runoff in the upper Santa Ana Valley, California. U.S. Geological Survey Water Resources Investigations, 73-41. <https://pubs.usgs.gov/wri/1973/0041/report.pdf>.
- Durbin, Timothy J., G.W. Kapple, and J.R. Freckleton. 1978. Two-Dimensional and Three-Dimensional Digital Flow Models of the Salinas Valley Ground-Water Basin, California. U.S. Geological Survey. Water Resources Investigations Report 78-113. Prepared in cooperation with the U.S. Army Corps of Engineers. 134 p.
- Durbin, Timothy. 2007. Groundwater Flow and Transport Model Seaside Groundwater Basin Monterey County, California, dated October 26, 2007.
- Durham, D.L. 1974. *Geology of the Southern Salinas Valley Area*. California, U.S. Geological Survey Professional Paper 819, 1974, 117 p.
- Feeney, M.B., and L.I. Rosenberg. 2003. Deep aquifer investigation - hydrogeologic data inventory, review, interpretation, and implications, 40 p. <https://www.co.monterey.ca.us/home/showdocument?id=19614>.
- Fugro, 1996. Additional Hydrogeologic Update, El Toro Area, Monterey County, California, February 1996.
- Flint, L.E. and A.L. Flint. 2014, California Basin Characterization Model: A Dataset of Historical and Future Hydrologic Response to Climate Change, (ver. 1.1, May 2017): U.S. Geological Survey Data Release, <https://doi.org/10.5066/F76T0JPB>.
- Gelhar, L. W., C. Welty, and K.R. Rehfeldt. (1992), A critical review of data on field-scale dispersion in aquifers, *Water Resources Research*, 28(7), 1955– 1974, doi:10.1029/92WR00607.
- Geoscience 2014. Monterey Peninsula Water Supply Project Hydrogeologic Investigation; Tech. Memo. #1; Summary of results – exploratory Boreholes. Prepared for California American Water; RBF Consulting. July 8, 2014.
- Geosyntec Consultants, 2007. El Toro Groundwater Study, July 2007.
- _____, 2010. Geologic Map and Cross-Sections from El Toro to Salinas Valley, June 2010.
- Geotechnical Consultants, Inc., 1986. HYDROGEOLOGIC UPDATE, FORT ORD MILITARY RESERVATION AND VICINITY, Monterey County, California. Prepared for US Department of the Army, Sacramento District Corps of Engineers.
- Gottschalk, I., R. Knight, Theodore Asch, Jared Abraham, and James Cannia, (2020), “Using an airborne electromagnetic method to map saltwater intrusion in the northern Salinas Valley, California,” *GEOPHYSICS* 85: B119-B131.
- Greene, H.G. 1970. Geology of Southern Monterey Bay and Its Relationship to the Ground Water Basin and Salt Water Intrusion. U.S. Geological Survey Open-File Report 70-141, 51 p. <https://www.co.monterey.ca.us/home/showdocument?id=61931>.



- _____, 1977. Geology of the Monterey Bay Region, California, U.S. Geological Survey OpenFile Report 77-718.
- Hanson, R.T., *et al.* 2002. Geohydrology of a deep-aquifer system monitoring-well site at Marina, Monterey County, California.
<https://pubs.usgs.gov/wri/wri024003/pdf/wrir024003.pdf>.
- Harding ESE. 2001. Hydrogeologic Investigation of the Salinas Valley Basin in the Vicinity of Fort Ord and Marina, Salinas Valley, California, prepared for Monterey County Water Resources Agency. 12 April. 166 p.
- HLA, 1994. Basewide Hydrogeologic Characterization, Fort Ord, California: prepared for U.S. Department of the Army, June 10, 1994.
- HydroMetrics, 2009. Seaside Groundwater Basin Modeling and Protective Groundwater Elevations, November 2009.
- JGOFS, 1997. *Assessing The Ocean's Role In The Global Carbon Cycle: The Joint Global Ocean Flux Study by Margaret C. Bowles and Hugh D. Livingston*. Chapter 5 Physical and thermodynamic data.
- Jordan *et al.*, 2005. Analysis of Aquifer Response, Groundwater Flow, and Plume Evolution at Site OU 1, Former Fort Ord, California, Lawrence Berkeley National Laboratory, February 21, 2005.
- Kang, S., R. Knight, G. Nelson, 2023. Integration of Airborne Electromagnetic Data into the Modeling of Saltwater Intrusion. Stanford University, Department of Geophysics. San Francisco.
- Kennedy/Jenks. 2004. Hydrostratigraphic Analysis of the Northern Salinas Valley. Prepared for Monterey County Water Resources Agency. 113 p.
- Jennings, C.W., with modifications by C. Gutierrez, W. Bryant, G. Saucedo, and C. Wills, 2010. Geologic map of California: California Geological Survey, Geologic Data Map No. 2, scale 1:750,000. https://www.conservation.ca.gov/cgs/Pages/Program-RGMP/2010_geologicmap.aspx.
- Johnson, Michael J., Clark J. Londquist, Julie Laudon, and Hugh T. Mitten. 1988. Geohydrology and Mathematical Simulation of the Pajaro Valley Aquifer System, Santa Cruz and Monterey Counties, California. U.S. Geological Survey Water-Resources Investigations Report 87-4281. <https://pubs.usgs.gov/wri/1987/4281/report.pdf>.
- MCWRA (Monterey County Water Resources Agency). 2017. Recommendations to Address the Expansion of Seawater Intrusion in the Salinas Valley Groundwater Basin. Special Reports Series 17-01. <https://www.co.monterey.ca.us/home/showdocument?id=57396>.
- Muir, 1982. Groundwater in the Seaside Area Monterey County California, September 1982.

- Niswonger, R.G., Sorab Panday, and Motomu Ibaraki. 2011, MODFLOW-NWT, A Newton formulation for MODFLOW-2005: U.S. Geological Survey Techniques and Methods 6-A37, 44 p.
- Panday, S., 2021; USG-Transport Version 1.9.0: The Block-Centered Transport Process for MODFLOW-USG, GSI Environmental, February 2022 <http://www.gsi-net.com/en/software/free-software/USG-Transport.html>.
- Panday, S., C.D. Langevin, R.G. Niswonger, Motomu Ibaraki, and J.D. Hughes. 2013, MODFLOW-USG version 1: An unstructured grid version of MODFLOW for simulating groundwater flow and tightly coupled processes using a control volume finite-difference formulation: U.S. Geological Survey Techniques and Methods, book 6, chap. A45, 66 p.
- Santa Cruz Mid-County Groundwater Sustainability Agency (GSA). 2022, Santa Cruz Mid-County Groundwater Basin Groundwater Sustainability Plan. Prepared by Montgomery & Associates. Submitted to the California Department of Water Resources January 2022.
- Spitz, K., Moreno, J. 1996. A Practical Guide to Groundwater and Solute Transport Modeling. New York: John Wiley and Sons.
- Tetra Tech, 2015, Salinas River Watershed Area Salt Modeling. Consultant's report to the California Central Coast Regional Water Quality Control Board and U.S. Environmental Protection Agency, Region IX. November 2015.
- Tinsley, J.C. III. 1975. Quaternary Geology of Northern Salinas Valley, Monterey County, California. Doctoral dissertation, Stanford University.
- Todd Engineers. 1989. Sources of Saline Intrusion in the Pressure 400-Foot Aquifer, Castroville Area, California.
- Thorup, R.R. 1976. Report on Castroville Irrigation Project Deep Test Hole and Freshwater Bearing Strata Below the Pressure 400-Foot Aquifer, Salinas Valley, CA. <https://www.co.monterey.ca.us/home/showdocument?id=61934>.
- US Department of the Army, Sacramento District, Corps of Engineers, 1975. Final Report, HYDROGEOLOGY OF FORT ORD AND VICINITY. Prepared for Fort Ord, Monterey County, California.
- Wagner, D.L., G. Greene, G.J. Saucedo, C. L. Pridmore, 2002. Geologic Map of the Monterey 30'x60' Quadrangle and Adjacent Areas, California. Regional Geologic Map Series, 1:100,000 Scale. Map No. 1, Plate 3 of 3. Digitized by Watkins, S. E., Little, J. D., Bizzarro, J. J.
- Wallace Group. 2021. Technical Memorandum: Corral de Tierra Subarea Water and Wastewater Usage Analysis. March 1, 2021.
- Watermark Numerical Computing. 2021. Groundwater Data Utilities software packages. August 2021.



WRIME, Inc. 2003. Deep Aquifer Investigation – Hydrogeologic Data Inventory, Review, Interpretation and Implications. Technical Memorandum.

Xu, M. and Y. Eckstein. 1995. Use of Weighted Least-Squares Method in Evaluation of the Relationship Between Dispersivity and Field Scale. *Groundwater*, 33: 905-908.
<https://doi.org/10.1111/j.1745-6584.1995.tb00035.x>.

Yates, Eugene B. 1988. *Simulated Effects of Ground-Water Management Alternatives for the Salinas Valley, California*. U.S. Geological Survey Water Resources Investigations Report 87-4066.

_____. 2005. Seaside Groundwater Basin: Update on Water Resource Conditions, April 14, 2005.

Appendix A

Simulated and Observed Water Level Hydrographs

See [AppendixA_Simulated and Observed Water Level Hydrographs.kmz](#), to be opened with Google Earth or Google Earth Pro



Appendix B

Integration of Airborne Electromagnetic Data into the Modeling of Saltwater Intrusion

Title: Integration of Airborne Electromagnetic Data into the Modeling of Saltwater Intrusion

Authors: Seogi Kang¹, Gregory Nelson², and Rosemary Knight¹

¹Stanford University

²Montgomery and Associates

Abstract

We created a robust numerical methodology that incorporates airborne electromagnetic (AEM) data into saltwater intrusion (SWI) modeling, utilizing commonly used tools and rock physics relationships in groundwater modeling and geophysics. With the calibrated SWI model and the AEM data obtained in the coastal region of California's Salinas Valley, we generated 105 SWI models and 500 resistivity models as priors. From these prior models, we obtained 75 resistivity models and 22 SWI models as posteriors; they have about 3 times lower data misfit between the simulated and observed AEM data than the baseline model, which assumed a homogeneous subsurface. The remaining 83 SWI models were falsified by the AEM data while all of them fit the in-situ data. Therefore, the accuracy of the SWI modeling was improved by constraining the modeling process with the AEM data. The developed and implemented methodology allows for the incorporation of AEM data to improve the accuracy of a regional-scale SWI model.

1. Introduction

Groundwater is a vital resource for the Salinas Valley of California, USA, providing nearly 95% of the water supply for the region (MCWRA, 2022). However, as sea levels rise and droughts become more frequent in the coastal area, the saltwater-freshwater interface is moving further inland. This poses a significant threat to freshwater security on land, as water quality in coastal aquifers is degraded, and a significant threat to coastal ecosystems offshore, as the nutrient supply delivered through submarine groundwater discharge is decreased. To proactively prevent or reverse SWI through changes in freshwater management, there is a need to both understand the current extent of saltwater intrusion in the region and to establish a plan for long-term monitoring. Saltwater intrusion (SWI) modeling has been widely used as a fundamental tool for managing freshwater resources in coastal areas (Guo & Langevin, 2002; Langevin et al., 2008; Masterson, 2004; Paulinski, 2021) and thus, obtaining an accurate SWI model is of paramount importance. In-situ data from water wells, including salinity, groundwater elevation, and descriptions of the geologic material, have been used to develop SWI models in order to predict future salinity distributions. While well data provide accurate point measurements, their low spatial density and coverage results in a large data gap between wells. This gap in data leads to a high level of uncertainty in future predictions from SWI models. Therefore, it is crucial to acquire new types of data that can fill this gap and reduce the level of uncertainty in predictions.

Airborne electromagnetic (AEM) methods, which can rapidly map out the distribution of electrical resistivity in the subsurface, over a large area and with a high spatial density has the potential to fill in this data gap between well data and decrease the uncertainty (Barfod et al., 2018; Foged et al., 2014; He et al., 2014; Kang, Knight, & Goebel, 2021; Kang, Knight, Greene, et al., 2021; Knight et al., 2018). Three-dimensional images of resistivity, obtained from AEM data in areas of concern for SWI, have been found to provide useful information, assisting in mapping out the location of the saltwater-freshwater interface (Goebel et al., 2019; Gottschalk et al., 2020; Viezzoli et al., 2010). Here we develop a methodology to integrate the AEM data into the modeling of saltwater intrusion in order to improve the accuracy of SWI models. We note that there is not a simple relationship electrical resistivity and salinity, as resistivity is also affected by sediment type. This complexity in the rock physic relationship, that links the measured parameter electrical resistivity to the subsurface properties, is accounted for in the developed methodology.

In the study area located along the Monterey Coast of the Salinas Valley, the coastal groundwater system is composed of two major sedimentary aquifer units, referred to as the 180-foot aquifer and the 400-foot aquifer. Both aquifers have been experiencing significant saltwater intrusion over the past several decades, with the freshwater-saltwater interface moving 10-20 km inland during this time, impacting water quality in many wells in the region. Saltwater intrusion has not occurred in, what is referred to as the Deep Aquifer, that underlies the 180-foot and 400-foot aquifers in the study area (MCWD & SVBGSA, 2022). Obtaining an accurate SWI model is essential for supporting efforts to achieve sustainable management of the saltwater intrusion in the area.

The goal of this study was to improve the modeling of saltwater intrusion in the study area covered by the two AEM data sets acquired in 2017 and 2019. Working with these data, we developed a novel numerical workflow that started with 105 SWI models and fit both data from wells (hydraulic head and salinity) and the time-lapse AEM data. While there have been previous studies that have utilized AEM data to characterize the saltwater intrusion (Fitterman & Deszcz-Pan, 2004; Goebel et al., 2019; Gottschalk et al., 2020), this is the first attempt to integrate time-lapse AEM data into an SWI model.

2. Obtaining input data for workflow

2.1 Calibrated SWI model

Obtaining an initial calibrated SWI model is the starting point of our workflow, the output of which is an improved SWI model. The initial SWI model was developed by Montgomery & Associates (M&A) (M&A, 2023). Required properties derived from this initial SWI model for the workflow were hydraulic conductivity, porosity, and salinity. While the hydraulic conductivity and porosity varied spatially and were fixed in time, the salinity at locations was allowed to vary in time as the model simulated SWI occurring from 1975 through 2020.

The SWI model is a variable-density flow model that extends from Monterey Bay in the northwest to Chualar Creek in the southeast. The boundary of the SWI model is shown in Figure 1. As SWI was the primary focus of this modeling, the model extent includes the coast from Seaside to Elkhorn Slough and simulates flow in the coastal area of the Salinas Valley in the principal hydrogeologic units of the valley (dune sands, Salinas Valley Aquitard, 180-Foot Aquifer, 180/400 Foot Aquitard, 400-Foot Aquifer, Deep Aquitard, Deep Aquifers). The lateral extent of the model is 50 km × 35 km with a uniform cell size of 150 m × 150 m (~500 feet x 500 feet). In the vertical dimension, there were 11 layers with variable thickness; each layer used the same lateral grid. The SWI model begins with a 500-year period, with no groundwater pumping or other human intervention where a saltwater wedge develops. This is followed by a 60 year period of pumping which simulates the initial SWI. These periods are then followed by the calibrated period between 1985 and 2020.

The SWI model was calibrated (through the process of history matching) to water levels and chloride concentrations measured in wells, and measured stream flows. Calibration involved the adjustment of hydraulic parameters (hydraulic conductivity, specific yield, porosity, specific storage, recharge) until an acceptable match was obtained between measured and simulated data (i.e., water levels and chloride concentrations). Parameters and results from the SWI model (hydraulic conductivity, porosity, and salinity) were then utilized in our workflow.

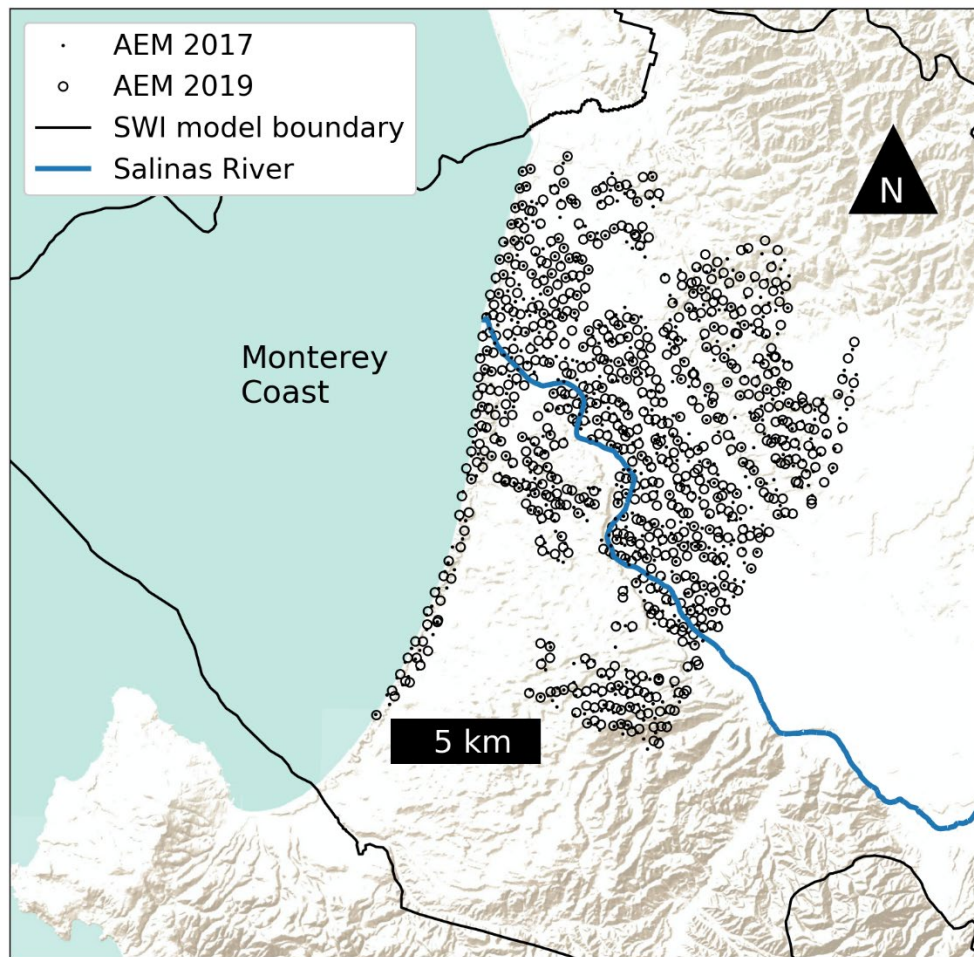


Figure 1. Location map displaying the boundary of the saltwater intrusion (SWI) model and the two AEM data sets, displayed as the sounding locations, acquired in 2017 and 2019.

2.2 Time-lapse AEM data

The airborne electromagnetic (AEM) system comprises a source loop and a receiver loop deployed on an aircraft, in this case a helicopter, typically at a height of 30-40 meters above the ground surface. The time-varying current injected into the source loop generates magnetic fields both above and below the ground surface, inducing eddy currents in the subsurface. These rotating currents, which depend on the electrical resistivity of the subsurface, produce magnetic fields that can be measured as voltages at the receiver loop. The measured data, consisting of 30-50 voltage values at time gates ranging from several microseconds to several milliseconds, provide information about the subsurface electrical resistivity. The voltage values measured early in time contain more information about shallow subsurface, while those measured later provide information about deeper regions. During the flight of the aircraft, voltage data are continuously acquired and stacked over 30-40 meter intervals – along the direction of flight, resulting in a set of voltage values, corresponding to the location of each interval, referred to as an AEM sounding.

Two AEM surveys were conducted in Monterey County located in the Salinas Valley of California, to monitor the changes in saltwater intrusion. The first survey was conducted in the first week of May 2017

using the SkyTEM 304 system, and the second survey was conducted in the last week of April 2019 using the SkyTEM 312 system. The SkyTEM 304 system has a depth of investigation of 150-300 m and vertical resolution near the ground surface of 1-3 m. The SkyTEM 312 system has a greater depth of investigation of 200-400 m, but a decreased near-surface resolution of 3-5 m.

After processing the data using Aarhus Workbench, which included the manual removal of noisy data and spatial smoothing using a trapezoidal filter (Auken et al., 2018), the number of AEM sounding locations for the 2017 and 2019 surveys were 9857 and 24697, respectively. The flight lines for both surveys were spaced 300-500 m apart. The soundings from the two surveys were typically within 70 m. The processing was carried out by Aqua Geo Framework (Asch et al., 2020). The 2019 AEM survey data covered mountainous regions in the southern part of the study area, not included in the 2017 survey.

The workflow was developed so as to have no more than two AEM soundings (one from the 2017 data and the other from the 2019 data) per cell of the SWI grid; this was to prevent underfitting the AEM data due to the lower spatial resolution of the SWI model than the AEM data at the surface. In order to equally weight the 2017 and 2019 AEM data, in selecting AEM soundings we aimed to select the same number of soundings from each data set. To satisfy these two conditions, we began with the 2017 AEM data which covered a smaller area than the 2019 AEM data. Given that the cell size of the SWI grid was larger than the spatial interval between soundings, there were instances where there were more than one 2017 AEM sounding present within a single SWI cell. To resolve this, in an SWI cell with multiple 2017 AEM soundings, the sounding closest to the centroid of the cell was retained and other soundings discarded. We repeated the same selection process with the 2019 AEM soundings. As a result, the number of soundings per each cell was no greater than two. However, this resulted in a greater number of soundings for the selected 2019 AEM data than for the selected 2017 AEM data due to the additional coverage of the 2019 AEM data over the mountainous regions. To equally weight the two AEM data sets, we selected the portion of the 2019 AEM soundings that had the smallest separation distance to a 2017 sounding location. This was repeated until the number soundings of the two data sets was the same. The resulting number of soundings of the two data sets were 769. These selected AEM data sets are referred to as the time-lapse AEM data.

3. Methodology

Our objective was to use the AEM data, along with other ancillary data, to reduce the uncertainty in the predictions obtained with SWI models. Specifically, out of 105 starting SWI models, we identified a reduced set compatible with both the conventional in-situ data and the time-lapse AEM data. The inputs for our workflow were 1) an SWI model calibrated to the in-situ data and 2) the time-lapse AEM data. The workflow was divided into five steps. Step 1: M&A utilized the PEST utilities provided by Doherty (2020) to generate 105 SWI models using the null-space Monte Carlo technique. Step 2: We transformed the hydrogeologic properties obtained in the first step into a resistivity model defined at the SWI grid, taking into account several parameters that had a range of possible values. The parameter values were sampled randomly, resulting in 500 SWI resistivity models. Step 3: We interpolated the 500 resistivity models onto the AEM grid resulting in 500 resistivity models that were used in simulating acquired AEM data; this step was needed to utilize the conventional 1D forward modeling algorithm widely used for inverting AEM data for hydrogeologic applications (e.g., Kang et al., 2017; Viezzoli et al., 2010). Step 4: We simulated an AEM response for each AEM resistivity model, thereby yielding 500 sets of time-lapse AEM data as outputs of our workflow. In this step, we also selected a portion of the AEM resistivity models which fit the time-lapse AEM data so as to find a reduced set of SWI models fitting both the in-situ and the AEM data.

2.1 Step 1: Generating multiple SWI models

The PEST utilities were utilized to generate 104 models through the use of null-space Monte Carlo methodology. The result was 105 SWI models, each of which agreed well with the in-situ data. The models comprised unique combinations of parameters including horizontal and vertical hydraulic conductivity, specific yield, porosity, specific storage, and recharge. To progress the workflow, the horizontal hydraulic conductivity distribution, porosity distribution, and two simulated salinity distributions (corresponding to the two times when the time-lapse AEM surveys were conducted) were extracted from each of the 105 SWI models. In the following sections of the paper, we will only use the horizontal hydraulic conductivity to obtain the resistivity, so the vertical hydraulic conductivity is ignored. Hence, the horizontal hydraulic conductivity will be referred to simply as hydraulic conductivity for clarity and conciseness. Ignoring vertical hydraulic conductivity when estimating resistivity was based upon the higher sensitivity of the AEM data to the horizontal resistivity than the vertical resistivity due to the parallel nature of the induced currents in the subsurface to the layered hydrogeologic structure.

2.2 Step 2: Transforming hydrogeologic properties to electrical resistivity

The objective of this stage was to use the hydrogeologic properties of hydraulic conductivity, porosity, and salinity to estimate electrical resistivity at the SWI grid scale. From 105 sets of the hydrogeologic properties we created 500 SWI resistivity models to account for uncertainties associated with required parameters for transforming hydrogeologic properties to resistivity.

For estimating an SWI resistivity model from the hydrogeologic properties, we employed an extension of the approach developed by (Gottschalk, 2020). This approach included two major processes: 1) estimating resistivity at a smaller scale than the SWI grid and 2) upscaling resistivity at the smaller scale onto the SWI grid. At the smaller scale, we assumed that the sedimentary aquifer system was a binary system composed of sand and clay.

The first process starts with calculating fluid resistivity, ρ_f , which linearly relates to the salinity in the form of total dissolved solids (TDS; mg/L):

$$\rho_f = (k_{\text{TDS}}\text{TDS} + p_{\text{TDS}})^{-1} \times 10^4 \quad (1)$$

where k and p stands for constants associated with the slope and intercept, respectively; subscript indicates an input variable to define a linear curve. The SWI model calculated the chloride concentration, CL, and therefore we needed another relationship between TDS and chloride:

$$\text{TDS} = (k_{\text{CL}}\text{CL} + p_{\text{CL}}) \quad (2)$$

Determined values from the linear regression of in-situ samples were $k_{\text{TDS}} = 1.42$, $p_{\text{TDS}} = 332.71$, $k_{\text{CL}} = 1.709$, $p_{\text{CL}} = 447.94$.

The resulting fluid conductivity was an input for calculating a resistivity value of the smaller scale clay using the Waxman-Smiths equation (Waxman & Smits, 1968):

$$\rho_{\text{clay}} = F(\rho_f^{-1} + Q_v B)^{-1} \quad (3)$$

where the formation factor is $F = \phi^{-m}$; ρ_f is the fluid resistivity; ϕ and m indicate porosity and cementation factor, respectively; Q_v and B are parameters related to clay materials. For calculating the resistivity of the smaller scale sand, $Q_v B$ in equation (2) was set to be zero (i.e., $\rho_{\text{sand}} = F\rho_f^{-1}$).

Within the second process, we upscaled the smaller scale resistivity values onto the SWI grid using the upper Hashin-Shtrikman bound (Hashin & Shtrikman, 1963):

$$\rho = \rho_{\text{clay}} \left(1 - \frac{3(1 - \text{CF})(\rho_{\text{clay}}^{-1} - \rho_{\text{sand}}^{-1})}{3\rho_{\text{clay}}^{-1} - \text{CF}(\rho_{\text{clay}}^{-1} - \rho_{\text{sand}}^{-1})} \right)^{-1}, \quad (4)$$

where CF indicates the clay fraction. Therefore, given resistivity values of the smaller scale sand and clay along with the clay fraction, it is possible to determine the resistivity value of a single cell of the SWI model.

The clay fraction was the link between the hydrogeologic properties from the SWI model (hydraulic conductivity and porosity) and the resistivity. Hence within the second process, it was needed to estimate the clay fraction. We extended Gottschalk (2020)'s approach to address this. For estimating the clay fraction, we first converted the hydraulic conductivity and porosity into d_{10} , which represents the size of the grain that passes 10% through a sieve. This was achieved using the Kozeny-Carman equation, which can be expressed as

$$d_{10} = \left(\frac{Kv(1 - \phi)^2}{gC_K\phi^3} \right)^{0.5} \quad (5)$$

where K is the hydraulic conductivity (m/s); ϕ is the porosity, v is the fluid kinematic viscosity ($1.1 \times 10^{-6} \text{ m}^2/\text{s}$); g is the gravitational acceleration ($9.81 \text{ m}/\text{s}^2$); C_K is a unitless coefficient, 1/180, determined by flow in capillary tubes or beds of spheres. We then randomly selected a threshold value for d_{10} , $\text{thres}_{d_{10}}$, for dividing the sample into two categories: clay poor (cp) and clay rich (cr). Finally, we randomly assigned a CF value to each of the two categories.

The two processes were repeated 500 times with bootstrapping of SWI models and random sampling of the associated parameters summarized in Table 1; these parameters were cementation factors for smaller scale sand and clay (m_{sand} , m_{clay}), clay fractions for clay poor and clay rich (CF_{cp} , CF_{cr}), and $\text{thres}_{d_{10}}$. This resulted in 500 SWI resistivity models.

Table 1. Summary of sampled parameters associated with the transform of hydraulic properties to the clay fraction. U and $\text{Log}_{10}U$ indicate the uniform and log uniform distributions, respectively.

Parameter	Distribution	Unit
m_{sand}	$U(0.5, 1.5)$	Dimensionless
m_{clay}	$U(0.5, 1.5)$	
CF_{cp}	$U(0, 0.5)$	
CF_{cr}	$U(0.5, 1)$	
$\text{thres}_{d_{10}}$	$\text{Log}_{10}U(0.02, 0.5)$	mm

2.3 Step 3: Interpolating SWI resistivity models onto AEM grid

In this step, we interpolated each SWI resistivity model onto the AEM grid resulting in an AEM resistivity model. The AEM resistivity model was composed of the vertical 1D resistivity profiles at each sounding location. Each vertical resistivity profile had 30 cells with the same vertical discretization in all

profiles: the cell thickness was 3 m at the surface and increased with a constant rate of 1.07 for each consecutive cell. Although we reinforced to have no more than two AEM soundings at a SWI cell, still there was a need to interpolate resistivity values on the SWI grid to the AEM grid due to increasing lateral sampling volume of resistivity with depth. Further, the vertical dimension of the SWI grid was variable along the lateral dimensions, while that of the AEM grid was uniform. To reconcile these differences between the AEM and SWI grids, we devised an interpolation method based on volumetric averaging (Kang et al., 2022). Using this approach, we interpolated all SWI resistivity models onto the AEM grid resulting in 500 AEM resistivity models.

2.4 Step 4: Simulating AEM response

Using the 1D forward modeling algorithm, we simulated AEM data at each lateral location of an AEM resistivity model using a corresponding vertical resistivity profile. This was repeated for all 500 AEM resistivity models resulting in 500 sets of the time-lapse AEM data. For each set, we calculated the root mean square error (RMSE) between the observed and predicted AEM data, providing a metric to evaluate the accuracy of each of the 500 AEM resistivity models. For each of the 500 resistivity models, there was a corresponding RMSE value, SWI model, and set of sampled parameters. These 500 resistivity models and parameters were referred to as the prior models and parameters, respectively. We organized the models based on increasing RMSE values and selected the top 75 models, which were referred to as the posterior models and their associated parameters as the posterior parameters. In addition, we selected the two resistivity models with the lowest and highest RMSE values from the 500 resistivity models. Associated SWI models with these two resistivity models were referred to as the lowest-fit SWI model and the highest-fit SWI model.

3. Results and Discussion

Based upon the RMSE values, we selected 75 posterior resistivity models from the 500 prior resistivity models. Within the 75 posterior resistivity models, there were 22 unique SWI models. These 22 SWI models were designated as the posterior SWI models. The baseline misfit was calculated assuming a uniform subsurface resistivity of 20 Ωm , which was used as a starting resistivity model for inverting the 2017 AEM data (Gottschalk et al., 2020), resulting in a misfit value of 14.

Figure 2 displays the distribution of calculated RMSE values, which vary between 4.2 and 10. All of the resistivity models demonstrate lower data misfit than the baseline homogeneous resistivity model. The lowest data misfit is approximately 2.5 times smaller than the highest data misfit. It is worth noting that all SWI models fit the in-situ data to a similar degree. Therefore, the difference in data misfit between these two extremes demonstrates the ability of AEM data to distinguish the better SWI models (posterior) from the many sampled SWI models (prior).

Figure 3 presents a comparison of the distributions of prior and posterior parameters related to the estimation of resistivity using hydraulic conductivity, porosity, and salinity from the SWI model. No significant differences can be observed between the prior and posterior parameters, indicating a high degree of uncertainty in determining these parameters using AEM data alone. This is largely due to the non-unique nature of the parameters, meaning that many combinations of these parameters can produce the same resistivity value. This issue could be addressed by incorporating other in-situ data, such as resistivity logs and sediment type logs, which can provide additional constraints and reduce uncertainty.

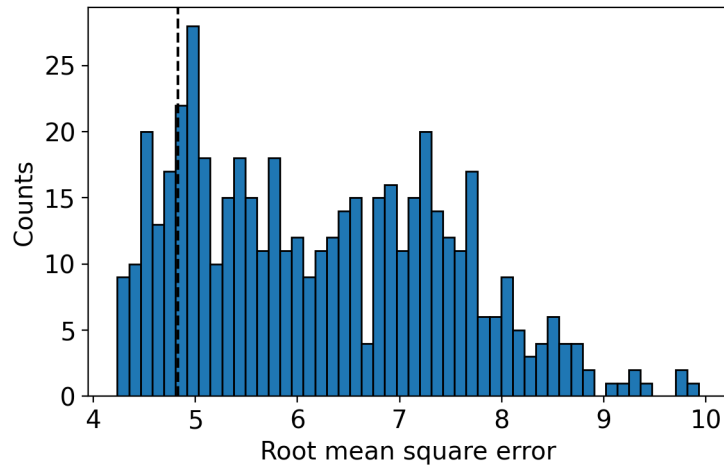


Figure 3. Distribution of Root Mean Square Error (RMSE) between the simulated and observed time-lapse AEM data for 500 resistivity models. The black vertical dashed line indicates the RMSE value of the top 75th percentile of the models.

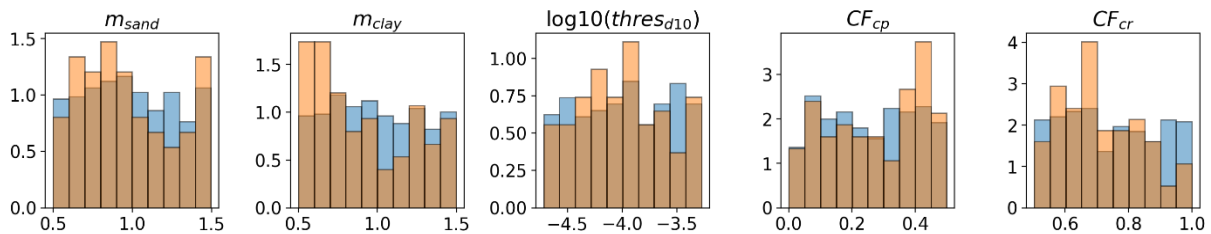


Figure 3. Comparing distributions of prior parameters and posterior parameters. Blue and orange bars distinguish prior and posterior parameters.

In Figures 4 and 5, we present a comparative analysis of the chloride concentrations and hydraulic conductivity distributions, respectively, for the lowest-misfit and highest-misfit SWI models within the 180-foot aquifer. The coastline and the Salinas River are represented by black and blue lines, respectively, and the high chloride concentration value of 9000 mg/L is denoted by a black dashed line. The regional-scale features of the chloride concentrations from both models are in agreement, with a large extent of saltwater intrusion (approximately 20 km from the coastline) observed near the center of the coastline and a decreasing extent to the north and south. This was mainly due to the first step of our workflow, which sampled SWI models fitting the in-situ chloride concentration data. We do observe, however, significant differences at a local scale. The highest-misfit model exhibits a local-scale intrusion at the upper part of the intrusion front as indicated in Figure 4b with a white dashed circle while the lowest-misfit model does not exhibit the similar feature. This is attributed to the presence of a high hydraulic conductivity zone as indicated in Figure 5b. In addition, the intrusion fronts with the high concentration value from the two models show significant difference. The lowest-misfit model shows an anomalous intrusion at the center of the coastline, as depicted by the shape of the high chloride concentration contours (Figure 4a) while this feature anomalous feature was absent in the highest-misfit model (Figure 4b). This difference is attributed to the presence of a high hydraulic conductivity zone in the vicinity as indicated in Figure 5b.

This analysis highlights the importance of considering both regional- and local-scale features in evaluating models of saltwater intrusion, and demonstrates the added value of incorporating AEM data in the model selection process.

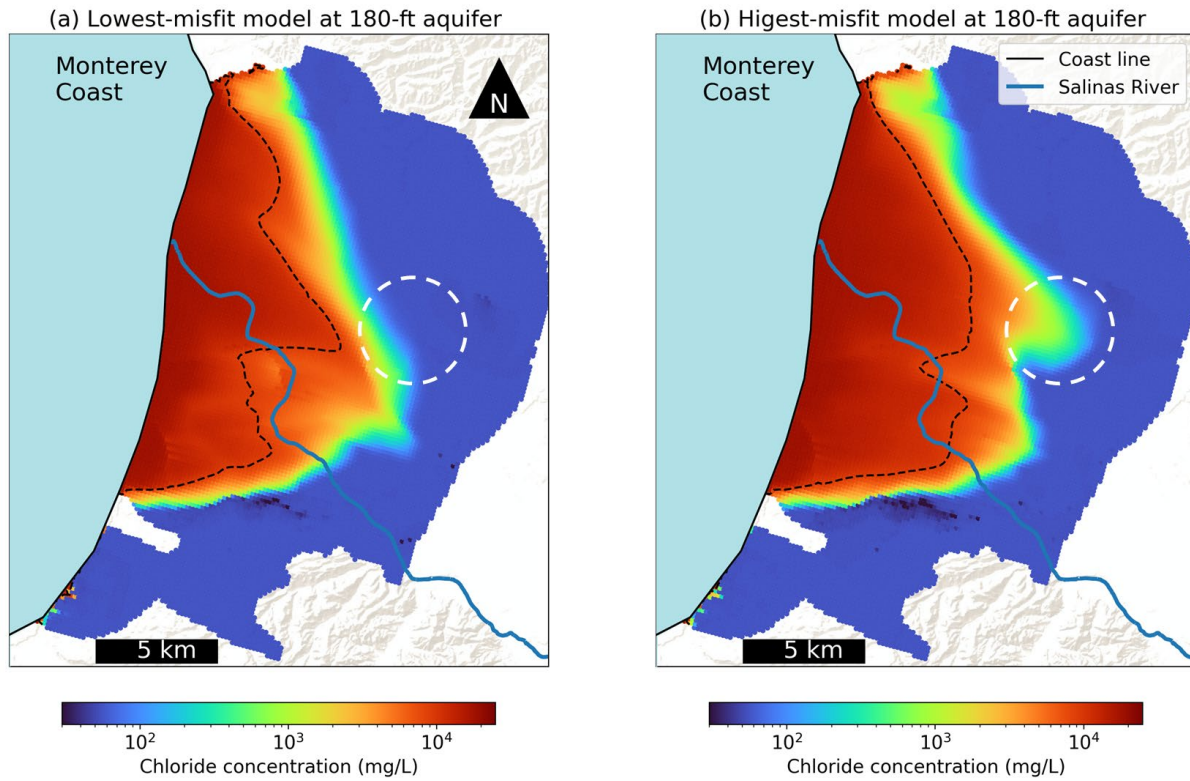


Figure 4. Comparison of the chloride concentrations from (a) the lowest-misfit SWI model and (b) the highest-misfit SWI model. The chloride concentration within the 180-foot aquifer is displayed on a plan view map. The black dashed line contours a high chloride concentration value of 9000 mg/L. White dashed circle highlights the region where a local-scale saltwater intrusion is present in the highest-misfit SWI model.

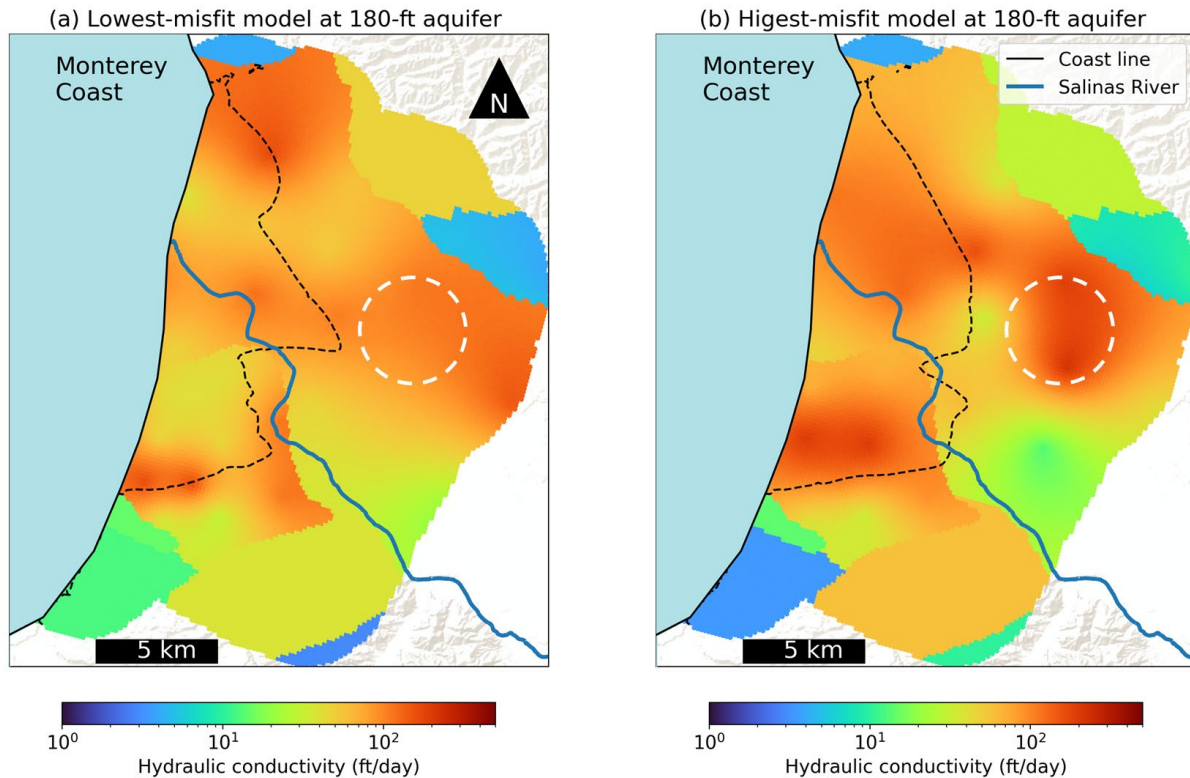


Figure 6. Comparison of the hydraulic conductivity distributions from (a) the lowest-misfit SWI model and (b) the highest-misfit SWI model. The hydraulic conductivity distribution in the 180-foot aquifer is displayed on a plan view map. The black dashed line contours a high chloride concentration value of 9000 mg/L from the corresponding SWI model. White dashed circle highlights the region where a local-scale saltwater intrusion is present in the highest-misfit SWI model.

4. Conclusions

The AEM method presents a significant opportunity to enhance the accuracy of saltwater intrusion models in numerous coastal areas. To achieve this, it is imperative to establish a strong numerical approach that seamlessly integrates AEM data into the modeling process.

Our methodology was developed with a focus on leveraging existing methodologies and relationships widely used in related fields. To generate multiple saltwater intrusion (SWI) models that fit in-situ data, we applied the null-space Monte Carlo technique, commonly adopted for uncertainty analysis in groundwater modeling. Hydrogeologic properties from the SWI models were transformed into electrical resistivity, a geophysical property that is sensitive to AEM data, using well-established rock physics relationships that can be easily implemented without extensive prior knowledge. The fast 1D AEM simulation algorithm was utilized to simulate AEM response; this algorithm has proven to be an effective approach for inverting AEM data for hydrogeologic applications.

Use of the AEM data in our analysis allowed us to falsify 83 SWI models and identify 22 SWI models as posteriors. All posterior models were not only constrained by the conventional in-situ data but also by the time-lapse AEM data. From visual inspection of the lowest-misfit and highest-misfit SWI models, we

expected and confirmed that the salinity distributions from both models show consistent regional-scale features. However, there were noticeable differences in local-scale features, which demonstrated the value of the AEM data for improving the accuracy of the SWI model at local-scale.

With the growing concern about sea-level rise and heightened demand for groundwater in coastal regions, it is expected that more areas will require the development of localized saltwater intrusion models. This, combined with the increasing adoption of AEM methods for hydrogeologic applications, has the potential to expand the coverage of AEM data in these areas. Our methodology is designed specifically for regions where both a local saltwater intrusion model and AEM data are available, making it readily transferable to other regions through its use of widely adopted numerical tools and rock physics relationships. In addition to improving saltwater intrusion predictions, our methodology also has the potential to be applied to the integration of AEM data with regional groundwater models, demonstrating its broad applicability.

Deliverables

Output table containing 500 resistivity models and associated parameters composed of model number, RMSE, and parameters related to the transform of hydrogeologic properties to electrical resistivity.

Filename: all_500_sets.csv [\[downloadable link\]](#)

References

- Asch, T., Abraham, J. D., & Cannia, J. C. (2020). *2017 & 2019 Airborne Geophysical Investigations for Marina Coast Water District*. Monterey, CA. Retrieved from https://storage.googleapis.com/wzukusers/user-27297781/documents/5e5d8a3a6b6610W4Ktvh/ASCH_MCWD2019_25Feb2020_v1_reduced.pdf
- Barfod, A. A. S., Møller, I., Christiansen, A. V., Hoyer, A. S., Hoffmann, J., Straubhaar, J., & Caers, J. (2018). Hydrostratigraphic modeling using multiple-point statistics and airborne transient electromagnetic methods. *Hydrology and Earth System Sciences*. <https://doi.org/10.5194/hess-22-3351-2018>
- Fitterman, D. V., & Deszcz-Pan, M. (2004). Characterization of saltwater intrusion in south Florida using electromagnetic geophysical methods. *US Geological Survey*, 405–416.
- Foged, N., Marker, P. A., Christiansen, A. V., Bauer-Gottwein, P., Jørgensen, F., Høyer, A. S., & Auken, E. (2014). Large-scale 3-D modeling by integration of resistivity models and borehole data through inversion. *Hydrology and Earth System Sciences*, 18(11), 4349–4362. <https://doi.org/10.5194/hess-18-4349-2014>
- Goebel, M., Knight, R., & Halkjær, M. (2019). Mapping saltwater intrusion with an airborne electromagnetic method in the offshore coastal environment, Monterey Bay, California. *Journal of Hydrology: Regional Studies*, 23, 100602. <https://doi.org/https://doi.org/10.1016/j.ejrh.2019.100602>
- Gottschalk, I. P. (2020). *Hydrogeophysical modeling of saltwater intrusion*. Stanford University.
- Gottschalk, I. P., Knight, R., Asch, T., Abraham, J., & Cannia, J. (2020). Using an airborne electromagnetic method to map saltwater intrusion in the northern Salinas Valley, California. *GEOPHYSICS*, 85(4), B119–B131. <https://doi.org/10.1190/geo2019-0272.1>
- Guo, W., & Langevin, C. D. (2002). *User's guide to SEAWAT; a computer program for simulation of three-dimensional variable-density ground-water flow* (Supersedes). *Techniques of Water-Resources Investigations*. <https://doi.org/10.3133/twri06A7>
- Hashin, Z., & Shtrikman, S. (1963). A variational approach to the theory of the elastic behaviour of multiphase materials. *Journal of the Mechanics and Physics of Solids*, 11(2), 127–140. [https://doi.org/https://doi.org/10.1016/0022-5096\(63\)90060-7](https://doi.org/https://doi.org/10.1016/0022-5096(63)90060-7)
- He, X., Koch, J., Sonnenborg, T. O., Flemming, J., Schamper, C., & Refsgaard, J. C. (2014). Transition probability-based stochastic geological modeling using airborne geophysical data and borehole data. *Water Resources Research*, 1–23. <https://doi.org/10.1002/2013WR014593>.Received
- Kang, S., Heagy, L. J., Cockett, R., & Oldenburg, D. W. (2017). Exploring nonlinear inversions: A 1D magnetotelluric example. *The Leading Edge*, 36(8), 696–699. <https://doi.org/10.1190/tle36080696.1>
- Kang, S., Knight, R., Greene, T., Christina, B., & Fogg, G. (2021). Exploring the Model Space of Airborne Electromagnetic Data to Delineate Large-Scale Structure and Heterogeneity Within an Aquifer System. *Water Resources Research*, 57(10), e2021WR029699. <https://doi.org/https://doi.org/10.1029/2021WR029699>
- Kang, S., Knight, R., & Goebel, M. (2021). Improved Imaging of the Large-Scale Structure of a Groundwater System with Airborne Electromagnetic Data. *Earth and Space Science Open Archive*, 34. <https://doi.org/10.1002/essoar.10508422.1>
- Kang, S., Knight, R., & Goebel, M. (2022). Improved Imaging of the Large-Scale Structure of a Groundwater System With Airborne Electromagnetic Data. *Water Resources Research*, 58(4), e2021WR031439. <https://doi.org/https://doi.org/10.1029/2021WR031439>

- Knight, R., Smith, R., Asch, T., Abraham, J., Cannia, J., Viezzoli, A., & Fogg, G. (2018). Mapping Aquifer Systems with Airborne Electromagnetics in the Central Valley of California. *Ground Water*. <https://doi.org/10.1111/gwat.12656>
- Langevin, C. D., Thorne Jr., D. T., Dausman, A. M., Sukop, M. C., & Guo, W. (2008). *SEAWAT Version 4: A Computer Program for Simulation of Multi-Species Solute and Heat Transport. Techniques and Methods*. <https://doi.org/10.3133/tm6A22>
- M&A. (2023). *Salinas Valley seawater intrusion model. Prepared for Salinas Valley Basin Groundwater Sustainability Agency*. Monterey, CA.
- Masterson, J. P. (2004). *Simulated interaction between freshwater and saltwater and effects of groundwater pumping and sea-level change, lower Cape Cod aquifer system, Massachusetts. Scientific Investigations Report*. <https://doi.org/10.3133/sir20045014>
- MCWD, & SVBGSA. (2022). *Salinas Valley Groundwater Basin Monterey Subbasin Groundwater Sustainability Plan*.
- MCWRA. (2022). Groundwater Level Monitoring. Retrieved from https://bit.ly/mcwra_gw_level_monitoring
- Paulinski, S. (Ed.). (2021). *Development of a groundwater-simulation model in the Los Angeles Coastal Plain, Los Angeles County, California. Scientific Investigations Report*. Reston, VA. <https://doi.org/10.3133/sir20215088>
- Viezzoli, A., Munday, T., Auken, E., & Christiansen, A. V. (2010). Accurate quasi 3D versus practical full 3D inversion of AEM data – the Bookpurnong case study. *Preview*, 2010(149), 23–31. Retrieved from <http://www.publish.csiro.au/paper/PVv2010n149p23>
- Waxman, M. H., & Smits, L. J. M. (1968). Electrical Conductivities in Oil-Bearing Shaly Sands. *Society of Petroleum Engineers Journal*, 8(02), 107–122. <https://doi.org/10.2118/1863-A>